

## Durham E-Theses

---

*The application of ESCA to structure and bonding  
with particular reference to synthesis and surface  
modification of polymers*

Abu-Shbak, Mohammad Mahmoud

### How to cite:

---

Abu-Shbak, Mohammad Mahmoud (1983) *The application of ESCA to structure and bonding with particular reference to synthesis and surface modification of polymers*, Durham theses, Durham University. Available at Durham E-Theses Online: <http://etheses.dur.ac.uk/7708/>

### Use policy

---

The full-text may be used and/or reproduced, and given to third parties in any format or medium, without prior permission or charge, for personal research or study, educational, or not-for-profit purposes provided that:

- a full bibliographic reference is made to the original source
- a [link](#) is made to the metadata record in Durham E-Theses
- the full-text is not changed in any way

The full-text must not be sold in any format or medium without the formal permission of the copyright holders.

Please consult the [full Durham E-Theses policy](#) for further details.

The copyright of this thesis rests with the author.  
No quotation from it should be published without  
his prior written consent and information derived  
from it should be acknowledged.

A thesis entitled

THE APPLICATION OF ESCA TO STRUCTURE AND BONDING  
WITH PARTICULAR REFERENCE TO SYNTHESIS AND  
SURFACE MODIFICATION OF POLYMERS

submitted by

MOHAMMAD MAHMOUD ABU-SHBAK, B.Sc.  
(Riyadh University)  
Saudi Arabia

A candidate for the Degree of Doctor of Philosophy

Graduate Society,  
University of Durham

July 1983



22.10.1983

To my parents,  
my brothers and sisters  
and all my family.

- ACKNOWLEDGEMENTS -

This thesis could not have been written without the help and assistance of a number of individuals whom I would like to thank. First and foremost I would like to extend my most sincere and greatest thanks in this acknowledgement to my supervisor Professor David T. Clark for his enthusiasm, guidance and encouragement during my studies with the ESCA group at Durham.

I would like also to thank and extend my sincere appreciation to my colleagues Dr. Hugh Munro, Bill Brennan, Steve Johnson, Andy Fowler and Jeff Eaves together for the friendship we developed. I am also grateful to all other members of the ESCA group over the past three years. Thanks are also due to a former colleague Dr. Mohammad Z. AbRahman, for his early advice.

I am indebted to Mrs. Elizabeth Nevins for her great assistance in preparing all the figures in this thesis and to Mr. Glyn Metcalfe. Also many thanks to Miss Jean Eccleston for her great secretarial skill and patience in typing this thesis.

Thanks are also due to Dr. Isam F. El-Saafin for his friendship and encouragement whilst at Durham University.

Finally, but not least, I extend my thanks to all my family and all my friends who gave me much support for doing this degree.

## - ABSTRACT -

Electron mean free paths as a function of kinetic energy have been measured by the substrate overlayer technique for in-situ polymerised films of polyparaxylylene, using a  $\text{Ti}_{k\alpha_{1,2}}$  ( $h\nu = 4510 \text{ eV}$ ) X-ray source. The results are compared with those previously reported at lower kinetic energies using  $\text{Mg}_{k\alpha_{1,2}}$  (1254 eV) and  $\text{Al}_{k\alpha_{1,2}}$  (1487 eV) photon sources.

ESCA is used to study structure, bonding and reactivity of polymeric materials, in particular those prepared by R.F. (radio-frequency), "glow discharge techniques", (plasma polymerisation).

Plasma polymerised films of perfluoropyridine have been investigated for a range of operating parameters, in both free-standing and in-situ reactors. A comparison of the stoichiometries and rates of deposition has been drawn with plasma polymers produced under comparable conditions from perfluoro and pentafluorobenzenes.

Ultra thin polymers produced by plasma techniques from three isomeric perfluorinated diazines (pyrazine, pyrimidine and pyridazine) have been investigated. The polymer produced from the 1,2-diazine is discussed in some detail. A combination of ESCA and microanalytical studies show that the C:F and C:N stoichiometries are closely similar to those for the starting monomers, over a range of operating parameters. The surface hydrolysis of these polymers with water as a function of time has been studied. The rates of polymer deposition are discussed as a function of the composite parameter  $W/FM$ . The rates of deposition reveal distinctive

differences between the isomeric diazines and those of plasma polymer films for isomeric fluorinated benzenes.

Laminate films based on LDPE and PET adhesively bonded with polyurethane adhesives have been investigated by ESCA. The change of surface chemistry of these films has been compared with the non-laminated base polymer of LDPE and PET. Migration and segregation phenomena in the laminates has been investigated.

ESCA has been used to investigate the surface chemistry of heat treated LDPE (low and high-slip agent) and PET. The results indicate that thermally promoted reactions at the surface may well be different than those in the bulk.

## - MEMORANDUM -

The work described in this thesis was carried out at the University of Durham between May 1980 and July 1983. It has not been submitted for any other degree, and is the original work of the author except where acknowledged by reference.

Work in this thesis has formed the whole, or part, of the following publications:-

1. Electron Mean Free Paths as a Function of Kinetic Energy: A Substrate Overlay Investigation of Polyparaxylylene Films on Gold Using a  $Ti_{k\alpha}$  X-ray Source, D.T. Clark, M.M. Abu-Shbak and W.J. Brennan, J. Elect. Spec., and Rel. Phen., 28, 11 (1982).
2. Plasma Polymerization. IX. A Systematic Investigation of Materials Synthesized in Inductively Coupled Plasmas Excited in Perfluoropyridine, D.T. Clark and M.M. Abu-Shbak, J. Polym. Sci., Polym. Chem. Ed., in press (1983).
3. Plasma Polymerization. X. A Systematic Investigation of Materials Synthesized in Inductively Coupled Plasmas Excited in Tetrafluoropyridazine, D.T. Clark and M.M. Abu-Shbak, J. Polym. Sci., Polym. Chem. Ed., in press (1983).
4. Plasma Polymerization. XI. A Comparison of the Plasma Polymerization of the Isomeric Perfluorinated Diazines, D.T. Clark and M.M. Abu-Shbak, J. Polym. Sci., Polym. Chem. Ed., in press (1983).

5. An ESCA Investigation of the Surface Chemistry of Heat Treated Polyethylene Terephthalate and Polyethylene, D.T. Clark and M.M. Abu-Shbak, *Polymer*, Ed., in press (1983).



CONTENTS

	<u>Page No.</u>
Acknowledgements	i
Abstract	ii
Memorandum	iv
Contents	vi
 <u>CHAPTER ONE:</u>	
ELECTRON SPECTROSCOPY FOR CHEMICAL APPLICATION (E.S.C.A.)	1
1.1. Introduction	2
1.2. Processes Involved in ESCA	4
1.2.1. The ESCA Experiment	4
1.2.2. De-excitation Processes	6
1.2.3. Relaxation Phenomena	10
1.2.4. Shake-up and Shake-off Phenomena	11
1.2.5. Energy Loss Processes	13
1.3. Feature of Core Electron Spectra	14
1.3.1. Binding Energy and Chemical Shifts	14
1.3.2. Line Shape Analysis	17
1.3.3. Line Widths	19
1.4. Fine Structure	21
1.4.1. Multiplet Splitting	21
1.4.2. Spin-Orbit Splitting	23
1.4.3. Electrostatic Splitting	24
1.5. Signal Intensities	27
1.5.1. Fixed Angle Studies	28
1.5.2. Analytical Depth Profiling	32
1.5.3. Angular Dependence	36

	<u>Page No.</u>
1.6. Energy Referencing	37
1.7. Sample Handling	40
1.8. Instrumentation	42
1.8.1. X-ray Equipment	43
1.8.2. Sample Chamber	46
1.8.3. Analyser	47
1.8.4. Electron Detection	49
1.9. General Aspects of ESCA	49
1.9.1. Advantages of ESCA	49
1.9.2. Disadvantages of ESCA	51
1.9.3. Hierarchy of ESCA Information	51

## CHAPTER TWO:

ESCA APPLIED TO POLYMERS	53
2.1. Introduction	54
2.2. Sample Preparation	56
2.2.1. Powders	56
2.2.2. Solution Cast Films	57
2.2.3. Pressed or Extruded Films	57
2.2.4. "In-situ" Preparation	58
2.3. Static Studies	58
2.3.1. Chemical Compositions	59
2.3.2. Percentage Comonomers in Copolymers	60
2.4. Structural Details	61
2.4.1. Repeat Units in Polymers - Substituent Effects	61
2.4.2. Repeat Units in Copolymers	64
2.5. Fine Structural Details	67
2.5.1. Shake-up Studies	67

	<u>Page No.</u>
2.6. Valence Band Studies of Polymers	69
2.7. Auger Parameters	69
2.8. Sample Charging Effects	70
2.9. Dynamic Studies	71
2.9.1. Surface Modification of Polymers	71
(i) Modification by plasma and corona discharge	71
(a) Corona-discharge treatment	72
(b) Inert gas plasmas	74
(c) Oxygen plasmas	75
(ii) Modification by chemical treatments	78
(a) Surface oxidation and sulphonation	79
(b) Surface fluorination	80
(c) Nitration and denitration	81
2.9.2. Migration and Segregation Phenomena	82
2.9.3. Polymer Degradation	84
Weathering Phenomena	84
2.9.4. In-situ Polymerisation	87

### CHAPTER THREE:

ELECTRON MEAN FREE PATHS AS A FUNCTION OF KINETIC ENERGY: A SUBSTRATE OVERLAYER INVESTIGATION OF POLYPARAXYLENE FILMS ON GOLD USING A $Ti_{k\alpha}$ X-RAY SOURCE	88
3.1. Introduction	89
3.2. Experimental	91
3.3. Results and Discussion	97
3.3.1. Introduction	97
3.3.2. Comparison of Electron Mean Free Paths for Photoelectrons Excited from the $Au_{4f}$ Levels	102

	<u>Page No.</u>
3.3.3. Au <sub>4d</sub> Levels Studied with Ti <sub>k<math>\alpha</math>1,2</sub> X-ray Source	104
3.3.4. Au <sub>4p<sub>3/2</sub></sub> Levels Studied with the Ti <sub>k<math>\alpha</math>1,2</sub> X-ray Source	105
3.3.5. Au <sub>3d</sub> Levels Studied with the Ti <sub>k<math>\alpha</math>1,2</sub> X-ray Source	107
3.3.6. Au <sub>3p<sub>3/2</sub></sub> Level Studied with Ti <sub>k<math>\alpha</math>1,2</sub> X-ray Source	109
3.3.7. The Cu <sub>L<math>\alpha</math></sub> Excited Au <sub>4f</sub> and Au <sub>3d</sub> Levels	110
3.3.8. Comparison of Data with Previous Studies of Polymer-Metal Systems by the Substrate-Overlayer Technique	112

#### CHAPTER FOUR:

PLASMA POLYMERISATION. A SYSTEMATIC INVESTIGATION OF MATERIALS SYNTHESISED IN INDUCTIVELY COUPLED PLASMAS EXCITED IN PERFLUOROPYRIDINE	116
4.1. Fundamental Aspects of Plasmas	117
4.1.1. Definition and Characterisation	117
4.1.2. Plasma Techniques	122
4.1.3. Reactive Species in Plasmas	123
4.1.4. Advantages and Disadvantages of the Glow Discharge Technique	124
4.2. Polymer Characterisation Techniques	126
4.3. Plasma Polymerisation	129
4.4. Polymer Films Produced by RF Plasma in Perfluoropyridine	132
4.4.1. Introduction	132
4.4.2. Experimental	134

	<u>Page No.</u>
4.4.3. Results and Discussion	137
(i) In-situ depositions	137
(a) Gross chemical structure	137
(b) Power dependence	140
(c) Rate of deposition	146
(d) Time dependence	148
(ii) Deposition in the free-standing reactor	151
(a) Gross chemical structure	151
(b) Rate of deposition	153
(c) Comparison of "monomers"	154
(d) Other measurements	156
(1) Contact angle	156
(2) Infra-red and UV studies	157
(3) TG and DSC studies	158

#### CHAPTER FIVE:

PLASMA POLYMERISATION: A SYSTEMATIC INVESTIGATION OF MATERIALS SYNTHESISED IN INDUCTIVELY COUPLED PLASMAS EXCITED IN TETRAFLUOROPYRIDAZINE	160
5.1. Introduction	161
5.2. Experimental	162
5.3. Results and Discussion	165
5.3.1. In-situ Deposition	165
(i) Gross structure	165
(ii) Power and pressure dependence	167
(iii) Time dependence	170
(iv) Rate of deposition	172

	<u>Page No.</u>
5.3.2. Deposition in the Free-Standing Reactors	174
(i) The bulk and surface analysis	174
(ii) Rates of deposition	179
(iii) Site of deposition	181
(iv) Other measurements	186
(a) Contact angles	186
(b) Infra-red studies	189
(c) Thermogravimetry (TG)	190
(d) Adhesion	191
(v) Sleeve effects	191

#### CHAPTER SIX:

PLASMA POLYMERISATION: A COMPARISON OF THE PLASMA POLYMERISATION OF THE ISOMERIC PERFLUORINATED DIAZINES	194
6.1. Introduction	195
6.2. Experimental	196
6.3. Results and Discussion	197
6.3.1. Introduction	197
6.3.2. Perfluoropyrimidine	197
(i) Gross structural features and composition	197
(ii) Angular dependent studies	200
(iii) Rates of deposition	203
(iv) Contact angle with water as a function of time	206
6.3.3. Perfluoropyrazine	208
(i) Gross structural features and composition	208
(ii) Rates of deposition	210

	<u>Page No.</u>
(iii) Time dependence	210
(iv) Contact angle with water as a function of time	212
6.3.4. Comparison of Plasma Polymer Films from Perfluoropyridine and the Isomeric Diazines	213

## CHAPTER SEVEN:

THE ESCA INVESTIGATION OF THE SURFACE CHEMISTRY OF POLYETHYLENE AND POLYESTER LAMINATE FILMS	219
7.1. Introduction	220
7.2. Experimental	228
7.3. Results and Discussion	231
7.3.1. Base Polymer Films	231
(i) Low density polyethylene	231
(a) Low-slip	231
(b) High-slip	235
(ii) Polyethyleneterephthalate	238
7.3.2. Polyurethane Adhesives	241
(i) Adhesive A	241
(ii) Adhesive B	246
(iii) Adhesive C	250
(iv) Adhesive D	251
(v) Adhesive E	253
(vi) Adhesive F	253
(vii) Adhesive G	254
7.3.3. Laminate Films	255
(i) Adhesive A	258
(ii) Adhesive B	260
(iii) Adhesive C	262

	<u>Page No.</u>
(iv) Adhesive D	263
(v) Adhesive E	264
(vi) Adhesive F	266
(vii) Adhesive G	268
7.4. Conclusion	270

## CHAPTER EIGHT

AN ESCA INVESTIGATION OF THE SURFACE CHEMISTRY OF HEAT TREATED POLYETHYLENE TEREPHTHALATE AND POLYETHYLENE	280
8.1. Introduction	281
8.2. Experimental	290
8.3. Results and Discussion	292
8.3.1. High-slip polyethylene (HSPE)	292
8.3.2. Low-slip polyethylene (LSPE)	297
8.3.3. Polyethylene terephthalate (PET)	301

## REFERENCES

## APPENDICES



CHAPTER ONE

CHAPTER ONEELECTON SPECTROSCOPY FOR CHEMICAL  
APPLICATIONS (E.S.C.A.)Abstract

A brief review of the fundamentals of ESCA experiment is presented along with a discussion of the more important experimental observables. A description of the instrumentation employed in this thesis is also given.



### 1.1. Introduction

In common with many other spectroscopic techniques X-ray photoelectron spectroscopy is a technique originally developed by physicists and is now extensively utilized by both inorganic and organic chemists as a tool for investigating structure, bonding and reactivity.<sup>1</sup>

At the beginning of the 20th century Robinson<sup>2-4</sup> and De Broglie<sup>5</sup> investigated the energy distribution of electrons in various elements by the X-ray irradiation of thin foils, producing photoemission via the photoelectric effect. The distribution of the electron energies for the transmitted photoelectrons was recorded photographically and analysed using a homogeneous magnetic field. These distributions were characterized by long tails with edges at the high energy end. Measurement of these edge positions gave a determination of the energies of the photoelectrons ejected from the different atomic levels and therefore with a knowledge of the energy of the exciting X-ray line, binding energies were calculated. Except for a few isolated attempts<sup>6-10</sup> to extend the work of Robinson and De Broglie, X-ray photoelectron spectroscopy went into a recession until the early 1950's when Siegbahn and co-workers at the University of Uppsala, Sweden, developed an iron-free magnetic double-focussing electron spectrometer with high resolution properties.<sup>11</sup> In 1954<sup>12,13</sup> the instrument was ready to use to record high resolution photoelectron spectra excited by X-ray and they observed that the sharp line could be resolved from the edge of each electron veil (see Figure 1.1.).

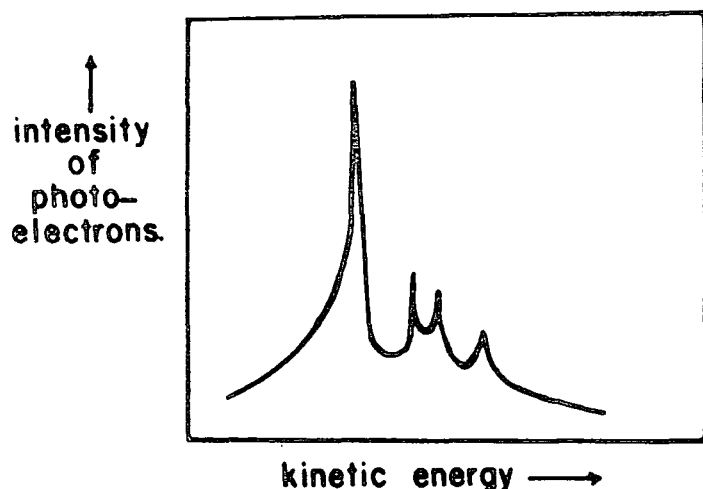


Figure 1.1. Electron spectra of MgO with  $\text{Cu}_{k\alpha}$  X-Rays.

From that point onwards the field of ESCA grew quickly through adolescence into its present day maturity.

The technique is primarily a tool for investigation of the binding energies of core electrons in atoms and molecules. Although the core electrons are not explicitly involved in bonding, the core energy levels of a molecule encode a considerable amount of information concerning the chemical environment of the atom.<sup>14,15</sup> Using this technique in 1958, Siegbahn and co-workers<sup>16</sup> first studied chemical shifts for a number of copper oxides. However, the general utility was fully appreciated only in 1964, after they observed the two distinct 1s peaks from the different oxidation states of sulphur in sodium thiosulphate.<sup>17,18</sup> The early development of electron spectroscopy (pre-Siegbahn) has been recently documented by Jenkin, Leckey and Liesegang.<sup>19</sup>

Over the past 30 years the technique of photoelectron spectroscopy has largely been developed by Siegbahn and his co-workers<sup>13</sup> and much of the early work was extensively

documented in 1968 in "ESCA, Atomic, Molecular and Solid State Structure Studied by Means of Electron Spectroscopy". Later works by this group were well documented in a series of publications.<sup>20-24</sup> Siegbahn originally coined the term ESCA (Electron Spectroscopy for Chemical Analysis), which he later amended to Electron Spectroscopy for Chemical Applications.

The technique of ESCA is also known as:-

- (1) X-ray Photoelectron Spectroscopy (XPS)
- (2) High Energy Photoelectron Spectroscopy (HEPS)
- (3) Induced Electron Emission Spectroscopy (IEES)
- (4) Photoelectron Spectroscopy of the Inner Shell (PESIS).

## 1.2. Processes Involved in ESCA

### 1.2.1. The ESCA Experiment

When an atom in a molecule or lattice is irradiated with a monoenergetic beam of soft X-rays, electrons with specific kinetic energies can be photoejected.<sup>13</sup>

The most commonly used photon sources are,  $Al_{K\alpha_{1,2}}$  and  $Mg_{K\alpha_{1,2}}$  with photon energies of 1486.6 eV and 1253.7 eV respectively. In principle all electrons, from the core to the valence levels may be ejected (Figure 1.2.), though the latter are usually studied<sup>25</sup> using Ultraviolet Photoelectron Spectroscopy (UPS) with He(I) radiation 21.22 eV, or He(II) radiation 40.8 eV. Typically, the life-times of the core hole state produced in the photoemission processes are in the range  $10^{-13}$  -  $10^{-17}$  seconds,<sup>26</sup> emphasising the extremely short time-scales involved in ESCA compared with most of the spectroscopic techniques.

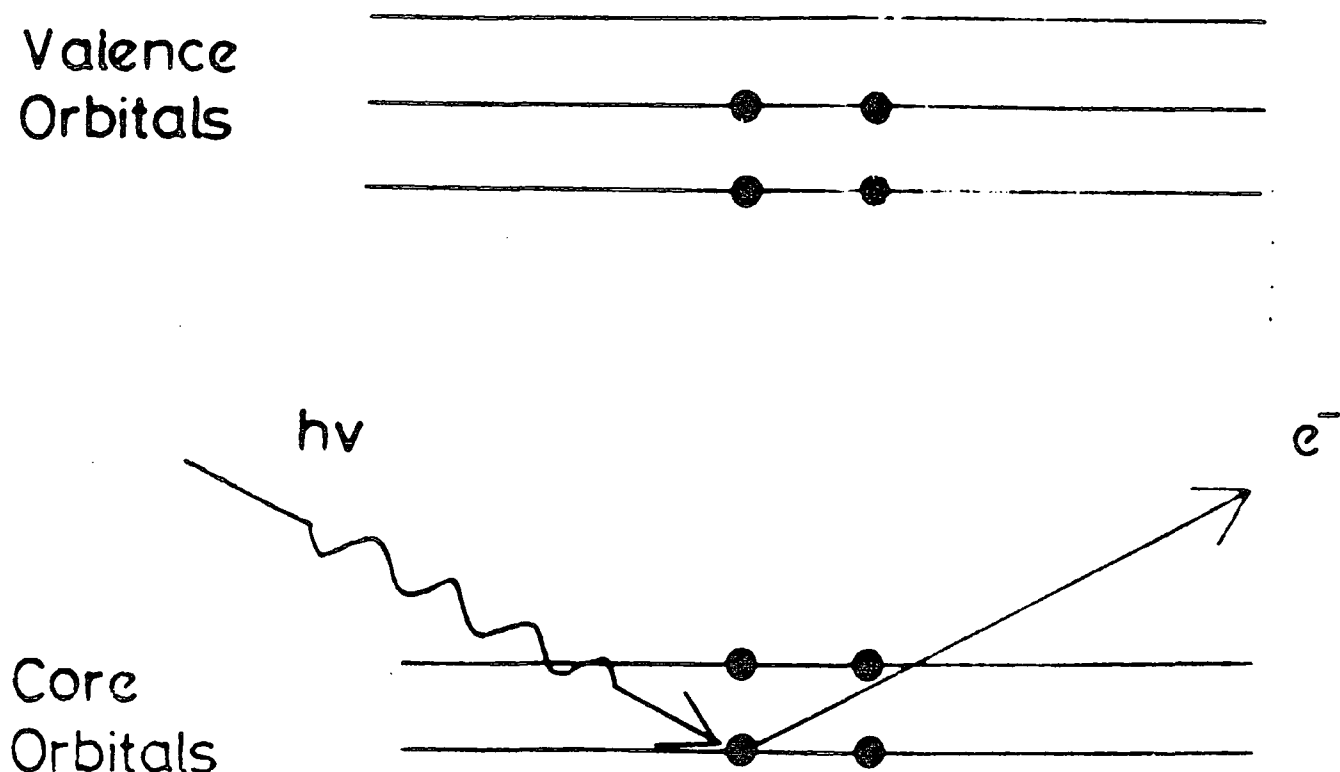


Figure 1.2. The photoionisation of a core level electron.

The total kinetic energy (K.E.) of the photoejected electrons is given by the equation

$$\text{K.E.} = h\nu - \text{B.E.} - E_r \quad 1.1.$$

where  $h\nu$  is the energy of incident photon,  $h$  is Planck's constant,  $\nu$  is the frequency of the X-rays, B.E. is the binding energy of the photoejected electrons<sup>†</sup>, and  $E_r$  is the recoil energy of the atom or molecule. Using  $\text{Al}_{K\alpha_{1,2}}$  (1486.6 eV), Siegbahn and co-workers,<sup>13</sup> have calculated that the recoil energy of atoms decreases with increasing atomic number, e.g. H = 0.9 eV, Li = 0.1 eV, Na = 0.04 eV, K = 0.02 eV

<sup>†</sup> Binding energy (B.E.) is defined as the energy required to remove an electron to infinity (vacuum level) with zero kinetic energy.

and  $Rb = 0.01$  eV. Therefore it is evident that the  $E_r$  term only has significance for the lighter elements, when compared with instrumental line widths obtained with the present study of elements from carbon upwards in the periodic-table.

The recoil energy is generally considered to be negligible for routine studies when using typical X-ray sources, for example  $Mg_{k\alpha_{1,2}}$  and  $Al_{k\alpha_{1,2}}$ . Recent studies by Cederbaum and Domcke<sup>27</sup> have shown that for accurate studies with high energy photon sources these effects are not negligible and can lead to modifications of the vibrational band envelopes of molecules containing lightest atoms. Therefore with the resolution available today, discrete rotational and vibrational transitions are seldom observed to contribute to the overall band profiles. Equation 1.1. for a free molecule therefore reduces to

$$K.E. = h\nu - B.E. \quad 1.2.$$

Binding energies are referred to the Fermi level when dealing with solids. This level for a conducting sample is defined as the highest occupied level, and is sometimes referred to as the 'electron chemical potential' and is located at the interface of the valence band and the conduction band. The relationship between the binding energies for solid and gaseous samples will be dealt with in more detail in a later section, (section 1.3.1.).

#### 1.2.2. De-excitation processes

The photoejection of a core electron from an atom creates a hole on that atom and there are then two principal routes

by which this core level vacancy can be filled.<sup>13</sup> These are Auger electron emission and X-ray fluorescence. These fundamental processes are shown schematically in Figure 1.3.

Auger electron emission may be viewed as a two step process involving the ejection of an electron from an inner orbital by a photon followed by an electron dropping down from a higher orbital to the vacancy in the inner orbital with the simultaneous emission of a second electron.<sup>28-32</sup> When the electron drops from a valence orbital to fill the

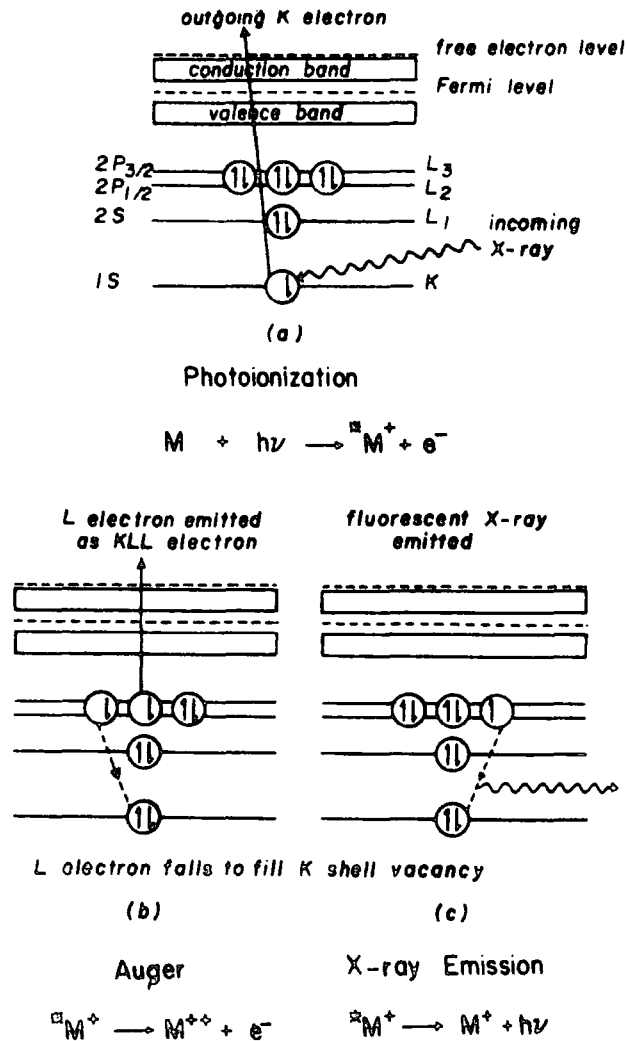


Figure 1.3. Photoionisation, Auger and X-ray Fluorescence.



inner orbital vacancy, the chemical shifts involved are related to both outer and inner orbitals, and in a few suitable cases, information can be gained on the binding energies of both levels. Where the electronic vacancy in the inner shell is filled by an electron from another inner shell (Coster-Kronig transition), the Auger spectrum is related to the inner orbital transition. These are very efficient and lead to very short life times with well resolved Auger spectra.<sup>30,31</sup> For a Coster-Kronig process to occur, the difference in the binding energies of the two inner orbitals must be sufficiently large to eject an electron from a higher orbital. Because of this limitation Coster-Kronig processes are only observed in elements of atomic number less than 40.

The other mode of de-excitation, X-ray emission, is not very efficient for lighter elements and is negligible for energies less than 500 eV, while the Auger efficiency is approximately comparable to X-ray emission at about 2000 eV.

The probability of Auger emission and X-ray fluorescence as a function of atomic number<sup>13</sup> is illustrated in Figure 1.4. It can be seen that Auger emission is important for the lighter elements and X-ray fluorescence for the heavier elements.

Both Auger electron and X-ray emission provide powerful techniques for the investigation of structure, bonding and elemental composition.

Auger Electron Spectroscopy (AES), as conventionally applied, is based on the analysis of the energy of electrons

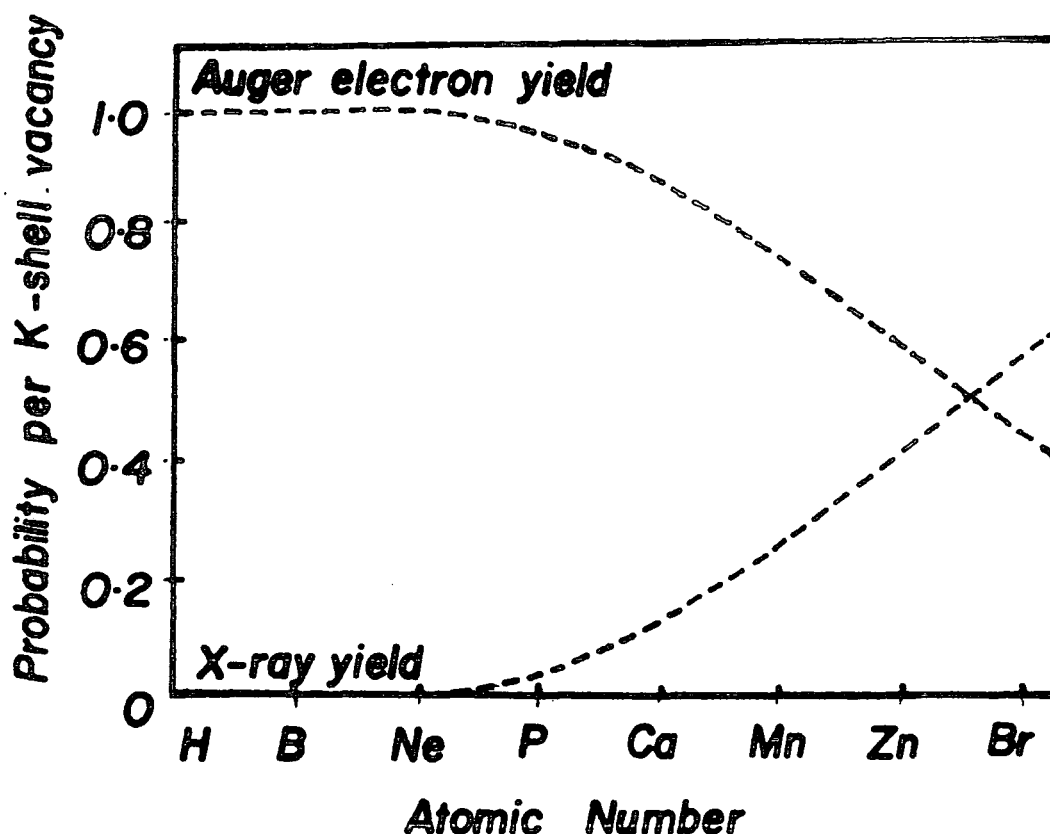


Figure 1.4. Yields of the Auger and X-ray fluorescence processes as a function of atomic number.

that are ejected from a sample as a consequence of excitation by a primary electron beam typically 3 to 10 kV at 1 to 30  $\mu$ A. This technique is truly a surface analysis technique in that the penetration depth for the exciting electrons is typically only about 5 atomic layers, or approximately  $\sim 20\text{\AA}$ .<sup>33</sup>

Essentially, there are three types of chemical information which may in principle be obtained from Auger spectra:-

- (i) The chemical shift due to the shifts of inner orbitals energy levels arising from changes in valence electron distribution;
- (ii) The second pertains to valence levels themselves;

- (iii) Information from the "molecular orbital energy spectra". If the molecular orbitals are known for a specific compound then the valence energy levels can be compared.

Auger chemical shifts can be larger than those corresponding to direct photoemission.

It should be noted that Auger spectroscopy is used particularly for surface analysis of metals and semiconductors. However, the incident beam of electrons in Auger spectroscopy is approximately three orders of magnitude greater in flux than a normal ESCA photon beam, and radiation damage is therefore a severe problem<sup>34</sup> when studying polymer surfaces.

The emission of X-rays instead of electrons leads to X-ray fluorescence (secondary-emission analysis), and the energies of emitted X-ray give information on the differences in energy levels in the samples. X-ray fluorescence spectroscopy is an excellent method of quantitative analysis for elements with atomic number greater than ten.<sup>35</sup> Concentration down to 0.1% for most elements and 0.01% for heavier elements have been detected.

### 1.2.3. Relaxation Phenomena

The photoionization of a core electron is accompanied by substantial electronic relaxation of the valence electrons.<sup>36-38</sup> Theoretical and experimental studies have shown that relaxation energy (R.E.) is a sensitive function of the electronic environment of a molecule.<sup>39-43</sup> It is of considerable importance in determining not only the absolute

binding energy of a core electron, but also in determining the line shapes of observed peaks by means of vibrational fine structure. Binding energies of the emitted photoelectrons, depend on the properties of both initial and the final wave functions. Therefore, using Koopmans' theorem<sup>44</sup> in the calculation of the absolute binding energies does not account for electronic relaxation energy, whereas self-consistent field ( $\Delta$ SCF) calculations do take account of R.E. and provide a method by which to investigate relaxation energies.<sup>43</sup> It has been shown that differences in relaxation energies within a series of related molecules are small and therefore cause only small changes in binding energies, but the R.E.'s have been found to be considerable<sup>43</sup> and are caused by the reorganisation of the valence electrons in response to the decreased shielding of the nuclear charge.

#### 1.2.4. Shake-up and Shake-off Phenomena

As well as the relaxation processes described in the previous section, the sudden perturbation of the valence electron cloud accompanying core ionisation gives rise to a finite probability for photoionisation by simultaneous emission of a valence electron from an occupied orbital to a virtual orbital (shake-up), or ionisation of a valence electron (shake-off),<sup>20,45,46</sup> as illustrated in Figure 1.5.

These phenomena are manifestations of electronic relaxation, therefore a revision of equation 1.2. is needed to take account of these multi-electron processes

$$\text{K.E.} = h\nu - \text{B.E.} - \bar{E} \quad 1.3.$$

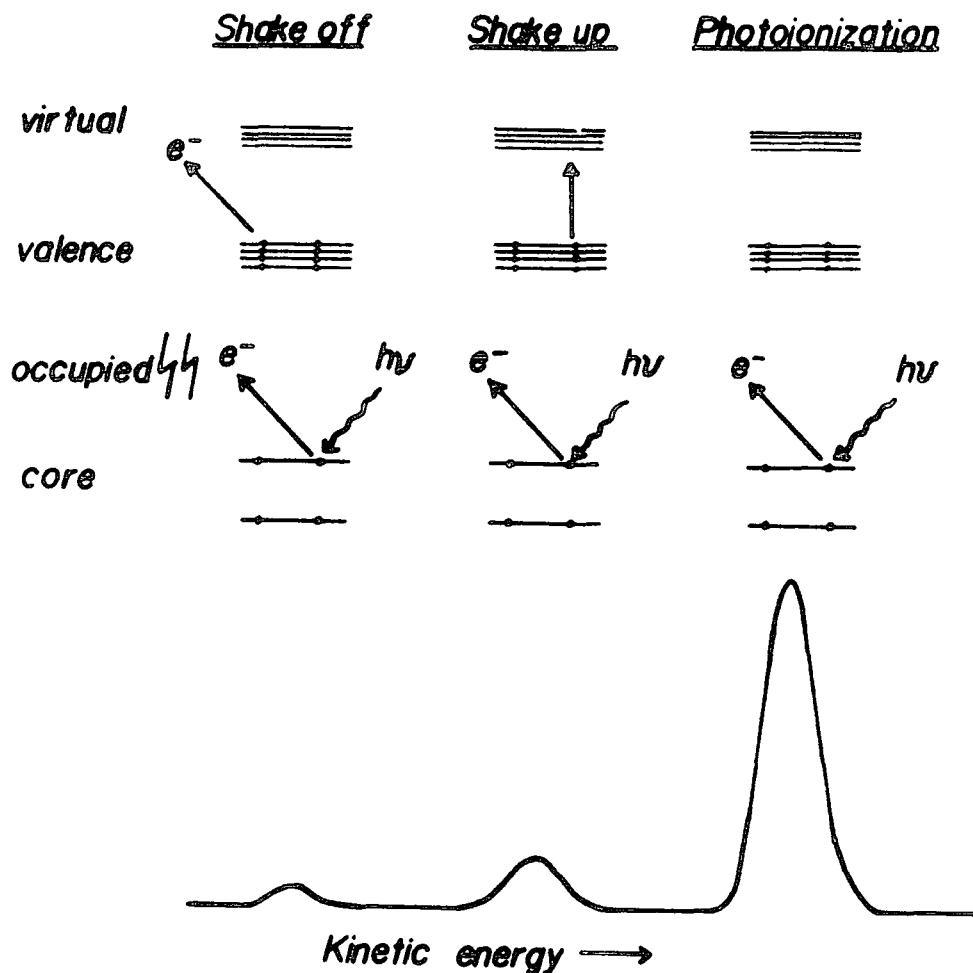


Figure 1.5. Photoionisation, shake-up and shake-off.

where  $\bar{E}$  is the energy of multi-electron processes.

Since these phenomena take place on a similar time-scale to photoionization they result in a modification of the primary photoelectron signal. The shake-up processes to a first approximation obey monopole selection rules<sup>20</sup> and may be viewed as an analogue of ultraviolet (u.v.) spectroscopy in ESCA. These processes have received much attention both from the experimental and theoretical standpoint.

The theoretical relationship between shake-up and shake-off satellite intensities to the relaxation energy has been discussed,<sup>47,48</sup> and calculations have been carried out on

the satellite structure of a number of small molecules.<sup>26,49,50</sup> The transition probabilities for high energy shake-off processes are relatively small compared to shake-up processes, and this is shown schematically in Figure 1.6.

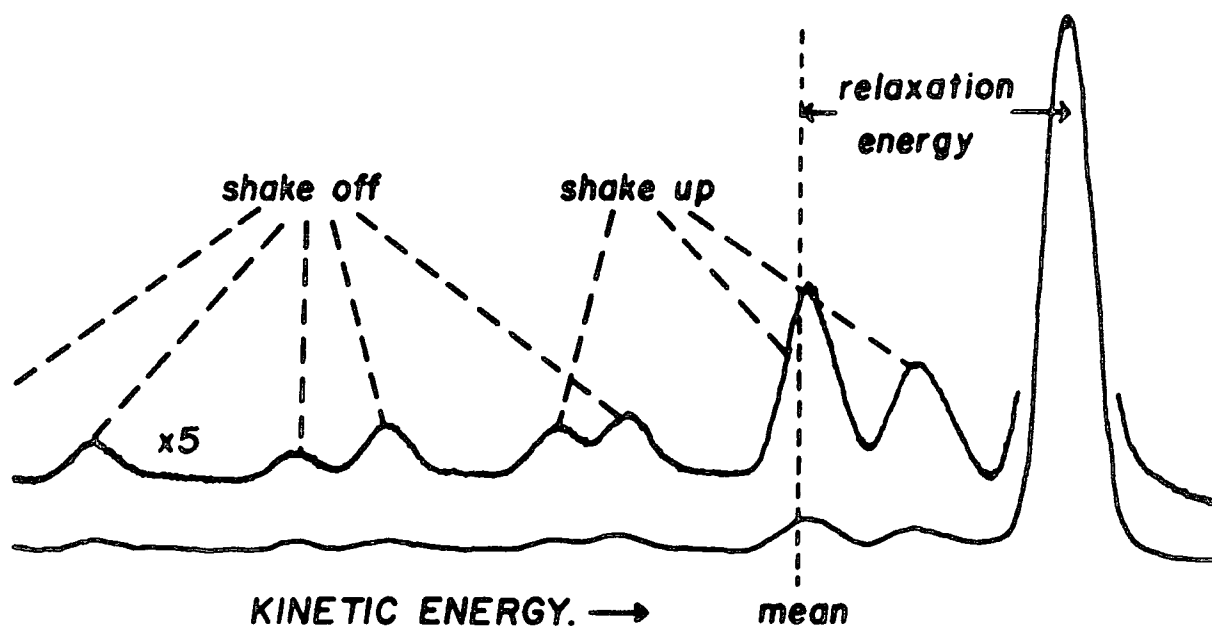


Figure 1.6. Relationship between relaxation energy and relative intensities of photoionisation, shake-up and shake-off peaks.

Shake-up and shake-off structure has been studied in a range of organic<sup>51,52</sup> and inorganic<sup>53,54</sup> materials with particular attention to the transition elements.

Recently work has been carried out on the use of shake-up to elucidate fine details of structure and bonding in polymer systems which are not directly attainable from the primary information levels in ESCA,<sup>55-59</sup> and a review of shake-up effects has been published.<sup>60</sup>

#### 1.2.5. Energy Loss Processes

In the case of a gas phase study, the electron distribution

found to the high binding energy side of a primary photo-ionisation peak is due entirely to shake-up and shake-off. When working at high gas pressure and with solids (or liquids) non-discrete energy losses become important, these are the so-called inelastic<sup>61,62</sup> losses of the photoionised electron, due to interaction between the photoelectrons and other electrons in the surface region of the sample (especially conductors).

An inelastic loss can also arise from the interaction with secondary electron emission resulting from autoionization.<sup>63</sup>

These are generally observed as broad tails to the low energy side of the primary peak.

### 1.3. Features of Core Electron Spectra

#### 1.3.1. Binding Energy and Chemical Shifts

Core levels are essentially localized on atoms, their energies are characteristic for a given element<sup>1</sup> and are sensitive to the electronic environment of an atom.<sup>13,20</sup> Thus, for a given core level of an element, while the absolute binding energy for that level is characteristic for the element. Typical examples of approximate core electron binding energies for some elements are shown in table 1.1. A knowledge of B.E.'s thus allows the ready detection or identification of elements in a sample.<sup>13</sup>

Variations of B.E. within a given core level are a sensitive function of the electronic environment of an atom,<sup>13,20,64</sup> and thus differences in the electronic environment

Table 1.1. Approximate core binding energies for 1st and 2nd row elements (eV).

	Li	Be	B	C	N	O	F	Ne
1s	55	111	188	284	399	532	686	867
	Na	Mg	Al	Si	P	S	Cl	Ar
1s	1072	1305	1560	1839	2149	2472	2823	2303
2s	63	89	118	149	189	229	270	320
2p <sub>1/2</sub>	31	52	74	100	136	165	202	247
2p <sub>3/2</sub>	31	52	73	99	135	164	200	245

of a given atom in a molecule give rise to a small range of B.E., or chemical shifts, often representative of a particular structural feature. The classic illustration of chemical shifts is the C<sub>1s</sub> spectrum of ethyl trifluoroacetate,<sup>20</sup> is shown in Figure 1.7.

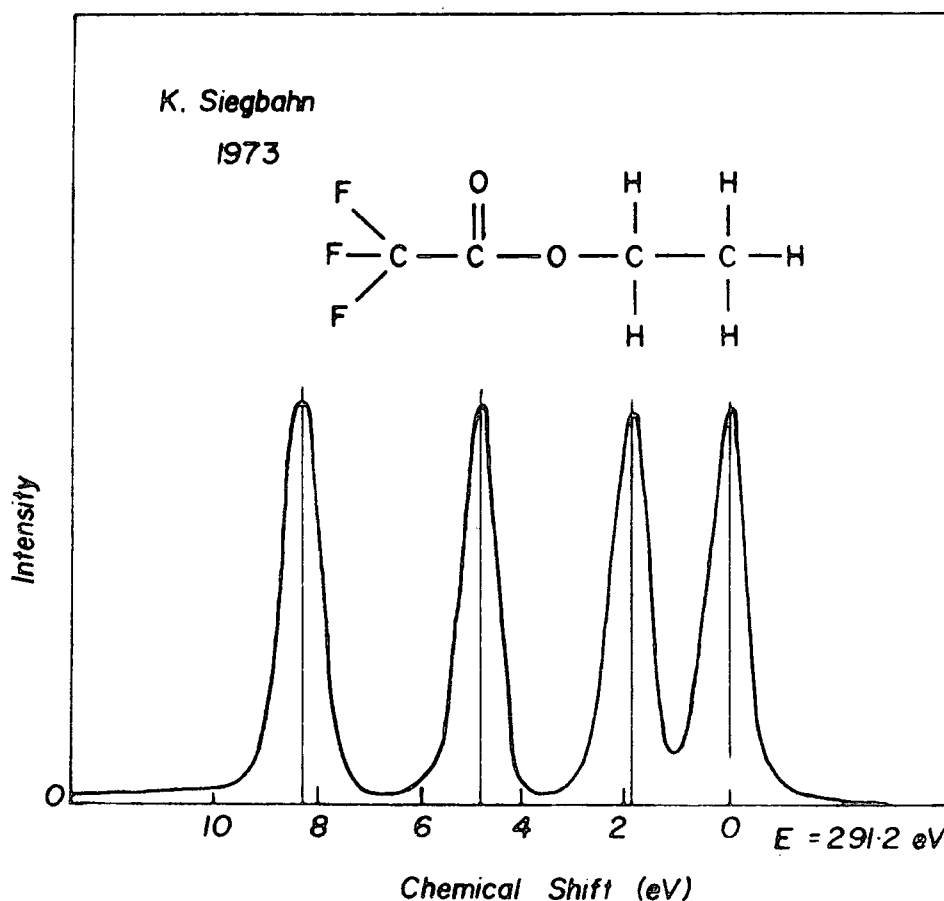


Figure 1.7. C<sub>1s</sub> spectrum of ethyl trifluoroacetate.



An extensive theoretical study, over a range of systems containing carbon-oxygen functionalities carried out by Clark and co-workers,<sup>65</sup> has suggested the additive nature of these shifts in B.E. as being a function of the number of bonds to the oxygen substituents. Thus a shift of  $\sim 1.5$  eV corresponds to carbon singly bonded to an oxygen, whilst a shift of  $\sim 3$  eV can correspond to either a carbon singly bonded to two oxygens or doubly bonded to one oxygen, on this basis, carboxylic acids and esters, and carbonate would be expected to exhibit shifts of  $\sim 4.5$  eV and 6 eV respectively, in good agreement with experimentally determined values.<sup>13,20,66-68</sup> These values will be discussed in detail in Chapter two.

Much attention has been paid to the theoretical interpretation of the chemical shift phenomenon observed experimentally. The following distinct, but inter-related approaches have been used:-

- (i) Koopmans' Theorem;<sup>44</sup>
- (ii) Core hole calculations,<sup>66,70</sup> linear combination of atomic orbitals - molecular orbital - self-consistent field method (LCAO - MO - SCF),  $\Delta$ SCF.
- (iii) Equivalent cores model;<sup>71</sup>
- (iv) Charge potential model.<sup>20</sup>
- (v) Quantum mechanical potential model.<sup>72-74</sup>
- (vi) Many bodied formalism.<sup>74</sup>

The relation between the experimental, Koopmans' and  $\Delta$ SCF binding energy is shown in Figure 1.8.

An account of the physical processes involved in electron

photoemission and their effects from a theoretical standpoint has been given by Fadley.<sup>75</sup>

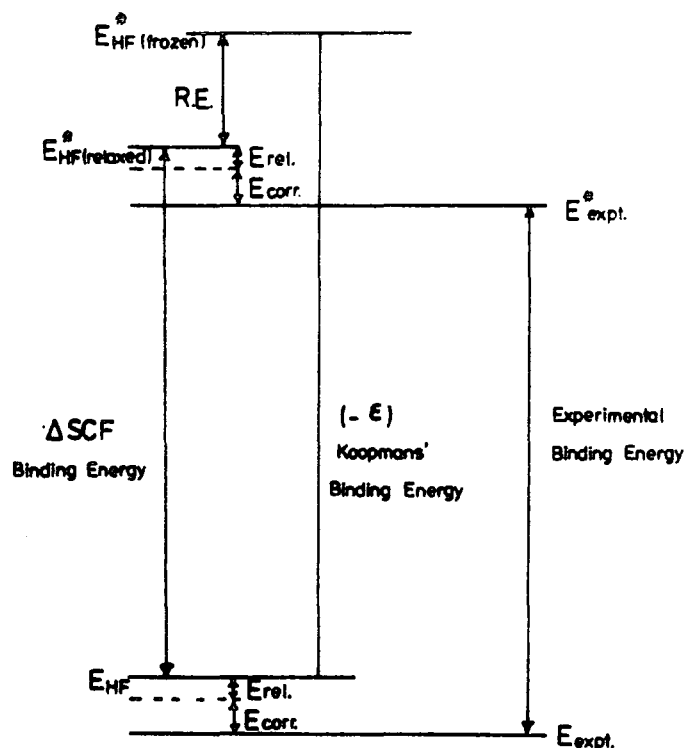


Figure 1.8. The relation between Koopman's Theorem,  $\Delta SCF$  and Experimental Binding Energy.

### 1.3.2. Line Shape Analysis

The need for line shape analysis (deconvolution) arises when the chemical shift of a level is smaller than the line width of that level. This is the most common situation encountered in ESCA and in fact, one of the major weaknesses of ESCA compared to say n.m.r.<sup>13</sup>

The measured line widths of component peaks for a core level may be expressed as

$$(\Delta E_m)^2 = (\Delta E_x)^2 + (\Delta E_s)^2 + (\Delta E_l)^2 \quad 1.4.$$

where  $\Delta E_m$  is the width (eV) at half height of the observed

photoelectron peak (FWHM).

$\Delta E_x$  is the FWHM of the exciting X-ray source, typical values being 0.7 eV<sup>76</sup> for  $Mg_{k\alpha_{1,2}}$  and 1.0 eV for  $Al_{k\alpha_{1,2}}$ .<sup>76</sup>  
 $\Delta E_s$  is the contribution to the FWHM due to spectrometer aberrations and is dependent on the emission energy and the choice of slits.

$\Delta E_l$  is the natural width of the core level under investigation.

The contributions to  $\Delta E_m$  from  $\Delta E_x$  for the commonly used photon sources (i.e. Mg and Al) are essentially Lorentzian line shapes. The characteristics for the energy distribution in  $Mg_{k\alpha}$  radiation are essentially comprised of four major component lines,  $\alpha_1$ ,  $\alpha_2$ ,  $\alpha_3$  and  $\alpha_4$ , the relative positions to the  $\alpha_1$  line are -0.33, +8.4 and 10.2 eV, with relative intensities 100, 50, 12.8 and 6.9.<sup>77</sup> The  $\alpha_3$  and  $\alpha_4$  lines are significantly removed from the  $\alpha_1$  and  $\alpha_2$  lines and manifest themselves as satellite peaks to the high kinetic energy side of the intense primary photoionisation signal in the ESCA spectrum. A similar situation is true for  $Al_{k\alpha}$  radiation.<sup>77</sup>

The contribution to  $\Delta E_m$  from  $\Delta E_s$  is considered to be Gaussian, whereas the natural line width is Lorentzian in shape. The convolution of these line shapes produces a hybrid shape with a Gaussian distribution dominating the overall line shape and with Lorentzian character in the tails. The use of pure Gaussian shapes introduces only small errors in line shape analysis.<sup>20</sup>

Deconvolution procedures may be grouped into two main categories:

- (i) Deconvolution by mathematical methods which have been reviewed by Carley and Joyner;<sup>78</sup>
- (ii) Curve fitting by simulation, either in analogue or digital fashion.

The second category requires close control over a number of variables, for example, binding energy, line width and peak height. These parameters are most conveniently controlled in the analogue mode, and the work in this thesis predominantly used this method (on a Dupont 310 curve resolver). The basic approach to curve simulation is outlined in Table 1.2.

When using either form of deconvolution method a certain amount of caution is required, as it is often possible to obtain more than one solution. When dealing with complex line shapes a detailed knowledge of prototype systems is very important, such that the solution is one based on chemical uniqueness.

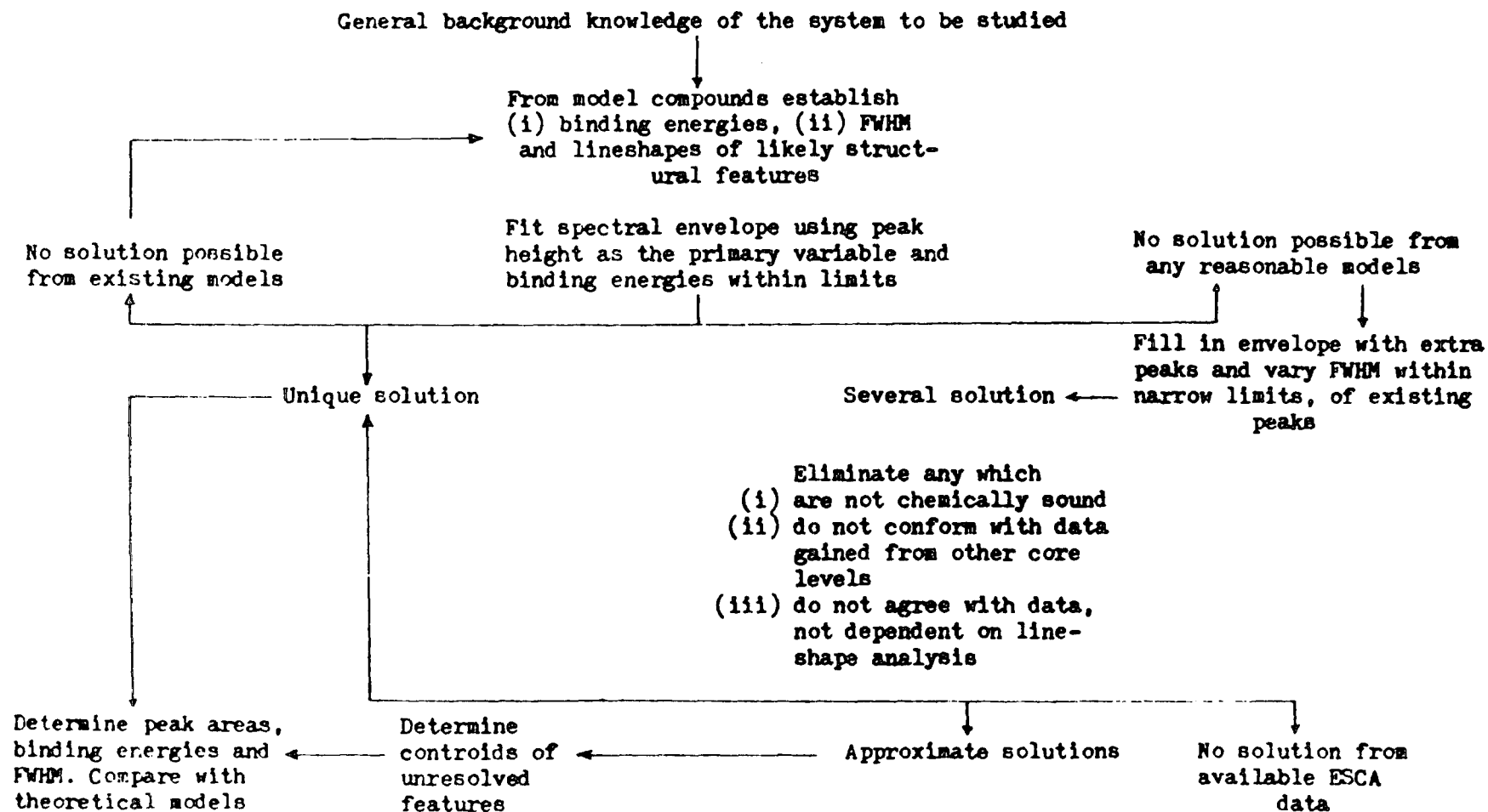
### 1.3.3. Line Widths

The various effects contributing to the total line width  $\Delta E_M$  will be discussed in section (1.8.3.). The natural line width of half maximum height peak (FWHM) of the core level under investigation,  $\Delta E_q$  and that of the incident radiation  $\Delta E_x$  (unless monochromatization is used) depend on the uncertainty principle.<sup>79</sup>

$$\Delta E \cdot \Delta t \geq \hbar/2$$

1.5.

Table 1.2. Line-shape analysis by curve fitting; schematic of logic procedure.



Where  $\hbar = \frac{h}{2\pi}$  and  $\Delta t$  is the lifetime of the state and  $h$  is Planck's constant. From the equation 1.5. above, a line width of  $\sim 1$  eV corresponds to a lifetime of approximately  $6.6 \times 10^{-16}$  sec.<sup>80</sup> Table 1.3. displays some natural line widths of core levels derived from X-ray spectroscopic studies.

Table 1.3. Full width at half maximum of natural line width  $\Delta E_{\ell}$ , for some core levels (eV).

level	S	Ar	Ti	Mn	Cu	Mo	Ag	Au
$1_s$	0.35	0.5	0.8	1.05	1.5	5.0	7.5	54
$2p_{3/2}$	0.10	-	0.25	0.35	0.5	1.7	2.2	4.4

Table 1.3. emphasizes the fact that there is no particular virtue in studying more tightly bound core levels, for Au, for example, the FWHM of  $\sim 54$  eV for the  $1_s$  level would swamp any chemical shift.

#### 1.4. Fine Structure

##### 1.4.1. Multiplet Splitting

Multiplet splitting occurs in paramagnetic systems and is the result of interactions between unpaired electrons present in the system and the unpaired core orbital electrons remaining after photoionisation. Examples can be found in the core level spectra obtained from compounds of transition elements.<sup>81,82</sup> The theoretical interpretation of multiplet effects is only straightforwardly understood for S-hole states and is based upon Van Vleck's vector coupling model.<sup>83</sup>

The magnitude of the splitting for a given ion can give valuable information concerning the localization or delocalization of the unpaired valence electron in compounds.<sup>13,84,85</sup> Since the greater the localization and spin densities on an atom the greater will be the observed splitting.

A simple example of multiplet splitting was demonstrated by Siegbahn and co-workers.<sup>20</sup> The gas-phase spectrum for  $N_2$  shows no indication of splitting, whilst spectra of NO and  $O_2$   $1s$  core levels are observably split, and this is illustrated in Figure 1.9. In the case of the NO molecule, the single unpaired electron is delocalized over nitrogen and oxygen so that the magnitude of multiplet splitting of the  $O_{1s}$  and  $N_{1s}$  core levels will depend upon the unpaired spin densities on the two atoms.

The pronounced satellite splitting (see Figure 1.9.), for the  $N_{1s}$  but not for the  $O_{1s}$  levels indicates that most of the unpaired spin density is on nitrogen. For the  $N_{1s}$  level, there is an energy separation of 1.5 eV, in the case of the  $O_{1s}$  level the separation is 0.7 eV leading to line-broadening of 0.3 eV.

The two peaks of multiplet splitting are often observed in such cases and the point of interest here is that the separation between the peaks varies depending upon the environment of the atom concerned.

Multiplet splittings in photoelectron spectroscopy have been reviewed in some detail by Fadley.<sup>84</sup>

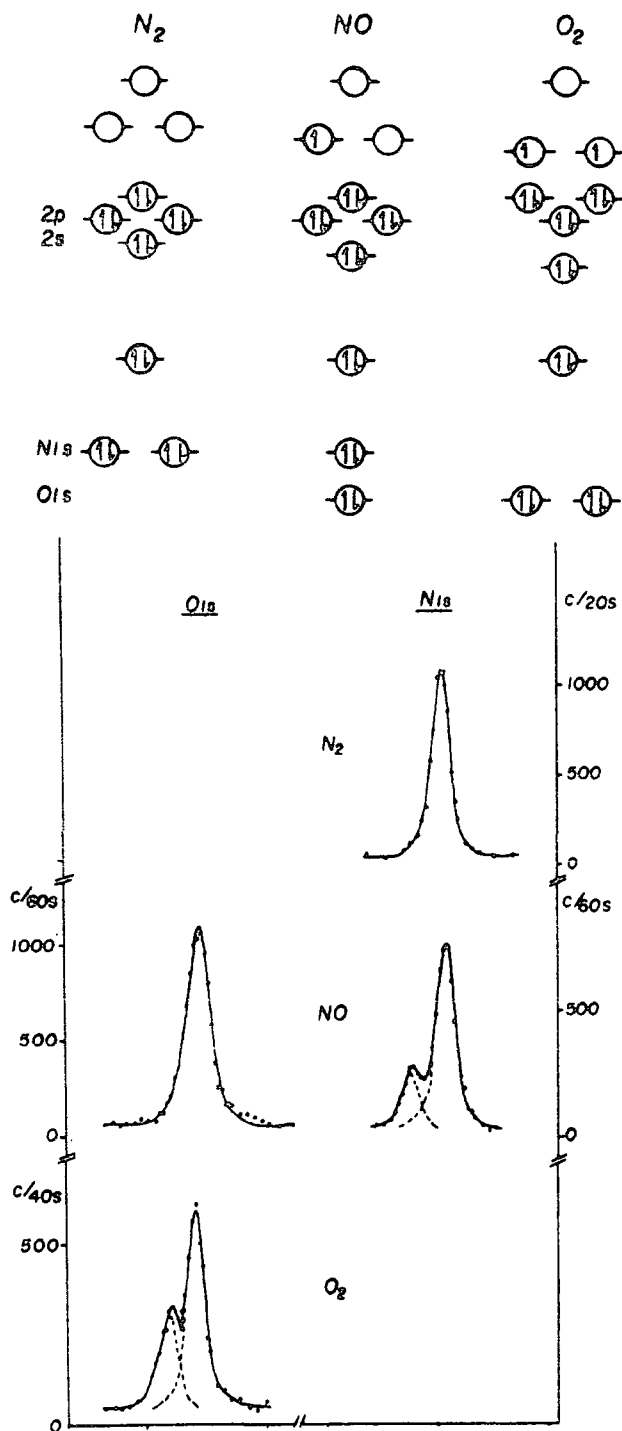


Figure 1.9. Diagram of orbital levels in  $N_2$ ,  $NO$  and  $O_2$ .

#### 1.4.2. Spin Orbit Splitting

If photoionisation takes place from an orbital which has an orbital quantum number ( $l$ ) greater than 1 (i.e.



p, d or f), then a doublet structure is observed in the XPS spectrum.<sup>13</sup> This arises from a coupling of the spin (S) and orbital (L) angular momenta of the electrons to yield momentum (J).

$$J = S + L \quad 1.6.$$

A doublet, which is sometimes well-resolved is then observed in the spectrum instead of single peak.<sup>13</sup> The relative intensities of the component peaks of the doublet structure observed are proportional to the ratio of the degeneracies of the states defined by the  $2J + 1$  rule. The relative signal intensities of the J states for the s, p, d and f orbitals are shown in Table 1.4.

Table 1.4. Intensity ratios for different levels.

Orbital	Orbital Quantum No.	Total Quantum No.	Intensity ratio
	$l$	$J = (l \pm s)$	$(2J + 1) : (2J + 1)$
s	0	1/2	singlet
p	1	1/2, 3/2	1:2
d	2	3/2, 5/2	2:3
f	3	5/2, 7/2	3:4

Examples of experimentally observed peaks from  $C_{1s}$ ,  $Cl_{2p}$ ,  $Ag_{3d}$  and  $Au_{4f}$  are shown in Figure 1.10.

#### 1.4.3. Electrostatic Splitting

This type of splitting has been interpreted from differential interaction of an external electrostatic field with the spin states of the core level being

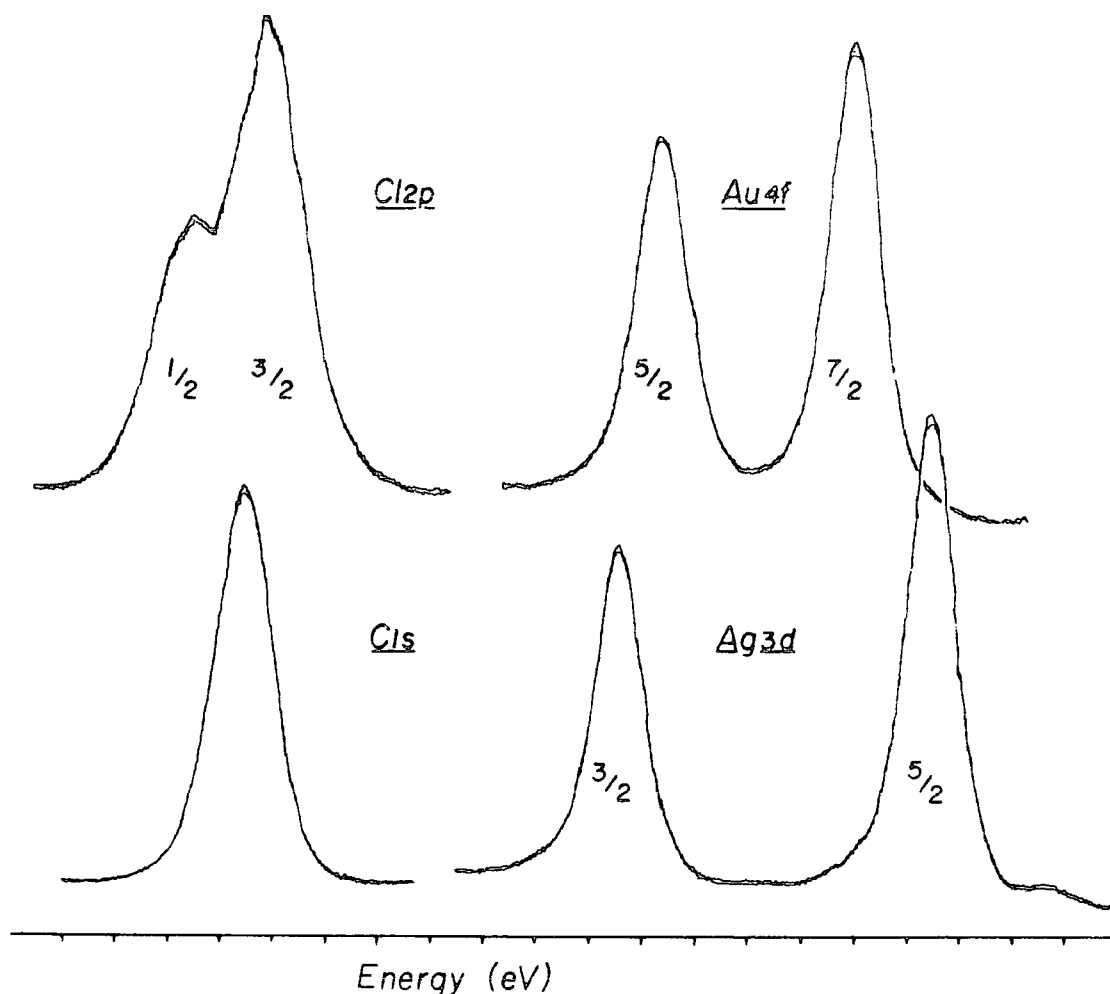


Figure 1.10. Examples of spin-orbit splitting in the p, d and f levels.

investigated. It has been observed for a number of systems, for example, the  $5p_{3/2}$  levels of uranium and thorium and in some compounds of gold.<sup>79</sup> A typical example of this splitting is shown in Figure 1.11. Correlations have been observed between this type of splitting and the quadrupole splittings obtained from Mossbauer spectroscopy<sup>86</sup> which arise from the interaction of the nuclear quadrupole moment with an inhomogeneous electric field. The splittings have been observed for a number of systems.<sup>87-88</sup>

A summary of the type of splitting encountered in ESCA is shown in Figure 1.12.

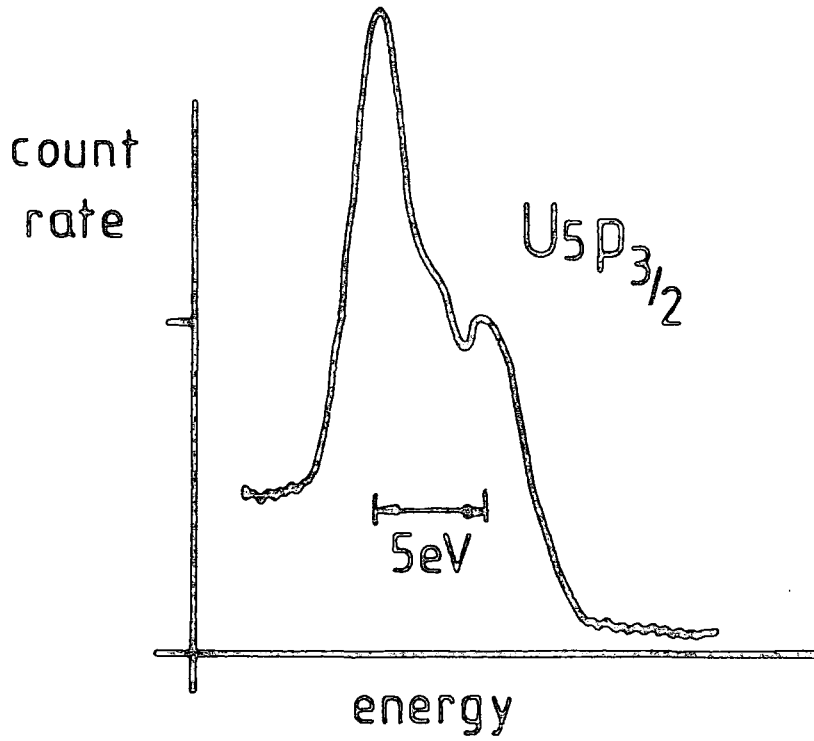


Figure 1.11. Electrostatic splitting in the  $5p_{3/2}$  levels of U metal.

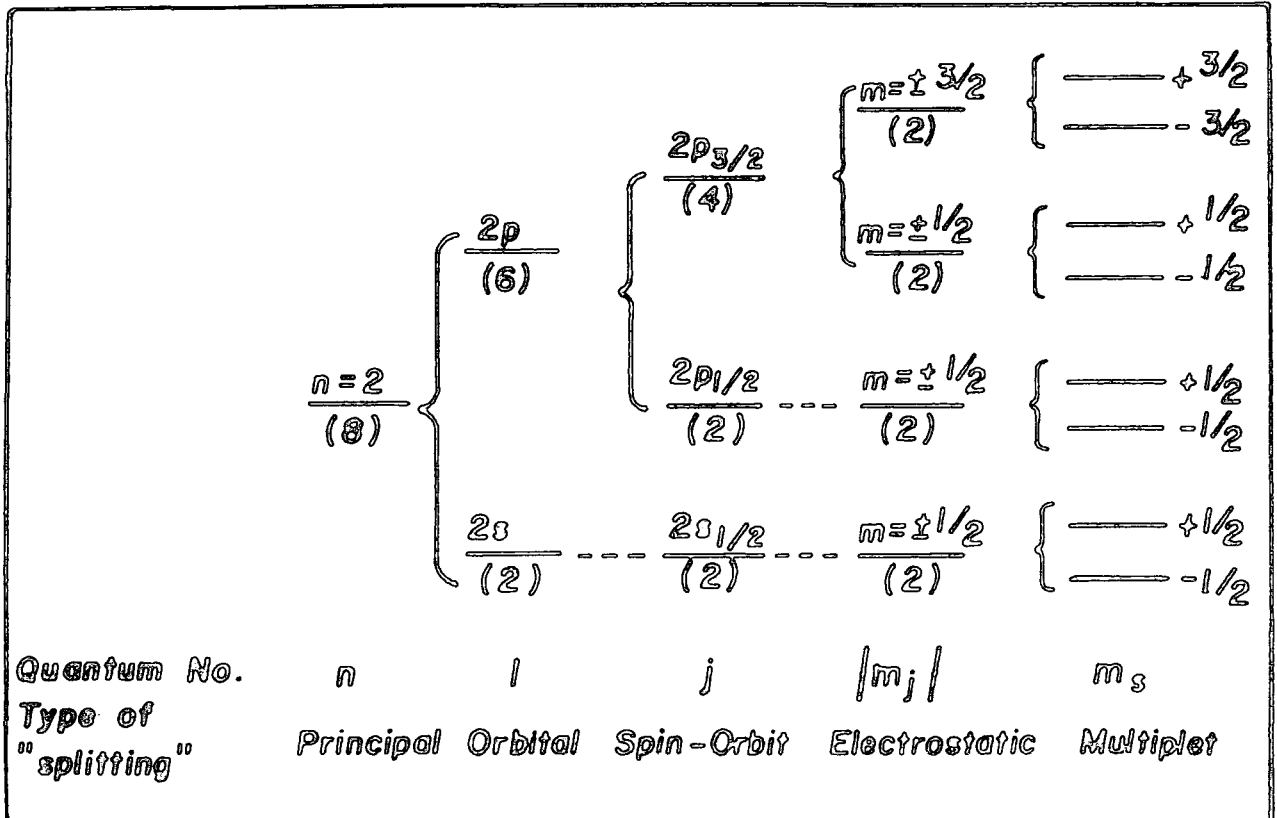


Figure 1.12. Splittings encountered in ESCA.

### 1.5. Signal Intensities

Figure 1.13. shows the general geometry employed in an ESCA experiment employing a fixed arrangement of analyser and X-ray source.  $h\nu$  represents the incident photon beam and  $e^-$  the fraction of photoemitted electrons entering the electron energy analyser.  $\phi$  is the angle between the X-ray source and the analyser entrance slit and  $\theta$  describes the angle of the sample in relation to the analyser. If the photoelectrons are emitted from a depth,  $d$ , of the sample as shown in Figure 1.13. the true path length of the photoemitted electrons will be  $d'$  where -

$$d' = d / \cos \theta$$

1.7.

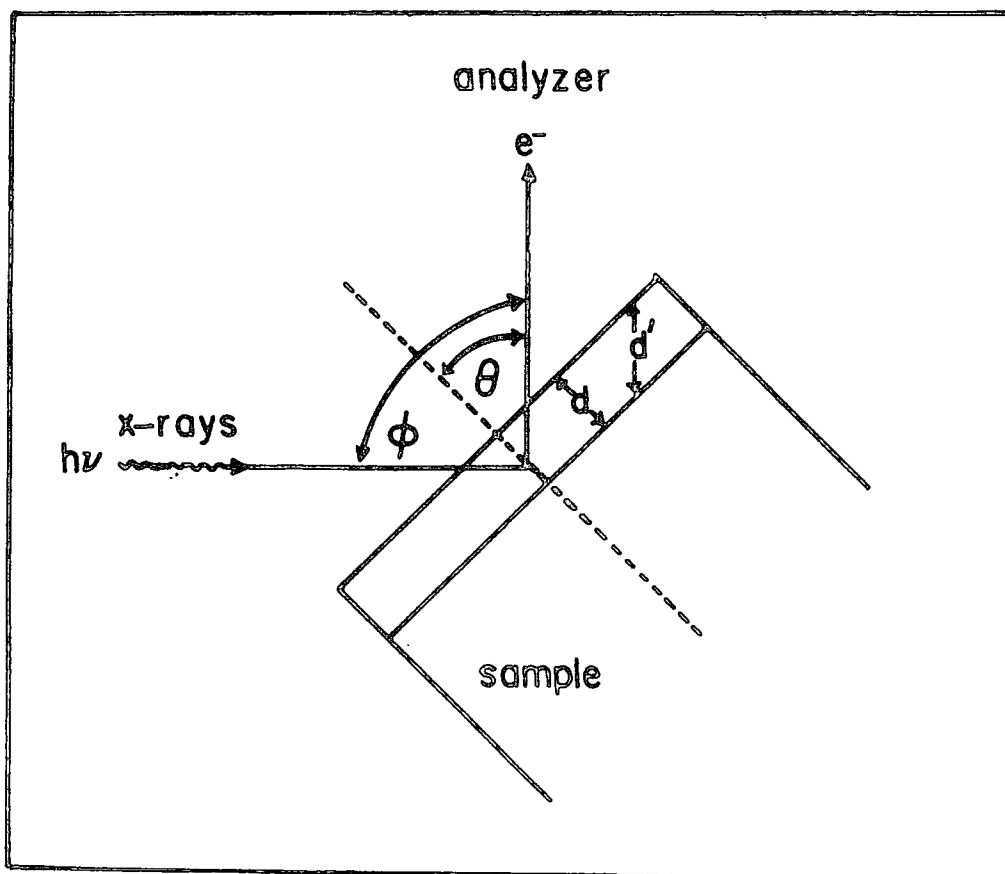


Figure 1.13. Geometry employed in an ESCA experiment.

Due to the short mean free paths of electrons (for K.E. > 50 eV) in solids (see section 1.5.2.), it is possible to enhance surface features with respect to bulk and subsurface<sup>89</sup> by conducting experiments involving the grazing exit of the photoemitted electrons, which are analysed, that is with  $\theta$  approaching  $90^\circ$ . This feature will be referred to in a later section.

### 1.5.1. Fixed Angle Studies

For an infinitely thick homogeneous sample, the intensity (I) of the elastic (no energy loss) photoionisation peak corresponding to photoionisation from a core level  $i$ , may be expressed as:

$$dI_i = F\alpha_i N_i k_i e^{-x/\lambda_i} dx \quad 1.8.$$

where:

$I_i$  is the intensity arising from core level  $i$ ;

$F$  is the exciting photon flux;

$\alpha_i$  is the cross-section for photoionisation from core level  $i$ ;

$N_i$  is the number of atoms per unit volume on which core level  $i$  is located;

$k_i$  is a spectrometer dependent factor for  $i$ ;

$\lambda_i$  is the inelastic mean free path for the photoemitted electrons.

In integrated form the equation becomes:

$$I_i = \int_0^\infty F\alpha_i N_i k_i e^{-x/\lambda_i} dx \quad 1.9.$$

$$\text{and } I_i = F\alpha_i N_i k_i \lambda_i \quad 1.10.$$

The following discussion will deal with each of these variables individually.

X-ray flux, F. - The flux is primarily determined by the power applied to, and efficiency of the X-ray gun. The angle of incidence on the sample surface is of importance for angular dependent studies. The mean free path of X-ray photons is typically in the region  $> 10,000\text{\AA}$  for solids.<sup>90</sup> This is some two or three orders of magnitude greater than electron mean free paths,<sup>91-94</sup> and so the X-ray flux will remain essentially unattenuated over the sample depth.

However, the angle of incidence  $\phi$  of the X-rays and the analyser and  $\theta$  do have an effect on the intensity of the photoionisation peak.

The cross-section for photoionisation of core level,  $i$ ,  $\alpha_i$ , is a parameter which describes the probability of the core level being ionised when irradiated by a photon of known energy.<sup>95</sup> This only includes the fraction of the total number of electrons photoemitted into the solid angle of acceptance of the analyser.  $\alpha_i$  is a function of the core level to which it relates and of the energy of the incident photon. Values of  $\alpha_i$  may be calculated from the fundamental properties of the atom<sup>96</sup> or determined experimentally from gas-phase ESCA experiments.<sup>20</sup> The geometry of the X-ray source with respect to the analyser entrance slit affects  $\alpha_i$  values, but for a particular spectrometer and using the same X-ray source and with a fixed value of  $\phi$  then  $\alpha_i$  is normally constant.

With  $\text{Mg}_{k\alpha_{1,2}}$  and  $\text{Al}_{k\alpha_{1,2}}$  the cross-section for photo-

ionisation from core levels of most elements is within two orders or magnitude of that for the  $C_{1s}$  level, therefore ESCA has a convenient sensitivity range for most elements. The cross-section for core levels are normally considerably higher than those for valence levels.

The spectrometer factor. - This factor,  $k_i$ , which varies from one instrument to another, includes effects due to detector efficiencies, analyser transmission characteristics which are both dependent on the kinetic energies of the core electrons being analysed, and geometric factors such as the solid angle of acceptance of the analyser.

Electron mean free path. - The inelastic mean free path of photoemitted electrons, (sometimes referred to as the escape depth for the photoemitted electrons),  $\lambda_i$  is defined as the distance in the solid through which the photoemitted electrons will travel before  $1/e$  of them have not suffered energy loss through inelastic collision. Both experimental<sup>93,94,97</sup> and theoretical calculations<sup>92</sup> of  $\lambda_i$  have been undertaken.  $\lambda_i$  is a function of the kinetic energy of the photoemitted electron and typically ranges in magnitude from  $\sim 4\text{\AA}$  for electrons of about 80 eV kinetic energy to  $\sim 37\text{\AA}$  for electrons of about 4500 eV. Further discussion on the direct determination of electron mean free path will be presented in a later chapter in this thesis.

The sampling depth is typically defined as that from which 95% of the signal, arising from a given core level, derives and may be related to  $\lambda$  by:

$$\text{Sampling depth} = -\lambda \ln 0.05 \approx 3\lambda.$$

As an example, for carbon  $1s$  levels studied by a  $Mg_{K\alpha 1,2}$  X-ray source the kinetic energy of the photoemitted electrons is  $\sim 960$  eV and the mean free path of the electrons is  $\sim 15\text{\AA}$ , 50% of the signal seen by ESCA derives from the outermost  $10\text{\AA}$  and 95% from the top  $45\text{\AA}$ . This illustrates that ESCA is indeed a very powerful tool for surface analysis.

Number density  $N_i$  is the number of atoms per unit volume in the sample on which the core level is localized. Although  $N_i$  is not directly related to the density of the sample, it is generally observed that for similar materials of different density the ESCA signal for a given core level will be more intense for the higher density material (e.g. high density polyethylene vs. low density polyethylene).<sup>98</sup> The most important consequence of  $N_i$  is that the relative signal intensities for the core levels of various atoms in a homogeneous sample are directly related to the overall stoichiometries of the atoms in the sample.

Thus for two core levels  $i$  and  $j$ :

$$\frac{I_i}{I_j} = \frac{F\alpha_i N_i k_i \lambda_i}{F\alpha_j N_j k_j \lambda_j} \quad 1.11.$$

where  $I_i$  is the signal intensity for core level  $i$ , and  $I_j$  is the signal intensity for core level  $j$ . If  $i$  and  $j$  are the same core level in differing chemical environments (e.g.  $C_{1s}$  in  $\underline{CH}_3-\underline{CF}_3$ ) then

$$k_i \alpha_i \lambda_i = k_j \alpha_j \lambda_j \quad \text{and} \quad \frac{N_i}{N_j} = \frac{I_i}{I_j} \quad 1.12.$$

If however,  $i$  and  $j$  are different core levels, then



$$k_{i,i,\lambda_i} \neq k_{j,j,\lambda_j} \quad 1.13.$$

may be determined experimentally from standard samples of known stoichiometry containing  $i$  and  $j$ . This ratio is usually referred to as the instrument sensitivity ratio of the given levels.

#### 1.5.2. Analytical Depth Profiling

Analytical depth profiling is important in cases where it is necessary to determine if the surface of a sample is characteristic of the bulk. The most favourable case is that of a single homogeneous component or of a surface coating of thickness  $d$  on a homogeneous base. This is often referred to as the substrate/overlayer model and is illustrated in Figure (1.14.).

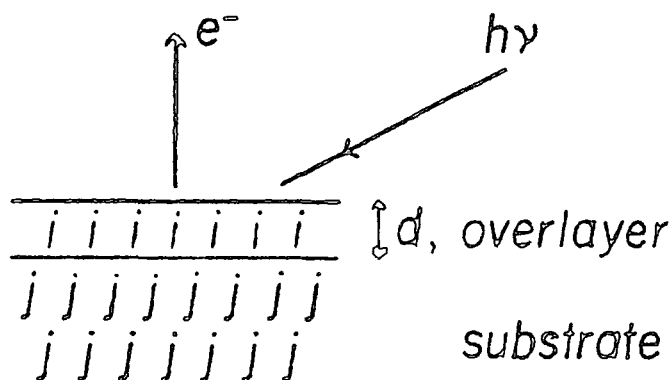


Figure 1.14. Substrate overlayer model.

The intensity of a signal arising solely from the overlayer can be expressed from equation 1.9 integrating between  $X = 0$  and  $X = d$ .

$$I_i^{\text{over}} = F\alpha_i N_i k_i \lambda_i (1 - e^{-d/\lambda_i}) \quad 1.14.$$

Similarly, integrating between  $X = d$  and  $X = \infty$  gives the intensity of a signal arising solely from the substrate.

$$I_j^{\text{subs.}} = F\alpha_j N_j k_j \lambda_j e^{-d/\lambda_j} \quad 1.15.$$

Figure 1.15. gives the general behaviour of electron mean free paths as a function of kinetic energy. It is clear that the data falls into a broad band. In the energy

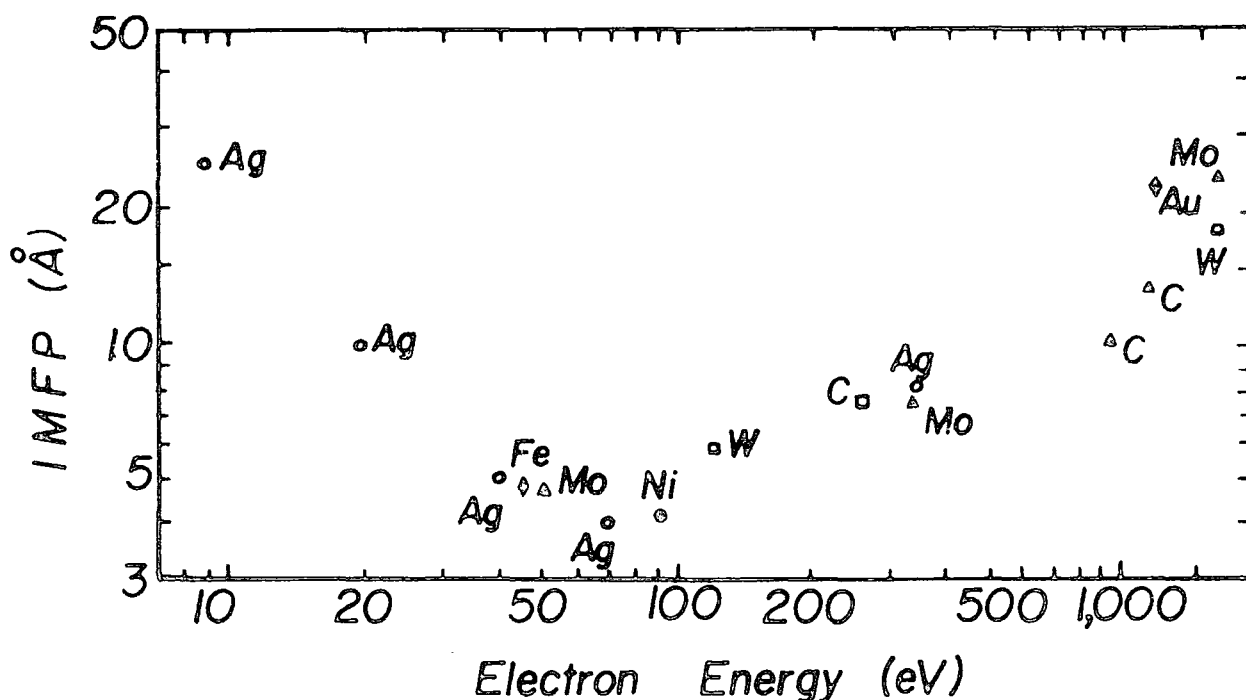


Figure 1.15. Electron mean free path as a function of kinetic energy.

range of interest to ESCA ( $> 300$  eV) the mean free path increases with kinetic energy.<sup>91</sup> As a consequence, the attenuation of a signal arising from a core level in the substrate by an overlayer will depend strongly on the kinetic energy of the photoemitted electrons. For example, a non-fluorine containing overlayer on a fluorine

containing substrate will result in a decrease in the  $F_{1s}/F_{2s}$  ratio.

Therefore, in order to analytically depth profile a sample, it is necessary to determine accurately the Inelastic Mean Free Paths (IMFP) at the kinetic energy of interest, through the material of interest. The IMFP in elements, inorganics, and organics are presented in Figures 1.16, 1.17 and 1.18.

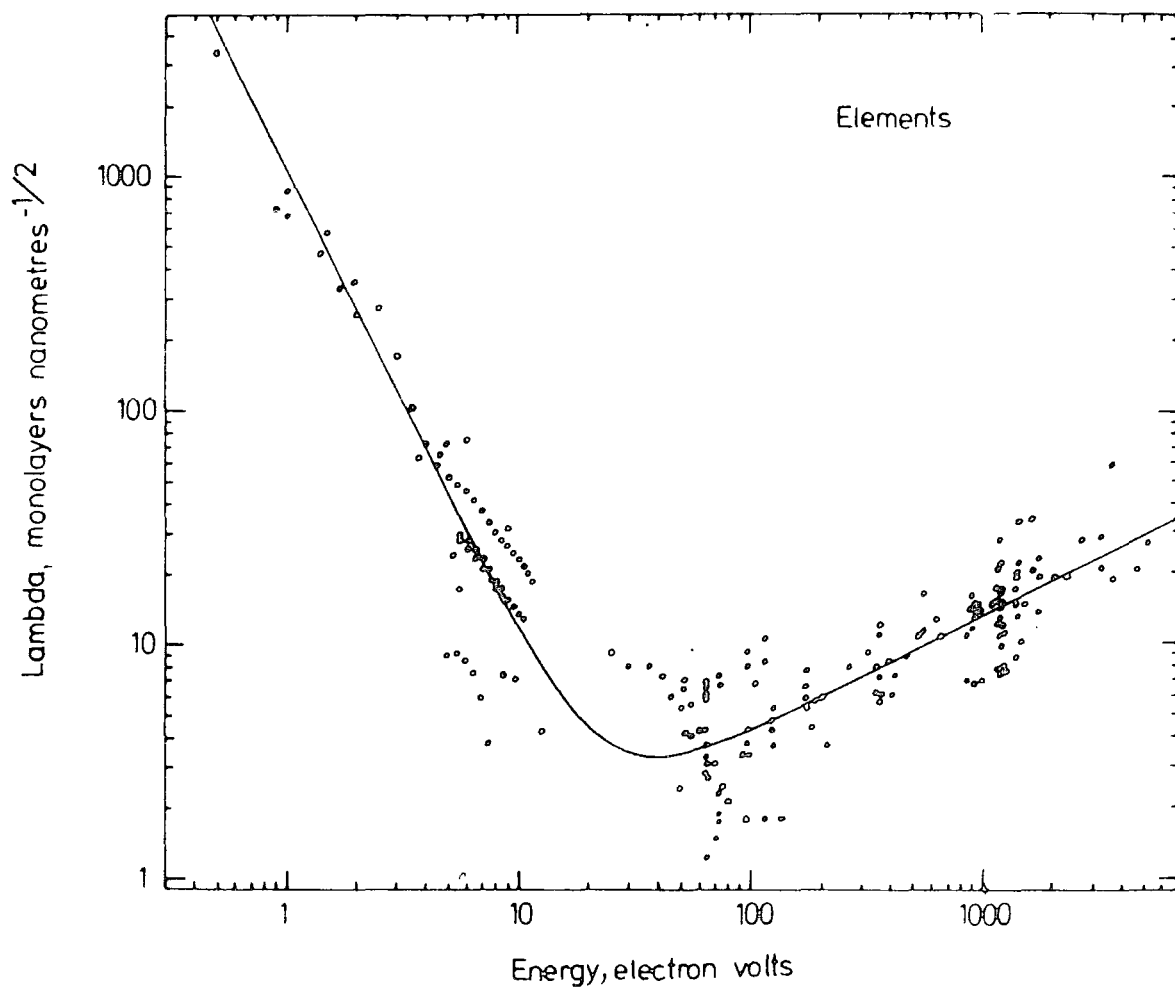


Figure 1.16. IMFP for elements  $\lambda_m = \frac{538}{E^2} + 0.41 (aE)^{\frac{1}{2}}$  monolayers.

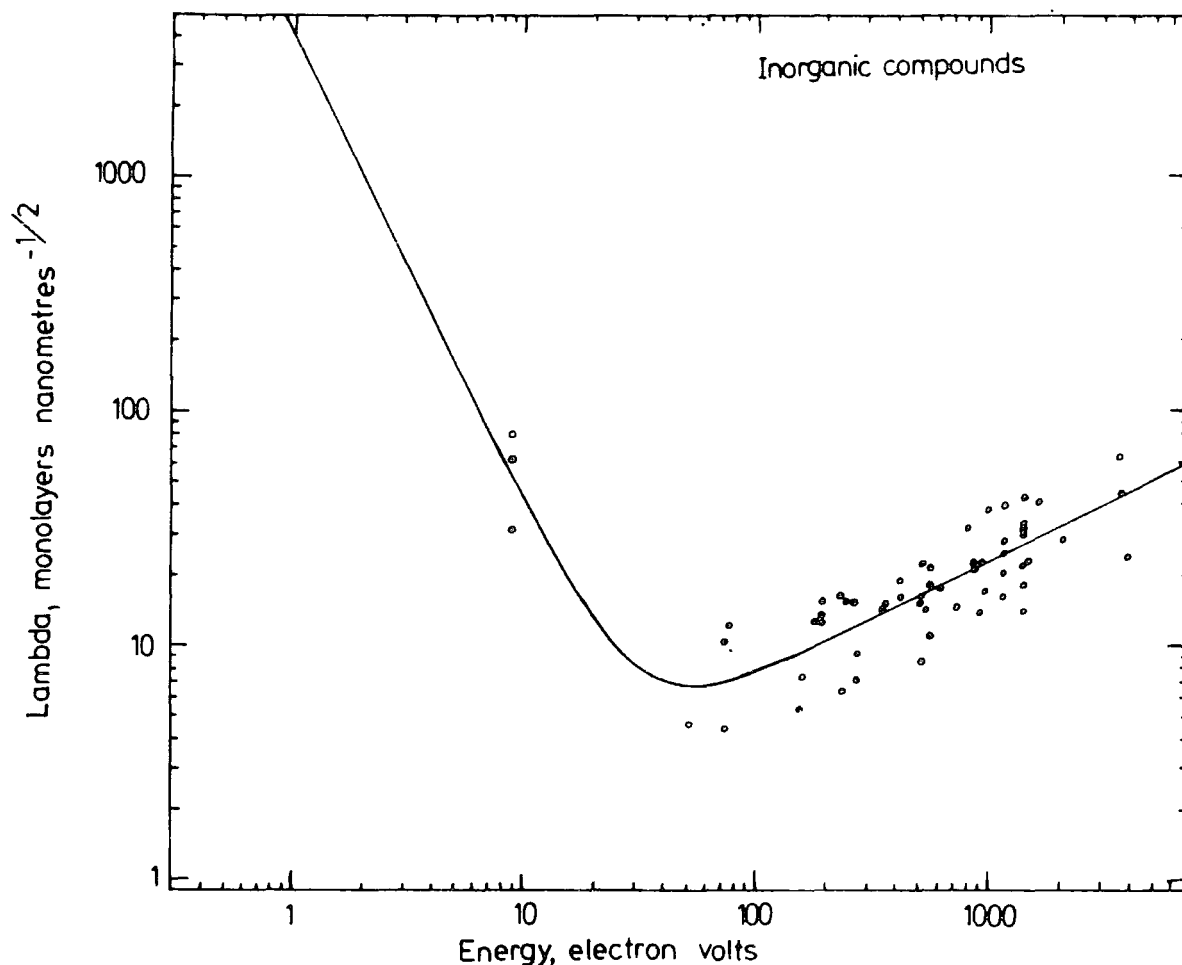


Figure 1.17. IMFP for inorganic  $\lambda_m = \frac{2170}{E^2} + 0.72 (aE)^{\frac{1}{2}}$  monolayers.

The electron mean free paths, which have been recently directly determined in this laboratory by Clark and co-workers<sup>93,99-101</sup> are  $\sim 22\text{\AA}$ ,  $\sim 14\text{\AA}$  and  $\sim 10\text{\AA}$  corresponding to  $\text{Au}_{4f}$  (1170 eV),  $\text{C}_{1s}$  ( $\sim 960$  eV) and  $\text{F}_{1s}$  ( $\sim 560$  eV) using  $\text{Mg}_{k\alpha_{1,2}}$  exciting radiation through polymeric materials. In more recent work, IMFP's have been measured for kinetic energies from 600 eV to 4430 eV corresponding to mean free path of  $15\text{\AA}$  to  $37\text{\AA}$  respectively. A detailed discussion of the experimental determination of these values are presented in chapter three.

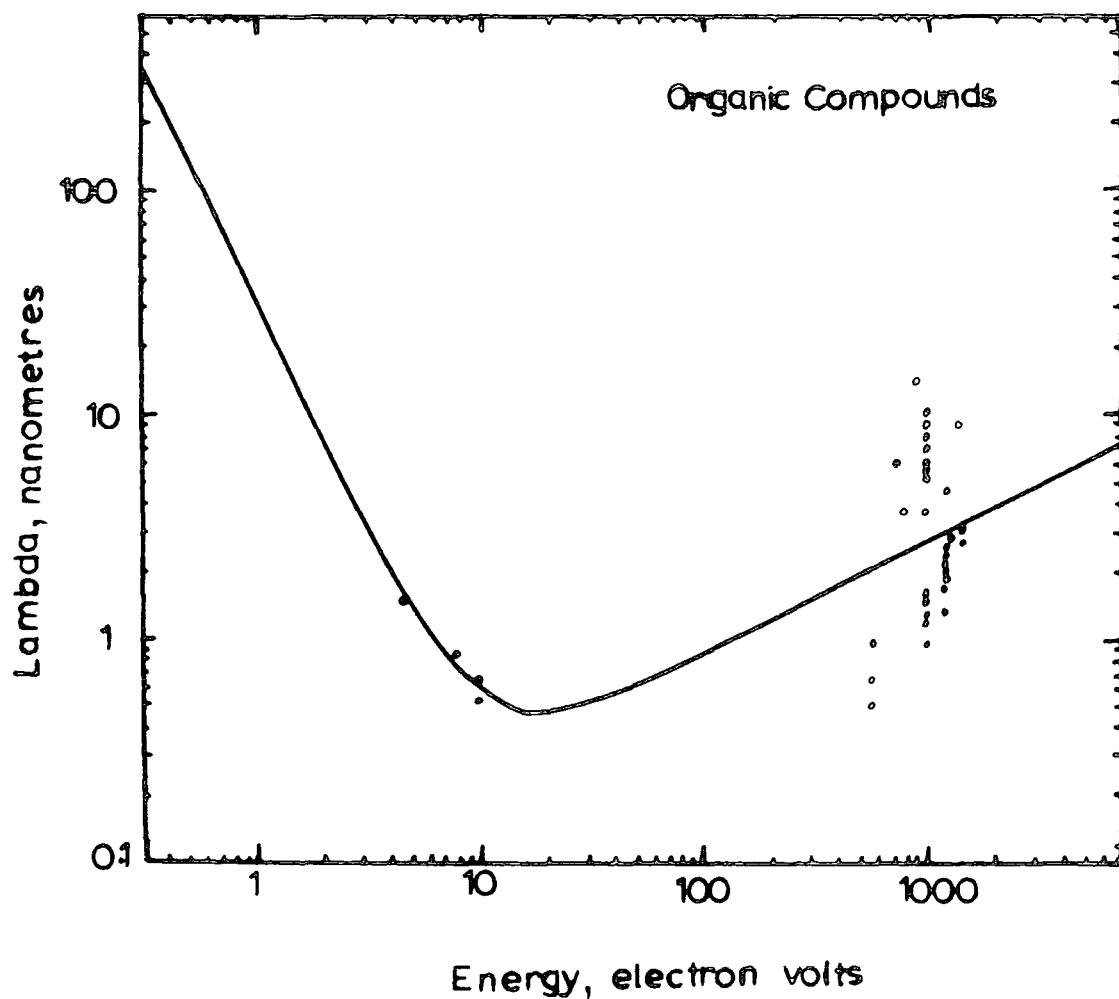


Figure 1.18. IMFP for organic  $\lambda_m = \frac{49}{E} + 0.11 E^{\frac{1}{2}} \text{ mg.m}^{-2}$ .

### 1.5.3. Angular Dependence

It should be pointed out that equation 1.10. does not accommodate two further effects of varying the angle  $\theta$ . The first effect is illustrated in Figure 1.19. The figure draws a comparison between a narrow X-ray beam and a beam which is broader than the width of the sample  $W$ .

For the narrow beam the total flux which hits the sample is not affected by varying  $\theta$  within limits. However, for the broader beam the total flux hitting the sample varies as

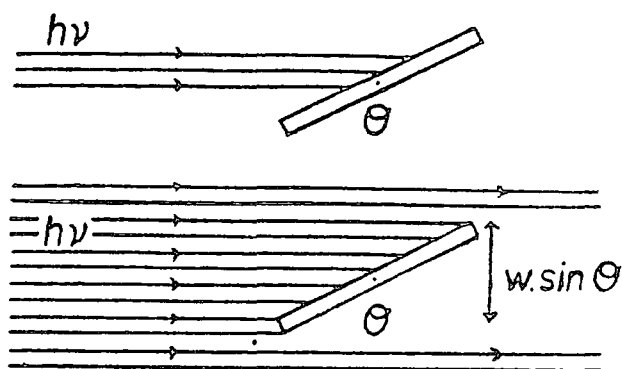


Figure 1.19. Narrow and wide X-ray beams.

$W \sin \theta$ . Therefore as  $\theta$  is increased this effect tends to increase the signal intensity. The second effect is concerned with the electrons which are photoemitted in the direction of the analyser. For a given value of  $\theta$  the entrance slit of the analyser "sees" a sample area proportional to  $W \cos \theta$ . Therefore as  $\theta$  is increased this effect tends to decrease the signal intensity.

The convolution of these two effects, acting in the opposite sense produces an overall function of  $\theta$ ,  $f_j(\theta)$  for a core level  $i$ , which exhibits a maximum value.

Equation 1.10. therefore may be replaced by

$$I_i = f_i(\theta) F \alpha_i N_i k_i \lambda_i \quad 1.16.$$

where  $f_i(\theta)$  can be determined empirically.

### 1.6. Energy Referencing

The reference level in ESCA is normally taken as the vacuum level when dealing with gaseous samples, and the Fermi level for solids. The relationship between the Fermi level and the vacuum level for a solid is shown in Figure 1.20.

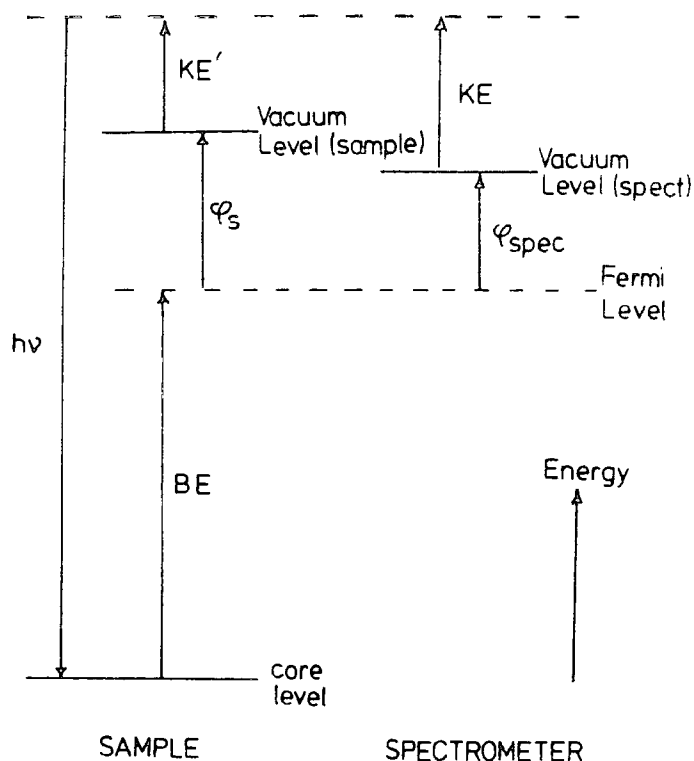


Figure 1.20. Binding energy level in solids.

For a conducting sample in electrical contact with the spectrometer the Fermi levels will be equal, and direct measurement of binding energies should be possible. However, with non-conducting samples, or samples not in electrical contact with the spectrometer, this will not be the case, and in order to correct for the sample charging due to photoionisation from the surface regions some calibration procedure must be adopted.<sup>104</sup>

For gaseous samples this can be accomplished by mixing with a gas whose core level binding energies are accurately known (e.g. Ar).

For solid samples the work-function  $\phi_s$  is defined to be the energy gap between the free electron (vacuum) level and the Fermi level in the solid. Although the Fermi levels of

both the solid and the spectrometer are equivalent their vacuum levels may be different, and then the electron will experience either an accelerating or retarding potential equal to  $\phi_s - \phi_{\text{spec}}$ , where  $\phi_{\text{spec}}$  is the work function of the spectrometer.<sup>102,103</sup> In ESCA it is the K.E. of the electron when it enters the analyser that is measured, and taking zero B.E. to be the Fermi level of the sample, the following equation results:

$$\text{B.E.} = h\nu - \text{K.E.} - \phi_{\text{spec.}} \quad 1.17.$$

This is illustrated in Figure 1.20.

The B.E. referred to the Fermi level does not depend on the work function of the sample but only on that of the spectrometer  $\phi_{\text{spec}}$ , and this represents a constant correction to all B.E.'s.

For samples deposited in thin film on a conducting substrate in the spectrometer source, since the mean free path of the incident X-ray beam is very large<sup>13</sup> it is possible, depending on conditions, for films of the order  $10^{30}$  Å to have sufficient charge carriers to be in electrical contact with the spectrometer. This is most readily shown by applying a bias voltage to the sample probe and if this is the case then the apparent shift in energy scale will exactly follow the applied bias. By shifting the position of the true zero of the K.E. scale, it is possible to study the secondary electron distribution and this provides a direct energy reference.<sup>105</sup> If the samples have been deposited on a substrate such as gold it is possible to measure



the core levels of the sample, whilst monitoring the  $\text{Au}_{4f_{7/2}}$  core level (84.0 eV) and this provides a convenient means of energy referencing.<sup>1</sup>

The most reliable method of energy referencing is to follow a controlled build up of hydrocarbon at the surface (B.E.  $\text{C}_{1s}$  285 eV).<sup>13,104</sup> This may be present as a thin layer of hydrocarbon material on the sample surface, or as  $\text{CH}_2$  environments already present in the sample. Work from this laboratory has shown how the build up of extraneous hydrocarbon material in the ES200 spectrometer can be selectively controlled.<sup>106</sup>

In general, the most useful calibration lines are those due to  $\text{C}_{1s}$  and  $\text{Au}_{4f_{7/2}}$  when used as a substrate.

## 1.7. Sample Handling

### Solid Samples

The most straightforward method for an involatile solid is to mount the sample onto a spectrometer probe tip by means of double sided adhesive tape. This means that the sample is not in electrical contact with the spectrometer. An alternative is to use electrically conducting adhesive tape.

Wherever possible, a more satisfactory technique is to deposit a thin layer of the sample onto a conducting substrate (gold) as a film by evaporation from a suitable solvent, or by other means (see chapter 2).

Other techniques include:

- (i) Pressing a disc of a powder sample and mounting

this onto the probe;

- (ii) A powder sample may be pressed into a wire gauze on the probe;
- (iii) Samples in the form of foils or sheets can be attached directly to the probe.

### Liquids

Here two methods may be used, namely condensation of the liquid onto the probe tip, or direct study of the liquid or solution in the spectrometer housing. Only the first technique is at present viable on commercially available instruments and involves the injection of the liquid into a heatable ( $25^{\circ}\text{C}$  -  $150^{\circ}\text{C}$ ) evacuated reservoir shaft followed by diffusion of the vapour through a metrosil leak and subsequent condensation onto a cooled gold plate on the tip of the sample probe (typical working temperature being in the range  $-50^{\circ}\text{C}$  to  $-150^{\circ}\text{C}$ ). This method ensures the sample surface is continually renewed and contamination and radiation damage effects are reduced.

Two techniques for studying liquids and solutions have been developed by Siegbahn where samples are studied as submillimeter beams,<sup>107</sup> or as a film on a wire passing through the X-ray beam parallel to the analyser entrance slit.<sup>108</sup>

### Gases

Gases may be studied by condensation onto a cooled probe, but several electron spectrometers have facilities to study gases in the gas phase. Such studies have the

following advantages:<sup>39</sup>

- (i) No inherent broadening of the levels due to solid state effects;
- (ii) Problems of sample charging removed;
- (iii) Increased signal to background ratio;
- (iv) Radiation damage, if it occurs, is of no importance unless the sample is recirculated;
- (v) Relatively easy calibration by mixing with standard gases;
- (vi) Possibility of distinguishing between inelastic losses and shake-up or shake-off processes by varying sample pressure;
- (vii) Direct comparison with theoretical results is simplified.

#### 1.8. Instrumentation

Since the appearance of the first commercial ESCA instrument in 1969, several designs have been marketed commercially. The majority of the work in this thesis was carried out on AEI ES200AA/B and Kratos ES300 spectrometers, (particularly using  $Ti_{k\alpha_{1,2}}$  X-ray, see chapter three). A schematic of the essential components of a typical ESCA spectrometer is given in Figure 1.21.

The description of the apparatus may be considered under four headings:

- (i) X-ray Equipment;
- (ii) Sample Chamber;
- (iii) Analyser;
- (iv) Electron Detection.

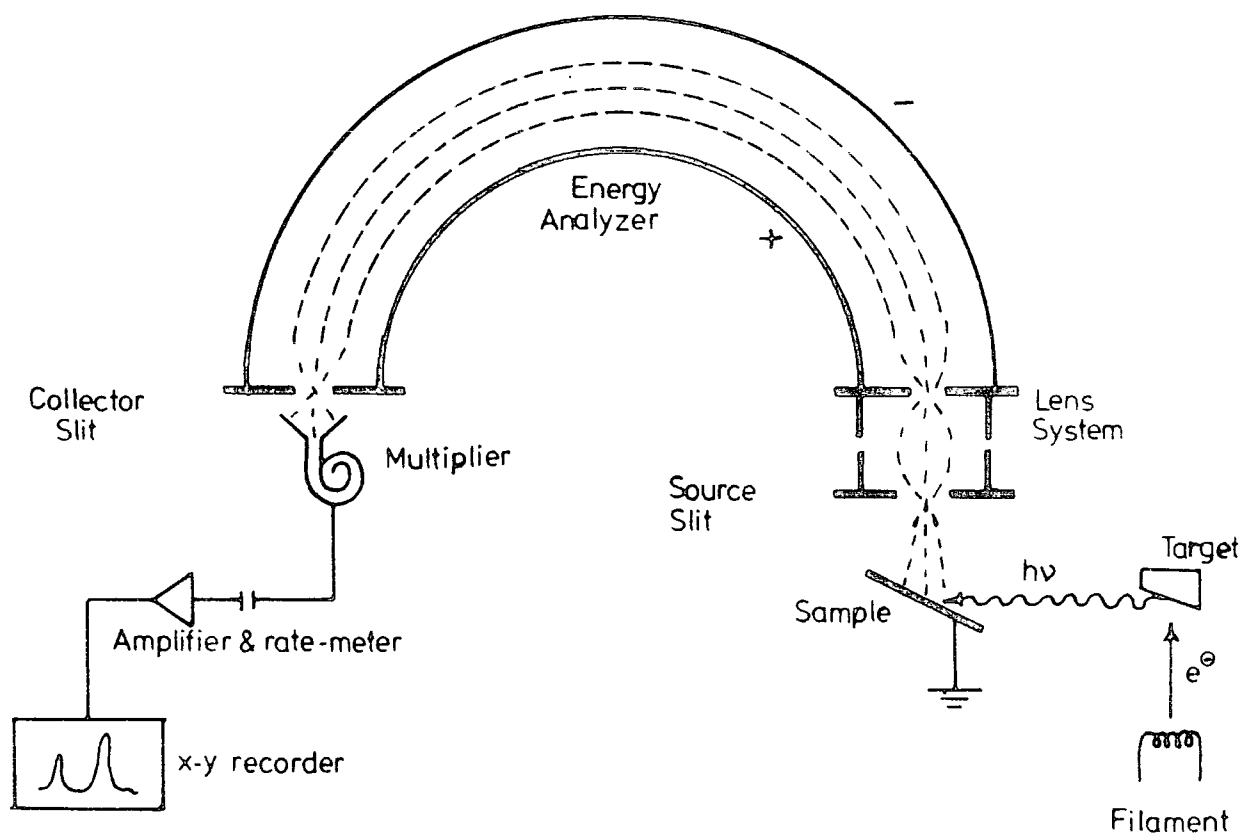


Figure 1.21. Some of the components of the ES200 spectrometer.

#### 1.8.1. X-ray Equipment

The equipment consists for the ES200AA/B spectrometer a Marconi Elliot GXS high voltage supply, whilst that for the ES300 is a solid state generator of Kratos design.

The X-ray beam is produced by the bombardment of a target (anode) with high energy electrons.

The X-ray photon sources are of the hidden filament or Henke<sup>109</sup> design, this reduces risk of contamination of the target by evaporated tungsten from the electron gun filament.

The ES200 spectrometer equipped with soft X-ray source ,

non-monochromatised  $Mg_{k\alpha_{1,2}}$  ( $h\nu = 1253.7$  eV), typical operating conditions  $< 10^{-7}$  torr, 12 kV, 13 mA.

The ES300 spectrometer is equipped with a dual-anode<sup>110</sup> ( $Mg_{k\alpha_{1,2}}$  and  $Ti_{k\alpha_{1,2}}$ ), and monochromated  $Al_{k\alpha_{1,2}}$  sources. The  $Ti_{k\alpha_{1,2}}$  has been used extensively in the work presented in this thesis.

In both spectrometers  $Al_{k\alpha}$  radiation can be monochromatised by using a crystal diffraction technique<sup>20</sup> to eliminate X-ray satellite and unwanted background (Figure 1.22.).

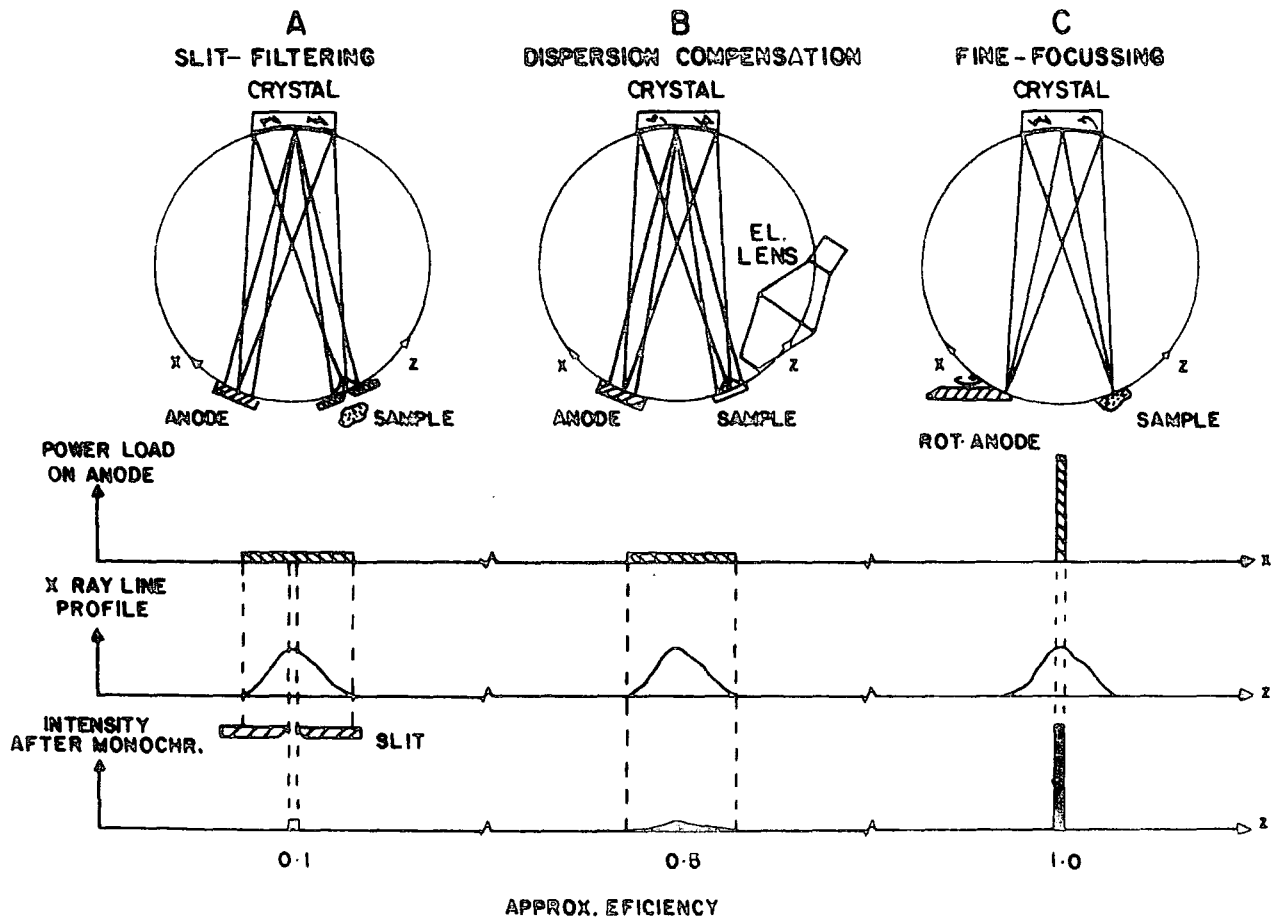


Figure 1.22. Techniques of monochromatisation of X-rays.

In both spectrometers non-monochromatised sources are isolated from the sample chamber by a thin (0.003") Al window which ensures that electrons scattered from the target or filament do not enter the sample region. In order to reduce the risk of scattered electrons exciting X-radiation from the Al window, the filament is operated at near ground potential (+ 10V) and the anode at high positive voltage. A typical, non-monochromatic X-ray spectrum (a tungsten anode) is shown in Figure 1.23. The spectrum consists of the characteristic line spectrum

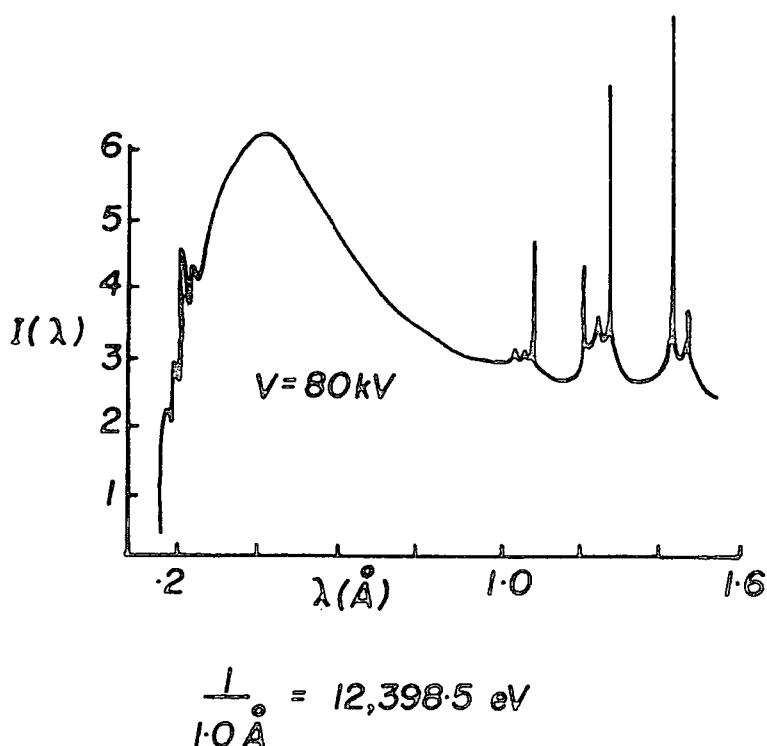


Figure 1.23. X-ray spectrum of a tungsten target.

superimposed on a continuous spectrum (Bremsstrahlung).<sup>108</sup> The continuous shape depends only on the energy of the incident electrons on the anode, and not on the nature of

the anode material.

### 1.8.2. Sample Chamber

Figure 1.24. displays a schematic drawing of the ES200AA/B spectrometer equipped with monochromator and reveals the relative disposition of the sample, X-ray sources and analyser.

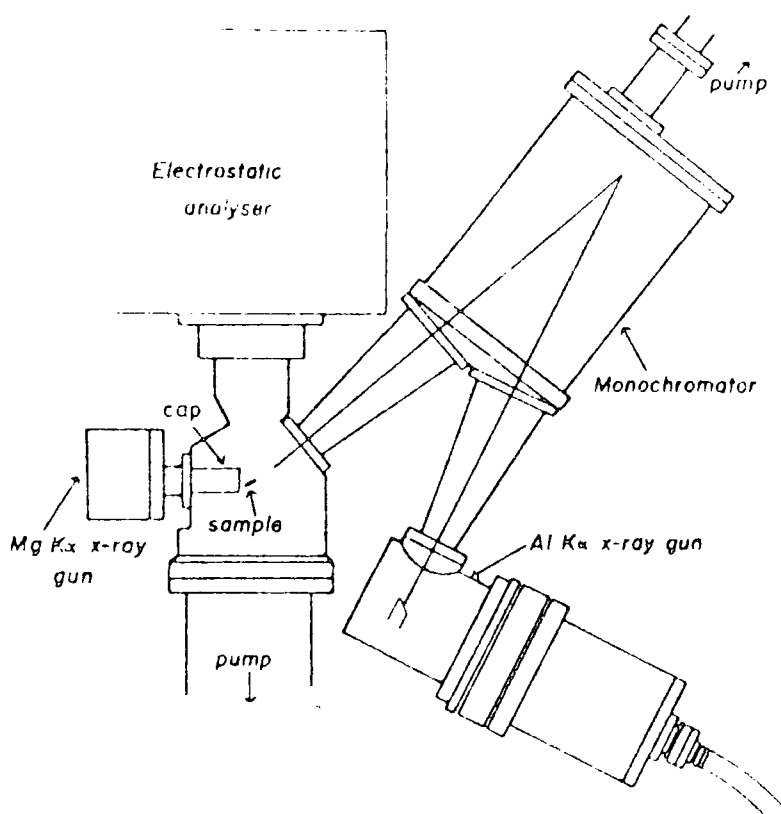


Figure 1.24. AEI ES200AA/B spectrometer.

The sample chamber of both ESCA instruments are equipped with several access ports for sample introduction and treatments. The preferred method of introduction is via an insertion lock system and high vacuum gates or ball valves, which allows samples to be studied on the tip of a probe whilst maintaining a base pressure of  $10^{-8}$  torr in

the system. Purpose-built reaction chambers may be attached to the source chamber via an insertion lock and this provides facilities for "in situ" polymerisation. By probe rotation, the optimum signal intensity may be obtained, or angular dependent studies performed.

The ES300 spectrometer has a permanently mounted preparation chamber attached to the source chamber, pumped by a diffusion pump, catering for the needs of the research interests. The source region is pumped separately from the analyser using Alcatel air-bearing, air-turbine turbo-molecular pumps having nominal pumping speeds of 450 and 120 l s<sup>-1</sup>, respectively. The base pressure is typically of the order 5 x 10<sup>-9</sup> torr.

### 1.8.3. Analyser

The electron energy analyser should have a resolution of 1 in 10<sup>4</sup> in order to carry out ESCA studies. The analyser used on the ES200B is a hemispherical double focussing analyser based on the principle described by Purcell,<sup>111</sup> which is screened from external magnetic interference by means of Mu-metal shields. The resolution,  $\Delta E/E$ , where E is the energy of the electrons, depends upon the mean radius of the hemispheres (R) and the combined widths of the entrance and exit slits, W.

$$\frac{\Delta E}{E} = \frac{R}{W} \quad 1.18.$$

Therefore the resolution can be improved in three distinct ways:

- (i) Reduce the slit widths, which reduce the signal intensity;



- (ii) Increase the radius of the hemisphere, which increases engineering costs and pumping requirements;
- (iii) Retard the electrons before entry into the analyser.

With reasonable compromise made on the slit widths to obtain sufficient signal intensity, and on the size of the hemisphere to prevent mechanical distortion and keep costs down, a retarding lens is also employed to slow the electrons down before entry into the analyser and cuts down on the resolution requirements of the analyser. Also, the lens system allows the analyser<sup>112</sup> to be located at a convenient distance physically from the source chamber which permits a maximum flexibility in sample handling.

Electrons of the required kinetic energy may be focussed at the detector slit by either of two methods:

- (a) Scanning the retarding potential applied to the lens and keeping a constant potential between the hemispheres;
- (b) Scanning the retarding potential and the potential between the analyser hemisphere simultaneously maintaining a constant ratio between the two.

The first method of fixed analyser transmission (FAT) has greater sensitivity at low kinetic energies (< 500 eV), and the second fixed retardation ratio (FRR) has greater sensitivity at higher electron kinetic energies. The mode employed in this work is FRR.

#### 1.8.4. Electron Detection

The electrons focussed by the analyser are detected by an electron multiplier and the pulses obtained are amplified and fed into the counting electronics. The signals fed into the counting system generate the ESCA spectra in two ways:

- (i) The continuous scan, where the electrostatic field is increased from the present starting K.E. continuously, while the signals from the multiplier are monitored by the rate meter. When the signal to background ratio is sufficiently high, a graph of the electron counts per second versus the K.E. of the electrons is plotted onto an X-Y recorder;
- (ii) The step scan, in which the field is increased by pre-set increments (typically 0.1 eV) and at each increment, (a) the counts may be measured for a fixed length of time, or (b) a fixed number of counts may be timed. The data obtained from the step scans is stored in a multichannel analyser (MCA), so that many scans can be accumulated to average random fluctuations in the background.

### 1.9. General Aspects of ESCA

#### 1.9.1. Advantages of ESCA

ESCA is an extremely powerful tool with wide-ranging applicability in respect of the surface studies. The principle advantages of the technique may be summarized as follows:

- (1) Samples may be solid, liquid or gas, and sample sizes are small being 1 mg solid, 0.1  $\mu$ l liquid and 0.5  $\text{cm}^3$  of a gas (at STP);
- (2) The technique is non-destructive in that the X-ray flux is quite small ( $\sim$  0.1 millirad./sec.).<sup>113</sup> This is especially advantageous over Auger spectroscopy where the electron beam produces many surface changes, particularly in polymeric systems where cross-linking and degradation can occur;
- (3) The technique is independent of the spin properties of the nucleus and all elements, with the exception of H and He, can be studied;
- (4) Materials may be studied "in-situ" in their working environments with a minimum of preparation;
- (5) The technique provides a large number of information levels from a single experiment and has a higher sensitivity than many other analytical techniques;
- (6) The data is often complementary to that obtained by other techniques;
- (7) For solids, ESCA has the capability of differentiating the surface from subsurface and bulk phenomena, facilitating analytical depth profiling;
- (8) The information obtained is directly related to molecular structure and bonding, and is applicable to both the inner and valence level of the molecule;
- (9) The information levels are such that "ab-initio" investigations are feasible and the theoretical basis is well understood.

### 1.9.2. Disadvantages of ESCA

There are surprisingly few disadvantages associated with ESCA:

- (1) The overall costs are quite high;
- (2) Whilst the technique has superior depth resolution,  $\sim 100\text{\AA}$ , the spatial resolution is poor and typically an area of  $0.3\text{ cm}^2$  is normally sampled;
- (3) If the surface differs from the bulk then it is not possible to say anything about the bulk structure by means of ESCA without sectioning the sample.

### 1.9.3. Hierarchy of ESCA Information

The ESCA experiment provides a large number of information levels per experiment with such wide-ranging capabilities is as follows:

- (1) The technique gives absolute binding energies, relative peak intensities, binding energy shifts, elemental analysis, analytical depth profiling, identification of structural features, etc.;
- (2) Shake-up and shake-off satellites may be observed. Monopole excited states, energy separation with respect to direct photoionisation peaks short and longer range effects directly;
- (3) Multiplet effects. For paramagnetic systems, spin state, distribution of unpaired electrons;
- (4) For valence energy levels, it allows the investigation of longer range effects directly and provides a fingerprint of gross structure;

- (5) Angular dependent studies. For solids with a fixed arrangement of analyser and X-ray source varying the take-off angle between the sample and analyser provides a means of differentiating surface from subsurface and bulk effects;
- (6) Sample charging phenomena which provide an additional means of monitoring structure and bonding in surface regions and electrical properties of polymer films can be investigated from biasing experiments.

CHAPTER TWO

CHAPTER TWO

## ESCA APPLIED TO POLYMERS

Abstract

A description of typical sample preparation techniques is given, and a review of the important aspects of the application of electron spectroscopy to the study of polymers presented.

## 2.1. Introduction

It has become increasingly evident over the past few years, by the number of publications on the subject emerging from laboratories throughout the world, that X-ray photoelectron spectroscopy (XPS or ESCA) has gained widespread recognition as the single most powerful tool for the non-destructive elaboration of the surface aspects structure, bonding and reactivity of polymeric systems. It is a topic of considerable current interest and the numerous reviews which have appeared over the past few years attest to the increasing awareness of the wide-ranging capability of the technique in this area.<sup>1,26,98,114-123</sup> This chapter presents a concise summary of some aspects of the investigations which have been carried out to date, with a bias towards areas of particular interest to this thesis.

From the latter part of 1970,<sup>1,114</sup> the general philosophy behind the initial work was to establish a data bank pertaining to relative peak intensities, binding energies and chemical shifts, from which trends could be drawn and comparisons made with simple monomer systems. This allowed the development of a theoretical framework within which results could be quantified. This also provided a strong basis for studying more complex systems.

In the early 1970's ESCA studies of polymers were initiated by Clark at Durham, the main emphasis being placed on fluoro-polymer systems.<sup>114-117</sup> The rationale behind the choice of fluorine containing systems may be summarised as follows. Firstly, fluorine is the most electronegative element in the



periodic table. It induces a large chemical shift and as a substituent greatly eases the problem of interpretation of the ESCA data. Secondly, fluoropolymers are of considerable academic and technological interest, and finally, by virtue of their general insolubility and intractability fluoropolymer systems are often difficult to study by other spectroscopic techniques.<sup>114</sup>

From 1970 up until the present time the ESCA investigation of polymeric materials has diversified to encompass non-fluorine containing systems,<sup>57,58,66,124</sup> and a number of other areas of considerable technological<sup>125</sup> and industrial<sup>126-128</sup> concern.

In this chapter much of the material is drawn from the work of Clark and co-workers and covers the period 1977 to 1982.

The areas of study may be divided into two main groups, and these are set out below.

(i) Static studies

- (1) Chemical compositions
  - (a) elemental compositions
  - (b) % comonomers in copolymers
- (2) Structural details
  - (a) structural repeat units in copolymers
  - (b) domain structure in block copolymers
- (3) Fine structure details
  - (a) structural isomerisms
  - (b) shake-up studies
- (4) Valence band studies

- (5) Auger parameters
- (6) Sample charging effects
- (ii) Dynamic studies
  - (1) Surface treatments
    - (a) plasma and corona discharge treatments, e.g. inert gas plasmas, oxygen plasma
    - (b) chemical treatments, e.g. oxidation, fluorination, nitration and denitration
  - (2) Polymer degradation, e.g. weathering phenomena
  - (3) Migration and segregation phenomena
  - (4) In-situ polymerisation.

## 2.2. Sample Preparation

The choice of the method of sample preparation is often governed by the physical state of the sample; whether prepared or as received and, for dynamic studies the nature of the experiment. The ultimate aim is to mount the sample onto a probe tip approximately 7 mm. x 14 mm. x 1 mm. The area actually irradiated by the X-ray beam is in fact substantially smaller than the size of the sample.<sup>129</sup>

### 2.2.1. Powders

When the polymer sample is available as a powder it is often convenient to study it as such by applying the powder to double sided "Scotch" adhesive tape mounted on the probe tip. Care must be taken such that no extraneous signals are observed from the sample backing and that no chemical reaction occurs between the sample and substrate. Uneven topography of samples prepared in this way generally leads to

lower signal/noise ratios than polymers studied as films.

### 2.2.2. Solution Cast Films

If the polymer is sufficiently soluble then thin films may be cast directly onto a backing (preferably gold foil) by conventional dip or bar coating, or spin casting. It is important to use clean apparatus and pure solvents containing no involatile residues which would segregate at the surface on evaporation of the solvent.

### 2.2.3. Pressed or Extruded Films

Because of the problems of possible contamination associated with solvent cast films, it may be convenient to study polymers in the form of pressed or extruded films mounted on a suitable backing (e.g. gold). For elastomers it is often possible to "melt" a small amount of the sample and allow it to spread in the form of a thin film on the tip of a sampling probe or to slice a thin film from a larger sample. In preparing samples from powders it is often convenient to press films between sheets of clean aluminium foil at an appropriate temperature and pressure. There are two precautions to be taken in doing this:

- (a) The temperature and pressure used should be such that no decomposition or adhesion of surface contamination occurs;
- (b) Since typically only the top  $\sim 50\text{\AA}$  of the sample is studied by ESCA it is important to avoid chemical reaction at the surface during preparation. For example, pressing polyethylene films in air at the minimum temperature necessary results in considerable

surface oxidation. This may be obviated by pressing in an inert atmosphere (e.g. N<sub>2</sub> or Ar).<sup>125</sup>

#### 2.2.4. "In-situ" preparation

A convenient and often contamination-free method of preparing polymer films is by direct polymerisation onto the probe tip. This is usually done from the gas phase by u.v. or electron irradiation, glow discharge polymerisation, (Chapters 4, 5 and 6) or pyrolysis of appropriate monomers, (Chapter 3). Surface treatments of polymers may also be achieved "in-situ", (see section 2.9.1.).

The experimental arrangement for these processes often involves pre-treatment chambers directly attached to the spectrometer, thereby eliminating any contamination or reaction due to exposure to air prior to investigation.

#### 2.3. Static Studies

As a preliminary to this section the information which may be derived from an ESCA experiment, as discussed in Chapter one, is summarised in Table 2.1.

Table 2.1. Information levels in ESCA.

- (1) Primary information levels
  - (a) Relative and absolute binding energies
  - (b) Relative peak intensities
- (2) Secondary information levels
  - (a) Shake-up structure
  - (b) Angular dependence of peak intensities
  - (c) Auger parameter
  - (d) Sample charging

### 2.3.1. Chemical Compositions

It is quite apparent from the discussions in Chapter one that ESCA is capable, in principle, of being able to study the core and valence levels of any element (with the exceptions of hydrogen and helium) regardless of the nuclear properties, such as magnetic or electric quadrupole moments. This particular feature of the technique makes it very useful for an understanding of surface treatments of polymers such as oxidation, fluorination, RF plasma treatments, etc., which will be discussed in the following sections. Thus, by carrying out a wide survey scan an elemental "map" may be produced. The use of two photon sources (commonly  $Mg_{k\alpha_{1,2}}$  at 1253.7 eV and  $Al_{k\alpha_{1,2}}$  at 1486.6 eV) allows a straightforward distinction between those peaks due to direct photoionisation and those due to Auger transitions which are not dependent upon the energy of the exciting radiation. A simple example is given in Figure 2.1. for an ethylene-

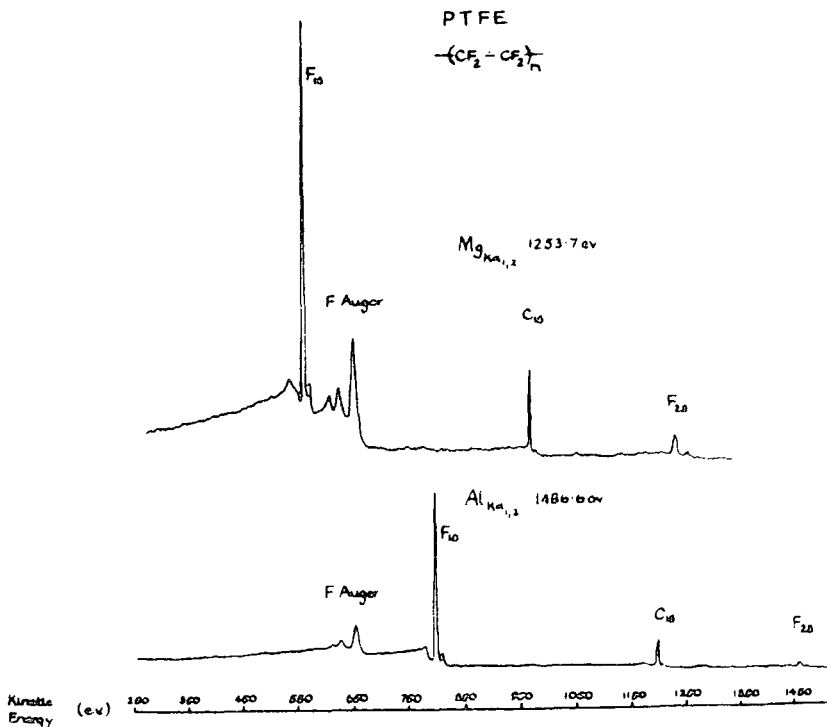


Figure 2.1. Survey scans of an *poly*-tetrafluoroethylene using  $Mg_{k\alpha_{1,2}}$  and  $Al_{k\alpha_{1,2}}$  photon sources.

tetrafluoro-ethylene copolymer. Such studies are extremely useful precursors to the detailed study of individual core levels.

Recent work<sup>101</sup> using harder X-ray sources e.g.  $Ti_{k\alpha_{1,2}}$  at 4510 eV provides excellent coverage of the kinetic energy range of 0 - 4500 eV. Chapter three will present the core levels of the gold substrate of polyparaxylylene overlayers using a  $Ti_{k\alpha_{1,2}}$  photon source.

### 2.3.2. Percentage Comonomers in Copolymers

A further application of the study of chemical compositions by ESCA has been in the determination of the percentage comonomer incorporated into a copolymer. Typical of the systems which have been studied are the Viton copolymers of hexafluoropropylene (HFP),<sup>1</sup> and vinylidene fluoride (VF<sub>2</sub>).<sup>1</sup> Since the core level shift on carbon due to fluorine is large, the spectra of these systems are easily resolved. The compositions for such materials may be directly determined from the fine structure of the C<sub>1s</sub> levels. For example,  $\underline{CF}_3$ ,  $\underline{CF}_2$ ,  $\underline{CF}$  and  $\underline{CH}$  components correspond to different absolute binding energies and thus the composition of thin polymer films prepared in RF discharge polymerisation may be determined, (detailed studies in later chapters in this thesis).

Clark and co-workers<sup>1</sup> were able to compute comonomer ratios by three different techniques which were all based upon the deconvolution of the C<sub>1s</sub> envelope, the area of the  $\underline{CF}_3$  peak, the total area of the ( $\underline{CF}_2 + \underline{CF}$ ) peak and the area of the  $\underline{CH}_2$  peak. Table 2.2. gives the results of the three methods of calculation.

Table 2.2. % Incorporation of HFP Calculated by Three Methods.

	Method of Calculation		
	(1)	(2)	(3)
Sample 40/60	39	42	40
Sample 30/70	33	30	32

## 2.4. Structural Details

### 2.4.1. Repeat Units in Polymers - Substituent Effects

Before the fine structural details of a series of polymers may be considered, studies of the qualitative and quantitative nature of substituent effects in ESCA need to be carried out. In Chapter one a brief survey of theoretical methods of interpreting chemical shifts were considered, and here the experimental determination of binding energy shifts is briefly discussed.

In a series of polymers studied by Clark et al.<sup>114,136</sup> the binding energies for the  $C_{1s}$  and  $F_{1s}$  levels were obtained. Studies have been extended to over one hundred standard polymers containing fluorine, oxygen, nitrogen, sulphur, chlorine and bromine.<sup>66,130-132</sup> Experimentally the binding energies have been reported for the core levels for a wide range of functionalities, a summary of which appear in Figure 2.2. along with theoretical chemical shift calculated within the CNDO/2 SCF formalism.

A considerable body of data<sup>65,67,70,119,121,133</sup> is now available on the influence of a wide range of substituents on the core binding energies of  $C_{1s}$ ,  $O_{1s}$  and  $N_{1s}$  levels which have been investigated experimentally and theoretically as

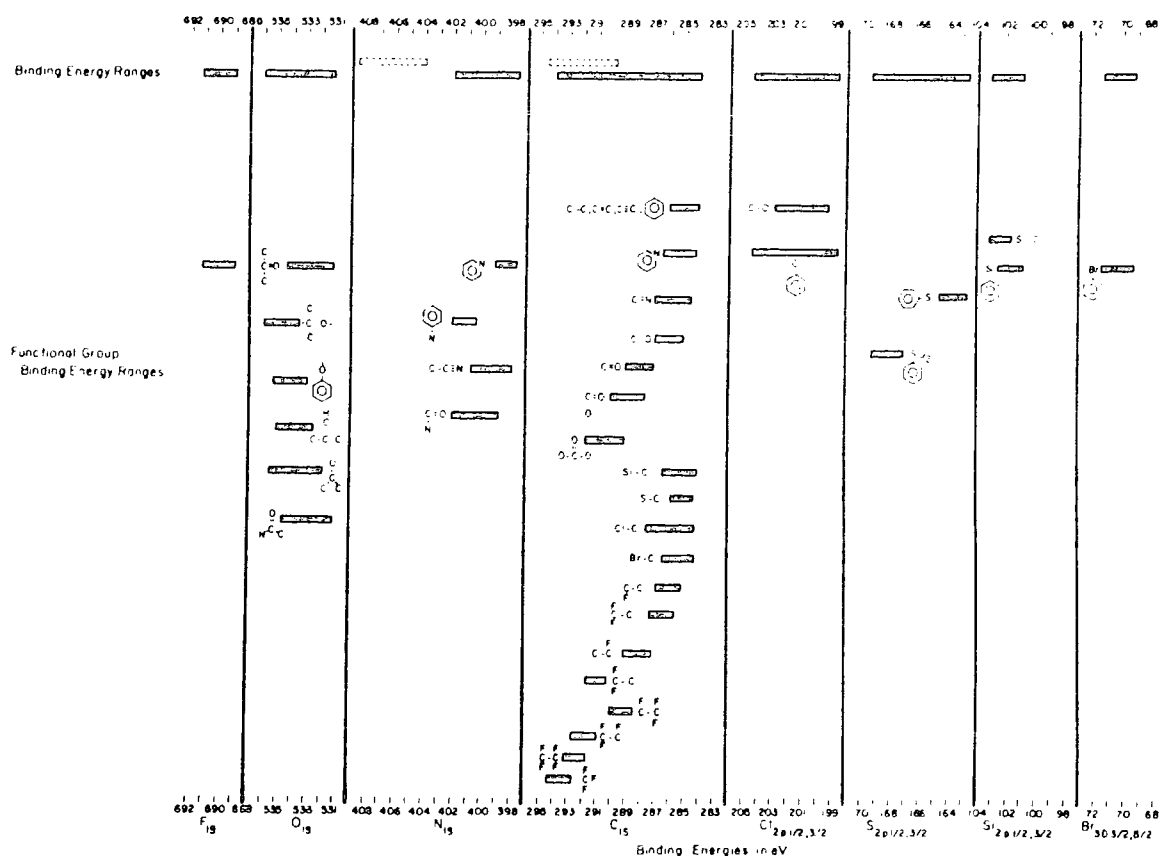


Figure 2.2. Correlation diagram for  $C_{1s}$  levels in polymeric systems as a function of electronic environment.

a function of electronic environment. In the data shown in Table 2.3. the experimental binding energies of  $C_{1s}$ ,  $N_{1s}$  and  $O_{1s}$  levels are compared with the theoretical data for model systems.<sup>70</sup> In general excellent agreement has been found between theory and experiment.



Table 2.3. A comparison of ASCF binding energies of  $C_{1s}$ ,  $N_{1s}$  and  $O_{1s}$  levels in the model systems with experimental data.

Molecule <sup>a</sup>	Comparison of Theoretical Model Compounds with Experiment						
	Solid Phase Experimental BE (eV)			Theoretical BE (eV) (corrected)			
	$C_{1s}$	$N_{1s}$	$O_{1s}$	$C_{1s}$	$N_{1s}$	$O_{1s}$	
<chem>CH3CN</chem>				286.8	287.5	400.4	
<chem>C(C)(C)C#N</chem>	285.0	286.4	399.5				
<chem>C(C)C#N</chem>	285.0	286.3	399.3				
<chem>CH3NO2</chem>		286.8	406.8	534.3	286.8	406.8	534.1
<chem>CH3ONO</chem>					286.8	404.9	534.9
<chem>CH3CH2CH2CH2ONO</chem>	285.0	286.7	405.0	534.2	535.2		
<chem>CH3ONO2</chem>					287.4	407.7	536.2
<chem>CH3CH2ONO2</chem>	285.0	287.0	408.1	535.0	534.2		
<chem>CH3CH2CH2ONO2</chem>	285.0	287.1	408.0	535.5	534.1		
<chem>CH3CH2CH2ONO2CH3</chem>	285.0	287.0	408.1	535.3	534.1		
<chem>CH3CH2CH2CH2ONO2</chem>	285.0	286.5	408.0	535.5	534.3		
<chem>CH3C(=O)NH2</chem>					284.8	288.4	399.5
<chem>C(C)C(=O)NH2</chem>		288.1	399.8	532.8			533.1
<chem>CH3O-C(=O)NH2</chem>					286.8	290.2	400.3
<chem>O=C(N)O</chem>							534.4
<chem>O=C(N)O</chem>							532.6
<chem>O=C(N)O</chem>		289.8	400.4	534.1	532.5		
	Gas Phase Experimental BE <sup>a</sup> (eV)			Theoretical BE (eV) (corrected)			
	$C_{1s}$	$N_{1s}$	$O_{1s}$	$C_{1s}$	$N_{1s}$	$O_{1s}$	
<chem>CH4</chem>	290.8			290.8			
<chem>NH3</chem>		405.6			405.6		
<chem>H2O</chem>			539.7			539.7	
<chem>HCN</chem>	291.5	406.8		294.0	407.4		
<chem>CH3CN</chem>	292.7	405.6		292.6	293.3	406.1	
<chem>CH3CH2CN</chem>	291.1	291.8	292.4	405.1			
<chem>CH3NH2</chem>	291.5	405.2		291.4	404.8		
<chem>CH3N2</chem>	291.3	404.8		291.0	404.2		
<chem>CH3NO</chem>	291.8		537.7	291.5	407.3	535.1	
<chem>CH3NO2</chem>	293.0	411.2	539.1	292.6	412.4	538.8	
<chem>CH3C(NO2)</chem>	291.43	292.6	411.5	538.7			
<chem>NH2CHO</chem>	294.5	406.4	537.7	294.9	405.9	537.3	
<chem>(NH2)2CO</chem>	294.8	406.1	537.2	295.1	405.8	535.9	

<sup>a</sup> Where there is ambiguity underlining denotes atoms of lower BE.

#### 2.4.2. Repeat Units in Copolymers

A series of ethylene-tetrafluoroethylene (E-TFE) copolymers been studied, and the copolymer composition calculated from the ESCA data in two ways.<sup>134</sup> Firstly from the relative ratios of the high to low binding energy peaks in the  $C_{1s}$  levels (attributed to  $CF_2$  and  $CH_2$  respectively), and secondly from the overall  $C_{1s}/F_{1s}$  intensity ratios taken in conjunction with the instrumentally dependent sensitivity factors.

It has been shown that these two methods of calculating the composition are in good agreement with bulk analytical methods (C and F elemental analysis). These techniques for the determination of C to F stoichiometries will be used in later chapters.

By considering the binding energies and chemical shifts of the components of the  $C_{1s}$  spectra obtained from the E-TFE copolymers and comparing these with those for regular homopolymers it has been shown that the system is largely alternating in structure. Further examination of the spectra revealed two features, the total line-widths (FWHM) were greater for the copolymer than the FWHM for the respective homopolymer, and the peak shapes were asymmetric. These two observations indicated that the spectra were envelopes of a number of overlapping peaks arising from different molecular environments.

While such techniques as contact angle measurements can clearly provide some indication of the immediate surface composition of the polymer films, many standard polymers are available for direct comparison with the structure and bonding

information levels obtained by ESCA (see Chapters 4, 5 and 6). ESCA offers the possibility of obtaining quantitative information on compositions and structure and bonding is not only the immediate surface, but also the subsurface typically to a depth of  $\sim 50\text{\AA}$ . The analytical depth profiling capability of the ESCA technique arises from the strong dependence on kinetic energy of the mean free path for photoemitted electrons corresponding to the elastic peaks in the ESCA spectrum, as was discussed in Chapter one. The intensity  $I$  of the signal from a given core level arising from a surface layer of thickness  $d$  is given by

$$I = I_{\infty}(1 - e^{-d/\lambda})$$

where  $I_{\infty}$  is the intensity observed for an infinitely thick layer and  $\lambda$  is the escape depth of the photoemitted electrons. Similarly, the intensity of a signal arising from the bulk of a sample under a surface layer of thickness  $d$  is

$$I = I_{\infty}e^{-d/\lambda}$$

These equations form the basis for determination of the surface structure by ESCA, and will be covered in Chapter three on the mean free paths of electrons in polyparaxylylene films.

The primary sources of ESCA data which have been routinely utilised in the application of the technique to polymers are absolute and relative binding energies, and relative peak areas.<sup>1</sup> It is becoming increasingly apparent, however, that the observation of shake-up satellites accompanying core ionisations can considerably increase the

scope of the technique in many applications, which will be discussed in detail in section 2.5.1. These considerations are readily apparent from comparing the intensity ratios of core levels of polystyrene and polydimethylsiloxane<sup>135a</sup> (PDMS) and on investigating the shake-up transitions for copolymers, it has been shown that for a wide range of bulk compositions the surface of the polymer consists essentially of a discrete phase of PDMS.

Other applications to the structure and bonding in polymer systems as studied by ESCA are given below.

A screening technique has been developed<sup>135b</sup> to determine protein quantity and quality (from the total nitrogen, ratio of side chain to backbone nitrogen and sulphur containing amino acid content) for a series of cereals and legumes. Good agreement was found between the ESCA data and that from standard Kjeldahl analysis. In recent work,<sup>121</sup> the ESCA technique has been used to determine the degree of substitution, DOS (average number of nitro-ester functionalities per glucose residue) for the nitration and denitration of cellulose materials. Again the ESCA data shows a good correlation with those determined from micro Kjeldahl bulk analysis.

Both ATR-IR<sup>136a</sup> and ESCA<sup>136b-d</sup> have shown that the polyetherurethanes<sup>136f</sup> (PEU's) and segmented polyurethanes (SPU's)<sup>136e</sup> have a surface structure which differs significantly from their bulk structure. One explanation for this difference might be the migration of low molecular weight components in PEU's and SPU's to the surface, this will be discussed in section 2.9.2.

The degree of polymerisation in a series of polyfluoro-carbonates was successfully determined from the ESCA data.<sup>135c</sup>

## 2.5. Fine Structural Details

### 2.5.1. Shake-up Studies

The observation of monopole excited states and their energy separation with respect to the direct photoionisation peaks and their relative intensities, allow information to be derived primarily on the nature of unsaturated features in the polymer.

An extensive study into shake-up phenomena in polymers, involving experimental investigations along with theoretical computations on shake-up intensities and transition energies, have been carried out.<sup>55-58</sup>

Investigation of shake-up phenomena in polymers has been undertaken by Clark and Dilks,<sup>56-58</sup> it has become apparent that the observation of low energy shake-up satellites for purely hydrocarbon polymers often provides the only useful level of information concerning their structure. The  $C_{1s}$  spectra of polyethylene, polybutadiene and polystyrene are displayed in Figure 2.3., for the latter two polymers  $\pi \rightarrow \pi^*$  shake-up satellites are evident. The effects of substituents on shake-up have also been investigated in some detail for a series of poly(para-substituted) styrenes and poly-4-vinylpyridine.<sup>58</sup> Shake-up has also been observed for substituents attached to an unsaturated structure.<sup>58</sup> Also shake-up has been employed to determine copolymer composition and morphology.<sup>57</sup>

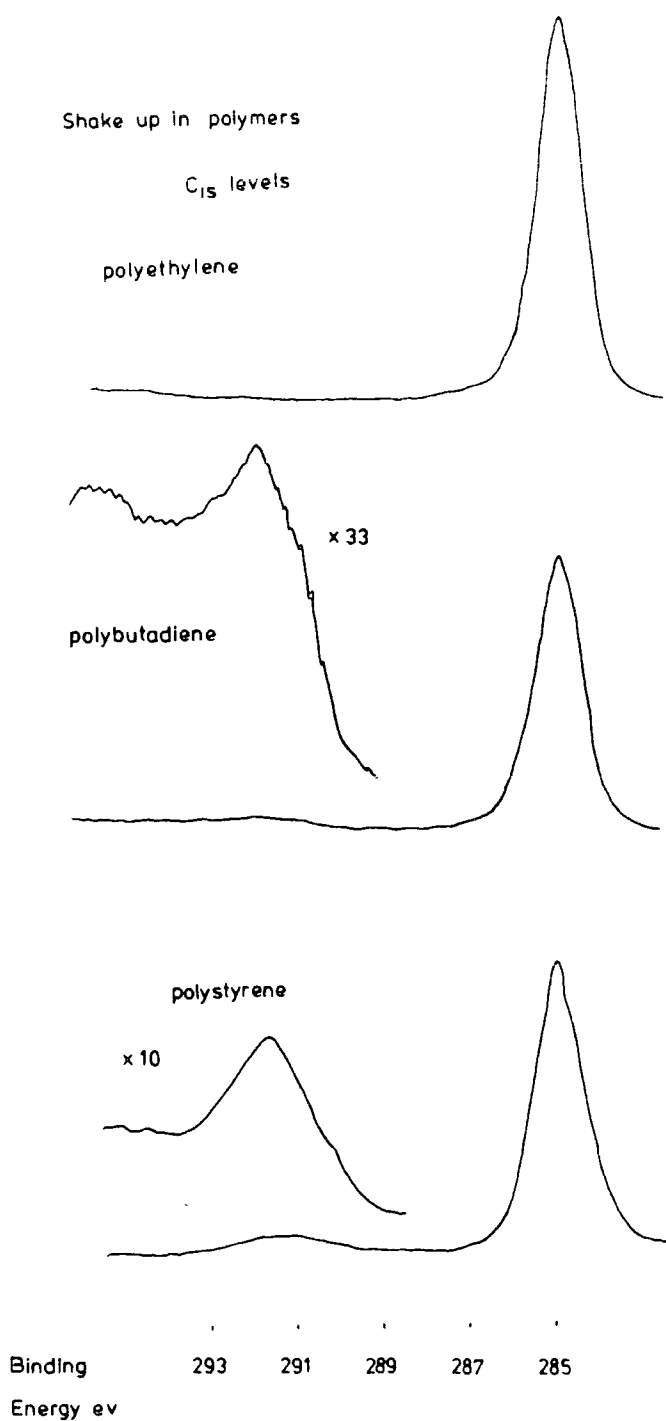


Figure 2.3. Core level spectra of polyethylene, polybutadiene and polystyrene showing the shake-up structure.

The use of shake-up structure arising from  $\pi \rightarrow \pi^*$  transitions to indicate the presence of unsaturation will be referred to in later chapters.

## 2.6. Valence Band Studies of Polymers

Structure and bonding in polymers is generally studied via the shifts in core binding energies which reflect the difference in valence electron distributions. When considering the direct investigation of valence levels by ESCA two distinct disadvantages compared with corresponding ultra-violet spectroscopy (UPS) measurements are apparent. Firstly, the cross-sections for photoionisation are much smaller than in UPS. Secondly, the inherent line-widths are much larger (e.g.  $\sim 5$  meV for He(I) versus  $\sim 700$  meV for  $\text{Mg}_{k\alpha_{1,2}}$ ).

Generally the valence levels of polymers have been studied by ESCA, and the band spectra of polymers are often useful finger-prints for a given polymer structure.<sup>98,121,137-138</sup>

Pireaux and co-workers have measured the valence band spectra for a variety of polymers, and the results contain valuable information related to the substituents effect, e.g. hydrocarbon based polymers,<sup>132,139</sup> fluoro-substituted polymers,<sup>140</sup> chlorine-containing polymers and oxygen-containing polymers.<sup>66,131</sup> Valence band spectra may also be used to study structural isomerism conductivity and adhesion of commercial polymers.<sup>141</sup>

## 2.7. Auger Parameters

Since the kinetic energies of the Auger electrons are determined by the difference in energy between the initial ion and the final ion in the transition, and since the chemical shifts of Auger and photoelectrons are different;

the Auger parameter, (difference in kinetic energy between the Auger and photoelectrons),<sup>145</sup> as a function of chemical state is very accurately determinable. When line energies of the most intense photoelectron peak are plotted against those of the most intense (sharp) Auger peak for compounds of the same element, the resulting two-dimensional chemical state provides an exceptionally fine technique for identifying chemical states.<sup>142-145</sup> Many of the chemical state plots relevant to polymers have been published.<sup>144</sup>

Recent studies extended the Auger parameter and provide Auger lines in reasonable intensity.<sup>146-148</sup>

For a limited number of substituted polymeric systems containing 2nd and 3rd row atoms (e.g. Cl, Br etc.), the observation of intense direct photoionisation and Auger peaks allows the determination of a charge independent Auger parameter.<sup>143-144</sup>

## 2.8. Sample Charging Effects

Sample charging of insulators has been considered as something of a disadvantage in ESCA. Since most polymers by their very nature are insulators under the conditions of ESCA experiment, energy referencing requires a knowledge of sample charging. Detailed studies<sup>149-150</sup> have shown that under a given set of instrumental conditions the shift in energy scale associated with sample charging phenomena is characteristic of the surface structure, and therefore constitutes a useful information level.

The effects of sample charging induced by using a



monochromatic source (e.g.  $Al_{k\alpha_{1,2}}$ ), is in general alleviated by either of two instrumental methods. The first involves the use of electron flood guns while, as an alternative, the second uses a low pressure mercury lamp to create a low energy electron flux from the walls of the sample chamber, by an ultra-violet photoemission process. The use of an "ultra-violet flood gun" improved matters considerably for the monochromatic source, providing a means of effectively "tuning" the sample charging.<sup>149</sup>

## 2.9. Dynamic Studies

### 2.9.1. Surface Modification of Polymers

The modification of a polymer film by either chemical or physical agents usually involves a change in structure and bonding which may permeate through surface, subsurface and bulk giving rise to inhomogeneities in these regions. The possibility, therefore, exists of employing ESCA for analytical depth profiling in which surface, subsurface and bulk may be differentiated. Nowhere in the field of polymer chemistry is ESCA more appropriate than in the study of surface modifications.

The ESCA technique has improved the level of understanding at a fundamental level in many of these modifications and we briefly consider a few representative examples.

#### (i) Modification by plasma and Corona discharge

The modification of polymer surfaces by electrical discharges (RF, Microwave, Corona) excited in a variety of

gases as a technique to improve their surface properties has been the subject of extensive research in both industrial and academic laboratories.<sup>119</sup>

The major virtues of these techniques are in producing profound changes in the surface properties of the polymer; the properties of the bulk material remain unchanged.<sup>151</sup>

(a) Corona-discharge treatment

The Corona discharge treatment of polymeric materials is one of the most widely used techniques for surface modification.<sup>152-153</sup> ESCA has been used by Millard and co-workers to investigate aspects of the surface treatment of wool fibres.<sup>154-155</sup> The Corona treatment in air allows the materials conveniently to be surface oxidised for improvement of printability, wettability and adhesive bonding.<sup>156-158</sup> Such a discharge treatment of polyethylene, polypropylene and polystyrene was carried out by Clark and co-workers.<sup>89,119,133,158</sup>

Briggs and co-workers<sup>159-162</sup> have used ESCA to examine Corona discharge treat of polyethylene (low density and high density), polypropylene and polyethylene terephthalate. The results suggested similar oxidised surfaces of PE and PET, and the change in surface properties have been followed as a function of ageing time.

Recent works<sup>163</sup> have investigated the surface changes in polyethylene (low density and high density) treated by Corona discharge in air, oxygen, nitrogen and argon by means of ESCA, the spectra show increases in the oxygen functionality of the surface in all the gases. In Chapter

seven, data will be presented in some detail showing that Corona treatment lowers the level of nitrogen functionality in the surface regions of low density polyethylene (LDPE) (low slip and high slip agent). Figure 2.4. presents the core level of LDPE high slip agent to show the surface before and after the Corona treatment.

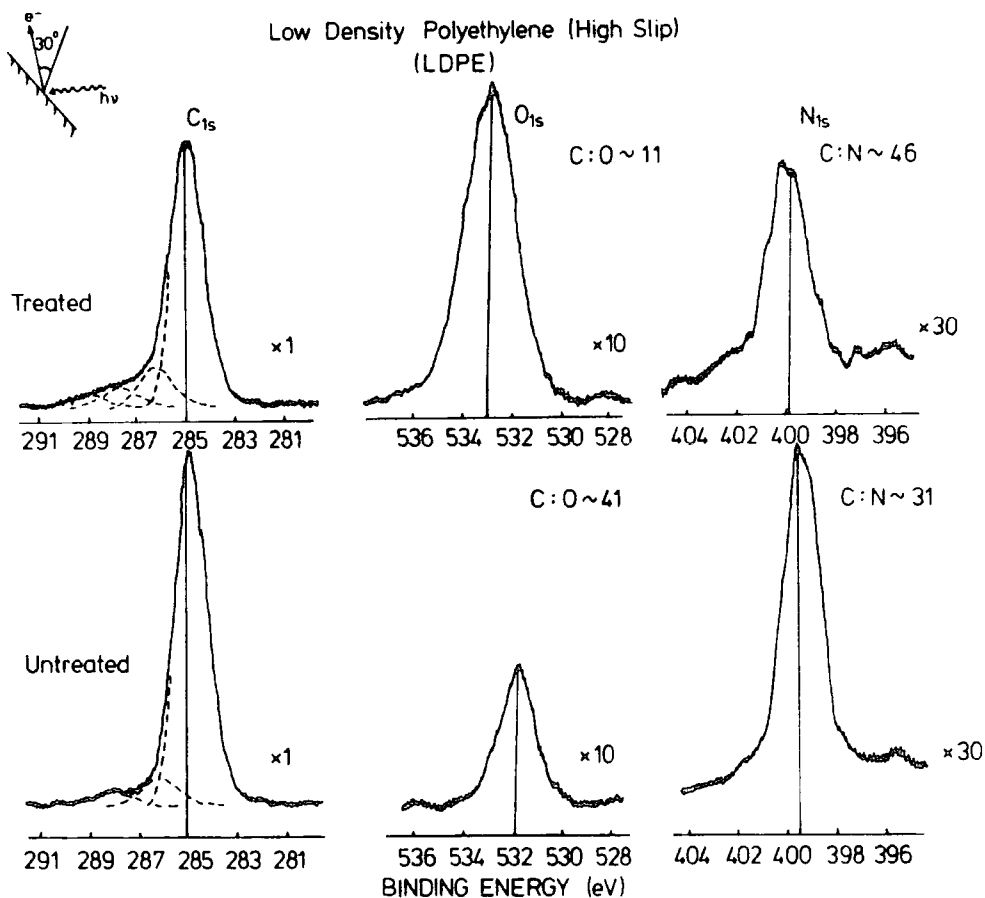


Figure 2.4. The  $C_{1s}$ ,  $N_{1s}$  and  $O_{1s}$  core levels of low density polyethylene (high slip agent) before and after Corona discharge treatment.

(b) Inert gas plasmas

The interaction of polymers with inductively coupled RF glow discharges excited in a variety of inert gases (He, Ne, Ar, Kr) has been investigated by means of ESCA.<sup>89,159,164-165</sup>

These investigations give a great deal of insight into many of the aspects of the ESCA experiments which have been outlined in a previous section (2.3.). The studies clearly demonstrated that a great deal of extra information can be obtained, qualitatively and semi-quantitatively by monitoring the angular dependence of the components of the relevant core level spectra.<sup>89</sup> The relative reactivities of particular structural features in the polymer, for example  $\text{CH}_2$  versus  $\text{CF}_2$ , may be obtained from the ESCA spectra by monitoring the relative intensities of the signals due to CF and CH.

***The effect of an Argon glow discharge on the  $\text{C}_{1s}$  spectrum of 48:52 ethylene-tetrafluoroethylene copolymer.***

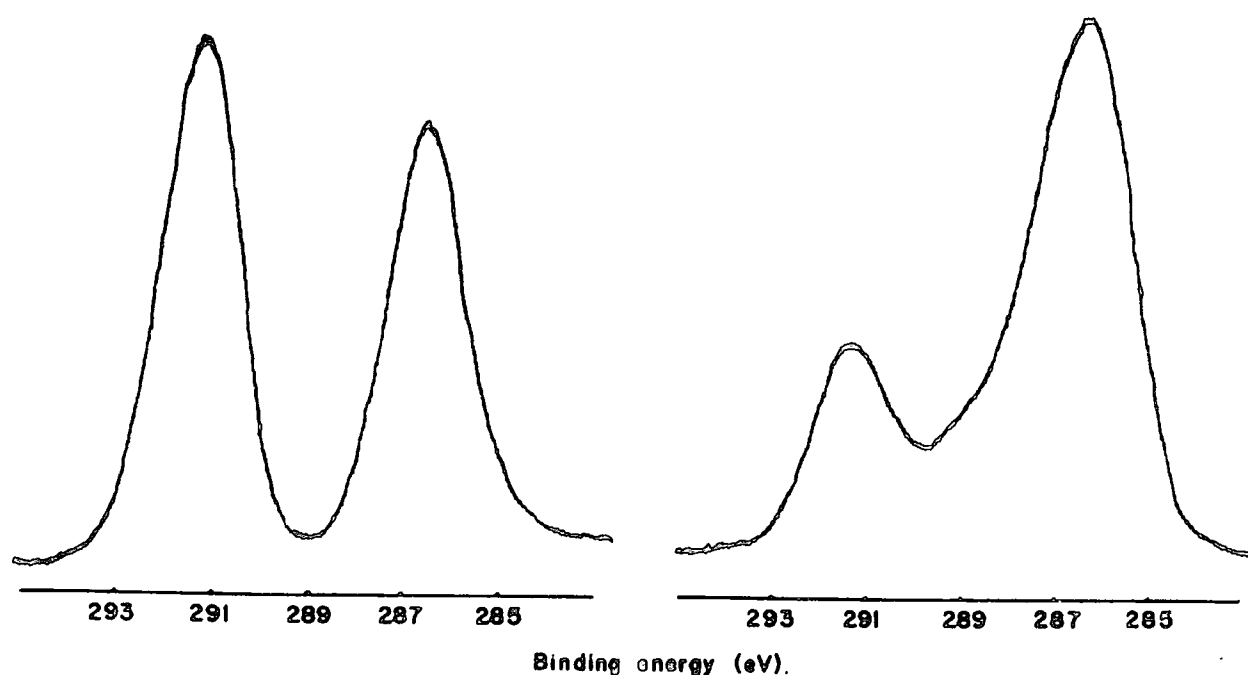


Figure 2.5.  $\text{C}_{1s}$  spectra of the ethylene-tetrafluoroethylene copolymer exposed to a discharge in Ar.

Typical core level spectra obtained in these studies are displayed in Figure 2.5. and Figure 2.6.

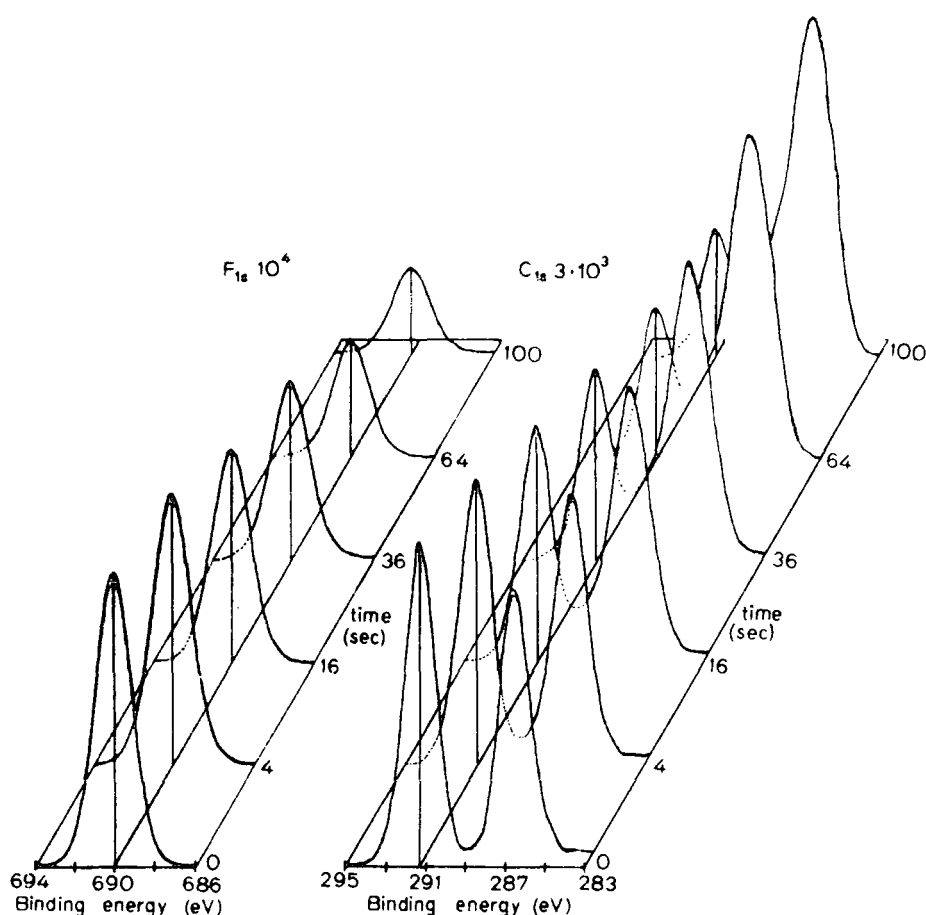


Figure 2.6. Modification of an E-TFE copolymer by a discharge excited in argon as a function of time.

(c) Oxygen plasmas

An area of considerable technological and industrial interest is the surface oxidation of polymers. In the particular case of oxygen plasmas, within the past few years several accounts have appeared on the use of ESCA to study the surface oxidation of polymers by oxygen containing radio-frequency plasmas.<sup>119,123</sup> Clark and Dilks<sup>133</sup> provided an example of the great applicability of ESCA coupled to glow discharge techniques in the oxygen plasma treatment of polyethylene (high and low density), polypropylene and polystyrene. Figures 2.7. and 2.8 show the core levels

of polyethylene and polystyrene before treatment and after exposure to an oxygen plasma respectively, these indicate that the reaction is rapid and is essentially complete after approximately five seconds at 0.2 torr and 0.4W, as far as the change in surface composition revealed by ESCA is concerned. However, at lower power (0.2 torr

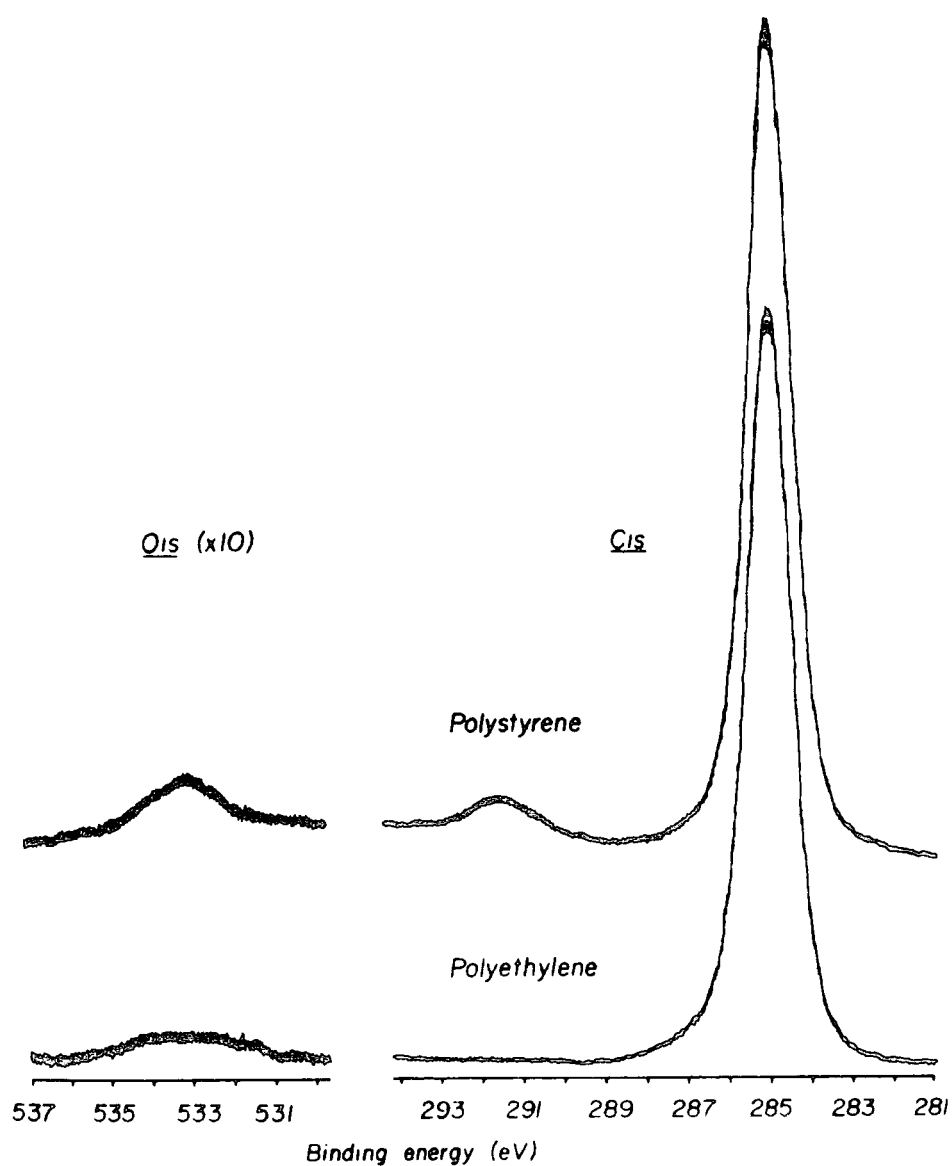


Figure 2.7. ESCA core level spectra of untreated samples of polyethylene and polystyrene films.

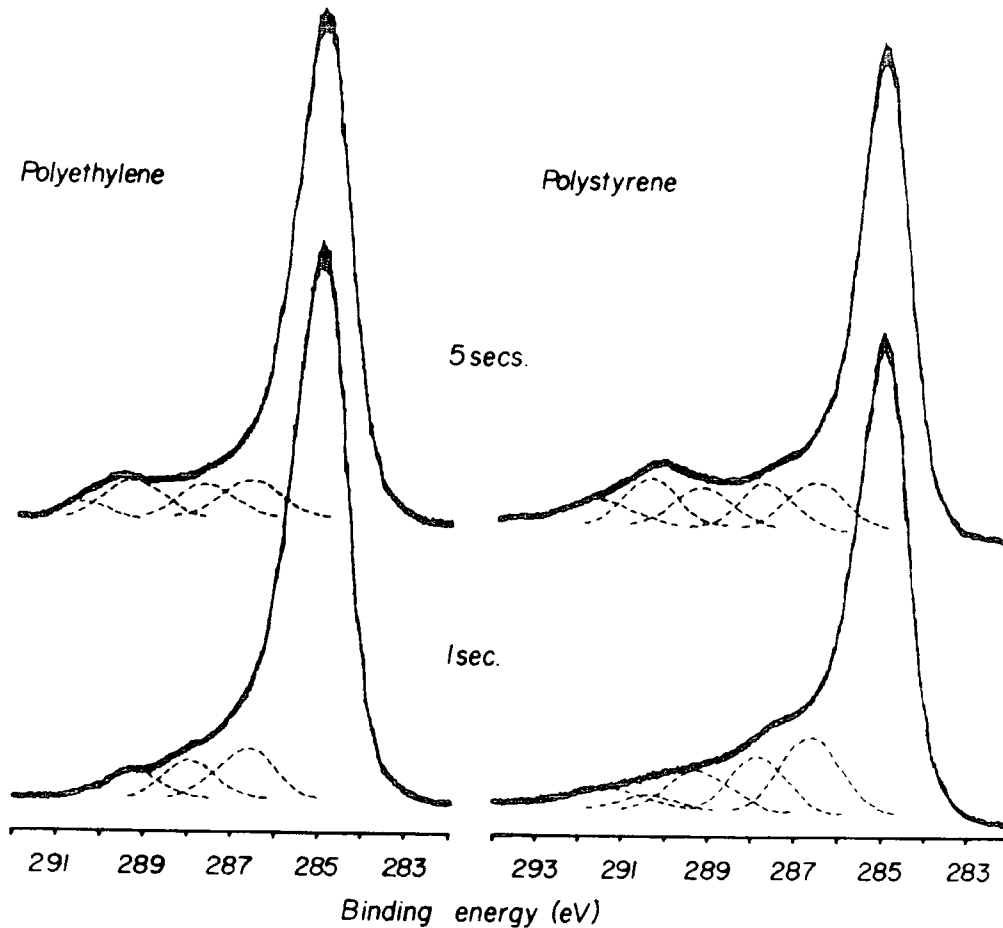


Figure 2.8.  $C_{1s}$  spectra for examples exposed to an oxygen plasma (0.2 torr, 0.4W) for 1 and 5 secs.

and 0.1W), the reaction will be slower and is a function of time as is evident from Figure 2.9., which presents the spectra of treated polyethylene films at 0.2 torr and 0.1W. It is evident that the components of the  $C_{1s}$  reach a constant intensity after approximately 16 seconds.

In a recent work,<sup>166</sup> it was shown that selective surface modifications of semi-conductors may also be accomplished by plasmas excited in both oxygen and hydrogen.

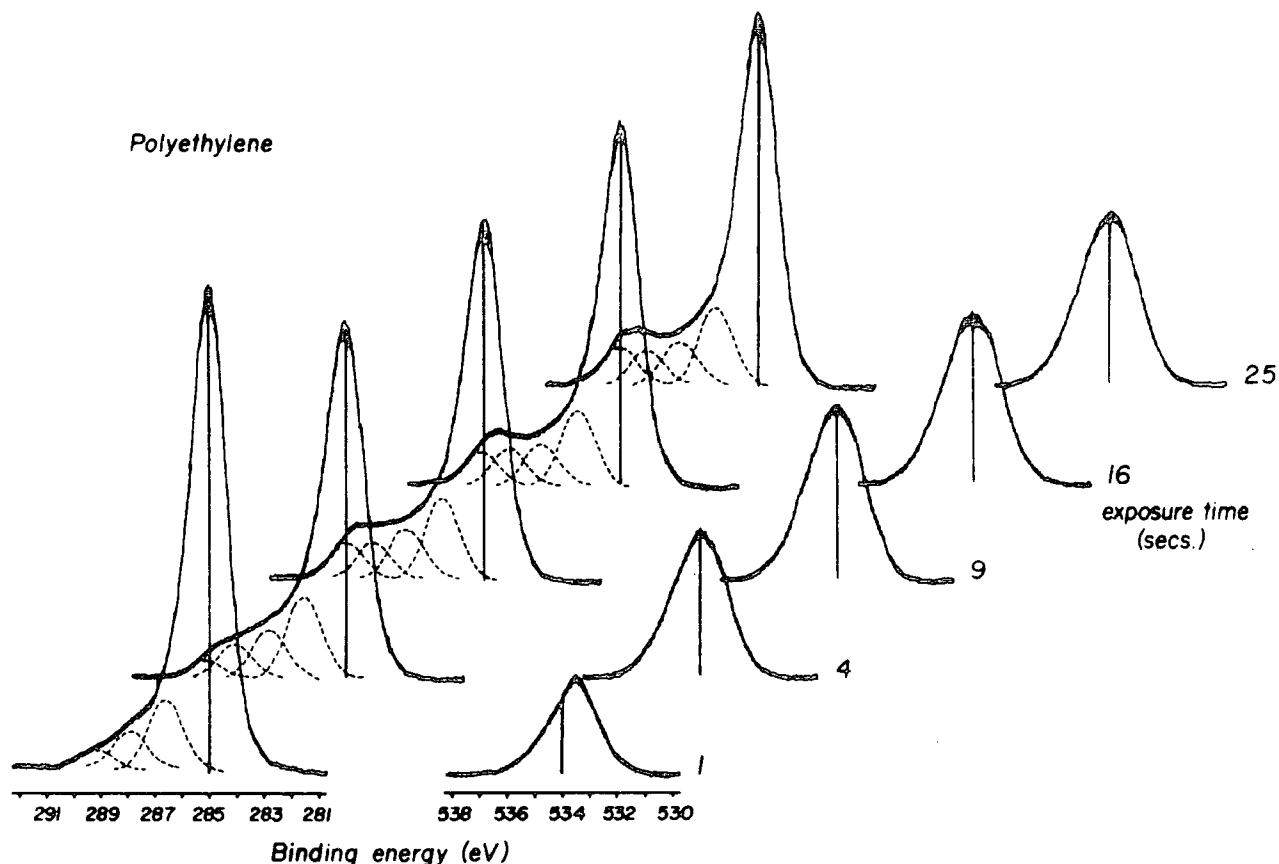


Figure 2.9.  $C_{1s}$  and  $O_{1s}$  spectra of polyethylene versus time of exposure to an oxygen plasma (0.2 torr, 0.1W).

More recent work investigated the changes in polymer films of high-density polyethylene (HDPE), polystyrene (PS), polyethylene terephthalate (PET) and Bisphenol-A polycarbonate. In all cases the oxygen plasma treatment gave rise to extensive oxygen functionalisation, with Bisphenol-A and PET exhibiting similar reactivities.

(ii) Modification by chemical treatments

Wet chemical treatments of polymers have received a great deal of attention in the literature. The interaction of polymers with chemically reactive species, typical examples



which will be considered include, oxidation (by interaction with molecular oxygen, and oxidising agents such as dichromate) to enhance its wettability and adhesion. Halogenation (acid and alkali treatments), sulphonation (concentrated or fuming sulphuric acid, or chlorosulphonic acid). The nitration and denitration by different mixtures of  $H_2SO_4$  and  $HNO_3$ .

Since the chemical reaction is initiated at the surface and is followed by diffusion into the bulk, the initial stages of reaction produces complex inhomogeneous systems. ESCA really comes into its own as a spectroscopic tool to study these complexities.

(a) Surface oxidation and sulphonation

In this section, we present illustrations of how ESCA may be used to detect the early stages of the oxidation and sulphonation treatment of polymers. In this connection it is important to point out that most commercially fabricated polymer samples exhibit a greater or lesser extent of surface oxidation which is not detected by other techniques.<sup>116</sup> As a simple example of how readily surface oxidation may be detected, a series of polyalkyl acrylates were measured, and the results obtained from the  $O_{1s}/O_{2s}$  ratios, which have widely different mean free paths, indicate that oxidation occurs primarily in the surface.<sup>66</sup>

Briggs and co-workers<sup>160,162,168</sup> have reported on ESCA investigations of low density polyethylene (LDPE), high density polyethylene (HDPE) and polypropylene (PP) films that were treated in sulphuric acid and chromic-sulphuric acid.

By studying both core and valence levels, several tentative conclusions may be drawn. Thus, after very mild treatment with chromic-sulphuric acid, the results indicate a substantial oxidation of LDPE, HDPE and PP. Modification by treatment with concentrated sulphuric acid was much slower and the observation of a high binding energy component in the  $S_{2p}$  levels confirms the presence of  $-SO_3H$  structural features, this indicates substantial sulphonation and oxidation. For the conditions used with both treatments the depth of chemical modification was less than  $90\text{\AA}$ . ESCA and MATR showed that as treatment time increase the oxygen functionalisation changes from keto-carbonyl to carboxyl (acid and ester).

Recent work has included ESCA investigations of polyethylene films treated in concentrated sulphuric acid at  $100^\circ\text{C}$  as a function of time. The ESCA data reveal that; the treatment increases the oxygen functionality, however, after 20 minutes treatment there is a slight decrease. The presence of the oxygen functionality in the ESCA spectra is due to the introduction of  $SO_3H$  group and this group reaches a maximum after 20 minutes, then slightly decreases.

(b) Surface fluorination

The interaction of polymers with various species are often diffusion controlled and hence lead to considerable inhomogeneities in structure and bonding in proceeding from surface to subsurface and into the polymer bulk. A particularly apposite example in this regard is provided by

the ESCA investigation of the surface fluorination of high density polyethylene carried out by Clark and co-workers.<sup>129,156</sup> The sensitivity of the technique is shown by the form of the core levels of samples that have been treated with gaseous fluorine (10% fluorine with nitrogen as diluent) for  $\frac{1}{2}$  sec. and 30 secs. respectively. The detailed analysis of the kinetics by ESCA produced a good description of the early stage of the fluorination process. From this study, estimates of electron mean free paths in the resultant polymer surface were made. It should be evident from this study that the time dependence of the chemical modification of polymers particularly in the initial stages may readily be followed by ESCA.

(c) Nitration and denitration

ESCA has been successfully<sup>169-172</sup> employed to interrogate the polymer surface during chemical reaction of the nitration and denitration of cellulose.

Figure 2.10a., shows the degree of substitution (DOS)

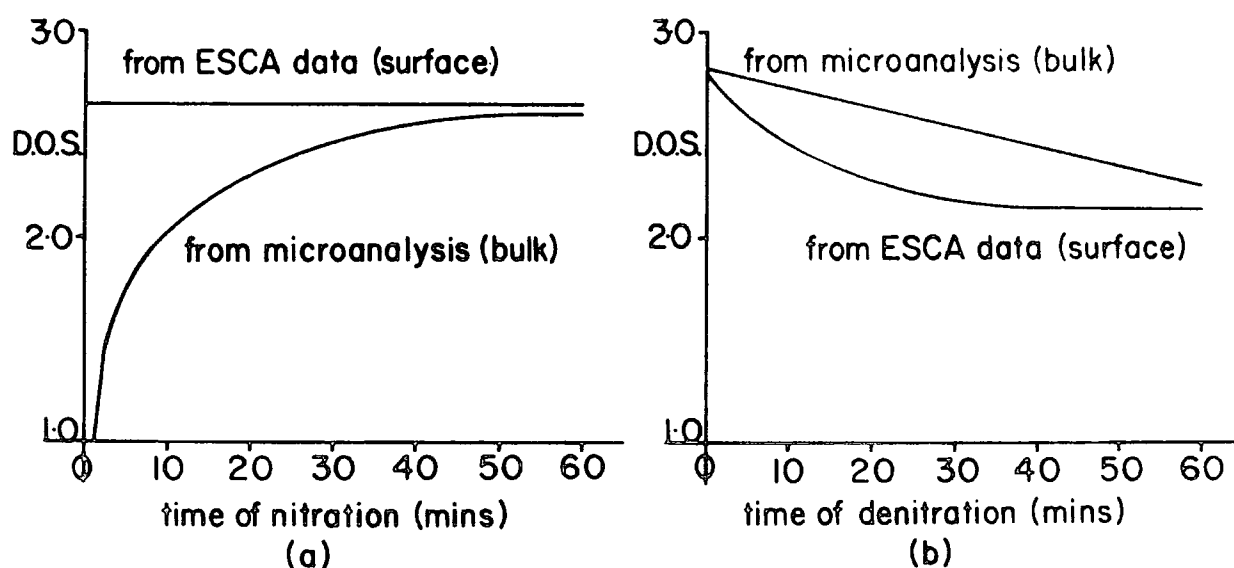


Figure 2.10. (a) Degree of substitution of the surface and in the bulk of a cellulose sample versus time of nitration.  
 (b) Degree of substitution of the surface and in the bulk of a nitrocellulose sample versus time of denitration.

derived from the ESCA data and microanalytical data for samples treated for various times at room temperature. The reaction at the surface of the fibres is fast and the maximum observed degree of substitution is reached within seconds. This type of analysis has been repeated for several nitration acid mixes, and in each case a similar situation was found.<sup>172</sup>

Figure 2.10b. shows that the relationship between surface and bulk reaction is less straightforward in the case of denitration.<sup>172</sup>

More recent work<sup>173</sup> of the nitration and denitration of cellulose has been carried out at lower nitration temperatures. At 10°C the DOS is similar to that at room temperature at -25°C it substantially decreases to a lower value of  $\sim 1.2$ .

#### 2.9.2. Migration and Segregation Phenomena

The migration and segregation of small molecules at polymer surfaces can be monitored by intensity changes of appropriate core levels as a function of take-off angle. A particularly intriguing application of this genre involves the migration of the low molecular weight silicone<sup>121</sup> material used as a release agent in double sided Scotch tape commonly employed for mounting purposes in ESCA experiments.

A priori migration of low molecular weight material could conceivably occur by two distinct mechanisms and this is indicated schematically in Figure 2.11. On the left hand side migration from one surface of a polymer to the other is by bulk migration involving permeation through the bulk. The alternative involves migration along the surfaces as indicated schematically on the right hand side of the figure.

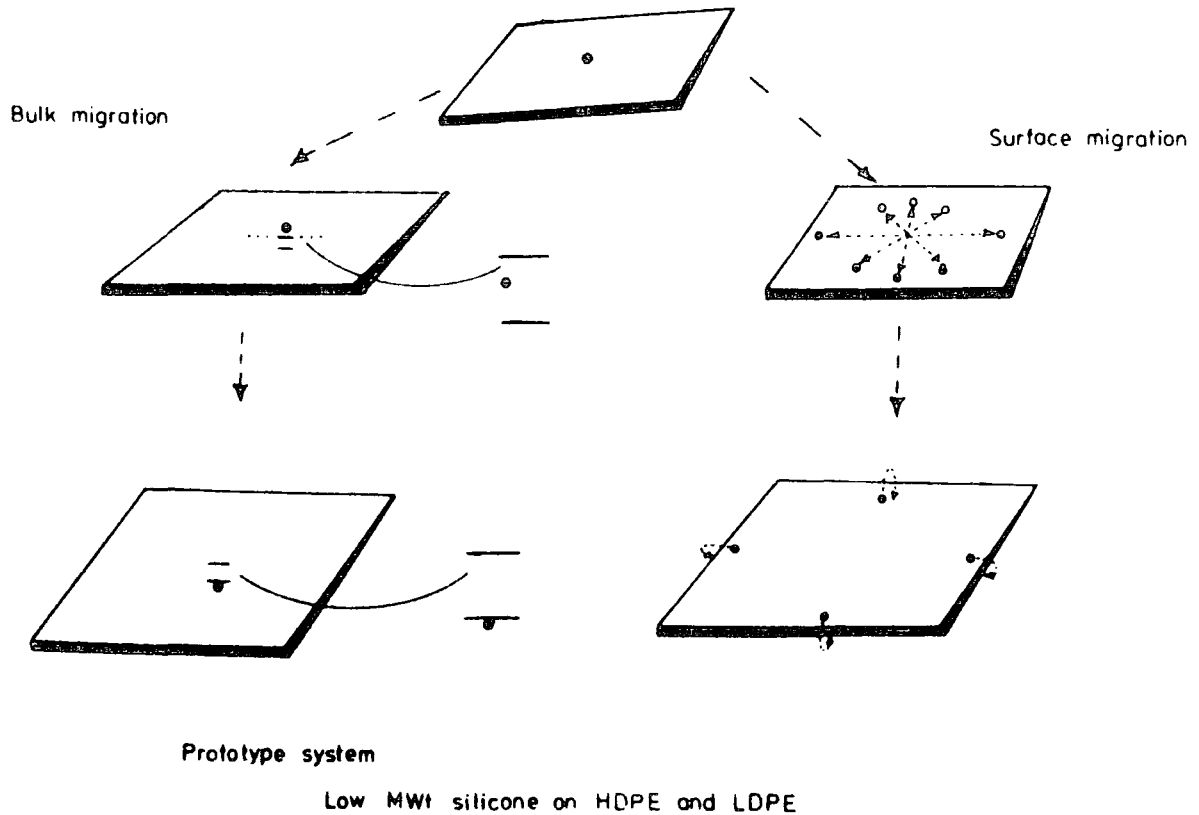


Figure 2.11. Migration phenomena: possible extremes for migration of low-molecular weight materials.

To demonstrate<sup>121</sup> the migration of the silicon material from the Scotch tape, a piece of tape was attached to a strip of high and low density polyethylene, the ESCA data after a period of 10 days show the potential for studying the mode of migration of small molecules both along and through surfaces and also point to the danger of long term exposure of samples to Scotch tape as might be used for example in securing samples for transporting purposes.

In Chapter seven, however, ESCA data illustrates the migration of nitrogen functionalities from the polyurethane adhesive into the laminate polyethylene (low and high slip) and polyethylene terephthalate surface regions. From the C:N stoichiometry (at different take-off angles) substantial

segregation of slip agent is evident on the surface of polyethylene. However, this will be covered in greater detail in Chapter seven.

### 2.9.3. Polymer degradation

Since all solids communicate with the universe by way of their surfaces, it is clear that any degradative procedure which depends intimately on the chemical, physical, electrical and mechanical properties of the surface regions is in principle directly amenable to investigation by ESCA. The environmental degradative procedures involving surfaces of polymeric materials are of considerable industrial and technological importance. In particular environmental degradation is of interest.

#### Weathering phenomena

The changes in structure of polymers on exposure to environmental conditions, (sunlight, precipitation and wind) causes degeneration of useful properties (e.g yellowing of fabrics and embrittlement of plastics). As the relative photon flux and partial pressures of oxygen and water at the surface will be higher than that in the bulk, it would be somewhat surprising if the reactions at the surface were entirely representative of those in the bulk.

The application of ESCA<sup>174-175</sup> in this area has a wide-ranging potential in the investigation of polymer degradation. Clark and Dilks<sup>176-177</sup> have investigated high density polyethylene exposed for about three months from February to May 1978 in San Jose, California. The sample exposure was effected under three sets of conditions: (a) shaded from

the sunlight, (b) under a 1 mm. thick pyrex glass slide and (c) fully exposed. In all cases extensive oxidative functionalisation of the surface occurred, and the  $O_{1s}/C_{1s}$  ratios increased to 8%, 24% and 50% for samples a, b and c respectively. These initial studies were extended by Clark and Munro<sup>178-180</sup> to compare natural weathering with controlled model exposures. As an example, polystyrene films were weathered in Dhahran, Saudi Arabia, for which the relevant  $C_{1s}$  core levels are displayed in Figure 2.12. This indicates an extensive oxygen incorporation in the surface occurred as is evident from the appearance of components arising from  $\underline{C}-O$ ,  $\underline{C}=O$  and  $O-\underline{C}=O$  functionalities on exposure. These observed changes were found to reveal similar trends with those in model studies.<sup>180</sup>

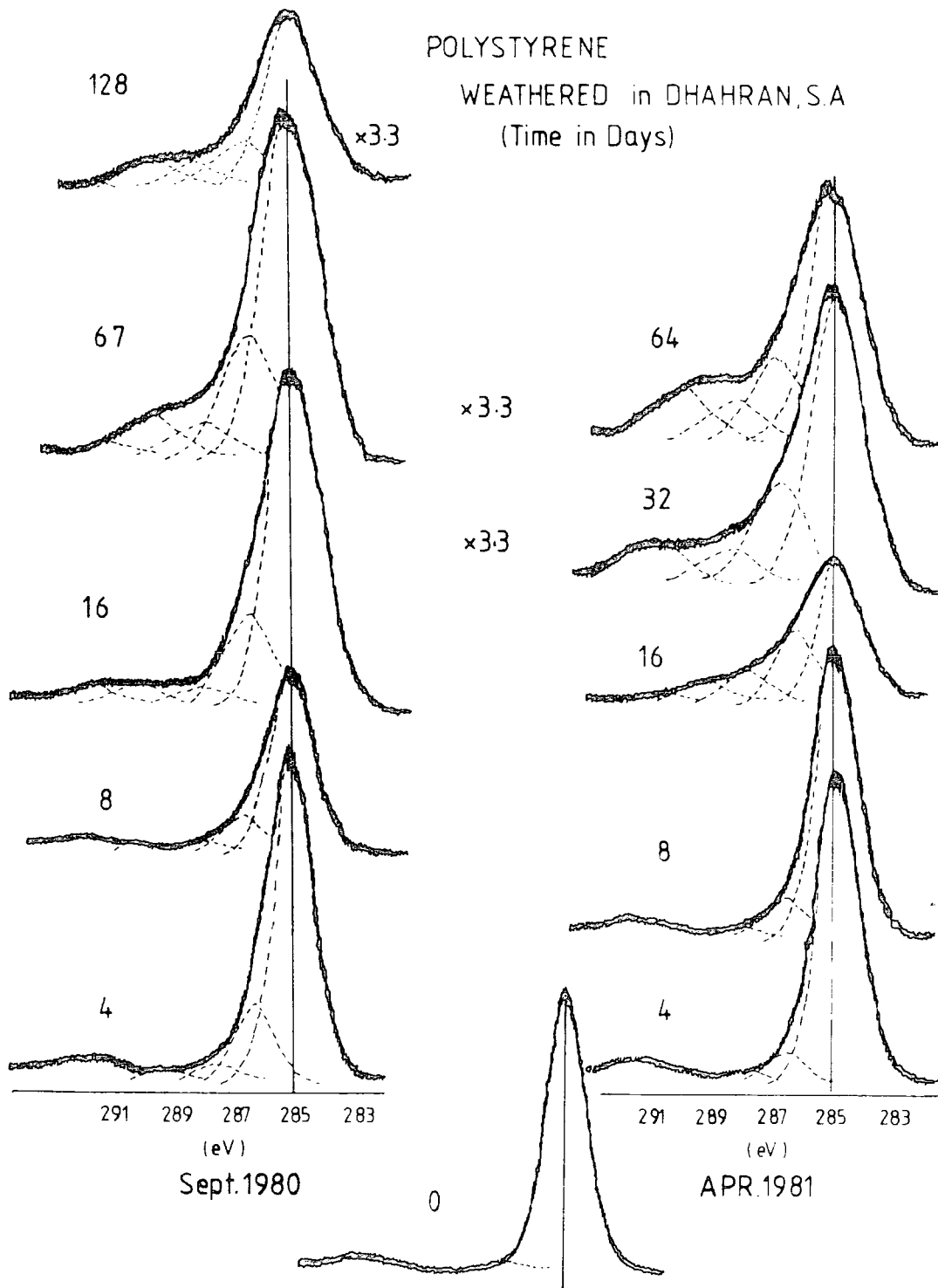


Figure 2.12.  $C_{1s}$  spectra of polystyrene weathered in Dhahran, S.A. (time in days).



#### 2.9.4. In-situ Polymerisation

The study of polymers prepared immediately prior to investigation has much to commend since such preparations often remove the possibility of surface contamination or reaction after preparation. Indeed, in many cases the polymers may not lend themselves readily to preparation by any other technique.

Later chapters in this thesis will deal with glow discharge polymerisation of organic molecules in some detail for in-situ polymerisation, whilst in Chapter three an investigation into the polymers produced by in-situ pyrolysis polymerisation of paracyclophane to determinations of electron mean free path as a function of kinetic energy in polymers will be described.

CHAPTER THREE

CHAPTER THREE

ELECTRON MEAN FREE PATHS AS A FUNCTION OF  
KINETIC ENERGY: A SUBSTRATE OVERLAYER  
INVESTIGATION OF POLYPARAXYLYLENE FILMS  
ON GOLD USING A  $Ti_{k\alpha}$  X-RAY SOURCE

Abstract

Electron mean free paths ( $\lambda$ ) have been determined for in-situ deposited polyparaxylylene by the substrate overlayer technique employing a  $Ti_{k\alpha_{1,2}}$  X-ray source ( $h\nu = 4510$  eV). By monitoring the attenuation of signals arising from the  $Au_{4f, 4d, 4p, 3d}$  and  $3p$  core levels excited by the  $Ti_{k\alpha}$  X-ray source and the  $Au_{4f}$  and  $4d$  levels excited by  $Cu_{L\alpha}$  X-rays ( $h\nu = 929.7$  eV) of the substrate mean free paths have been determined in the kinetic energy range from  $\sim 4430$  eV to  $\sim 590$  eV. The present results are compared with those previously reported at lower kinetic energies using  $Mg_{k\alpha_{1,2}}$  and  $Al_{k\alpha_{1,2}}$  photon sources. The results indicate that at kinetic energies of  $\sim 4000$  eV the typical sampling depth using the  $Ti_{k\alpha}$  source is  $\sim 150\text{\AA}$ .

### 3.1. Introduction

The past decade has witnessed an explosive growth in the application of ESCA to a wide variety of problems in both fundamental academic studies in surface science and applied projects of direct relevance to industry and technology. One of the most systematically developed areas has been the application of ESCA to the study of polymer surfaces and a substantial background is now available for the quantification of experimental data.<sup>98</sup> One of the most important aspects of this quantification procedure is a knowledge of electron mean free paths as a function of kinetic energy. For the most part the direct determination of electron mean free paths has been a neglected area of research and most attempts at quantification of data have generally relied on assumed values for a given material, with an empirical dependence of the mean free path on kinetic energy.<sup>181</sup>

The particular value of the direct investigation of the structure, bonding and reactivity of surface by means of ESCA in the particular case of polymers has been documented extensively in the literature;<sup>93,98,121</sup> polymers represent one class of materials for which detailed information is available, albeit over a limited kinetic energy range. Detailed studies by means of substrate overlayer techniques have been documented for both linear and cross-linked polymeric systems,<sup>93,99</sup> the main conclusion being that there is little dependence on structure for the mean free paths derived, which are somewhat comparable to those which

have been measured for typical metals and semi-conductors.<sup>93,99,182-183</sup> By contrast, for highly ordered organic overlayers of either a polymeric or monomeric nature, comparable studies<sup>183</sup> have shown that mean free paths depend distinctively on structure, and this has been rationalised on the basis of both packing density and channelling phenomena.<sup>183</sup>

Since the majority of ESCA investigations have been carried out with instrumentation involving either or both of  $\text{Al}_{\text{K}\alpha_{1,2}}$  and  $\text{Mg}_{\text{K}\alpha_{1,2}}$  it is clear that a necessary pre-requisite to the quantitative development of the technique is a knowledge of escape depths for electrons photoemitted from the commonly observed core levels. Recent work<sup>169,184</sup> has commented on the great potential of the use of harder X-ray sources (e.g.,  $\text{Ti}_{\text{K}\alpha}$ ) for extending the scale of depth profiling by means of ESCA, and it is interesting that the absence of data for mean free paths appropriate to this higher photon energy ( $h\nu = 4510 \text{ eV}$ ) is notable not only for polymers but for solids in general.<sup>98-99,121,181-182</sup> The considerable extension in the scope of depth profiling (particularly for fibrous or powdered samples, for which angular-dependent studies are inappropriate) provided by harder X-ray sources is of great importance in the study of polymeric systems, and a detailed study of electron mean free paths as a function of kinetic energy for the  $\text{Ti}_{\text{K}\alpha}$  X-ray source would therefore seem to be particularly apposite at this time.

Therefore, this chapter presents the investigation of

electron mean free paths for the kinetic energy range  $\sim$  600 - 4430 eV by means of substrate overlayer techniques involving gold substrates and in-situ deposited films of polyparaxylylene.

### 3.2. Experimental

The substrate-overlayer technique provides, in principle, the most straightforward and reliable method of measuring electron mean free paths, the experimental difficulties in implementation are considerable.<sup>185</sup>

For a variety of reasons which will become apparent, the study to be reported in this chapter involved the in-situ production of poly(p-xylylene) films by polymerisation of p-xylylene precursors generated in a pyrolysis flow system.

The major advantages of employing the synthetic route involving [2.2.]p-cyclophane starting materials may be summarized as follows:

- (1) The pyrolysis under appropriate conditions yields quantitative conversion to the polymer with no side reactions;<sup>186-188</sup>
- (2) Since the method allows close control of the rate of production and deposition rate of the intermediate p-xylylenes, uniform thin films may readily be produced;<sup>186-188</sup>
- (3) The thin films produced in this way, as opposed to other methods (e.g., solvent casting), are essentially free of impurities (e.g., solvent

impurities, antioxidants, catalysts, filler, anti-blocking agents, etc.);<sup>186-188</sup>

- (4) The poly(p-xylylene) polymers produced by this route have been well characterized in the literature;<sup>189-190</sup>
- (5) The films can be prepared in-situ in a sample chamber directly attached to the spectrometer source, which obviates any possibility of contamination which might arise if the samples were prepared elsewhere and then transferred to the spectrometer.<sup>191</sup>

A schematic of the synthetic route is shown in Figure (3.1.), where the sublimation and pyrolysis temperatures are in the range indicated.

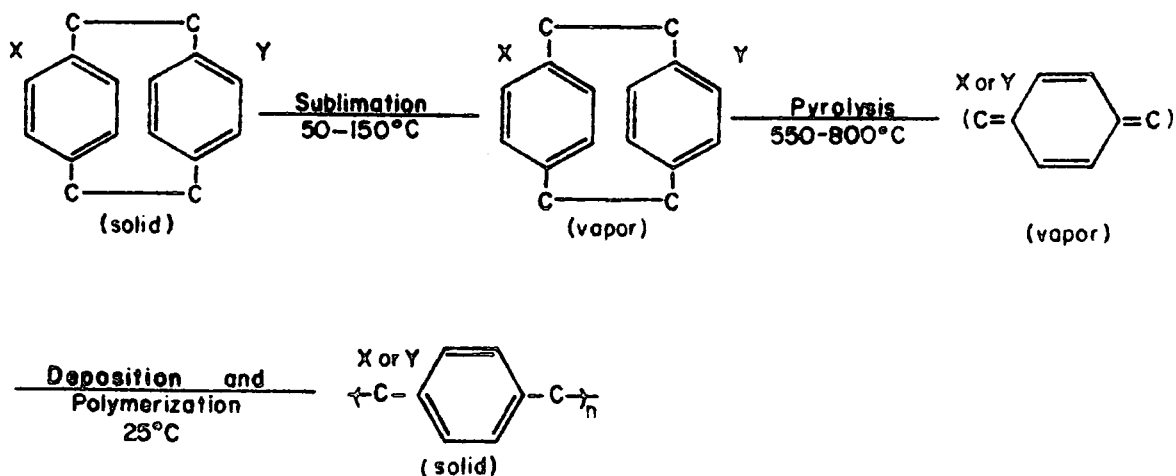


Figure 3.1. A schematic of the polymerisation process from the [2.2]paracyclophane to the polyparaxylylene.

The starting material [2.2]p-cyclophane was obtained from Union Carbide Corporation, Bound Brook, U.S.A. The starting material was recrystallised from appropriate solvents a minimum of three times, and characterised by VPC, melting points and by ultra-violet and infrared spectroscopy;<sup>13</sup> the purity was > 99.5%.

The final design of the apparatus employed in this work is shown in Figures 3.2a. and 3.2b. utilized the flexibility of the insertion lock system of the custom-designed Kratos ES300 spectrometer.

The purified [2.2]p-cyclophane starting material was placed in the temperature-controlled sublimation end of  $\frac{1}{2}$ " diameter quartz tube ca. 24" in length. The sample  $\sim$  2 g., was sublimed into the pyrolysis zone which extended over a length of  $\sim$  12", starting some 6" from the closed end of the tube. The Lindberg (Type 55035A, Lindberg, Watertown, Wis.) pyrolysis furnace enabled accurate control of the temperature profile over the pyrolysis zone. The post-pyrolysis zone of the quartz tube was connected via greaseless coupling to  $\frac{1}{2}$ " flexible tubing, (Cajon Corporation, Cleveland, Ohio) which lead to the deposition chamber, constructed from a stainless steel 70 mm. conflat flanged, four way adaptor, (Vacuum Generators, Sussex, England). This chamber could be isolated from the pyrolysis tube by means of a greaseless valve. Tubing between the pyrolysis zone and deposition chamber was maintained at a constant temperature  $\sim$  80°C, using electrical heating tape. The deposition chamber was mounted directly onto the spectrometer insertion lock





Figure 3.2a. The apparatus shown attached to the insertion lock system of the Kratos ES300 spectrometer.

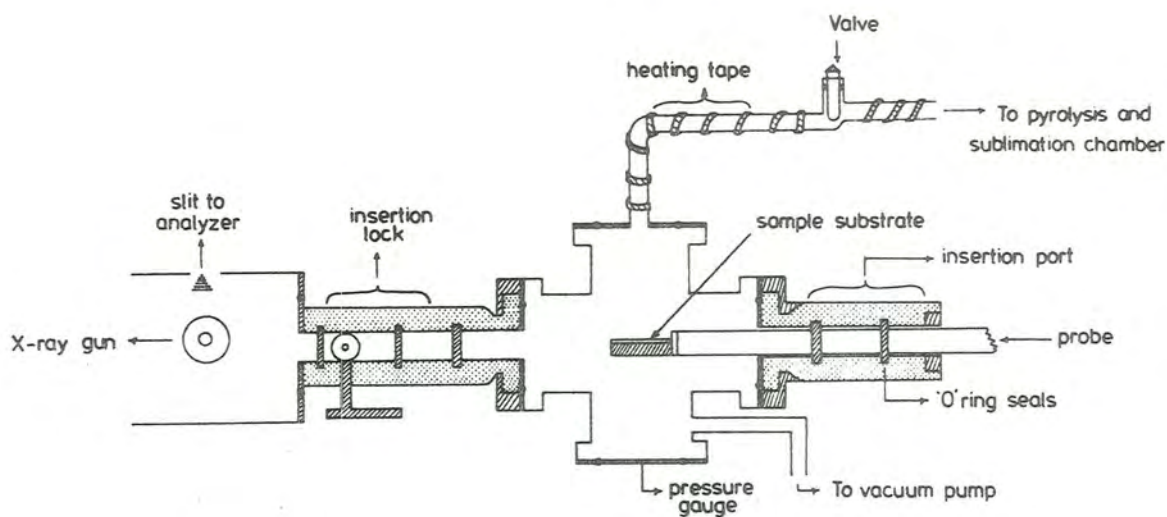


Figure 3.2b. Schematic diagram of deposition chamber directly attached to the ESCA insertion lock system for the preparation of in-situ deposited polyparaxylylene films.

system by means of a double sided flange fitted between the insertion lock edge and the deposition chamber, and sealed using a Viton 'O' ring. The insertion port on the deposition chamber contained 2 teflon omniseal 'O' rings. The gold foil substrate was mounted on the probe tip so that it was in electrical contact with the spectrometer. Pumping for the system was provided by a two stage rotary pump (Edwards ED50, Edwards High Vacuum, Crawley, England).

In a typical deposition the apparatus was pumped down to a pressure of  $\sim 5 \times 10^{-2}$  torr. The sublimation heater was then placed over the closed end of the quartz tube containing the [2.2]paracyclophane, with appropriate adjustment of sublimation temperature  $\sim 180^{\circ}\text{C}$  and the pyrolysis temperature  $\sim 600^{\circ}\text{C}$ . The polyparaxylylene films were deposited onto the gold substrate by opening the valve separating the deposition region from the pyrolysis tube. The deposition thicknesses were controlled approximately by timing, the deposition being evident by a higher pressure  $\sim 8 \times 10^{-2}$  torr. When a film of appropriate thickness had been deposited the pyrolysis chamber was valved off from the deposition chamber, and the sublimation heater removed. To minimise polymer deposition in the insertion lock roughing system of the spectrometer, 5 mins. were allowed to elapse before sample entry into the spectrometer sample chamber.

The absolute calibration of film thickness was carried out after each deposition by investigation of the signal attenuation of the  $\text{Au}_{4f}$  levels employing the  $\text{Mg}_{k\alpha_{1,2}}$  photon

source using the previously<sup>93</sup> determined mean free path for photoelectrons of K.E. 1170 eV of  $22\text{\AA}$ . Spectra were recorded at two different take-off angles ( $30^\circ$  and  $50^\circ$ ) and since the signal intensities proved to be very low for photoemission from the  $C_{1s}$  level of the polymer overlayer with the  $Ti_{k\alpha_{1,2}}$  photon source and since extended exposure times to this source also showed evidence of radiation damage attention was focussed in each experiment on a single substrate core level. The  $Mg_{k\alpha_{1,2}}$  spectra were recorded at 12.0 kV and 8 mA whilst the  $Ti_{k\alpha_{1,2}}$  spectra were recorded at 13.5 kV and 18 mA. Although initial experiments indicated that the peaks occurring at  $\sim 590$  eV and 845 eV kinetic energy arose from  $Ti_{k\alpha_{1,2}}$  excited  $M_{II}^{M,N} V VI$ ,  $M_{II}^{M,N} V VII$  and  $M_{II}^{M,N} V IV$ ,  $M_{II}^{M,N} V V$  Auger transitions, further work has confirmed the assignment as due to  $Cu_{L\alpha}$  excited  $Au_{4f}$  and  $4d$  levels respectively. Although the twin anode is symmetrically related to the sample position it is clear that incomplete coverage of the copper target with Ti leads to a significant contribution to the total spectrum when using the Ti target of  $Cu_{L\alpha}$  X-rays.

The first series of experiments involved the recording of the  $Au_{4f}$  and  $C_{1s}$  levels for the initial gold sample followed by the examination of the  $Ti_{k\alpha}$  excited spectra for the  $4f$ ,  $4d$ ,  $3d_{3/2}$ ,  $3d_{5/2}$  and  $3p$  levels and the  $Cu_{L\alpha}$  excited  $Au_{4f}$  and  $4d$  levels. After deposition of a polymer film of known thickness the spectra were re-recorded, however the  $Mg_{k\alpha_{1,2}}$  spectra were also re-recorded after exposure to the  $Ti_{k\alpha_{1,2}}$  source to monitor the radiation

damage. In this series of experiments seven different gold substrates were employed and the attenuation of signal particularly at the low kinetic energy limited studies to three deposition thicknesses per sample. The data obtained in this series of experiments revealed subtle changes in core level spectra (particularly the  $C_{1s}$  levels as measured by the  $Mg_{k\alpha_{1,2}}$  photon source) and the investigation for each substrate taken was limited to one core level studied with the  $Ti_{k\alpha_{1,2}}$  source but with  $\sim 5$  deposition thicknesses for each. This enabled the radiation damage to be kept to a negligible level with little evidence of change in the  $C_{1s}$  levels monitored using the  $Mg_{k\alpha_{1,2}}$  source between depositions. This involved 35 separate experiments using the two photon sources.

The spectrometer employed in this work was a customized Kratos ES300 spectrometer. The source region of the spectrometer was separately pumped from the analyser using Alcatel air bearing air turbine turbo molecular pumps of nominal pumping speeds  $450 \text{ l sec.}^{-1}$  and  $120 \text{ l sec.}^{-1}$  respectively. The base pressure of the system during measurement of the spectra was  $\sim 10^{-9}$  torr. Spectra were recorded in analogue fashion using the fixed retardation ratio mode of scanning. Area measurements were made using both a Dupont 310 analogue curve resolver and an Apple II microcomputer with graphics tablet.

### 3.3. Results and Discussion

#### 3.3.1. Introduction

Before considering the detailed interpretation of the ESCA data on mean free paths it is worthwhile briefly considering the particular advantage and disadvantage of using a  $\text{Ti}_{k\alpha_{1,2}}$  X-ray source. Figure 3.3. shows a wide scan spectrum of a gold substrate with a thin monolayer coverage of polyparaxylylene.

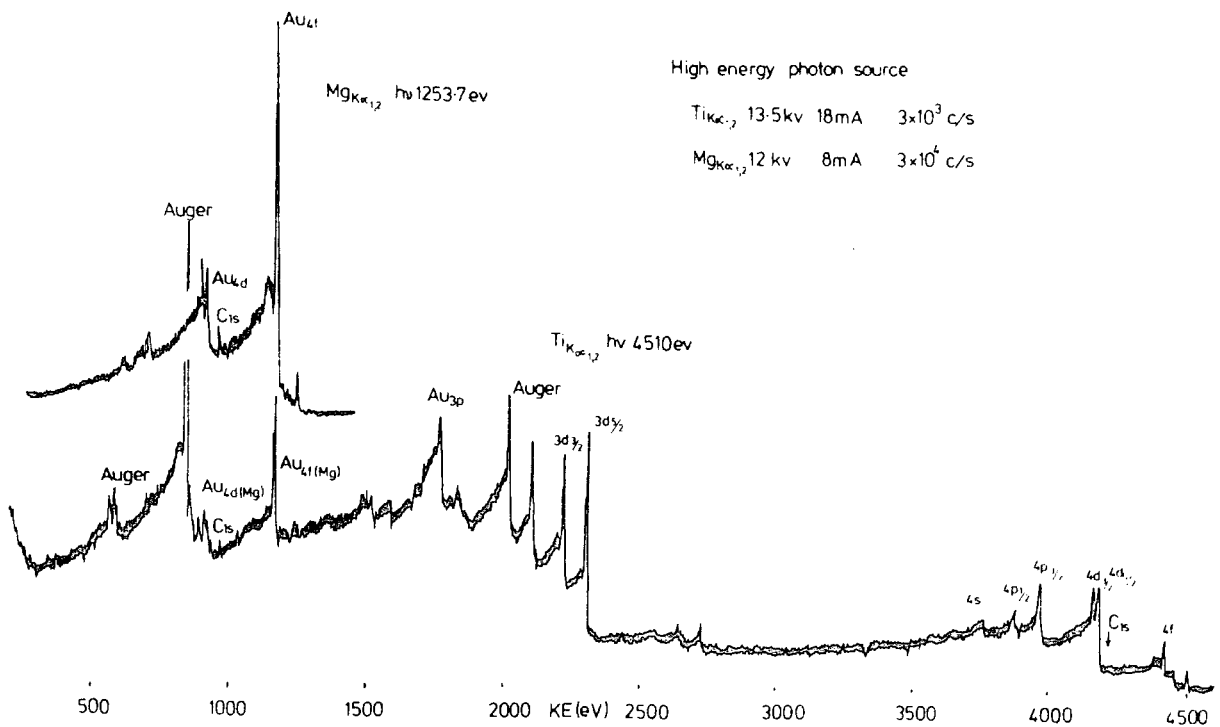


Figure 3.3. Wide-scan ESCA spectra excited using  $\text{Mg}_{k\alpha_{1,2}}$  and  $\text{Ti}_{k\alpha_{1,2}}$  photon sources for a gold substrate with  $\sim 12\text{\AA}$  of a polyparaxylylene overlayer.

The  $\text{Mg}_{k\alpha_{1,2}}$  excited spectra show strong photoemission from the  $\text{Au}_{4d}$  and  $\text{Au}_{4f}$  with a  $\text{C}_{1s}$  signal for the overlayer of detectable intensity. The great advantage of using the

Ti<sub>k $\alpha$ 1,2</sub> X-ray source in extending studies to much higher kinetic energy is evident from these data. The cross-section for photoemission from the 3p and 3d levels is considerable and the higher cross-section for photoemission from the 4p and 4d levels compared to the 4f levels is clearly evident from Figure 3.4. The position for the C<sub>1s</sub> level (excited by Ti<sub>k $\alpha$ 1,2</sub>) is as indicated but both the wide scan and high resolution scans of the level reveal negligible intensity for this level. This arises from two main contributory factors. Firstly the cross-section for photoemission is low, and secondly the mean free path for electrons photoemitted from C<sub>1s</sub> levels at  $\sim 4400$  eV is much larger than the film thickness ( $\sim 12\text{\AA}$ ) so that the intensity is negligible.

Instrumental parameters dictated that the Ti<sub>k $\alpha$ 1,2</sub> X-ray source was run at 13.5 kV and 18 mA which is less than optimum for characteristic radiation to bremsstrahlung output. The appearance of Cu<sub>L $\alpha$</sub>  excited spectra also shows the incomplete coverage of the target. However, even taking this into account, there is clearly a substantial difference in cross-section for the Au<sub>4f</sub> levels for a power input difference of a factor of 2.5 in going from Ti<sub>k $\alpha$</sub>  to Mg<sub>k $\alpha$</sub>  the intensity for photoemission from the 4f levels differ by at least three orders of magnitude for the two photon sources. (The spectra were recorded in the FRR mode,\* so the instrumental response function will be enhanced for electrons of greater kinetic energy.) The low cross-section for

---

\* Fixed Retardation Ratio.

photoionisation from substrate polyparaxylylene core levels and the greater proportion of bremsstrahlung to characteristic radiation poses particular problems in the direct determination of mean free paths using the substrate overlayer technique with the  $Ti_{k\alpha_{1,2}}$  X-ray source.

Thus the low count rates mean extended counting times and preliminary experiments using  $Mg_{k\alpha_{1,2}}$  investigations before and after  $Ti_{k\alpha_{1,2}}$  examination revealed evidence of radiation damage. In consequence fresh samples of polyparaxylylenes need to be deposited for each core level studied since extended studies with the  $Ti_{k\alpha_{1,2}}$  X-ray source of e.g. the 3p, 3d, 4p, 4d and 4f levels for a given sample shows the importance of the radiation damage in determining overall signal intensities.

The  $Ti_{k\alpha_{1,2}}$  X-ray source provides a characteristic doublet with intensity ratio 1:2 separated by 6 eV and under the instrumental conditions where the FWHM for the  $Au_{4f_{7/2}}$  level excited by  $Mg_{k\alpha_{1,2}}$  was 1.15 eV, that for the individual components of the  $Ti_{k\alpha_{1,2}}$  excited spectra were for the  $3d_{3/2}$  levels 2.4 eV. This illustrates the fact that under normal instrumental conditions the FWHM for the  $Ti_{k\alpha}$  spectra are largely dominated by the inherent width of the X-ray source.

In consequence it is a straightforward matter to analyse the rather complex lineshapes arising from the superposition of spin orbit split components for a given core level with the superposition of components excited by the spin orbit split  $Ti_{k\alpha_{1,2}}$  doublet. It should be emphasised however that

the attenuation of substrate core levels requires only that the total integrated intensity be determined and the analysis of electron mean free paths does not hinge on an analysis of the component contributions for a given level.

The data in Figure 3.3. shows that convenient core level spectra for the  $Au_{3p}$ ,  $3d$ ,  $4p$ ,  $4d$  and  $4f$  levels may be monitored to provide direct estimates of electron mean free paths at K.E.'s  $\sim 1768$  eV,  $2220$  eV,  $3970$  eV,  $4177$  eV and  $4430$  eV respectively. In addition the  $Cu_{L\alpha}$  excited  $Au_{4f}$  and  $4d$  levels at  $\sim 845$  eV and  $\sim 590$  eV conveniently extend the investigation to much lower kinetic energies.

It is clear that with the investigation previously reported using  $Mg_{k\alpha_{1,2}}$  and  $Al_{k\alpha_{1,2}}$  photon sources that investigation of these levels provides an excellent coverage of the kinetic energy range  $0 - 4500$  eV, and this represents the most complete study undertaken to-date of electron mean free paths as a function of kinetic energy for a given class of material over such a wide kinetic energy range.

Before considering the data for the mean free paths it is worthwhile briefly considering in a qualitative sense the strong dependence of mean free path on kinetic energy. This is dramatically illustrated by the core level data displayed in Figure 3.4.

For the  $Mg_{k\alpha_{1,2}}$  excited  $Au_{4f}$  levels at  $\sim 1170$  eV kinetic energy the deposition of  $\sim 70\text{\AA}$  of a polyparaxylylene over-layer results in a signal attenuation by a factor of  $\sim 50x$ . By contrast for the  $Au_{4f}$  levels excited using the  $Ti_{k\alpha_{1,2}}$  X-ray source the corresponding attenuation is by a factor of  $\sim 5x$ .





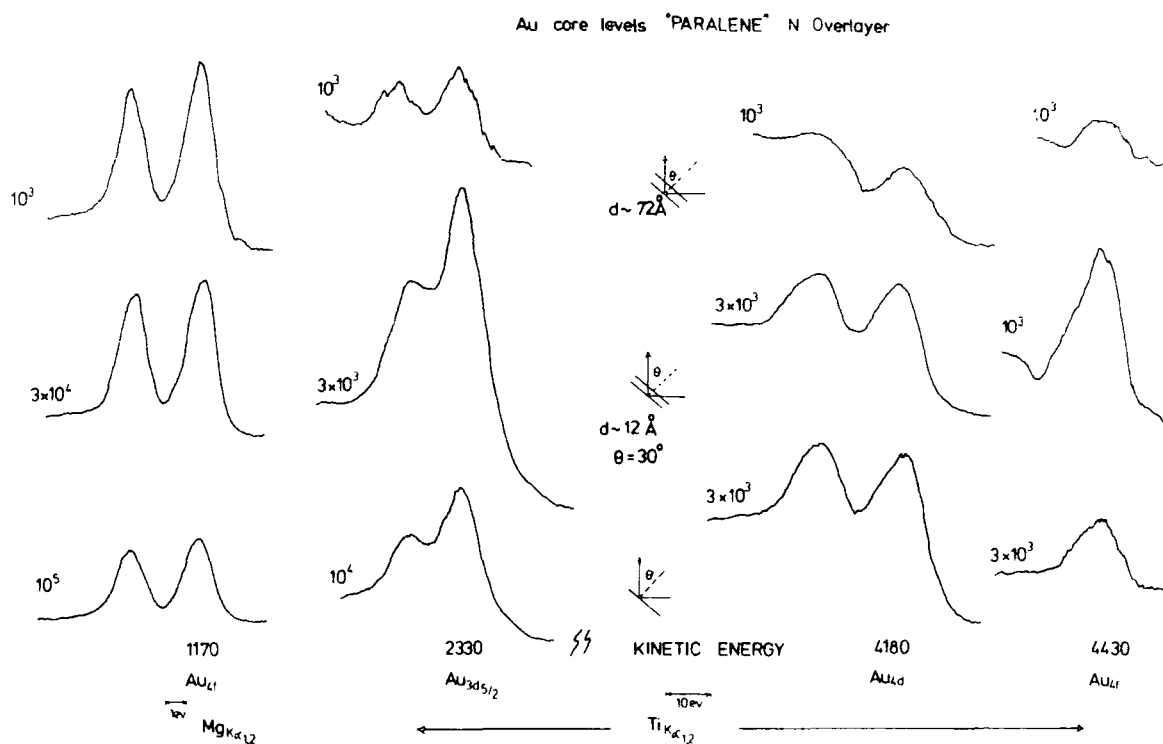


Figure 3.4.  $Au_{4f}$  ( $Mg_{K\alpha_{1,2}}$ ) and  $Au_{3d_{5/2}}$ ,  $Au_{4d}$  and  $Au_{4f}$  (all  $Ti_{K\alpha_{1,2}}$ ) core level ESCA spectra recorded at a take-off angle of  $30^\circ$  for a gold substrate with differing thicknesses of polyparaxylylene overlayer.

### 3.3.2. Comparison of electron mean free paths for photoelectrons excited from the $Au_{4f}$ levels

Previous work<sup>93</sup> has provided a detailed knowledge of electron mean free paths as a function of kinetic energy employing  $Mg_{K\alpha_{1,2}}$  and  $Al_{K\alpha_{1,2}}$  photon sources.<sup>4</sup> The data obtained from the study of the  $Au_{4f}$  substrate core levels using  $Mg_{K\alpha_{1,2}}$  has been employed to calibrate the film thickness for the studies made using the harder X-ray source. This has two distinct advantages firstly, it relates directly intensity ratios obtained from one photon source to

another, secondly it obviates the need for a deposition monitor and the apparatus is therefore somewhat simpler for the experiments described here compared with those detailed previously.<sup>93</sup> For the quantification of the data described in this chapter a mean free path of  $22\text{\AA}$  for photoelectrons of K.E. 1170 eV has been taken.<sup>93</sup>

As the data in Figures 3.3. and 3.4. reveal the cross-section for photoemission from the 4f levels using the  $\text{Ti}_{k\alpha_{1,2}}$  photon source is rather low and in consequence the overall signal intensities become very low for extensive coverage with the polyparaxylylene overlayer and as previously noted radiation damage precludes greatly extended counting times to improve the statistics. The statistical correlations for the 4f levels of K.E.  $\sim 4430$  eV photoemitted using the  $\text{Ti}_{k\alpha_{1,2}}$  X-ray source are therefore somewhat poorer than for some of the other levels, the relevant data are displayed in Figure 3.5. The mean free paths computed from the gradients of the plot  $\ln I_s/I_0$  vs.  $d/\cos \theta$  provides estimates of  $37\text{\AA}$  and  $37\text{\AA}$  for the data corresponding to take-off angles of  $30^\circ$  and  $50^\circ$  with correlation coefficients of 0.89 and 0.95 respectively. Considerable scatter is evident from the data in Figure 3.5., however the good agreement between the results at  $30^\circ$  and  $50^\circ$  take-off angles suggests that the coverage must be rather uniform and not in the form of patched overlayers. The data thus indicates that the mean free path increases by a factor of  $\sim 2$  in going from 1170 eV to  $\sim 4430$  eV, implying a square root dependence of MFP on K.E.

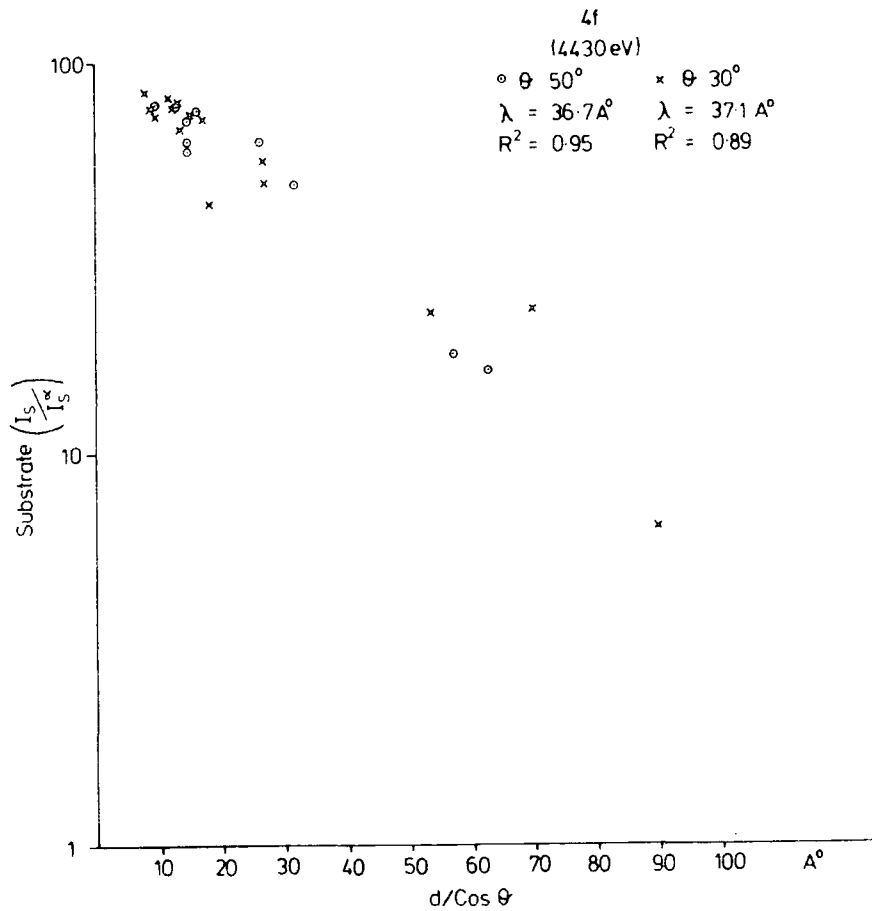


Figure 3.5. Plot of  $\ln \frac{I_s}{I_s^0}$  versus  $d/\cos \theta$  ( $\text{\AA}$ ) for the 4f levels of the Au substrate excited using the  $\text{Ti}_{k\alpha_{1,2}}$  photon source.

### 3.3.3. $\text{Au}_{4d}$ levels studied with the $\text{Ti}_{k\alpha_{1,2}}$ X-ray source

The cross-section for photoemission from the  $\text{Au}_{4d}$  levels is somewhat higher than for the  $\text{Au}_{4f}$  levels using the  $\text{Ti}_{k\alpha_{1,2}}$  X-ray source compared with the  $\text{Mg}_{k\alpha_{1,2}}$  X-ray source as is evident from Figure 3.3.

The data from which the mean free paths have been derived are shown in Figure 3.6. and the statistical analysis is reasonable. The absolute magnitude of the mean free paths

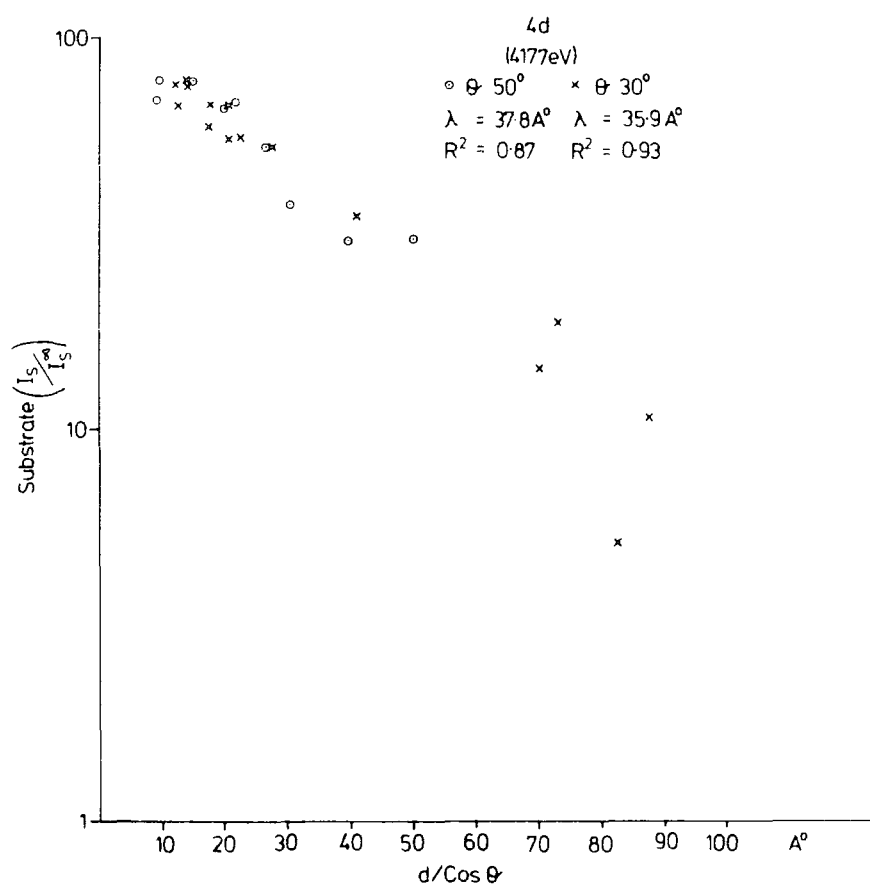


Figure 3.6. Plot of  $\ln \frac{I_s}{I_s^0}$  versus  $d/\cos \theta$  ( $\text{\AA}$ ) for the 4d levels of the Au substrate excited using the  $\text{Ti}_{k\alpha_{1,2}}$  photon source.

evaluated at take-off angles of  $50^\circ$  and  $30^\circ$  respectively, are essentially the same ( $38 \text{ \AA}$  and  $36 \text{ \AA}$ ) for electrons of K.E.  $\sim 4177$  eV (the total envelope of the spin orbit split components has been employed).

#### 3.3.4. $\text{Au}_{4p_{3/2}}$ levels studied with the $\text{Ti}_{k\alpha_{1,2}}$ X-ray source

The  $\text{Au}_{4p_{3/2}}$  levels show a greatly increased cross-section for photoionisation using the harder X-ray source as is also apparent from the spectra in Figure 3.3. This

considerably aids the study of overlayers extending to a considerably greater thickness particularly at higher take-off angles where the instrument response function is such that overall intensities tend to be low.

The data are displayed in Figure 3.7. and the correlation coefficients are significantly higher than for the data for the  $Au_{4d}$  or  $Au_{4f}$  levels described above.

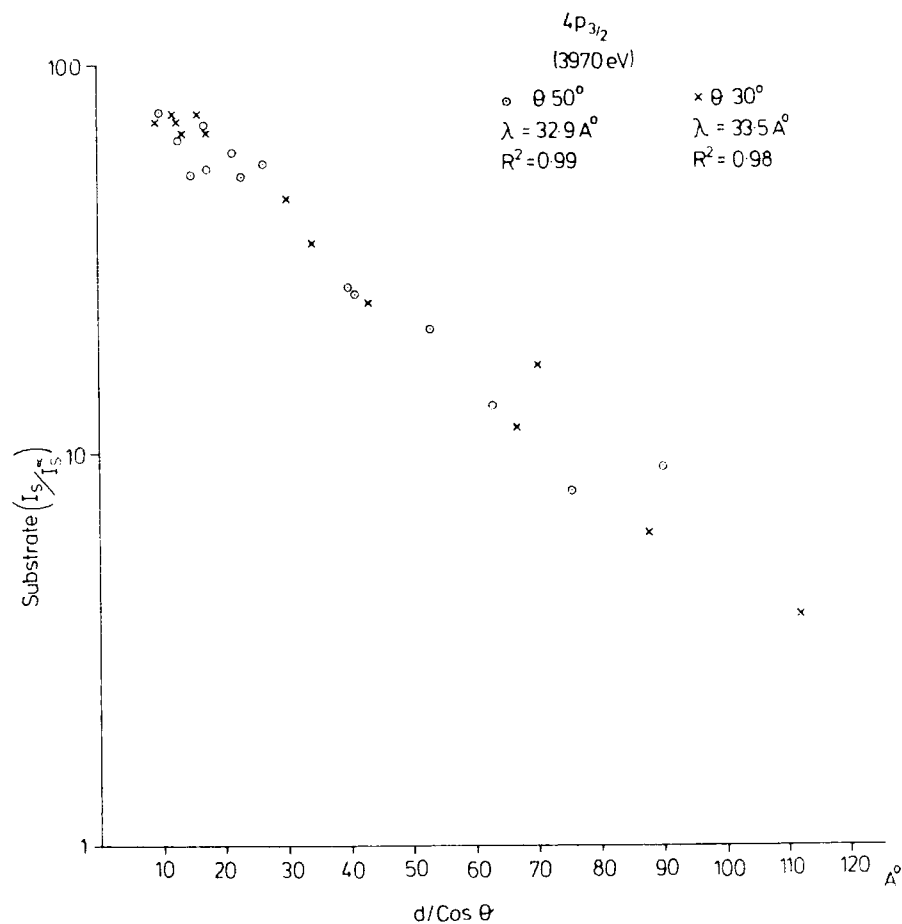


Figure 3.7. Plot of  $\ln \frac{I_s}{I_s^0}$  versus  $d/\cos \theta$  (Å) for the  $4p_{3/2}$  levels of the Au substrate excited using the  $Ti_{k\alpha_{1,2}}$  photon source.

The data pertaining to the two different take-off angles

of  $50^\circ$  and  $30^\circ$  provides estimates of mean free paths at  $\sim 3970$  eV K.E. of  $33\text{\AA}$  and  $34\text{\AA}$  respectively

### 3.3.5. Au<sub>3d</sub> levels studied with the Ti<sub>k $\alpha$ 1,2</sub> X-ray source

The cross-section for photoemission from the Au<sub>3d</sub> levels (unavailable using the softer X-ray source) is fairly high using the Ti<sub>k $\alpha$ 1,2</sub> X-ray source and the well resolved spin orbit doublet are immediately identifiable from the spectrum displayed in Figure 3.3. With the higher count rates and larger splitting available for the spin orbit split components it has proved possible to monitor the attenuation of signal for both components. The data for Au<sub>3d<sub>3/2</sub></sub> components are shown in Figure 3.8. whilst that for the Au<sub>3d<sub>5/2</sub></sub> levels are shown in Figure 3.9.

Considering the Au<sub>3d<sub>5/2</sub></sub> levels for which the correlation coefficients are somewhat higher, the computed mean free paths corresponding to the data taken at take-off angles of  $50^\circ$  and  $30^\circ$  respectively are  $28\text{\AA}$  and  $27\text{\AA}$  for a K.E. of  $\sim 2305$  eV. These values are significantly below those detailed above for electrons of higher kinetic energy.

The data for the Au<sub>3d<sub>5/2</sub></sub> levels (K.E.  $\sim 2220$  eV) provide estimates of  $28\text{\AA}$  and  $31\text{\AA}$  for mean free paths evaluated at take-off angles of  $50^\circ$  and  $30^\circ$  respectively, in tolerable agreement with those determined for the Au<sub>3d<sub>5/2</sub></sub> levels.

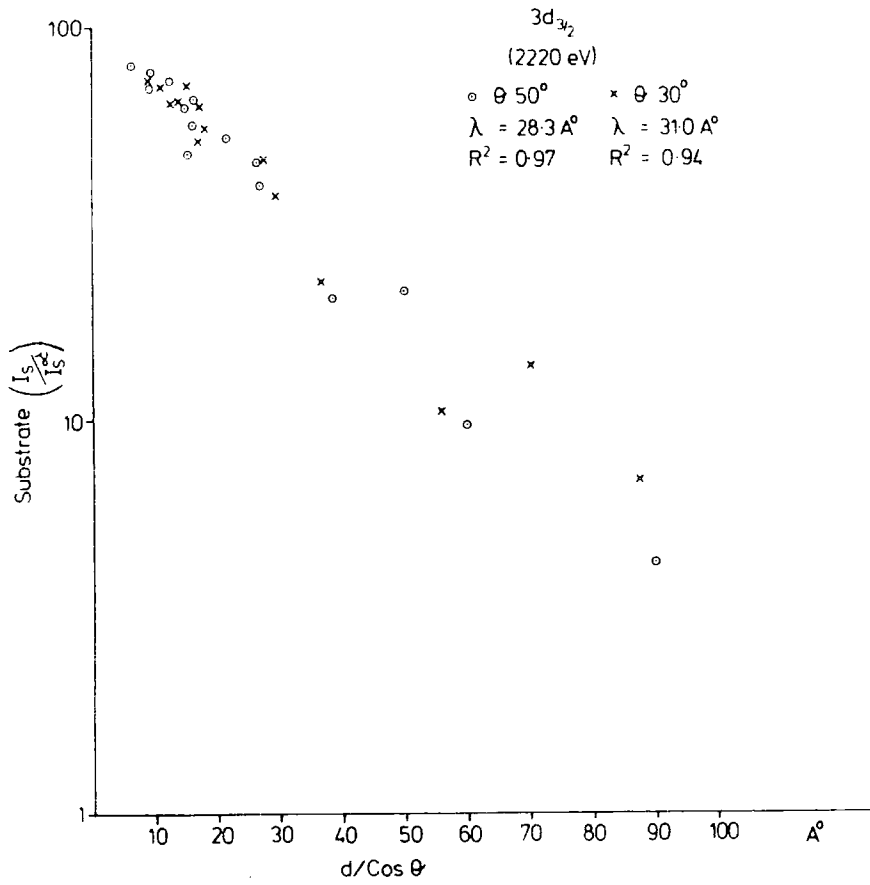


Figure 3.8. Plot of  $\ln \frac{I_s}{I_s^0}$  versus  $d/\cos \theta$  ( $\text{\AA}$ ) for the  $3d_{3/2}$  levels of the Au substrate excited using the  $\text{Ti}_{k\alpha_{1,2}}$  photon source.

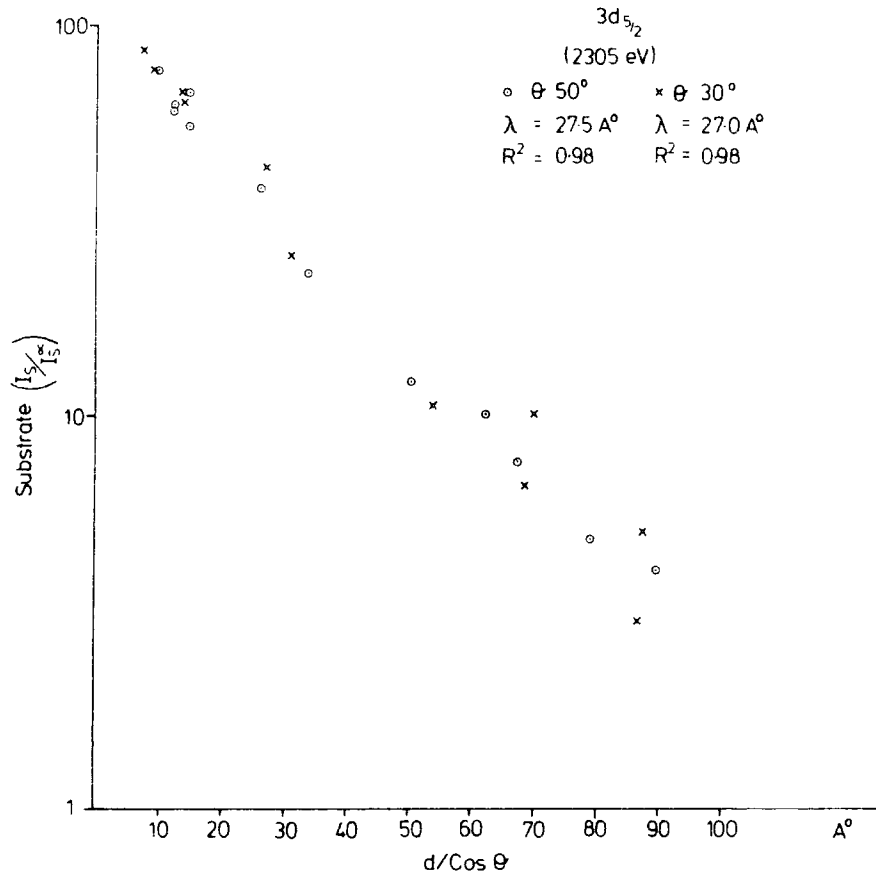


Figure 3.9. Plot of  $\ln \frac{I_s}{I_s^\infty}$  versus  $d/\cos \theta$  (Å) for the  $3d_{5/2}$  levels of the Au substrate excited using the  $Ti_{k\alpha_{1,2}}$  photon source.

3.3.6.  $Au_{3p_{3/2}}$  level studied with  $Ti_{k\alpha_{1,2}}$  X-ray source

The  $Au_{3p_{3/2}}$  level although having a much larger FWHM than for the  $3d_{3/2}$  levels is of comparable intensity when excited by the  $Ti_{k\alpha_{1,2}}$  X-ray source and provides a convenient intermediate kinetic energy (1768 eV) for the direct measurement of mean free paths. The data are shown in Figure 3.10. and the analysis provides estimates of 27Å and 23Å for take-off angle of 50° and 30° respectively.



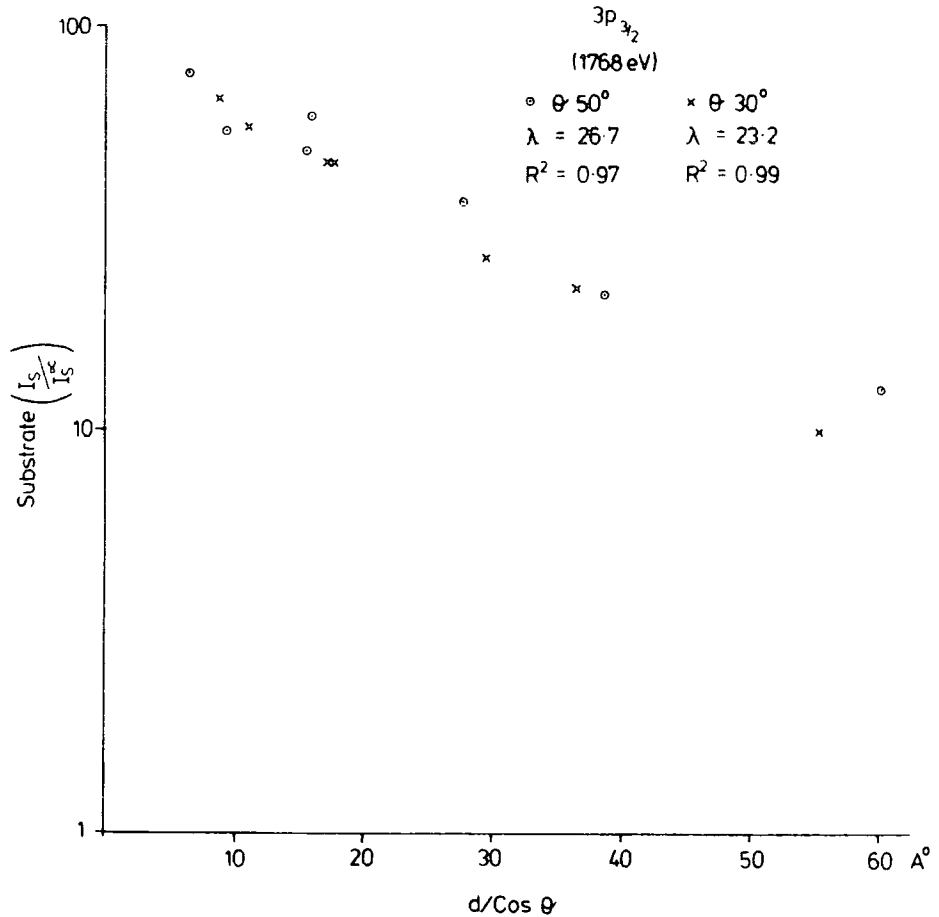


Figure 3.10. Plot of  $\ln \frac{I_s^\omega}{I_s^\infty}$  versus  $d/\cos \theta$  ( $\text{\AA}$ ) for the  $3p_{3/2}$  levels of the Au substrate excited using the  $\text{Ti}_{k\alpha_{1,2}}$  photon source.

### 3.3.7. The $\text{Cu}_{L\alpha}$ excited $\text{Au}_{4f}$ and $\text{Au}_{4d}$ levels

The wide scan ESCA spectrum in Figure 3.3. reveals intense peaks at  $\sim 845$  eV and  $\sim 590$  eV associated to  $\text{Au}_{4f}$  and  $\text{Au}_{4d}$  respectively. These are excited by  $\text{Cu}_{L\alpha}$  and provide direct measurements of electron mean free path as a function of kinetic energy at a somewhat lower energy than has previously been reported for polyparaxylylene.<sup>4</sup>

The data for the  $\text{Au}_{4f}$  at 845 eV are shown in Figure 3.11. The statistical correlations are very reasonable and

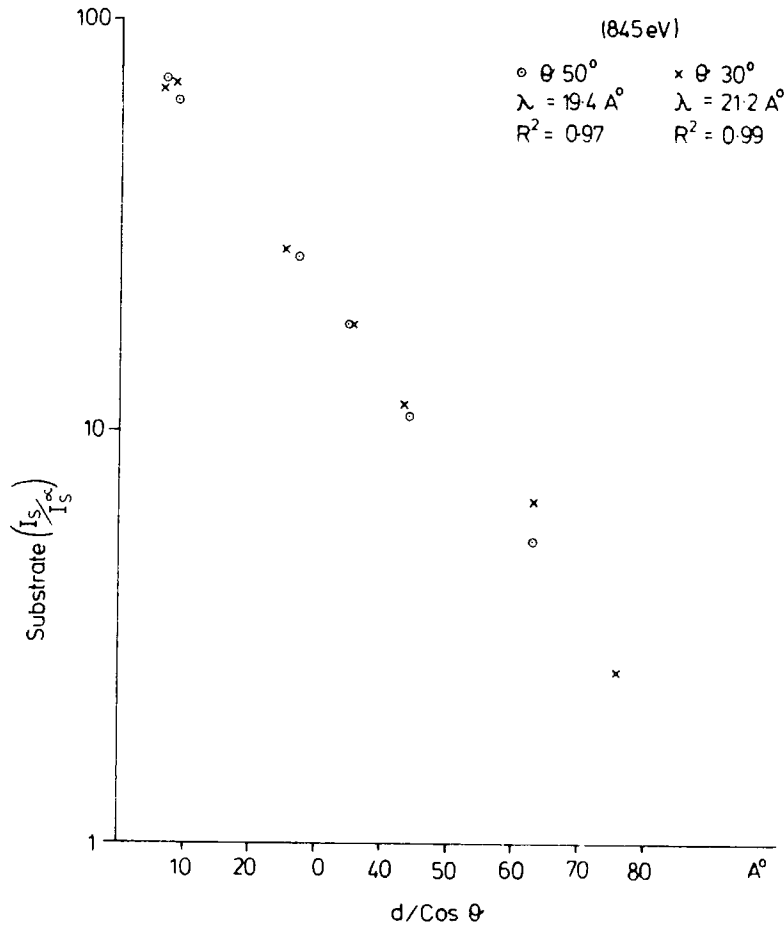


Figure 3.11. Plot of  $\ln \frac{I_s^\alpha}{I_s}$  versus  $d/\cos \theta$  (Å) for the  $Au_{4f}$  levels of the Au substrate excited using the  $Cu_{L\alpha}$  photon source.

the analysis for  $50^\circ$  and  $30^\circ$  take-off angles provides estimates of  $19\text{Å}$  and  $21\text{Å}$  respectively the same as the mean free path determined for the  $Au_{4f}$  levels employed as standard at kinetic energy 1170 eV excited using  $Mg_{k\alpha_{1,2}}$  X-ray source.

The corresponding data for the  $Au_{4d}$  at  $\sim 590$  eV K.E. are shown in Figure 3.12. the derived mean free paths at take-off angles of  $50^\circ$  and  $30^\circ$  being  $15\text{Å}$  and  $18\text{Å}$  respectively.

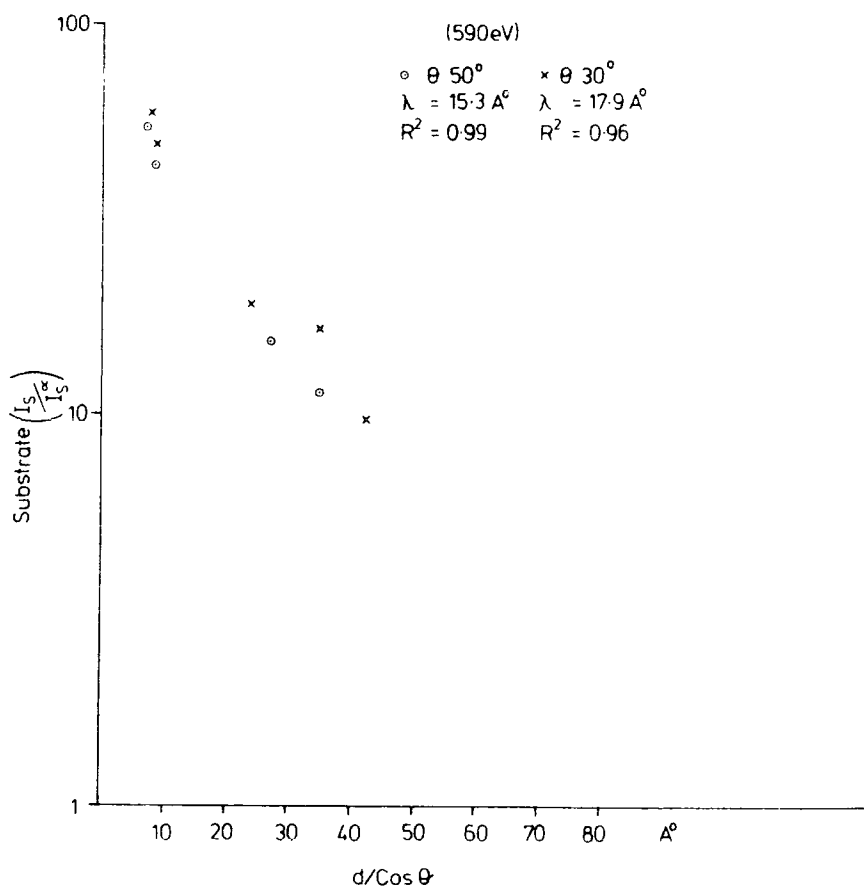


Figure 3.12. Plot of  $\ln \frac{I_s}{I_s^0}$  versus  $d/\cos \theta$  ( $\text{\AA}$ ) for the 4d levels of the Au substrate excited using the  $\text{Cu}_{L\alpha}$  photon source.

3.3.8. Comparison of data with previous studies of polymer-metal systems by the substrate-overlayer technique

Previous work<sup>93,99</sup> has shown how over a limited kinetic energy range mean free paths in typical linear and cross-linked polymers are very similar to those that have been determined over comparable energy ranges by the substrate overlayer technique for metals and semi-conductors.<sup>93,98-99,181</sup> It has also been shown<sup>183</sup> that ordered fatty acid overlayers do not provide a suitable model for typical polymers, the

mean free paths being somewhat larger at a given kinetic energy and showing a significant dependence on structure particularly the mean area per molecule.

There have been relatively few investigations of electron mean free paths in overlayers which extend over a wide kinetic energy range. By far the majority of investigations have been confined<sup>181</sup> to either the 0 -  $\sim$  100 eV region employing either or both of vacuum u.v. and synchrotron sources or in the 0 -  $\sim$  1250 eV or 0 -  $\sim$  1480 eV using conventional soft x-ray sources ( $\text{Mg}_{k\alpha_{1,2}}$ ,  $\text{Al}_{k\alpha_{1,2}}$ ).

An early study of evaporated Au and Al on chromium substrates, Nordling and co-workers<sup>192</sup> employing  $\text{Cr}_{k\alpha_{1,2}}$  ( $h\nu$  5414.7 eV) and  $\text{Al}_{k\alpha_{1,2}}$  ( $h\nu$  1486.7 eV) X-ray sources showed a roughly square root dependence of the mean free path on kinetic energy over a 3K eV range. Thus for gold the mean free path effectively doubles in going from 940 eV K.E. ( $19\text{\AA}$ ) to  $37\text{\AA}$  at a K.E. of 3208 eV.<sup>192</sup> However over a narrow range from 940 eV to 1403 eV the dependence of mean free path on kinetic energy is somewhat closer to being a linear rather than a square root function.

The previous work employing both  $\text{Mg}_{k\alpha_{1,2}}$  and  $\text{Al}_{k\alpha_{1,2}}$  X-ray sources on the polyparaxylylene<sup>93</sup> also suggested a much greater dependence of mean free path on kinetic energy in the limited range of the investigation, however the present study extending over the range to  $\sim$  4400 eV reveals that the dependence over this range follows roughly a square root dependence.

It is of interest to consider this dependence in somewhat

more detail and this is shown in Figure 3.13., this is the most complete set of data for any material in the kinetic energy range  $\sim 500 - 4500$  eV. The plot of  $\lambda$  versus  $K.E.^{\frac{1}{2}}$  is reasonably linear over the substrate levels studied in this work and the data confirm that over an extended energy range the dependence is roughly square root in nature. Also indicated in Figure (3.13.) are the points previously determined for the polyparaxylylene system using both substrate and overlayer core levels, using  $Mg_{K\alpha}$  photon source. Considering the error limits involved the data

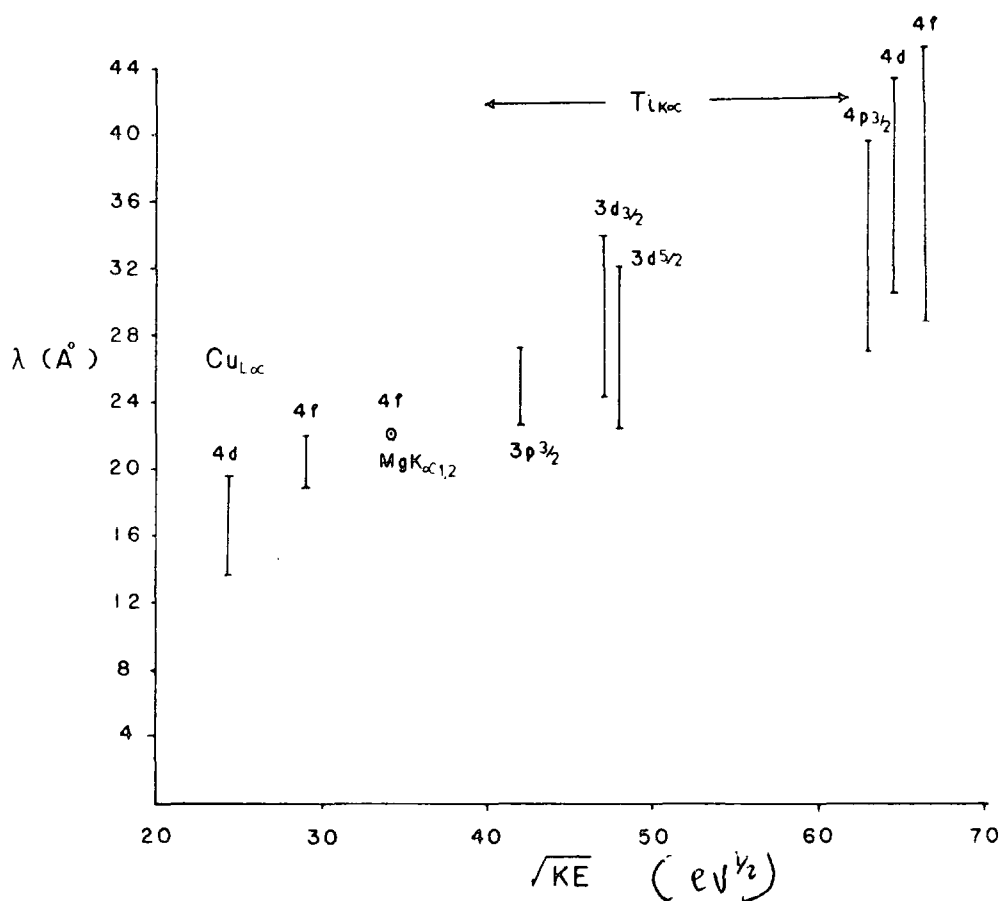


Figure 3.13. Plot of  $\lambda(\text{\AA})$  versus square root of kinetic energy for gold substrate with polyparaxylylene overlayers studied using  $Ti_{K\alpha c}$ ,  $Mg_{K\alpha}$  and  $Cu_{L\alpha}$  photon sources.

overall are in very reasonable agreement. The data illustrate the distinct advantage in terms of depth profiling of having a dual X-ray source with  $\text{Ti}_{k\alpha_{1,2}}$  and  $\text{Mg}_{k\alpha_{1,2}}$  and  $\text{Cu}_{k\alpha_{1,2}}$  photon sources. The considerable uncertainty of interpretation of data and the likelihood of artefacts arising in ion milling of polymer based systems makes the dual X-ray source attractive for depth profiling studies since for electrons with kinetic energies of  $\sim 600$  eV and  $\sim 4000$  eV the difference in sampling depth (defined in terms of  $3\lambda$ ) might typically amount to  $50\text{\AA}$  (dependent on take-off angle). In the case of powdered or fibrous samples where angular dependent studies are not realistically feasible the use of harder X-ray sources provides a basis for depth profiling which has not hitherto been available in such systems. The data presented in this chapter provides the basis for semi-quantitative interpretation of such data.

CHAPTER FOUR

CHAPTER FOUR

Plasma Polymerisation . A Systematic  
Investigation of Materials Synthesised  
in Inductively Coupled Plasmas Excited  
in Perfluoropyridine

Abstract

The RF plasma polymerisation of perfluoropyridine has been investigated for a range of operating parameters. The stoichiometries of the resulting thin films indicate a predominance of rearrangement mechanisms in their formation, with both nitrogen and fluorine being retained at approximately the same level as in the starting monomers. In appropriate cases, comparison has been drawn with plasma polymers produced under comparable conditions from perfluoro and pentafluorobenzenes. Whilst the plasma polymer films from the benzenes have a low critical surface tension that for the pyridine system changes with time with the surface becoming completely wettable with water. This is attributed to surface hydrolysis of the plasma polymer films produced from the perfluoropyridine.



#### 4.1. Fundamental Aspects of Plasmas

##### 4.1.1. Definition and Characterisation

Plasma may be defined as a gas discharge and can be obtained by subjecting a gas in the discharge tube to an electric field under appropriate conditions (e.g. pressure and power). Some of the gas molecules will be ionised into positive ions and free electrons. Under these circumstances the state of gas is known as a plasma.

A plasma may also be defined as a gaseous state or partially ionised gas composed of atoms, molecules, ions, metastables and the excited states of these species and electrons such that the concentration of positively and negatively charged species is approximately the same. A plasma must therefore be electrically neutral.

Various plasmas are found in nature and can also be created in the laboratory, e.g. in electrical discharges. Figure (4.1.) summarises the various plasma systems, either occurring naturally or produced in laboratories.<sup>193</sup> The area which has proved to be of greatest interest to chemists is that associated with charge densities of ca.  $10^{10} \text{ cm}^{-3}$  and average electron energies of ca. 1.0 eV.

Plasmas may be divided into two types. Firstly "hot" or "equilibrium" plasma, characterised by a high gas temperature and an approximate equality between the gas and electron temperatures. These plasmas are generally regarded as being of more interest to physicists, typical examples of "hot" plasmas including arcs and plasma torches. The second type of plasma, with which this thesis is to be concerned,

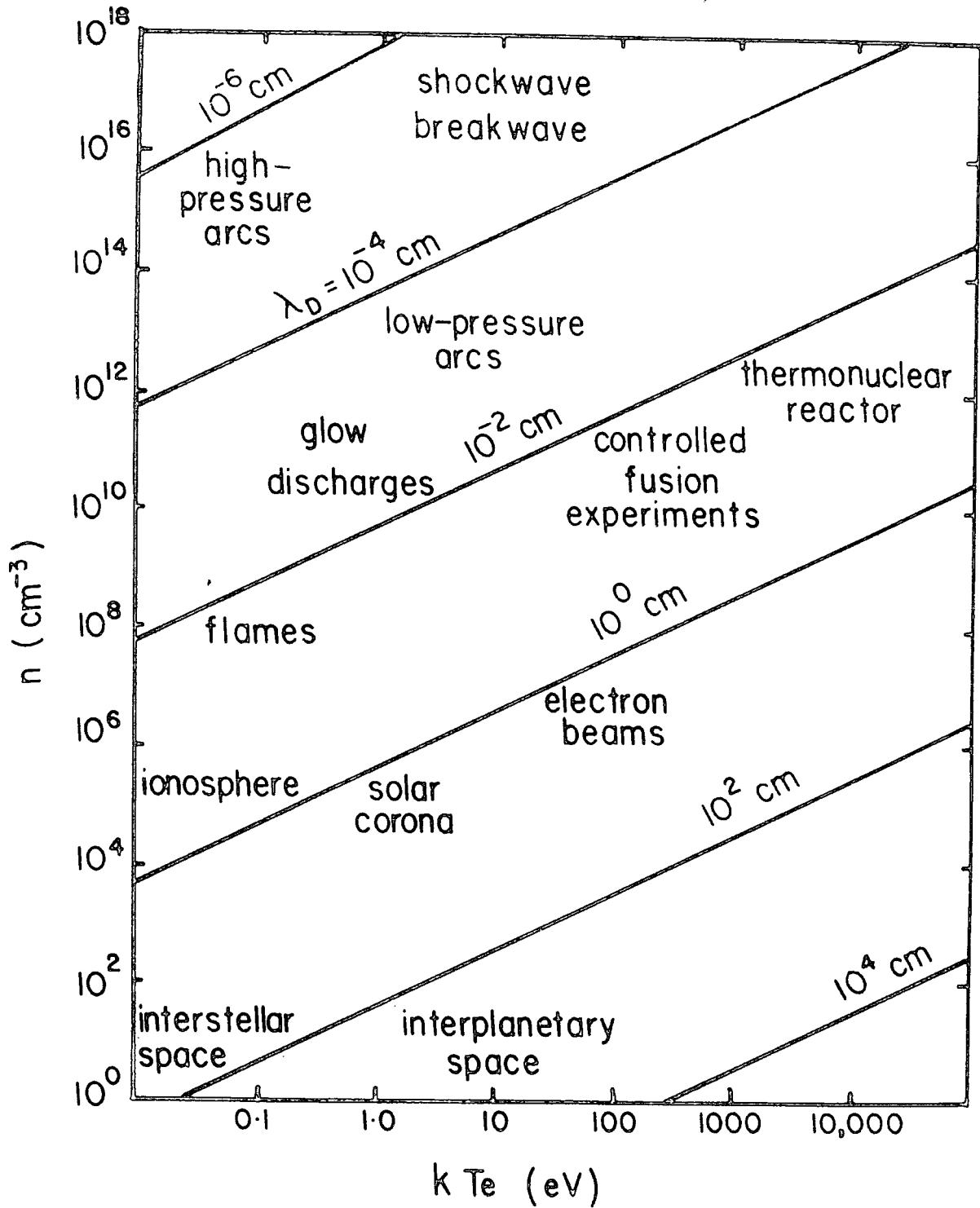


Figure 4.1. Plasmas found in nature and in the laboratory.

might be termed "cool" and is of primary interest to chemists. "Cool" or "non-equilibrium" plasmas have the characteristic feature that the Boltzman temperature of the ions and molecules is roughly ambient whilst that of the electrons is some two orders of magnitude greater.

Electrons within the plasma are accelerated by the electric field and produce further ionisation by collisions with other species. The collision process and some of its consequences are shown schematically in Figure (4.2.).

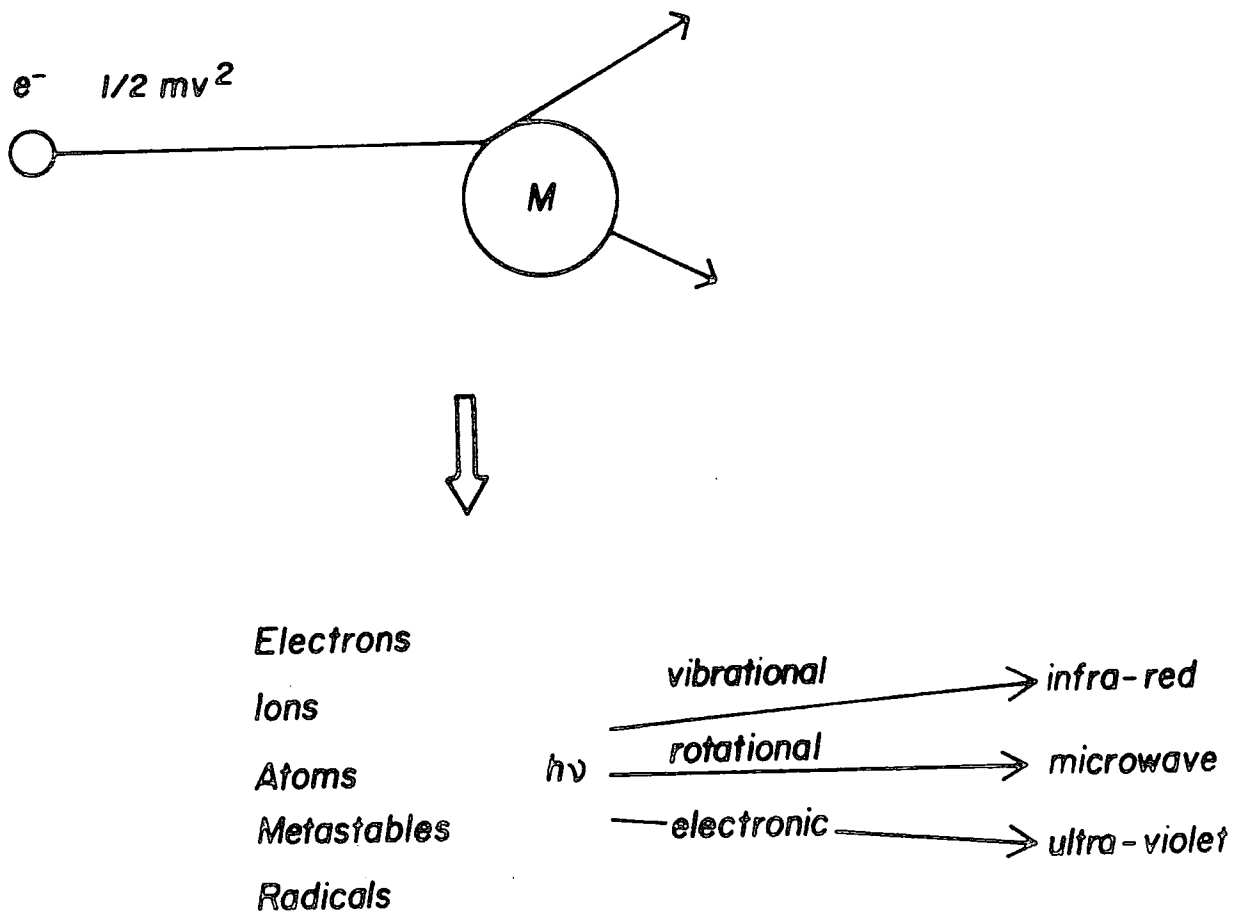


Figure 4.2. Schematic collision in a plasma leading to the production of numerous species and electromagnetic radiation.

Although the interaction of radio-frequency glow discharges with solids in general has been an active area of research in both industrial and academic laboratories, few attempts have been made to characterise the plasmas involved in terms of the energy distribution of electrons, ions and metastables. Expressions describing the electron energy distribution in reference to energy input, discharge dimensions and gas pressure lead to a Maxwellian distribution of electron energies, Figure (4.3.). This relationship holds strictly for simple systems only, for example hydrogen, as in

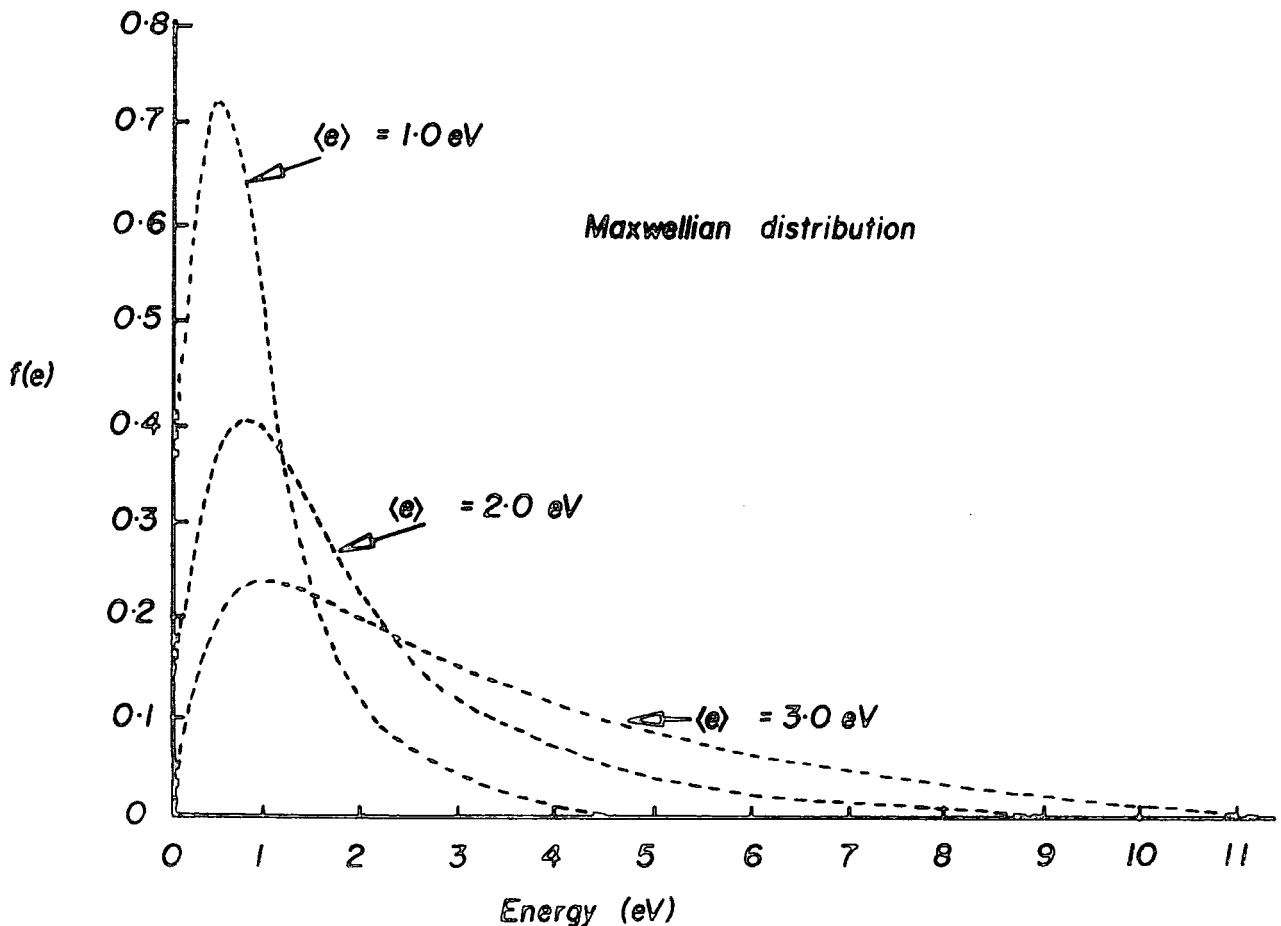


Figure 4.3. Maxwellian distribution function.

Figure (4.4.). For more complex systems, the average

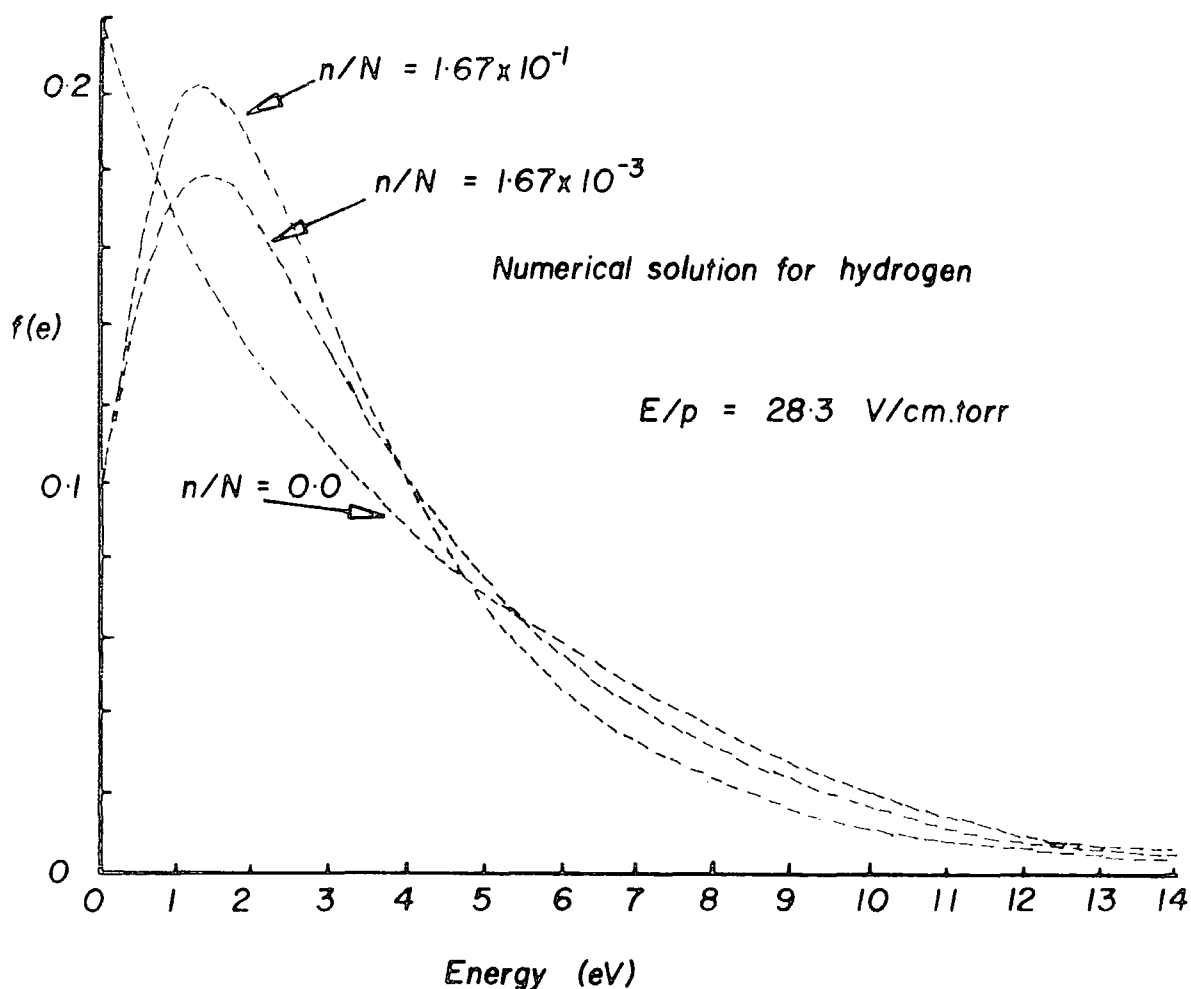


Figure 4.4. Numerical solution for hydrogen discharge.

electron energies may be analysed by electrical probe measurements,<sup>194-195</sup> and direct electron sampling.<sup>196</sup>

In general, plasmas are a plentiful source of electromagnetic radiation, through de-excitation of excited states, particularly in the u.v. and vacuum u.v. and indeed plasmas are often used as sources of electromagnetic radiation in these regions. In addition the relatively smaller output in the visible region gives rise to characteristic colours

for plasmas excited in a given system and hence the appellation "glow discharge".

#### 4.1.2. Plasma Techniques

The production of a non-equilibrium glow discharge may be accomplished in several ways, there are three distinct aspects which are of interest, namely the source of electrical power to sustain the plasma, the coupling mechanism, and what may loosely be termed the "plasma environment". This is illustrated schematically in Figure (4.5.)<sup>116</sup> and the combination selected for a given investigation is dependent

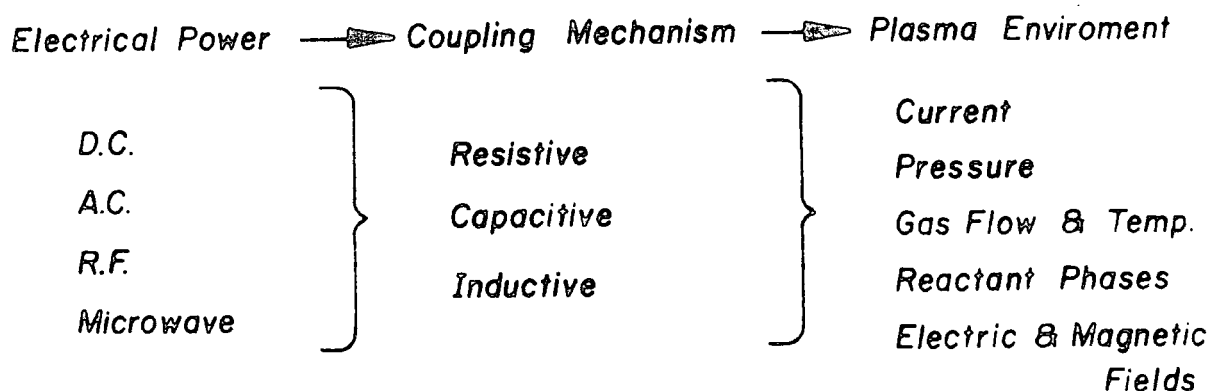


Figure 4.5. Elements of a glow discharge experiment.

on a number of factors such as cost, ease of construction, and convenience. Whilst most of the early work<sup>151,197-199</sup> involved AC and DC discharges, the greater flexibility and closer control over operating parameters has of recent years shifted the emphasis towards the investigation of inductively coupled RF and microwave plasmas, and the predominant emphasis in this work will be in this area.

The glow discharge experiment can be performed over a

wide range of frequencies from AC to the RF region. Yasuda and co-workers<sup>199</sup> have employed frequencies of 60 Hz (AC), 10 kHz (AF; Audio Frequency) and 13.56 MHz (RF). The distribution of power density in the glow region of glow discharge is modified in a magnetic field and so the glow discharge may be operated over a wider range of power levels, where it is magnetically focussed between the electrodes. Typical glow discharge experiments involve power of a few tens of watts or less, although it may vary from 0.1W to a few kilowatts. The operating pressure using RF discharge can range from  $\sim$  0.01 torr to 1.0 torr, and up to 1 atmosphere for a DC discharge. Using RF power it is possible to obtain stable glow discharge operating at low average power loading by pulsing the power input. When working with DC discharges at higher power levels (> 50W) some special cooling system for the electrodes is necessary.

#### 4.1.3. Reactive Species in Plasmas

A variety of species may be found in a plasma excited by an electrical discharge arising from collisions involving electrons, ions, metastables, neutral molecules and free radicals, in ground and excited states, together with photons of various energies. These species are potentially chemically active. Table (4.1.) displays some typical values of energies associated with species found in glow discharges compared with some typical bond energies for organic systems.<sup>116</sup>

With a wide variety of ions, radicals and excited states available from their excitation in plasmas, even for simple monomers it is evident that a variety of mechanisms is

Table 4.1. Energies associated with a glow discharge.

	<u>eV</u>
<i>Electrons</i>	0 - 20
<i>Ions</i>	0 - 2
<i>Metastables</i>	0 - 20
<i>U.V./visible</i>	3 - 40

***bond energies:-***

<i>C-H</i>	4.3	<i>C=O</i>	8.0
<i>C-N</i>	2.9	<i>C-C</i>	3.4
<i>C-Cl</i>	3.4	<i>C=C</i>	6.1
<i>C-F</i>	4.4	<i>C≡C</i>	8.4

available for polymerisation reactions in a glow discharge.<sup>200</sup>

4.1.4. Advantages and Disadvantages of the Glow Discharge Technique

The principal advantages and disadvantages of the glow discharge technique are set out in Table 4.2.

The glow discharge synthesis of polymer films or modification of polymer surfaces is a process of such flexibility that either batch or continuous operations can be employed whichever is the most desirable. This may prove to be a facility of great importance, especially when



Table 4.2.Advantages

- 1 - Applicable to batch or continuous processing.
- 2 - Low initial capital outlay.
- 3 - Suitable for application to a wide range of systems.
- 4 - Close control over experimental conditions.

Disadvantages

- 1 - Cannot produce films to a specific formula.
- 2 - Thick films are brittle and discoloured.

considering the integration of the technique into industrial processing or treatments.

The glow discharge polymerisation is essentially a one step process, which often proves to be cost effective in terms of power consumption and labour requirements. This contrasts with conventional solution phase techniques, which often employ several steps, require highly pure solvents, and temperatures higher than ambient.

The obvious advantages of the glow discharge technique compared with conventional polymer syntheses are that the plasma polymerised materials are deposited in the "clean" environment of a partial vacuum, and may be readily coated onto virtually any substrate.

The glow discharge technique facilitates great control over operating parameters (pressure, flow rate and power), and the appropriate conditions can readily be established for a wide range of starting materials to be plasma polymerised. 193,201-202

#### 4.2. Polymer Characterisation Techniques

Since the polymers produced by plasma polymerisation are system dependent, the variation in the operating parameters (e.g. power, pressure, etc.) often produces significant changes in the structure and properties of the polymer. Some of the analytical techniques which have been employed to study the bulk and the surface properties are considered briefly in Table 4.3.

Table 4.3.

##### A. Bulk properties

1. Micro-analysis
2. Electron spin resonance spectroscopy (e.s.r.)
3. Nuclear magnetic resonance (NMR)
4. Differential scanning calorimetry and thermal gravimetric analysis (DSC and TGA)
5. Infra-red spectroscopy (IR)
6. Dielectric properties

##### B. Surface properties

1. E.S.C.A.
2. Contact angle
3. Reflectance IR
4. Electron microscopy

In this thesis, the surface characterisation is considered in somewhat more detail, however, it is worthwhile to briefly summarise some of the results obtained from bulk studies.

Generally, the chemical compositions of the plasma

polymerised polymers bear no simple relationship to that of the starting materials, and the stoichiometry of the polymer depends upon the conditions under which the plasma polymerisation reaction is carried out. In this chapter, and later chapters, the stoichiometry of plasma polymerised polymers produced by R.F. glow discharges in the fluoro-heteroaromatic systems are investigated using microanalysis and ESCA. The results show that the stoichiometric ratios of C:F and C:N are roughly similar for the polymer and the starting monomer.

Electron spin resonance spectroscopy has been used to determine the spin density of the free radicals in the plasma polymerised material.<sup>203-204</sup>

High resolution solid state NMR spectroscopy<sup>205-206</sup> has also been used in studying the structure of plasma polymerised films

Differential scanning calorimetry (DSC) and thermal gravimetric analysis (TGA) have shown that plasma polymers have no phase transitions before decomposition occurs, reflecting in general the thermal stability of these materials.<sup>207</sup> Important information available from using both techniques will be presented in this chapter and later chapters.

The application of ESCA to the study of structure and bonding in polymer surfaces has been described in chapter two. However, some of the important information levels available from ESCA which may be of use in the study of plasma polymerised and modified surfaces are indicated in Table 4.4.

Table 4.4.

1. Elemental analysis
2. Functional group analysis
3. Shake-up studies to investigate unsaturation
4. Angular studies
5. Kinetic studies

The contact angle determinations have been used extensively to investigate the polarity of the polymer surfaces.<sup>208-209</sup> A discussion concerning contact angle studies will also be considered in this chapter and later chapters. Results from the determination of contact angles indicate more rapid wetting of the fluoroheteroaromatic systems than fluorinated benzenes. This is consistent with the rapid hydrolysis of C-F bonds in the plasma polymer reflecting the hydrolytic instability of the monomer where replacement of a ring CF by N on going from the benzene to the pyridine strongly influences the reactivity of the ring system to nucleophilic attack.

Reflectance IR spectroscopy has been used extensively, the results are in agreement with those of transmission IR, and the technique has provided further information on the structure of the system and the reactivity of the polymer.

The gross morphological features of plasma polymerised polymer surfaces have been investigated using electron microscopy.

#### 4.3. Plasma Polymerisation

Plasma polymerisation by a variety of means has been an active area of research in academic and industrial circles over the past ten years with the predominant emphasis being on the investigation of organic systems.

The distinctive feature of plasma polymerisation as opposed to conventional polymerisation is that a variety of organic compounds which do not contain particular functional groups may be polymerised.

The major points of interest in plasma polymerisation may be elaborated as follows:-

1. Under what conditions may a plasma excited in a given monomer produce a polymeric film and how does the rate of deposition depend on the operating parameters?
2. How does the structure of a plasma polymerised film depend on the operating parameters?
3. Under a given set of operating conditions how reproducible are the results?
4. How does the structure of a plasma polymerised film depend on the nature of the precursor and how does this vary as a function of polymer formed in different regions of a plasma reactor?

Such questions are circumscribed by having available techniques for characterising the samples and for monitoring the rate of deposition of films.

The advent of ESCA as a spectroscopic tool has transformed this situation and it is possible to directly

monitor rates of deposition and obtain information on structure and bonding in the polymer film in the same experiment.

In recent work<sup>99,210-218</sup> ESCA has been used to study the fundamental aspects of plasma polymerisation of simple fluorinated alkenes, aromatics, alicyclics and hetero-aromatics system. The reason for the interest in fluoropolymer systems lies in their ease of study by means of ESCA. Thus Figure 4.6. shows the distinctive nature of the  $C_{1s}$  core level spectra for various structural features which might arise in fluoropolymers.

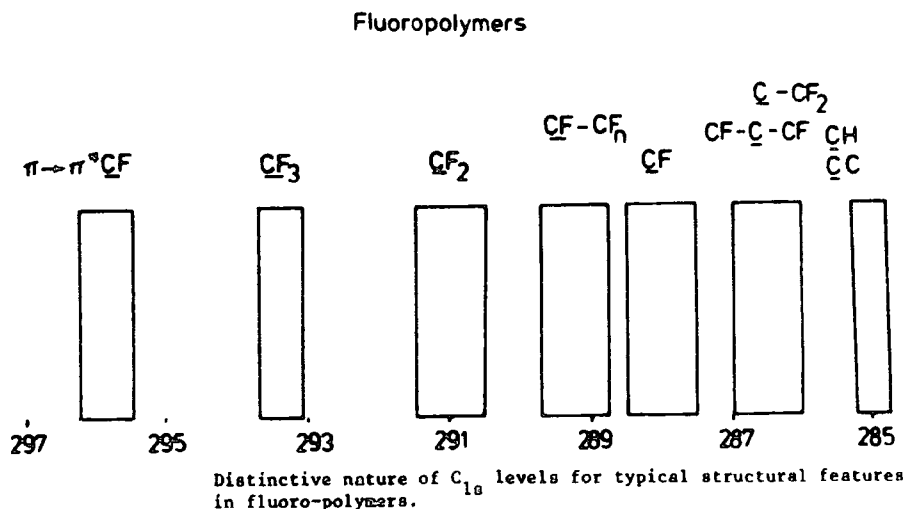


Figure 4.6. Distinctive nature of  $C_{1s}$  levels for typical structural features in fluoropolymers.

Yasuda and co-workers<sup>219</sup> introduced an important parameter (W/FM) which provides an indication of the total power dissipated in the plasma per unit weight of material. Thus if W is the total power (watt) input to the

plasma,  $F$  is the monomer flow rate (mole per unit time), and  $M$  is the molecular weight of the monomer in which the plasma is excited the  $W/FM$  is a conveniently definable parameter in the investigation of synthetic routes. A schematic of the typical behaviour of the deposition rate for polymer versus the  $W/FM$  is shown in Figure 4.7.

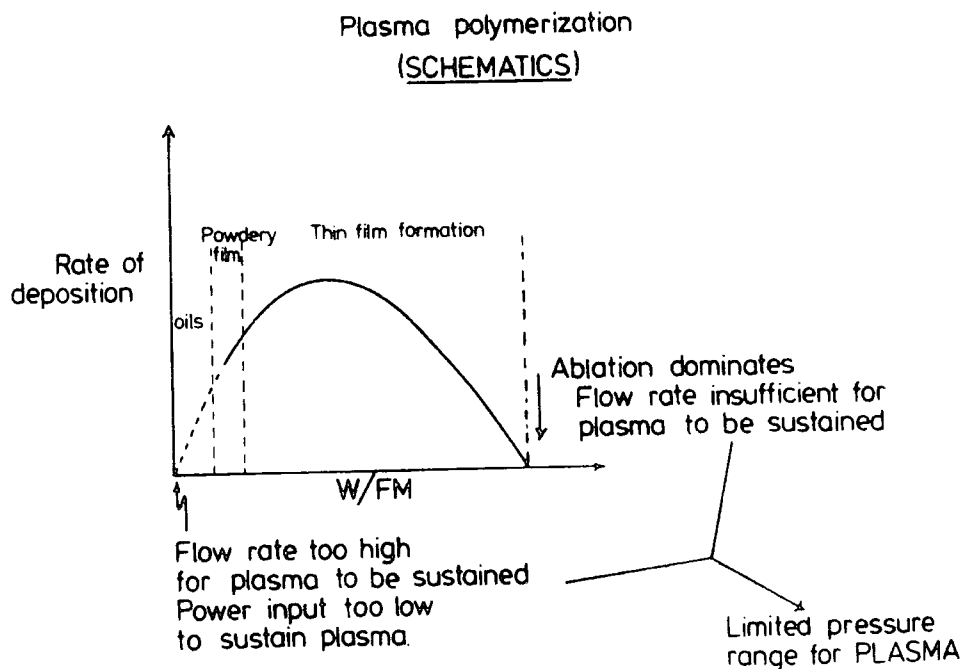


Figure 4.7. Plasma polymerisation schematic of rate of deposition as a function of  $W/FM$ .

The dynamic processes obtaining in a plasma polymerisation in glow discharges have been classified into "plasma-induced polymerisation" and "plasma-state polymerisation". The latter process is illustrated by Competitive Ablation and Polymerisation (CAP) mechanism and is shown schematically in Figure 4.8.

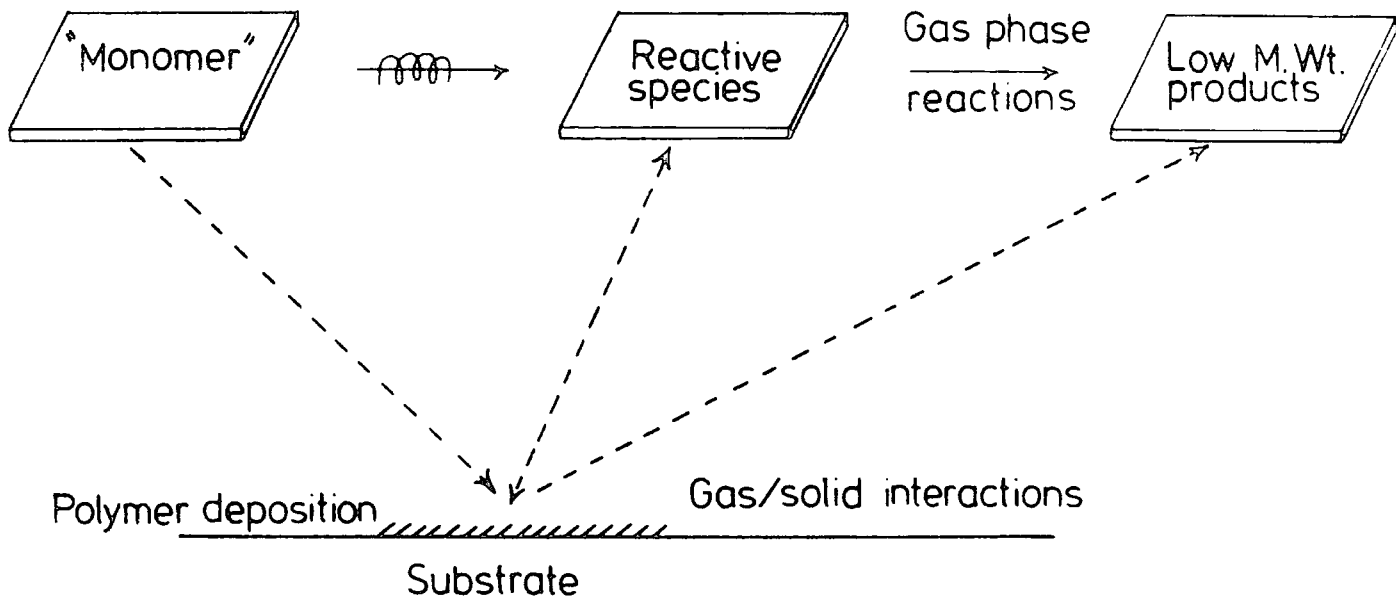


Figure 4.8. Dynamic processes in plasma polymerisation. Competitive Ablation and Polymerisation (CAP) mechanism.

#### 4.4. Polymer Films Produced by R.F. Plasma in Perfluoro-Pyridine

##### 4.4.1. Introduction

In this section the study of polymer films produced by glow discharge techniques as studied by ESCA is presented. Clark and co-workers have demonstrated the unique capabilities of ESCA as a spectroscopic tool for investigating aspects of structure, bonding and reactivity of polymer surfaces.<sup>114-117,219</sup>

Plasma polymerisation as a route to novel ultra thin coatings which may be deposited to a controlled thickness have excited considerable interest in both academic and industrial circles in recent years.<sup>193,199</sup> The considerable potential for technological exploitation of such films of novel, chemical, physical, electrical and



mechanical properties has spurred attempts to understand the relationship between the structure of the "monomer" in which the plasma is excited and the resultant cross-linked polymeric materials.<sup>116,193,199,219</sup>

Previous studies<sup>210-216</sup> have detailed investigations by means of ESCA of the gross structural features, compositions and rates of deposition of a wide variety of plasma polymers produced from perfluorinated aliphatic, alicyclic, aromatic and heterocyclic systems. In the particular case of the highly fluorinated benzenes, ESCA studies have shown that the dominant route to polymer formation involves rearrangement with evidence for ring scrambling processes which equilibrate isomeric substituted derivatives (e.g. the tetrafluorobenzenes).<sup>214</sup> There have been no previous studies of analogous fluoroheteroaromatic systems the study of which should yield considerable insight into the relationship between the "monomer" in which the plasma is excited and the polymer. The relative stability of benzenoid valence tautomers on going from the homoaromatic to the heteroaromatic system is increased whilst the reactivity to nucleophiles also increases dramatically.<sup>221</sup> This chapter presents an investigation of the plasma polymerisation of perfluoropyridine as a prototype for a perfluorinated heteroaromatic system and which therefore provides a convenient comparison with previous studies on perfluorobenzene and pentafluorobenzene.<sup>215-216</sup>

#### 4.4.2. Experimental

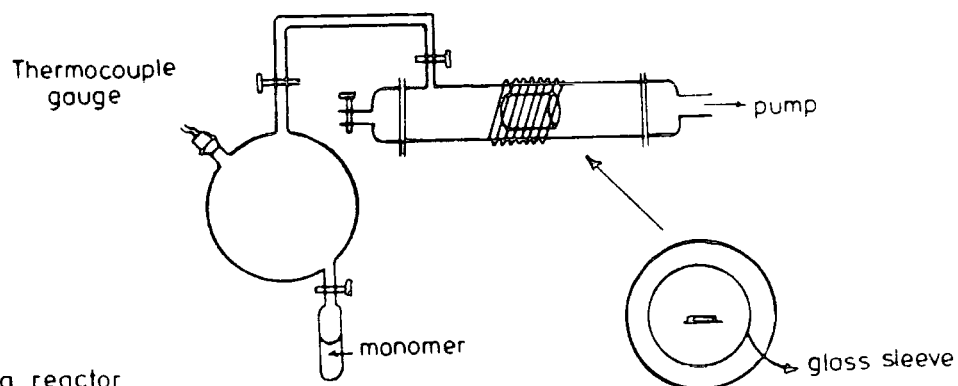
The work described in this chapter involved two polymerisation reactors, one (reactor A) consisted of a free-standing reactor incorporated into a grease-free vacuum line flow system. Samples prepared in this reactor configuration (A) were subsequently transferred to the ESCA spectrometer in air. The second reactor configuration (C) involved direct access to the insertion lock system of the ESCA spectrometer enabling samples to be prepared and studied in-situ without exposure to the atmosphere. Schematics of the reactor configurations (A and C) used in this study are shown in Figure 4.9.

The first reactor (reactor A) consisted a pyrex tube 5 cm. in diameter, 32 cm. long, sandwiched between ground glass flanges on "O" ring seals. The thin film of polymer was collected by deposition onto gold substrates located in a glass sleeve (1½" diameter, 8 cm. long), mounted along the bottom of the reactor in the centre of the coil. The rates of deposition of the polymer films were determined by deposition onto Al foil (2 x 1 cm.<sup>2</sup>), by measuring the weight increase of the foil using a CAHN electromicrobalance. For contact angle and multiple attenuated total reflectance (MATR) IR studies, however, the polymer films were deposited onto High Density Polyethylene (HDPE) substrates and were used soon after preparation.

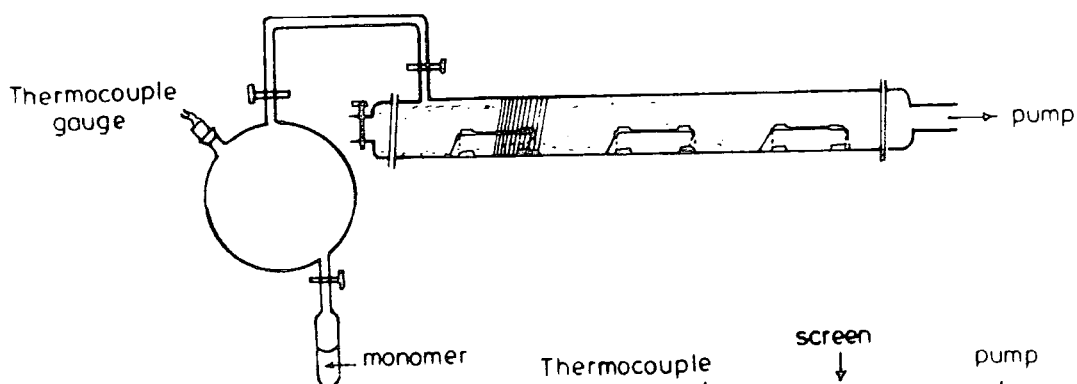
(MATR) IR spectra were recorded on a Perkin-Elmer 577 grating instrument with a 25 reflection ATR attachment. Optimization of the geometry for signal intensity and

## Reactor Configurations

## A) Short reactor (free standing rig.)



## B) Long reactor



## C) In-situ

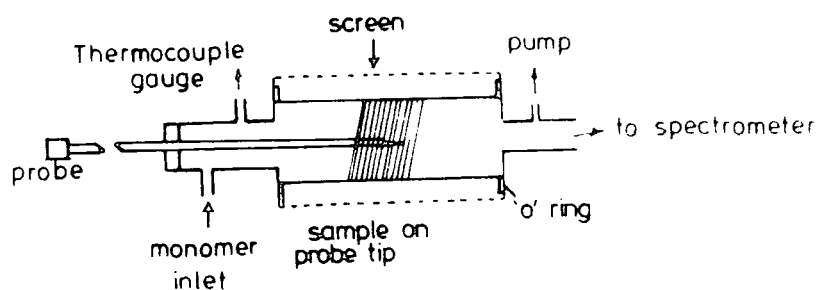


Figure 4.9. Schematic of the reactor configurations used in this study. (These are not to scale.)

resolution lead to incident/exit angles of  $45^\circ$  using a KRS 5 single crystal.

The second reactor used in this study is reactor (C), consisted of a pyrex tube 16 cm. long and 5 cm. diameter, sandwiched between stainless steel flanges by "O" ring seals, and enclosed in a copper mesh screen to prevent R.F.

interference with the electronics of the spectrometer. The polymer films were deposited onto gold substrates mounted on the ESCA probe tip by double-sided "Scotch" tape. The probe of  $\frac{1}{2}$ " diameter and 60 cm. long stainless steel was capable of passing through the reactor, on "O" ring seals and into the spectrometer for analysis.

Each of the systems (reactor A and C) was pumped by an Edwards ED50, 50 l min.<sup>-1</sup> two stage rotary pump, including cold trap to avoid the backstreaming of rotary pump oil.

In all cases, plasmas were excited using a Tegal Corporation R.F. generator operating at 13.56 MHz. Core level spectra were recorded on an AEI ES200A/B spectrometer using Mg<sub>k $\alpha$</sub> <sub>1,2</sub> x-radiation. The Au<sub>4f</sub><sub>7/2</sub> level at 84.0 eV and C1s level at 285.0 eV binding energies were used for energy calibration. Integration of spectra was accomplished on a Dupont 310 curve resolver.

In reactor (A) the flow rates were measured by monitoring the change of pressure as a function of time, for the relevant closed system, immediately after the pumping was valved off. For the small reactor (B) the monomer was directly vaporised into the inlet tube to the reactor, and the rate of deposition was measured by investigation of the signal attenuation of the substrate Au<sub>4f</sub> levels:

Microanalyses were made by combustion for carbon, hydrogen and nitrogen, and potassium fusion for fluorine. Sufficient quantities of samples for these analyses were obtained by removing the polymer which was deposited on the walls of the reactor inside the coil region.

The starting material pentafluoropyridine was prepared by fluorination of pentachloropyridine,<sup>220</sup> and was shown to be analytically pure by mass spectroscopy and G.L.C. The monomer was degassed in an auxiliary vacuum line pumped with an Edwards oil diffusion pump and two stage rotary pump by appropriate freeze-thaw cycles.

#### 4.4.3. Results and Discussion

##### (i) In-situ depositions

##### (a) Gross chemical structure

Preliminary experiments established that in the free-standing reactor plasma polymer deposition was rapid in the pressure and power regimes of 100 - 200 $\mu$ , and 10 - 35 watts respectively. However, ESCA analysis soon revealed that such samples were unstable in air with rapid uptake of oxygen, the spectra being consistent with nucleophilic displacement of fluoride by water. Pentafluoropyridine itself does in fact have a well developed chemistry based on nucleophilic aromatic substitution<sup>220</sup> and the effect of replacing a ring CF or CH group by nitrogen in going from perfluoro and pentafluorobenzene to perfluoropyridine has been well documented in this respect. The hydrophilic nature of the surface of the plasma polymers prepared in the free-standing reactor from pentafluoropyridine contrasts markedly with the distinctly hydrophilic nature of the plasma polymers from perfluoro or pentafluorobenzene produced under the same conditions.<sup>215-216</sup> There are obvious complications arising from surface hydrolysis of the polymer films arising from exposure to air at the typical laboratory (Relative

Humidity) RH of  $\sim 50\%$ , therefore the initial focus of attention was on plasma polymers prepared and studied in-situ, to avoid this complication.

As a starting point, briefly consider the core level spectra for plasma films deposited in-situ on gold substrates (1 watt,  $200\mu$ , 180 sec.). Whereas the core level spectra of fluoropyridine consist of  $C_{1s}$ ,  $N_{1s}$  and  $F_{1s}$  components centred at 290 eV, 402.3 eV and 690.7 eV respectively<sup>57</sup> with instrumentally and cross-section corrected area ratios corresponding to C:N:F stoichiometries of 5:1:5, the corresponding spectra for the plasma polymer shown in Figure (4.10) reveal evidence for extensive molecular rearrangement accompanying deposition. The  $C_{1s}$

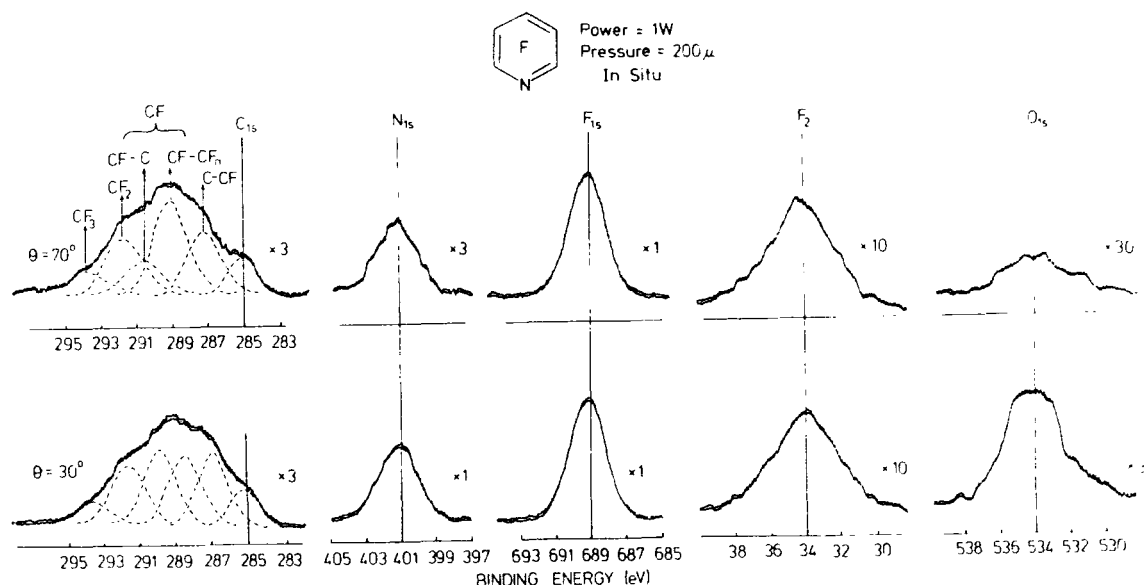


Figure 4.10.  $C_{1s}$ ,  $N_{1s}$ ,  $F_{1s}$ ,  $F_{2s}$  and  $O_{1s}$  spectra of the plasma polymer prepared in-situ at 1W discharge power and  $200\mu$  for 180 secs. at take-off angles of  $30^\circ$  and  $70^\circ$ .

levels for example show a broad structure extending from 285 eV to  $\sim$  294 eV with a standard line shape analysis revealing components arising from  $\underline{\text{CF}}_3$ ,  $\underline{\text{CF}}_2$ ,  $\underline{\text{C}}\text{-CF}$  and  $\underline{\text{C}}\text{H}$  components in addition to those arising from  $\underline{\text{C}}\text{F}$  centred at  $\sim$  288.5 eV and  $\sim$  290 eV ( $\underline{\text{C}}\text{F-C}$  and  $\underline{\text{C}}\text{F-CF}_n$ ). The angular dependent data reveals significant difference in the relative abundance of each structural feature as a function of depth into the sample and, as will become apparent, in contrast to films produced from the fluoroaromatics, the stoichiometry and structural features for the fluoroheteroaromatic system show distinct depth and time of deposition dependence.<sup>215-216</sup>

It is clear that nitrogen is retained in structure and the somewhat greater FWHM for the  $\text{N}_{1s}$  peak for the polymer compared with the monomer studied under the same conditions suggests that a range of molecular environments are present in the film. The centroid of the  $\text{N}_{1s}$  peak corresponding in binding energy to 401 eV may be compared with a value of  $\sim$  402.3 eV for the starting monomer.<sup>221</sup> Oxygen is detected at a low, but significant level and this could arise from traces of oxygen in the degassed monomer or more likely from the low level of  $\text{H}_2\text{O}$  and  $\text{O}_2$  desorbing from the internal surfaces of the reactor during plasma processing. An unusual feature clearly evident from the data in Figure 4.10. is the fact that relatively the intensity of the  $\text{O}_{1s}$  peak increases at lower take-off angle. This would suggest that the oxygen is not at the very surface but in the subsurface of the film. Previous work, would suggest that, the component at 285 eV arises from extraneous hydrocarbon contamination and indeed it does appear that the sticking coefficient for such

contamination which has not previously proved to be a problem is sufficiently high, that even for depositions carried out in-situ, low level contamination is not completely eliminated.

The total area ratios of 0.6(0.6), 2.8(2.5), and 13.8(11.8) for the  $C_{1s}/F_{1s}$ ,  $C_{1s}/N_{1s}$  and  $C_{1s}/O_{1s}$  levels at  $30^\circ$  and  $70^\circ$  take-off angles respectively suggests an "average" stoichiometry of approximately  $C_1:F_1:N_{0.3}:O_{0.05}$  compared with starting composition of  $C_1:F_1:N_{0.2}$ . This would indicate that the polymer is formed by rearrangement as in the benzene series,<sup>210-216</sup> with the low level of oxygen contamination corresponding to approximately 1 carbon in 20 having oxygen attached. Analysis of the  $C_{1s}$  line profile at take-off angle  $30^\circ$  gives the following component contributions in percentage terms  $\underline{CF}_3$  (7),  $\underline{CF}_2$  (20),  $\underline{CF}$  (49),  $\underline{C}$  (24) giving a C:F stoichiometry of 0.91 in reasonable agreement with that provided by the relative intensity ratios of the  $C_{1s}/F_{1s}$  levels. A possible source of error in determining the C:F stoichiometry from the components is the overlapping nature of shake-up<sup>57</sup> associated with  $\underline{C}$  and  $\underline{CF}$  structural features forming part of a conjugated system and which would increase in intensity the components attributed solely to  $\underline{CF}_3$  and  $\underline{CF}_2$  structural features. The net effect of this would be to slightly increase the derived "apparent" fluorine content of the film.

(b) Power dependence

Previous studies<sup>213,215</sup> have shown that for fluoroaromatic systems the gross structural features as a function of power (typically in the range  $W/FM \times 10^7 \text{ j kgm.}^{-1}$ ) at 10 - 50W



a given pressure are remarkably constant. The data for films deposited for 180 seconds at  $200\mu$  at a take-off angle of  $30^\circ$  are shown in Figure 4.11.

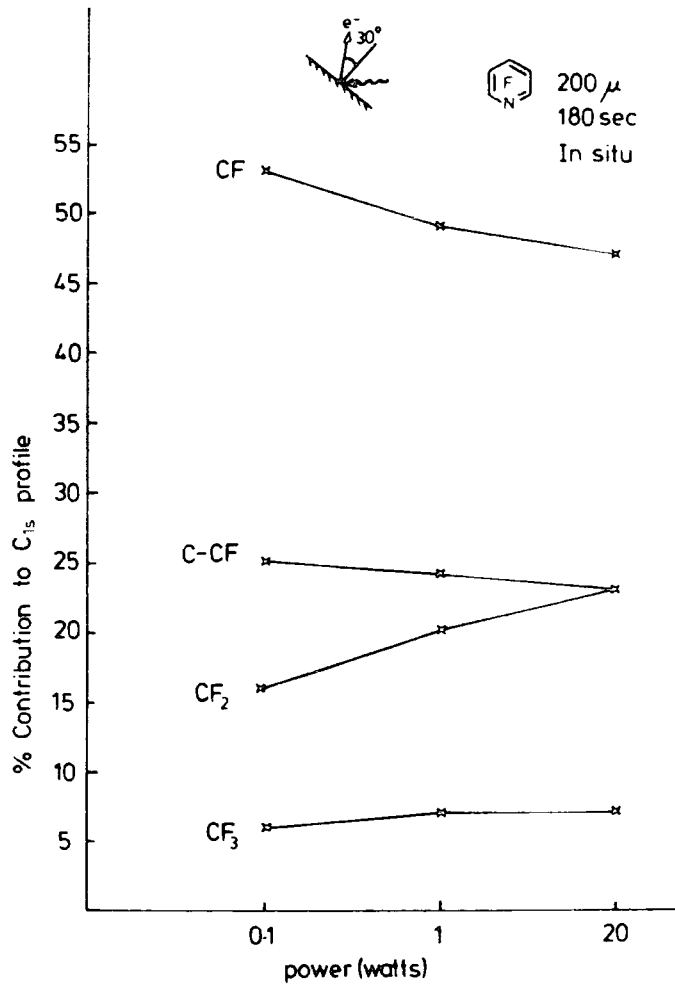


Figure 4.11. Percentage contribution to the  $C_{1s}$  envelope of the plasma polymers prepared in the in-situ reactor at  $200\mu$  as a function of power,  $\underline{CF}$  groups encompass ( $-\underline{CF}-C$  and  $\underline{CF}-CF_n$ ).

At higher powers there is a tendency for there to be a somewhat greater percentage contribution to the overall structure from  $\underline{CF}_2$  at the expense of  $\underline{CF}$  and  $\underline{C}-CF$  structural features, although the overall C/F stoichiometry remains

essentially the same. The C:F, C:N and C:O stoichiometries derived from the ESCA data are shown in Table 4.5. the results for the 30° and 70° take-off angle being, within experimental error, the same. Whereas the C/F overall

Table 4.5. C/F, C/N and C/O stoichiometries of in-situ plasma polymerised perfluoropyridine as a function of power and pressure.

power (W)	pressure (μ)	C/F component	C/F	C/N	C/O
0.1W	200μ	0.97	0.98	4.2	22.4
	100μ	0.85	1.2	3.1	-
0.4W	100μ	0.94	0.98	3.5	-
1W	200μ	0.91	0.98	3.3	20.7
	100μ	0.98	1.1	3.4	-
20W	200μ	0.88	1.0	2.7	14.1

stoichiometry remains the same, the C/N and C/O stoichiometries indicate increased incorporation of nitrogen and oxygen at higher powers. That the extraneous level of oxygen should be linked to the nitrogen content is not unreasonable since hydrogen bonding to amine functionalities would effectively scavenge any residual oxygen present in the form of water. At higher power desorption and ablation of -OH containing species from the reactor walls will also be of greater importance.

The N<sub>1s</sub> peak in each case consists of a broadened

(compared with the starting monomer) structure which may be analysed into two components centred at  $\sim 401.8$  eV and  $\sim 400.6$  eV respectively. The former corresponds reasonably closely with that for a nitrogen in a perfluoro environment as for example in the starting monomer (cf. 402.3 eV). The ratio of the two components are also indicated in Table 4.5. and it is worthwhile noting that perfluoropyridine itself is an extremely weak base.<sup>220</sup> The  $O_{1s}$  peak is also broadened indicating a variety of environments consistent with hydrogen bonding.<sup>65,70</sup>

The sensitivity of the overall C/N stoichiometry to the power dissipated in the plasma prompted the investigation of the power dependence at lower pressures in the range (0.1 - 1 watt) total power input using the pulsing facility with switching being on the microsecond scale, that shown in Figure 4.12.

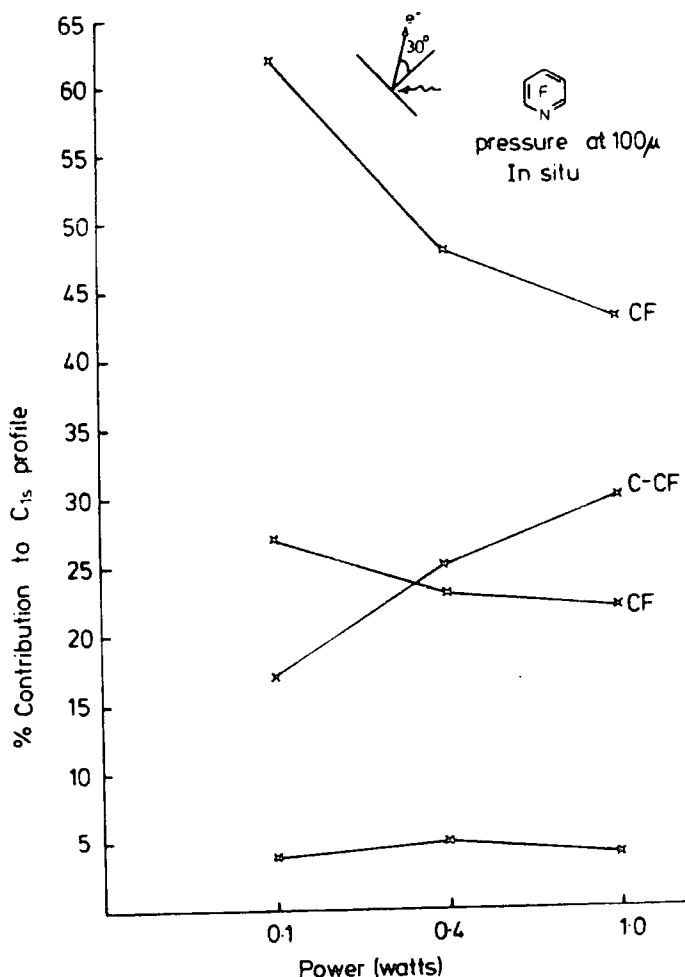
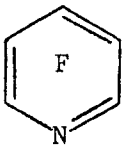

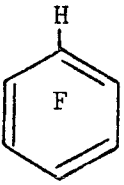


Figure 4.12. Percentage contribution to the  $C_{1s}$  envelope of the plasma polymers prepared in the in-situ reactor at  $100\mu$  as a function of power, CF groups encompass ( $-\underline{CF}-C$  and  $\underline{CF}-CF_n$ ).

For the in-situ depositions it is of interest to compare the C:F stoichiometry (relative to the starting monomer) and the components of the  $C_{1s}$  spectra of the films deposited under comparable conditions from pentafluorobenzene and from perfluorobenzene. The relevant data are shown in Table 4.6. At 1W and  $200\mu$ , comparison of the data for the nitrogen heterocycle and the fluoroaromatic of the same C:F stoichiometry, pentafluorobenzene suggests

Table 4.6. Comparison of C/F stoichiometry and percentage contribution of the  $C_{1s}$  envelope for in-situ plasma polymerised films of perfluoropyridine, perfluoro and pentafluorobenzenes as a function of power at  $200\mu$ .

polymer	power (W)	$\frac{C/F \text{ poly.}}{C/F \text{ mon.}}$	C/F	C-CF	CF	CF <sub>2</sub>	CF <sub>3</sub>	$\pi \rightarrow \pi$
	1W	0.9	0.91	24	49	20	7	-
	5W	0.9	0.93	21	55	20	4	-
	5W	0.9	0.92	25	47	18	8	2
	1W	1.0	1.2	33	50	9	4	4
	5W	0.92	1.1	32	47	14	4	4

that the heterocyclic system leads to a polymer with slightly higher fluorine content and this arises from a greater preponderance of  $CF_2$  structural features at the expense of carbons not carrying fluorine. The shake-up intensity also appears to be higher for the benzene based system.

A corresponding comparison between the perfluorinated heterocycle and aromatic system (perfluorobenzene) with films prepared at 5W and  $200\mu$  shows in Table 4.6. a close correspondence in the distribution of structural features.

The data indicate the subtle differences in gross structural features as a function of the structure of the starting monomer.

(c) Rate of deposition

Previous work indicates that one of the most distinctive features of thin film formation in the plasma polymer field is the close control which may be exercised in the rate of deposition.<sup>210-216</sup> The air sensitivity of the plasma polymer films produced from pentafluoropyridine makes the determination of rate of deposition somewhat complicated. However, for the in-situ depositions, the initial rates have been monitored by measuring the attenuation of the  $Au_{4f_{7/2}}$  levels of gold substrates. Figure 4.13. illustrates

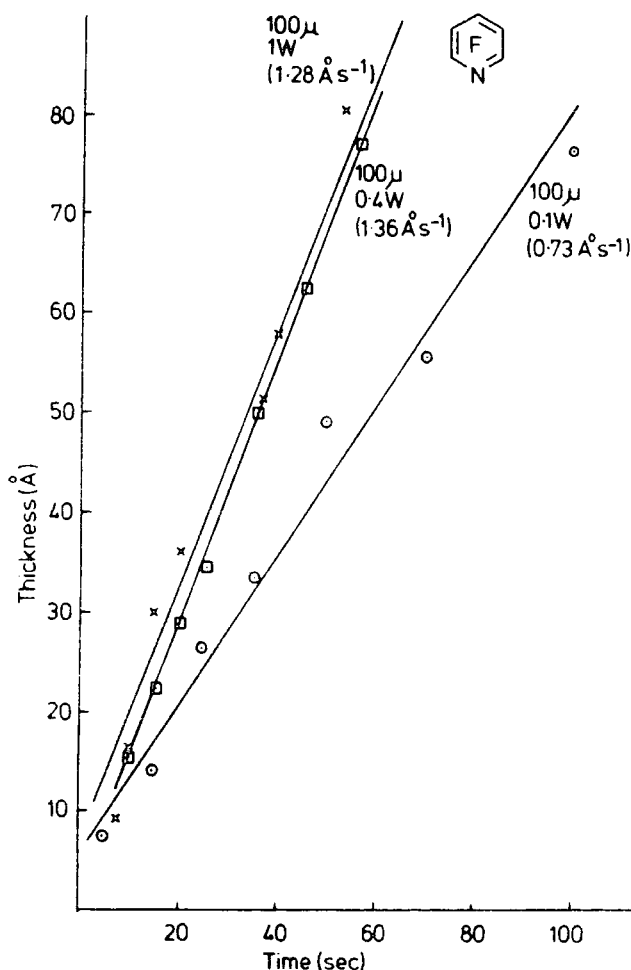


Figure 4.13. Thickness (Å) vs. time (secs.) for plasma polymers.

the initial deposition rates by means of ESCA, the data being displayed in Table 4.7. The rate of deposition at

Table 4.7. Rate of deposition of plasma polymerised films of perfluoropyridine prepared in-situ reactor at  $100\mu$  as a function of power, and comparison data with perfluoro and pentafluorobenzenes.

	power			
	0.1W	0.4W	1W	5W
perfluoropyridine	$0.73\text{\AA s}^{-1}$	$1.36\text{\AA s}^{-1}$	$1.28\text{\AA s}^{-1}$	-
perfluorobenzene	-	-	-	$11\text{\AA s}^{-1}$
pentafluorobenzene	-	-	$3.0\text{\AA s}^{-1}$	$2.0\text{\AA s}^{-1}$

$100\mu$  and 0.1W total input power is half that at 0.4W, and from Table 4.7. a comparison may be drawn with the rate of deposition at  $100\mu$  and 1W input power with pentafluorobenzene studied under the same conditions.<sup>215-216</sup>

The rate of deposition of the *homo*aromatic system is seen from this to be somewhat faster than for the *hetero*aromatic ( $3\text{\AA sec.}^{-1}$  vs.  $1.3\text{\AA sec.}^{-1}$ ).

(d) Time dependence

Previous studies<sup>213,216</sup> of the plasma polymerisation of fluoroaromatic systems indicate, that the depositions are uniform with time once the initial interface is established and that the composition does not vary with deposition time. Perfluoropyridine shows a striking departure from this behaviour, as is clearly evidenced by the component  $C_{1s}$  analysis presented in Figure 4.14. for films deposited at 1W

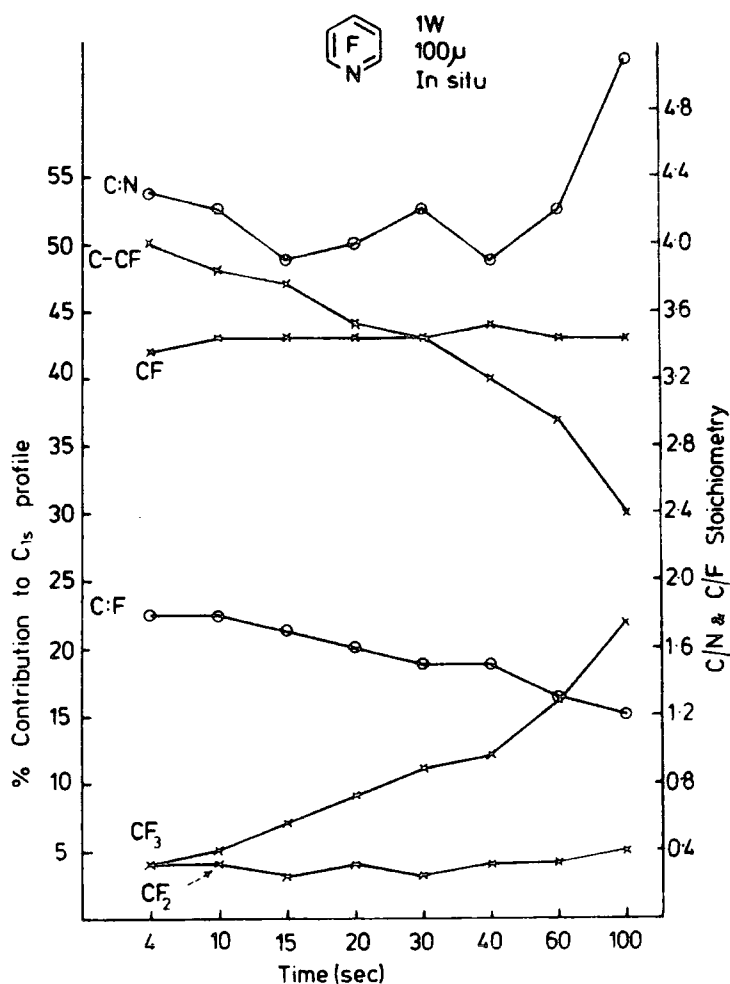


Figure 4.14. % contribution to the  $C_{1s}$  envelope and C:F and C:N stoichiometry of plasma polymer films prepared in-situ at 1W discharge power and 100μ as a function of time.



and  $100\mu$  for varying periods of time. Also shown in Figure 4.14. are the C:F and C:N stoichiometries as determined by ESCA, the C:F stoichiometry being derived independently from the component analysis and from the integrated intensities of the  $C_{1s}$  and  $F_{1s}$  levels. Initially the film deposited is lower in both fluorine and nitrogen content than that for the thick film deposited after 100 seconds. The representative spectra for the  $Au_{4f}$ ,  $C_{1s}$ ,  $N_{1s}$  and  $F_{1s}$  levels of perfluoropyridine deposited in-situ reactor C at 1W and  $100\mu$  as a function of time deposition are displayed in Figure 4.15. It is clear that over a range of varying periods of time of deposition, the gross chemical composition and structural features evidenced by ESCA show dependence on time of deposition. The possible reason for this could be that with the lower rate of deposition it is possible to study films at an earlier stage of deposition than for the fluoroaromatics previously described.<sup>213,216</sup> The ablative processes will obviously differ for the initial deposition, and the role of hydrolysis may be more important at the outset from any extraneous water in the system. As already been noted the plasma polymer films from perfluoropyridine are hydrolytically unstable, and this point will be considered in some detail in the next section of deposition in the free-standing reactor.

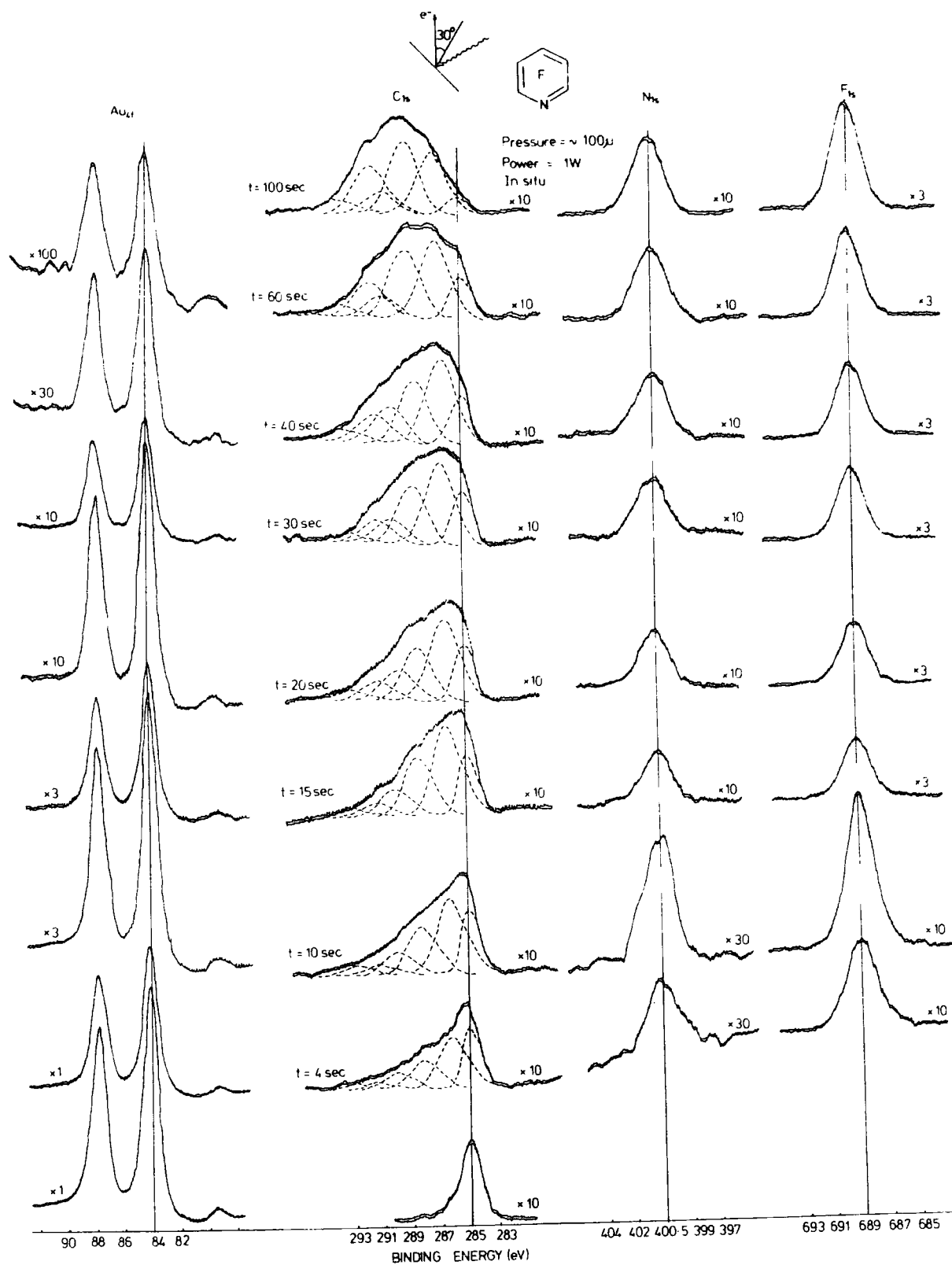


Figure 4.15. Au<sub>4f</sub>, C<sub>1s</sub>, N<sub>1s</sub> and F<sub>1s</sub> levels of plasma polymerized prepared in-situ reactor at 1W and 100 $\mu$ , as a function of time.

(ii) Depositions in free-standing reactor

(a) Gross chemical structure

The initial series of experiments were carried out in a free-standing reactor, A; the larger volume and higher pumping speed of which provides a lower value of  $W/FM$  for a given total power input.

The gross chemical composition and structural features have been investigated for plasma polymer films of perfluoropyridine deposited in the centre of the glow region of reactor A, at an input pressure of  $200\mu$  and power input 10, 25 and 35W, the ESCA spectra present the  $C_{1s}$ ,  $N_{1s}$  and  $F_{1s}$  levels in Figure 4.16. It is possible to say that over the range of powers and at a pressure of  $200\mu$ , the core levels of the plasma polymers obtained from perfluoropyridine are similar, but small differences are noticed when detailed line shape analyses of the  $C_{1s}$  level are considered. The peak at 285.0 is identified from the angular dependent studies as extraneous hydrocarbon contamination. This assignment of the peak at 285 eV is significantly higher than that of polymer films prepared in the in-situ reactor previously described.

The free-standing reactor provides a capability for obtaining sufficient material for microanalysis, and the results are shown in Table 4.8., together with the analysis based on ESCA. The surface and bulk compositions are in tolerable agreement, and show the same trend with power at fixed pressure. Thus higher power is associated with slightly lower fluorine content. Whilst the C/F stoichiometry

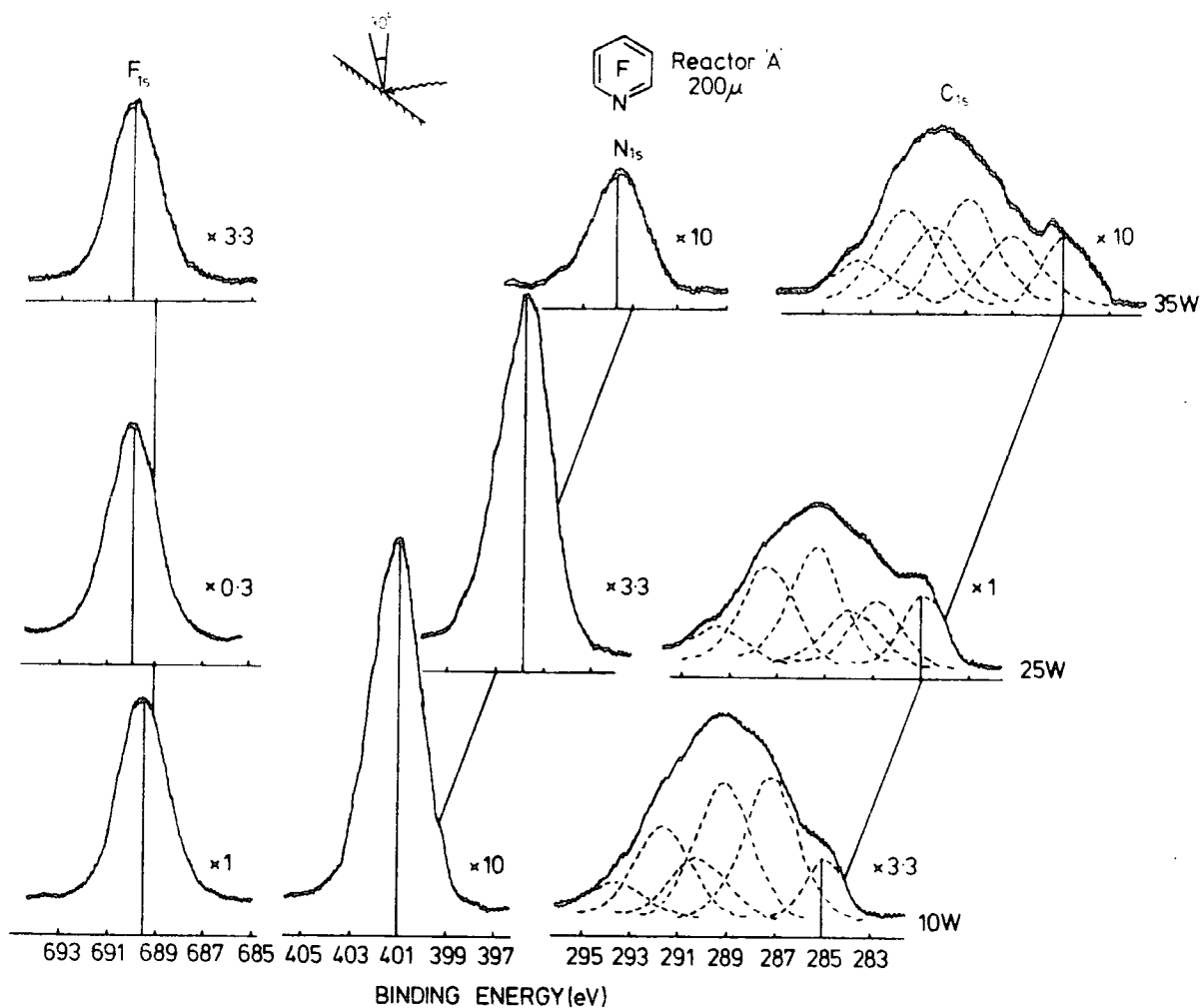


Figure 4.16.  $C_{1s}$ ,  $N_{1s}$ ,  $F_{1s}$  spectra of the plasma polymer prepared in reactor A at 200 $\mu$  and three discharge powers.

Table 4.8. Stoichiometric ratios of the bulk and surface of the plasma polymerised perfluoropyridine as a function of power.

Power and pressure	Bulk (Microanalysis)		Surface (ESCA)	
	C/N	C/F	C/N	C/F
10W 200 $\mu$	4.5	0.96	4.5	0.99
25W 200 $\mu$	4.0	1.1	4.5	1.0
35W 200 $\mu$	4.3	1.2	4.0	1.1



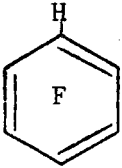
ratio is somewhat similar for the polymer and the starting monomer, the nitrogen content is significantly higher.

With the exception of one sample for which a small amount of silicon was detected, (arising from glass incorporated with the sample when it was mechanically removed from the reactor walls by means of a spatula) the level of oxygen was small. This indicates that extraneous oxygen functionalities are only at the very surface of the samples. The somewhat surprising thing in fact is that the level of oxygen detected by means of ESCA is not noticeably different for samples prepared in-situ, or in the free-standing reactor. This indicates that reaction occurs in the surface region extremely rapidly even with low levels of extraneous oxygen containing species (e.g.  $O_2$ ,  $H_2O$ ).

(b) Rate of deposition

It is of interest to measure rates of deposition for polymeric films produced in the free-standing reactor by direct measurement of weight increase of Al foils placed in the reactor. The data are shown in Table 4.9. At  $100\mu$  the rate of deposition decreases by  $\sim 2$  on going from 5W to 10W total input power whilst at  $200\mu$ , the rate effectively doubles on going to higher power. This reinforces the subtle control which may be exerted over deposition rate by means of the input power and pressure. Comparison may also be drawn with perfluorobenzene<sup>216</sup> and under one set of operating parameters, pentafluorobenzene.<sup>215</sup> In the case of perfluorobenzene the rate of deposition at

Table 4.9. Comparison of the rate of deposition of the plasma polymers prepared in reactor A, for perfluoropyridine, perfluorobenzene and pentafluorobenzene as a function of power.

power (W)	200 $\mu$		100 $\mu$	
	5W	10W	5W	10W
	10 $\text{\AA s}^{-1}$	17 $\text{\AA s}^{-1}$	2.3 $\text{\AA s}^{-1}$	1 $\text{\AA s}^{-1}$
	-	45 $\text{\AA s}^{-1}$		
	20 $\text{\AA s}^{-1}$			

200 $\mu$  pressure reaches a maximum at  $\sim 30$  watts. At 200 $\mu$  and 10 watts the deposition rate is  $\sim 3x$  higher than for the perfluoropyridine. For pentafluorobenzene the deposition rate at 200 $\mu$  and 5W is  $\sim 2x$  higher than for the perfluoropyridine under the same conditions.

(c) Comparison of "monomers"

The component analysis of the  $C_{1s}$  spectra for films deposited in the free-standing reactor as a function of "monomer" are shown in Figure (4.17.). As already alluded to the greater sensitivity to operating parameters of the plasma

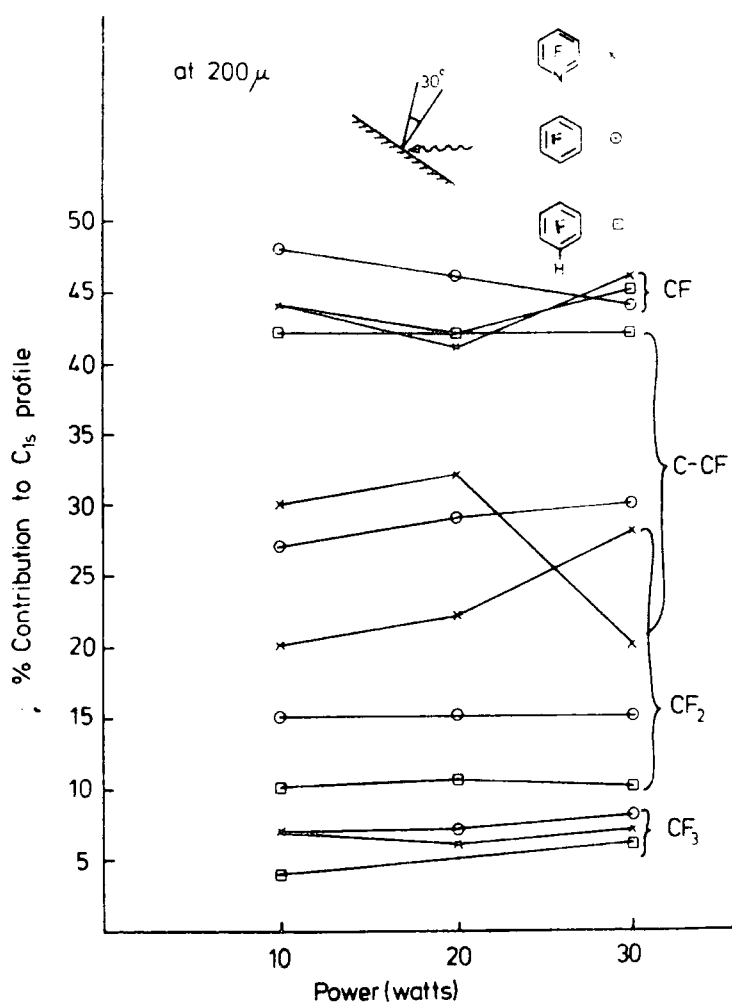


Figure 4.17. % contribution to  $C_{1s}$  envelopes for various structural features in the plasma polymers prepared in reactor A at  $200\mu$ .

films produced from pentafluoropyridine compared to the fluorinated benzenes,<sup>215-216</sup> is shown in the analysis presented in Figure (4.17.). In the range 10 - 30 watts the  $-CF_3$  contribution to the overall structure is comparable for all three monomers. Whilst for the fluorinated benzenes, the components for  $-CF_2$  groups remains essentially constant with power, for the perfluoropyridine there is an increase in the contribution from  $CF_2$  groups; the overall contribution in any case being higher for the pyridine ring system.

(d) Other measurements

Sufficient samples of material can be obtained from depositions in the free-standing reactor to make bulk measurements other than microanalysis which has previously been described.

(1) Contact angle

Films deposited onto either gold or high density polyethylene (HDPE) have been investigated with a view to following contact angle ( $H_2O$ ) as a function of time. Typical data are displayed in Figure (4.18.), and these

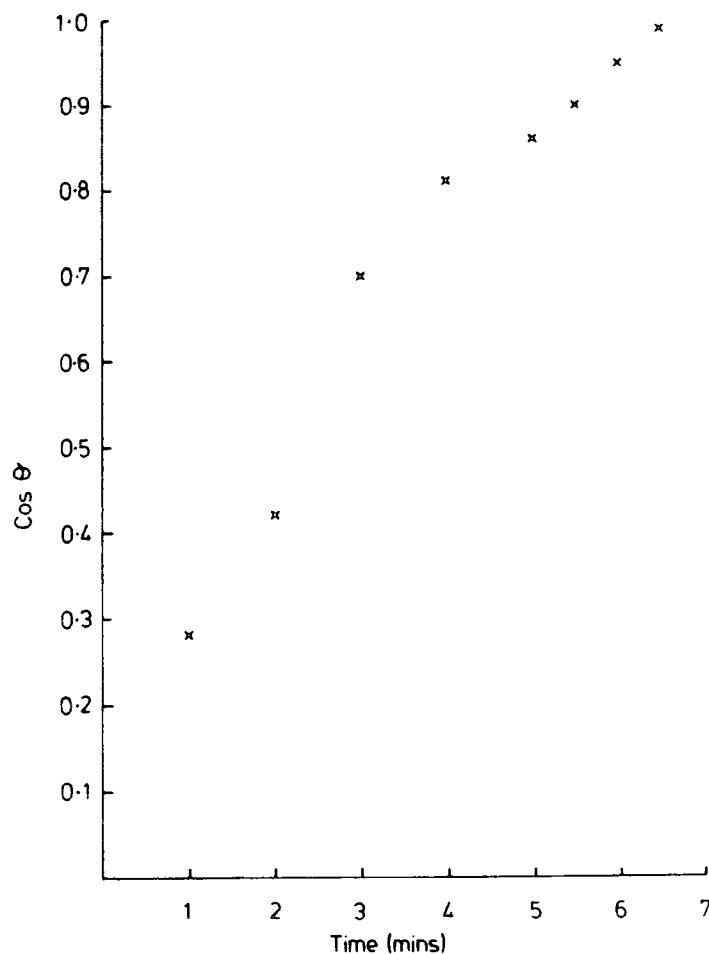


Figure 4.18. Cos. contact angle  $\theta$  vs. time (mins.)



indicate rapid wetting of the polymer film is striking contrast to the non-wetting (low critical surface tension) behaviour of the films produced from the fluorinated benzenes. This is consistent with rapid hydrolysis of C-F bonds in the plasma polymer reflecting the hydrolytic instability of the monomer where replacement of a ring CF group by N on going from the benzene to the pyridine strongly influences the reactivity of the ring system to nucleophilic attack.

## (2) Infra-red and UV studies

Powdered samples of the polymer have been studied in the form of KBr disks whilst samples deposited on HDPE have been employed in multiple attenuated total internal reflectance IR spectra. The spectra in both cases are displayed in Figure 4.19. and show relatively uninformative features being

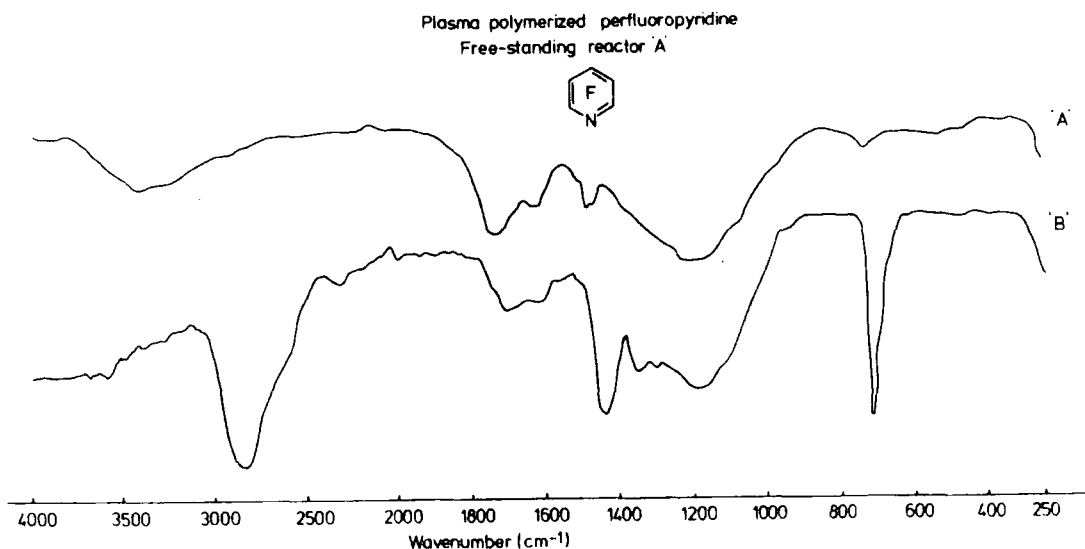


Figure 4.19. (a) IR spectra of plasma polymerised perfluoropyridine prepared in free-standing reactor, (KBr disk).  
(b) MATR-IR spectra of plasma polymerised perfluoropyridine film deposited onto HDPE at power 10W and 200 $\mu$  for 2 mins.

broad intense absorptions centred  $\sim 1200 \text{ cm.}^{-1}$  associated with  $\text{-C-F}$  structural features and low intensity broad absorptions in the region  $\sim 3400 \text{ cm.}^{-1}$  associated with  $\text{-O-H}$  stretching modes. The problems associated with the use of IR to elucidate structural features in fluorocarbon plasma polymer films has previously been discussed in the particular case of perfluoro-2-butyl-tetrahydrofuran<sup>213</sup> where the IR data is somewhat misleading.

$\sim 1000\text{\AA}$  thick films deposited onto HDPE ( $\sim 100\mu$ ) were investigated by means of difference UV spectra. Such films show only a very low level of end absorption.

### (3) TGA and DSC studies

Samples of the powder removed from the free-standing reactor have been investigated by both Thermal Gravimetric Analysis (TGA), and Differential Scanning Calorimetry (DSC), (Figure 4.20.). These studies indicate no well-defined

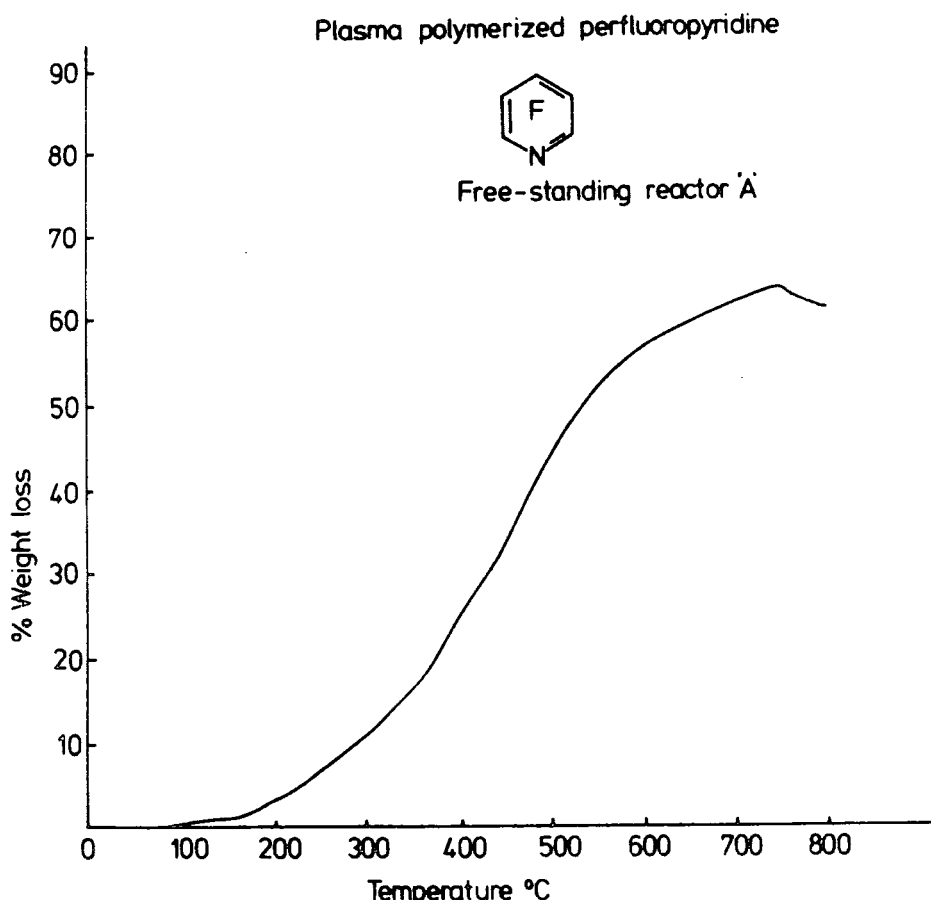


Figure 4.20. Thermogravimetry analysis of plasma polymerised perfluoropyridine in the free-standing reactor, (operating conditions, nitrogen atmosphere, heating rate  $20^\circ\text{C}/\text{min.}$ ).

transitions but a low rate of weight loss up to temperatures of  $\sim 600\text{K}$  at which stage there is a rapid onset of decomposition. This is somewhat similar in behaviour to the plasma polymer films produced from the fluorinated benzenes.<sup>213-216</sup> The low rate of weight loss at lower temperatures may well be associated with desorption of water and/or low M.wt. material based on the original monomer.

CHAPTER FIVE

CHAPTER FIVEPLASMA POLYMERISATION. A SYSTEMATIC INVESTIGATION  
OF MATERIALS SYNTHESISED IN INDUCTIVELY COUPLED  
PLASMAS EXCITED IN TETRAFLUOROPYRIDAZINEAbstract

A detailed investigation has been made by means of ESCA of the gross structural features and chemical composition of ultra thin plasma polymerised films prepared from tetrafluoropyridazine. The data reveals evidence of extensive rearrangement accompanying polymerisation with the C:F and C:N stoichiometries for the polymer films similar to those for the starting monomer. From an initially high contact angle with water the surfaces are found to become completely wettable with time and this is attributed to surface hydrolysis. Comparison has been drawn between surface and bulk compositions. Brief consideration is also given to sleeve effects.

### 5.1. Introduction

Clark and co-workers<sup>210-218</sup> have shown how the ESCA technique may be applied to the systematic investigation of how the structural features present in a polymer and its ultimate composition depend on the initial starting material and the operating parameters of the plasma instrumentation.<sup>219</sup>

Recent works<sup>211-216</sup> have considered in some detail the gross structural features and rates of deposition of plasma polymer films prepared under a variety of conditions from fluorinated monomers spanning aromatic, alicyclic and acyclic systems. In the particular case of the fluorinated benzenes,<sup>214-217</sup> plasma polymerisation provides a convenient route to materials of novel character and to complement these studies, an investigation of the related heteroaromatic system has been recently initiated.<sup>217</sup> A comparison between the gross structural features, compositions and rates of deposition of perfluorobenzene, pentafluorobenzene and pentafluoropyridine, (see chapter 4), is instructive and reveals the complex but well defined routes involved in the production of polymer films in the plasma reactor. The common theme relating plasma polymerisation of aromatic and heteroaromatic systems is the relative constancy of the composition of the polymers produced with respect to that of the initial monomer. In a previous chapter on perfluoropyridine for example, the C:N:F stoichiometry of the polymer is roughly the same as that of the monomer, indicating the dominance of rearrangement routes to the polymer as opposed to elimination. The incorporation of nitrogen in the

plasma polymer on going from perfluorobenzene to perfluoropyridine<sup>216-217</sup> strongly influences the final properties of the polymer. Thus whilst the plasma polymer from the nitrogen heterocyclic system becomes hydrophilic in contact with water that from perfluorobenzene is hydrophobic exhibiting a remarkably low critical surface tension of  $\sim 20 \text{ dynes cm.}^{-2}$ .

This chapter presents an investigation of tetrafluoropyridazine which a priori could conceivably eliminate molecular nitrogen directly and potentially lead to a solely fluorocarbon plasma polymer. An added interest in the 1,2-diazine is its greater propensity for rearrangement in the excited state (e.g. to prismanes, Dewar benzenes, benzvalenes and azafulvenes), and reactivity towards nucleophiles.<sup>220</sup>

Therefore the following have been studied:

- (i) The gross compositions and structural features as a function of power, pressure and site of deposition.
- (ii) Rates of deposition.
- (iii) Surfaces and bulk stoichiometries.
- (iv) Contact angle with water and thermal behaviour.

## 5.2. Experimental

Tetrafluoropyridazine has been studied in three reactor configurations at a variety of input powers, pressures and flow rates with a plasma being excited in an inductively coupled RF configuration. The range of these flow rates, powers, and pressures provided convenient deposition rates

for the polymer produced in the plasmas.

The three reactor configurations (A, B and C) used in this study are shown in Figure 4.9. Reactors A and C have been described in detail in Chapter 4.

Reactors A and B were used to produce polymer films which were subsequently transferred in air to the ESCA instrumentation for study.

Polymer films produced in reactor A were deposited onto gold substrates, located on a glass sleeve, mounted along the bottom of the reactor. Three types of glass sleeve have been used in this work.

Reactor B was specifically constructed to allow direct investigation of the structure of the polymer and rate of deposition as a function of site position in the reactor. This reactor in Figure (4.9.), consisted of an end-flanged pyrex glass tube, 100 cm. long and 5 cm. in diameter. Polymer films were deposited onto gold and aluminium foil substrates located at different sites along the reactor and deposition was studied as a function of position of the coil.

The structures of the polymers produced in reactor C have been studied as a function of power, pressure and time, the rates of deposition being measured by investigation of the signal attenuation of the substrate  $Au_{4f}$  levels.

In reactor A the rates of deposition of the polymer films onto Al foil ( $2 \times 1 \text{ cm.}$ )<sup>2</sup>, were determined by measuring the weight increase of the foil using a CAHN electromicrobalance. For contact angle and adhesion studies, however, the polymer films were deposited onto High Density



Polyethylene (HDPE), Al foil or gold substrates, and were used soon after preparation. Microanalysis was performed by combustion for carbon, nitrogen and hydrogen and potassium fusion for fluorine. Sufficient quantities of samples for these analyses and infrared (IR) measurements of KBr disks were obtained by removing the polymer deposited on the inside of the sleeve tube and from the walls of the pyrex reactor A, outside the coil region, and from the walls of the in-situ reactor C.

In all cases, plasmas were excited with a Tegal Corporation RF generator operating at 13.56 MHz and associated matching network. A pulsing facility was used at lower power levels with switching in the microsecond range.

Spectra were recorded on an AEI ES200B spectrometer with  $Mg_{K\alpha_{1,2}}$  x-radiation. The  $Au_{4f}$  level at 84.0 eV and  $C_{1s}$  level at 285 eV binding energy were used for energy calibration.

The gold substrates (Johnson Matthey, grade 2, sheet 0.3 mm. thick), were cut to a convenient size for direct mounting on the probe of the ESCA spectrometer.

The monomer was shown to be pure by GLC, and degassed at  $10^{-4}$  Torr before use. The starting material tetrafluoropyridazine was prepared by fluorination of tetrachloropyridazine according to the standard procedure.<sup>220</sup>

### 5.3. Results and Discussion

#### 5.3.1. In-situ Deposition

##### (i) Gross structure

Core level spectra for films deposited in-situ at 5W and 200 $\mu$  for a period of 180 secs. are shown in Figure 5.1. The  $C_{1s}$  levels show a broad envelope which at

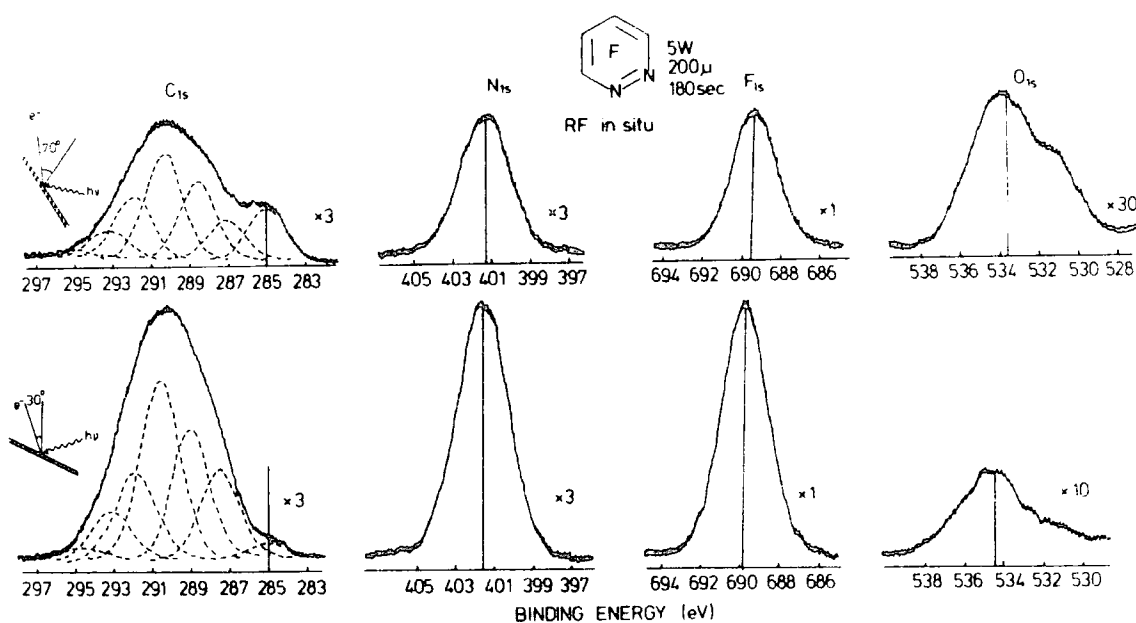


Figure 5.1.  $C_{1s}$ ,  $N_{1s}$ ,  $F_{1s}$  and  $O_{1s}$  spectra of the plasma polymer prepared in-situ reactor at 5W discharge power and 200 $\mu$  for 180 secs. at take-off angles of  $30^\circ$  and  $70^\circ$ .

$70^\circ$  take-off angle also shows evidence of a low binding energy (B.E.) hydrocarbon component. The fact that this is larger at  $70^\circ$  indicates the surface nature of this component

and the change in intensity with time indicates that the polymer film scavenges low levels of hydrocarbon background in the plasma reactor very efficiently compared with, for example, the plasma polymer films from perfluorobenzene.

The spectra reveal that nitrogen is retained in the polymer structure and there is also a low level of oxygen apparent; this is slightly greater at the very surface. Since the monomer itself is extremely reactive towards water this low level of extraneous reaction is not unexpected.

The integrated intensities obtained from the spectra at  $30^\circ$  and  $70^\circ$  take-off angles are  $C_{1s}/F_{1s}$  0.63(0.65),  $C_{1s}/N_{1s}$  1.6(1.8) and  $C_{1s}/O_{1s}$  13(11). The average stoichiometries calculated from these figures are C:F 1.1:1, C:N 2.1:1, compared with the corresponding figures for the "monomer" of C:F 1:1 and C:N 2:1, i.e. the polymer has slightly less fluorine and nitrogen than the starting "monomer". For comparison purposes the level of oxygen corresponds to  $\sim 1$  carbon in 20 having an oxygen attached.

Standard line shape analysis provides intensity ratios for the six components in the  $C_{1s}$  spectrum (other than extraneous hydrocarbon at 285 eV) corresponding to  $\underline{C}F-CF_n$  ( $\sim 287.5$  eV),  $\underline{C}F$  ( $\sim 289.0$  eV),  $\underline{C}F-CF_n$  ( $\sim 290.0$  eV),  $\underline{C}F_2$  (291.5 eV),  $CF_3$  ( $\sim 293.5$  eV) and a low intensity peak at  $\sim 294.0$  eV corresponding to a  $\pi \rightarrow \pi^*$  shake-up satellite of the  $\underline{C}F$  components (transition energy  $\sim 6.5$  eV).<sup>58</sup> The C:F stoichiometry derived from this data is 0.83:1 for both  $30^\circ$  and  $70^\circ$  take-off angles (excluding the low level hydrocarbon component in both cases). The discrepancy with

the stoichiometries derived from the  $C_{1s}/F_{1s}$  intensity ratios almost certainly arises from two principal causes. Firstly the low level of surface hydrocarbon contamination will attenuate the signal from the  $F_{1s}$  level more than that from the  $C_{1s}$  levels arising from the polymer. This is a consequence of the shorter mean free path of the photoemitted electrons from the  $F_{1s}$  level and leads to an underestimate of the fluorine content. The use of bulk derived sensitivity factors in this instance will also lead to a degree of uncertainty. Secondly the substituent effect of nitrogen leads to an overlap of the shake-up structure arising from lower binding energy components, and  $\underline{CF}_2$  and  $\underline{CF}_3$  structural features. This will have the effect of overestimating the fluorine content. The average of these two estimates suggests that under these reaction conditions, the polymer has a C:F stoichiometry which is essentially the same as that for the "monomer", i.e. 1:1.

(ii) Power and pressure dependence

The spectra displayed in Figure 5.1. reveal that polymerisation is accompanied by extensive molecular rearrangement. The gross structural features and derived stoichiometries as a function of power at constant pressure (200 $\mu$ ) are displayed in Table 5.1. It seems clear from this that at higher powers the C/F stoichiometric ratio tends to increase slightly, suggesting greater elimination of fluorine, whilst the C/N stoichiometric ratio decreases. At low powers there is evidence that there is a greater extent of nitrogen elimination. The gross structural features also

Table 5.1. C/F, C/N and C/O stoichiometric ratios and percentage contribution of C<sub>1s</sub> envelope of plasma polymers prepared in-situ reactor at two take-off angles 30° and 70° as a function of power at 200μ.

Power (W)	Angle θ	Stoichiometry Ratio				% C <sub>1s</sub> Contribution				
		C/F comp.	C/F	C/N	C/O	C-CF	CF	CF <sub>2</sub>	CF <sub>3</sub>	π→π*
0.1W	30°	0.91	0.89	2.9	26.8	23	48	24	5	-
	70°	0.83	1.0	2.5	22.4	21	42	31	5	1
0.5W	30°	0.93	1.04	2.3	-	19	60	15	6	1
	70°	-	-	-	-	-	-	-	-	-
5W	30°	0.86	1.0	2.0	20.7	17	56	17	8	2
	70°	0.83	1.1	2.2	17.2	22	58	20	8	2
10W	30°	1.0	1.0	1.9	48.4	29	46	19	6	-
	70°	1.0	1.1	2.0	-	29	48	19	4	-
20W	30°	1.0	1.1	1.9	-	27	50	17	4	2
	70°	0.86	1.3	2.0	-	25	41	25	8	1
30W	30°	0.91	1.2	1.7	20.6	25	45	25	5	-
	70°	0.83	1.3	1.7	-	18	40	27	9	-

reveal the subtle changes in microstructure as a function of polymerisation conditions; the results again indicating the much greater sensitivity to polymerisation conditions for the heterocyclic systems compared to the benzene system which have been studied previously.<sup>214-216</sup>

The dependence on pressure in the range 50 - 300μ has been investigated at a fixed input power of 10 watts. The

relevant data, on the stoichiometric ratios and the percentage contribution to the  $C_{1s}$  envelopes, are displayed in Table 5.2., and reveal that at high W/FM (low pressure), the

Table 5.2. C/F, C/N and C/O stoichiometric ratios and percentage contribution of the  $C_{1s}$  envelope of plasma polymer films prepared in-situ reactor at LOW discharge power as a function of pressure.

Pressure ( $\mu$ )	Angle $\theta$	Stoichiometry Ratio				% $C_{1s}$ Contribution				
		C/F comp.	C/F	C/N	C/O	C-CF	CF	CF <sub>2</sub>	CF <sub>3</sub>	$\pi \rightarrow \pi^*$
50 $\mu$	30 $^\circ$	1.6	1.4	1.5	6.1	55	30	11	4	-
	70 $^\circ$	-	-	-	-	-	-	-	-	-
100 $\mu$	30 $^\circ$	1.2	1.6	2.3	-	40	40	14	4	2
	70 $^\circ$	1.3	1.6	2.3	-	41	41	14	3	1
200 $\mu$	30 $^\circ$	1.0	1.0	1.9	48.4	29	46	19	6	-
	70 $^\circ$	1.0	1.1	2.0	-	29	48	19	4	-
300 $\mu$	30 $^\circ$	0.95	1.1	2.3	46.2	31	36	23	8	2
	70 $^\circ$	1.0	0.95	2.3	-	31	38	23	6	2

fluorine content of the polymer decreases, whilst the nitrogen content increases. These conditions also correspond to a significantly higher level of oxygen in the polymer, which considering the sensitivity of the monomer to moisture is remarkably low in any case. The  $C_{1s}$  spectra for 10 watts power at two take-off angles, 30 $^\circ$  and 70 $^\circ$ , (Figure 5.2.), reveal that polymerisation is accompanied by molecular rearrangement which is a function of pressure (50 - 300 $\mu$ ).

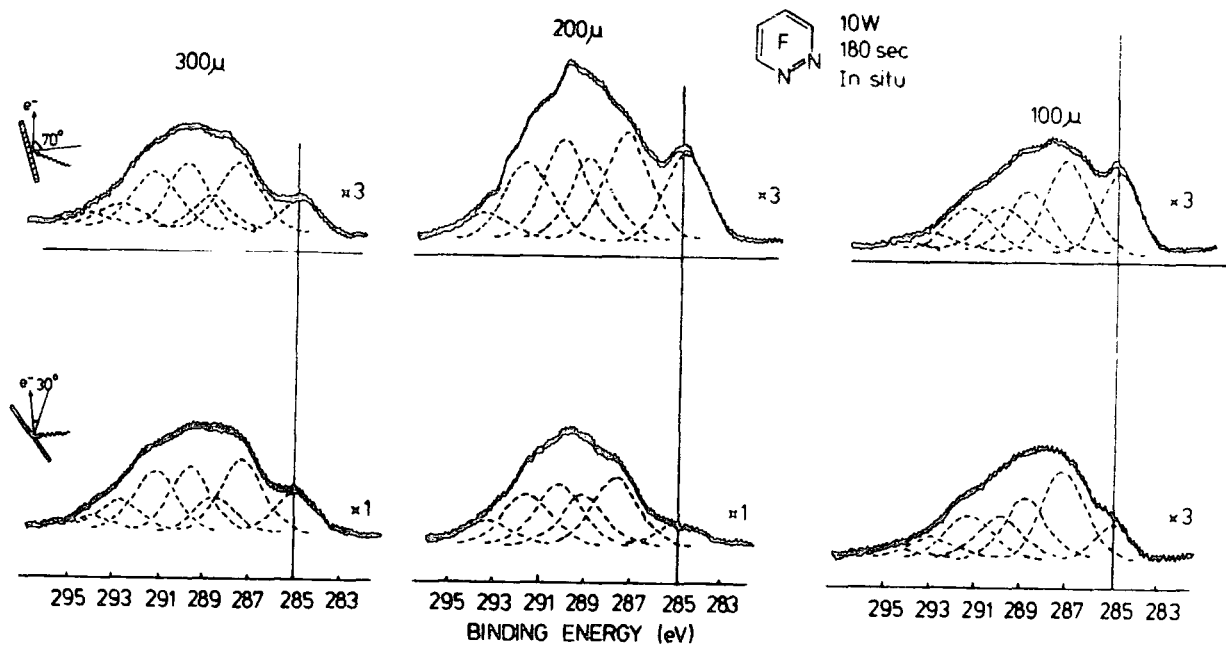


Figure 5.2.  $C_{1s}$  spectra of plasma polymers prepared in-situ reactor at 10W as a function of pressure at two take-off angles  $30^\circ$  and  $70^\circ$ .

(iii) Time dependence

Previous work<sup>217</sup> indicated that for the heterocyclic system perfluoropyridine, the composition of the plasma polymer film varied slowly as a function of time of deposition. This may reflect the high reactivity of the monomer system towards extraneous material in the plasma environment when the plasma is first initiated, and as evidence of this, Table 5.3., shows the relative intensity ratios for the core level spectra as a function of time for plasma polymers deposited at  $100\mu$  and 1.5 watts over a period of 35 seconds. From this it is clear that initially there is a large amount of oxygen in the polymer film which decreases as the film is deposited.

Table 5.3.  $C_{1s}/F_{1s}$ ,  $C_{1s}/N_{1s}$  and  $C_{1s}/O_{1s}$  and % contribution of the  $C_{1s}$  envelope of plasma polymer films prepared in-situ reactor of 1.5W and 100u as a function of time deposition.

Time	Area Ratios			% $C_{1s}$ Contribution			
	$C_{1s}/F_{1s}$	$C_{1s}/N_{1s}$	$C_{1s}/O_{1s}$	C-CF	CF	CF <sub>2</sub>	CF <sub>3</sub>
5 sec.	1.1	1.9	1.2	32	54	11	3
15 sec.	1.3	1.8	2.9	32	55	11	2
25 sec.	1.2	1.9	4.5	26	56	14	4
35 sec.	0.7	1.8	6.3	17	58	19	6

The components of the  $C_{1s}$  spectra suggest that as the film is deposited there is an increased proportion of  $\underline{CF}_3$  and  $\underline{CF}_2$  structural features and this is clear from the data displayed in Figure 5.3. This again suggests that initially deposited films of this reactive monomer are much more dependent on all of the operating parameters than for the corresponding fluorinated benzenes.



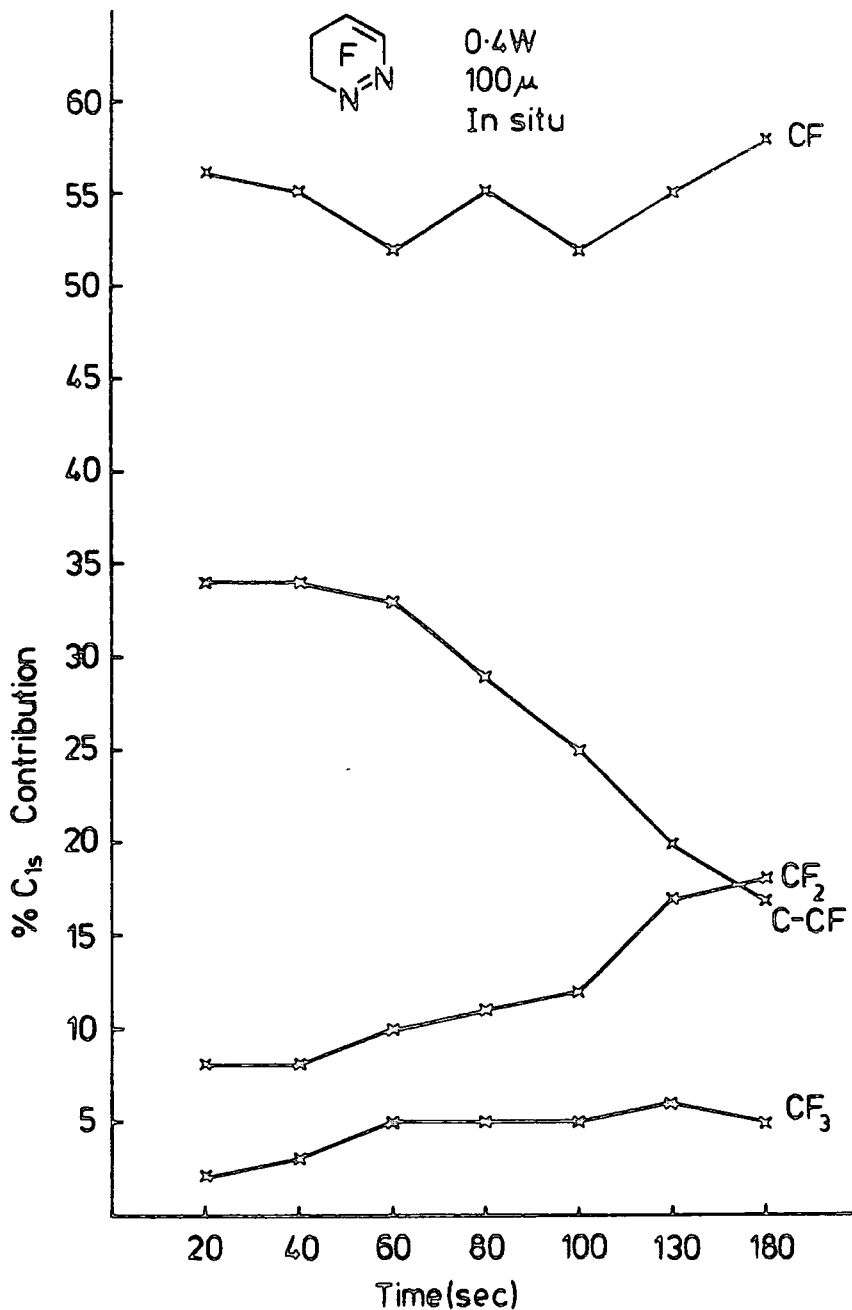


Figure 5.3. % contribution to the  $C_{1s}$  envelope of plasma polymer films prepared in-situ reactor at 0.4W discharge power and 100 $\mu$ , as a function of time deposition.

(iv) Rate of deposition

The sensitivity of the structure of the initially deposited film of the plasma polymer to the plasma conditions

leads to significantly greater error in directly measuring deposition rates compared with that for the previously studied fluorobenzenes.<sup>214-216</sup> Typical data obtained from the measurement of the attenuation of the  $Au_{4f_{7/2}}$  signal as a function of time are shown in Figure 5.4. The deposition rates follow a consistent trend. Thus at  $100\mu$  the rate

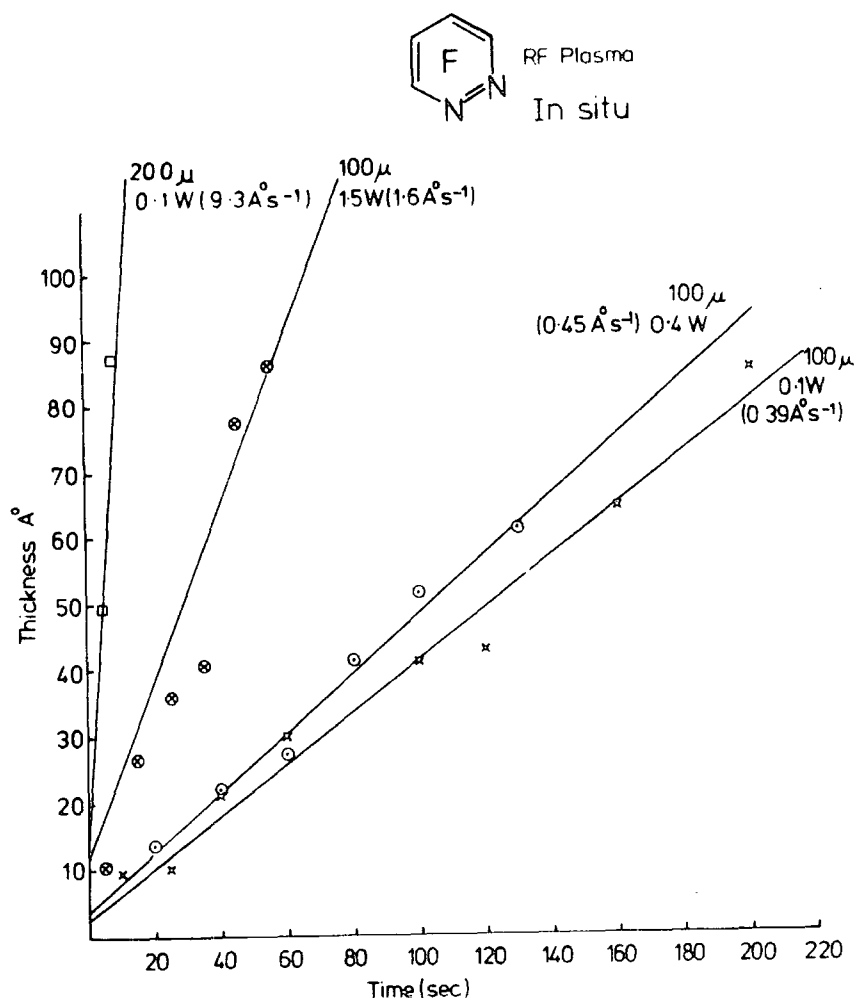


Figure 5.4. Thickness (Å) vs. time (secs.) for plasma polymer prepared in-situ reactor.

increases on going from a power input of 0.1 watt to 1.5 watts, the rate for the latter being  $1.6 \text{ Å sec.}^{-1}$ . The rate of

deposition increases so rapidly at the higher pressure of  $200\mu$  that it is not possible to accurately measure the rate from the attenuation of the  $Au_{4f}$  signal. A rough estimate from the data in Figure 5.4. suggests that at 0.1 watt the rate increases from  $\sim 0.4\text{\AA} \text{ sec.}^{-1}$  at  $100\mu$  to  $\sim 10\text{\AA} \text{ sec.}^{-1}$  at  $200\mu$ .

### 5.3.2. Depositions in the free-standing reactors

The initial experiments carried out in the free-standing reactor, and as already seen the depositions carried out in-situ indicate the sensitivity of the surface composition to low levels of extraneous contaminants in the atmosphere (e.g.  $H_2O$  and hydrocarbon). The focus of attention in studying plasma polymerisation of perfluoropyridazine in the free-standing reactor has been:-

- (a) The comparison of bulk (microanalysis) and surface compositions;
- (b) The rate of deposition;
- (c) The site dependence of deposition;
- (d) The investigation of contact angles, adhesion and thermal behaviour.

#### (i) The bulk and surface analysis

With depositions in reactor A sufficient samples have been available for microanalyses (C, H, N by combustion, F by potassium fusion), to enable a direct comparison of the bulk with surface chemistry determined by ESCA. Since the deposition occurs primarily in the coil region the bulk

stoichiometries of materials deposited both in the coil region or in the regions outside the region of maximum glow have been investigated. For convenience films deposited in the glow region were deposited on the inside surface of a close fitting pyrex glass tube (sleeve), covering the region 8 cms. either side of the centre line of the coil. The sleeve could be removed after each deposition, and the material then removed from the inside surface by gently abraiding with a stainless steel spatula. Under the conditions of the experiment, material deposited in the coil region formed yellowish clear films which could in fact be readily removed as a film from the glass surface. After removing the sleeve the material deposited either side of the coil region in the reactor walls, was also removed by means of a spatula. The material itself was noticeably different in physical form from that deposited in the coil region, being powdery in nature. Whilst the material deposited in the coil region was insoluble in any of the common solvents, that deposited outside was slowly soluble in acetonitrile, but not in hydrocarbon, aromatic or simple ester or ketone (e.g. ethylacetate, methyl ethyl ketone) solvents.

This perhaps suggests that the material deposited outside the coil region contains lower molecular weight material.

The microanalysis data and the derived stoichiometries for the polymer samples, and for comparison purposes the starting monomers, are shown in Table 5.4. The fact that the microanalysis data for the starting monomer is slightly low in

C/N ratio cf. 1.92 vs. theoretical value of 2.0, indicates the difficulty of analysing these materials even by traditional microanalytical techniques.

Table 5.4., also shows that the film material from the sleeve yields C/N and C/F ratios both of which are higher

Table 5.4. Stoichiometric ratios of the bulk and surface of the plasma polymerised tetrafluoropyridazine.

	Bulk (Microanalysis)		Surface (ESCA)		
	C/F	C/N	C/F	C/N	C/O
Monomer	1	1.92	1	2	-
Polymer film from the sleeve, at (10W, 200 $\mu$ )	1.18	2.44	0.99	2.0	14.3
Polymer powder from the reactor at (10W, 200 $\mu$ )	1.05	2.70	0.99	2.1	10.0
Polymer powder from the reactor at (10W, 200 $\mu$ ) after 6 months	1.45	2.56	0.77	1.8	2.0
Polymer film from the in-situ reactor at (10W, 200 $\mu$ )	1.18	2.44	1.0	2.0	48.4

than for the "monomer", indicating slightly less nitrogen and fluorine in the polymer. By contrast the corresponding ESCA data suggests a slightly increased nitrogen content, although the fluorine analysis agrees remarkably well.

If it is assumed that the deficit in the total micro-

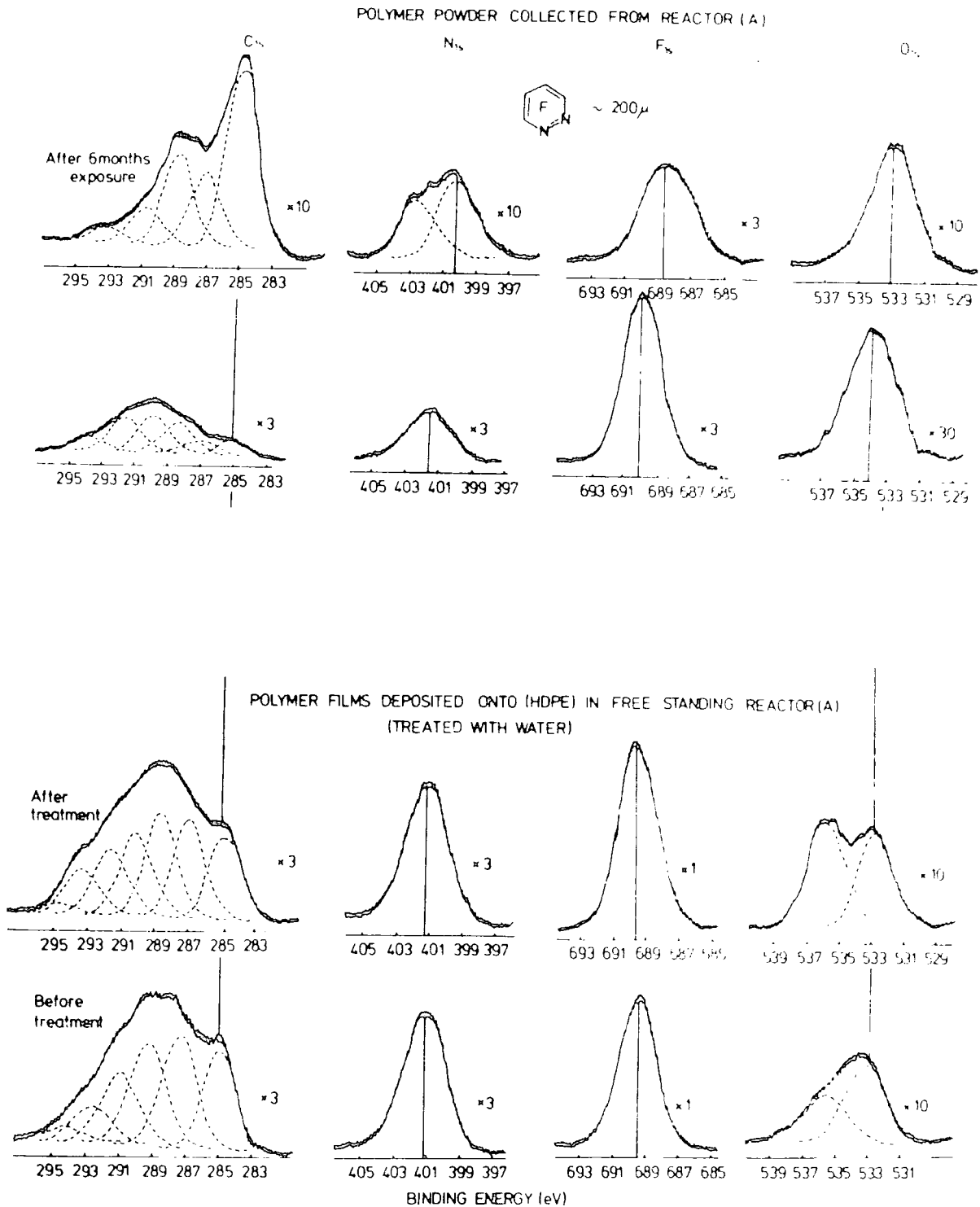
analysis figures arises from oxygen the ESCA data would indicate a level of oxygen in the surface regions  $\sim 2x$  that for the bulk.

The microanalysis for the powdery samples from outside the coil region suggests a C/F ratio similar to that of the film samples but a higher C/N ratio. The ESCA analysis, however, is remarkably similar to that for the film sample and for the starting "monomer". It is interesting to note **that in** this case the "deficit" in the microanalytical data is small and if it is again assumed that this arises from oxygen, the C/O ratio for the surface is very much higher than for the bulk.

A later section, briefly alludes to the changes in contact angle with time for the film samples, and these indicate a chemical reaction which is also evident from the microanalytical data.

Thus, also shown in Table 5.4., are microanalytical data for samples which have been exposed to air for a period of  $\sim 6$  months. For the bulk analysis it is clear that the effect of long term exposure to the laboratory environment is a decrease in fluorine content, the nitrogen content remaining about the same as the previous sample, (see Table 5.4.). That the major process occurring in this period, is hydrolysis is clear since the microanalysis reveals (by difference) a large uptake of oxygen accompanying loss of fluorine. The ESCA data reveal the apparent increase in fluorine (low  $C_{1s}/F_{1s}$  ratio), and the core levels spectra themselves (Figure 5.5.), show that hydrolysis produces fluoride,

(evident as the low binding energy component), and also indicate extensive rearrangement as a function of exposure.



**Figure 5.5.** Comparison of  $C_{1s}$ ,  $N_{1s}$ ,  $F_{1s}$  and  $O_{1s}$  spectra of the plasma polymer prepared in free-standing reactor at 15W and  $200\mu$ , before and after treatment by water, and polymer powder as a function of exposure.

Hydrolysis therefore releases fluoride which migrates to the surface of the samples. The component analysis of the  $C_{1s}$  spectra for the samples deposited in reactor A, also shown in Table 5.5., displays a remarkable correspondence with those for the in-situ deposition (e.g. 10W, 200 $\mu$ ).

Table 5.5. Comparison of percentage contribution of  $C_{1s}$  envelope of plasma polymerised tetrafluoro<sup>1s</sup> pyridazine prepared in free-standing reactor and in-situ reactor.

Polymer	C-CF	CF	CF <sub>2</sub>	CF <sub>3</sub>	$\pi \rightarrow \pi^*$
Film in the free stand reactor at (10W, 200 $\mu$ )	12	59	18	9	2
Powder from the free stand reactor at (10W, 200 $\mu$ )	21	52	17	10	-
Film in-situ reactor at (10W, 200 $\mu$ )	29	46	19	6	-

(ii) Rates of deposition

Rates of deposition measured by means of a capacitance microbalance, have been determined for a variety of operating conditions, as a function of site in reactor B. Polymer films deposited on Al foil substrates at 7 different sites in the reactor, corresponding to the coil being centrally located in the 1 meter reactor provides the data shown in Figure 5.6.; this pertains to samples deposited in reactor B at 10 watts input power and 200 $\mu$ , (deposition time 30 seconds). The deposition is fairly uniform in the



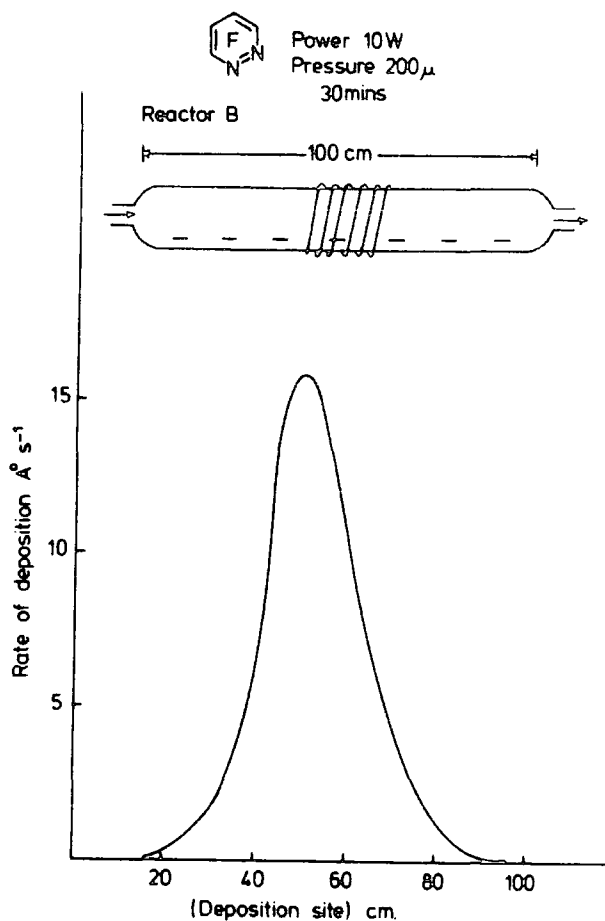


Figure 5.6. Rate of deposition  $\text{\AA s}^{-1}$  vs. site of deposition (cms.).

coil region and falls off on either side of the region of maximum glow, in a symmetric manner.

The rates of deposition also have been measured in the coil region in reactor configuration A as a function of power and pressure, and are shown in Table 5.6. Unfortunately it did not prove possible to maintain a stable glow at 5 watts and 200 $\mu$ ; the results, however, are in line with those produced in the in-situ reactor configuration. Thus the rate of deposition decreases sharply in going from 200 $\mu$  to 100 $\mu$  pressure. The rates of deposition, determined as an

Table 5.6. Rate of deposition of plasma polymer films prepared in free-standing reactor A as a function of power and pressure.

Power (W)	Pressure ( $\mu$ )	Rate of deposition $\text{\AA s}^{-1}$
5W	100 $\mu$	1.9 $\text{\AA s}^{-1}$
10W	100 $\mu$	2.2 $\text{\AA s}^{-1}$
10W	200 $\mu$	3.2 $\text{\AA s}^{-1}$

average from the weight increase of the Al foil substrates, are in line with those determined as initial rates by ESCA. Thus for closely similar W/FM parameters, the rate for the in-situ reactor (1.5W, 100 $\mu$ ) is 1.6 $\text{\AA sec.}^{-1}$ , and that in reactor A (10W, 100 $\mu$ ) is 2.2 $\text{\AA sec.}^{-1}$ .

(iii) Site of deposition

The design of reactor B allows an investigation of deposition in both glow and non-glow regions and shows how the structure of the deposited plasma polymer depends on its site of deposition.

Two configurations of reactor B have been investigated with differing positions of the coil region as noted in the experimental section.

Polymer films deposited onto gold substrates at 6 different sites in the reactor, with the coil being centrally located in the 1 meter reactor (configuration 1), provides the data shown in Table 5.7. This shows that the material

Table 5.7. Stoichiometric ratios and percentage contribution to the  $C_{1s}$  envelopes for various structural features in the plasma polymers prepared in reactor B on gold substrate at 10W and 200 $\mu$  as a function of site of deposition. (The coil located in the centre of the reactor.)

Position	C/F comp.	C/F ratio	C/N	C/O	C-CF	CF	CF <sub>2</sub>	CF <sub>3</sub>	$\pi \rightarrow \pi^*$
20 cm.	1.0	0.85	1.1	-	27	52	7	10	4
30 cm.	0.96	0.88	2.1	22.3	26	49	18	6	1
40 cm.	0.99	1.00	2.0	15.3	25	47	22	8	1
50 cm.	0.87	1.00	1.80	12.2	24	45	23	8	-
60 cm.	0.82	0.80	1.5	8.8	14	58	18	9	1
70 cm.	0.79	0.80	1.6	8.2	8	64	20	7	1

deposited either well downstream or well upstream of the coil region has a higher fluorine and nitrogen content than in the coil region, where the stoichiometry for the polymer is somewhat similar to that for the monomer. The level of oxygen is somewhat higher for the materials deposited downstream of the coil. Representative spectra for the  $C_{1s}$ ,  $F_{1s}$  and  $N_{1s}$  levels of polymer films deposited at 10 watts and 200 $\mu$  as a function of site deposition are displayed in Figure 5.7. As evidenced by ESCA it is clear that the gross chemical composition and structural features, show dependence on the site of deposition. This effect is reinforced when the

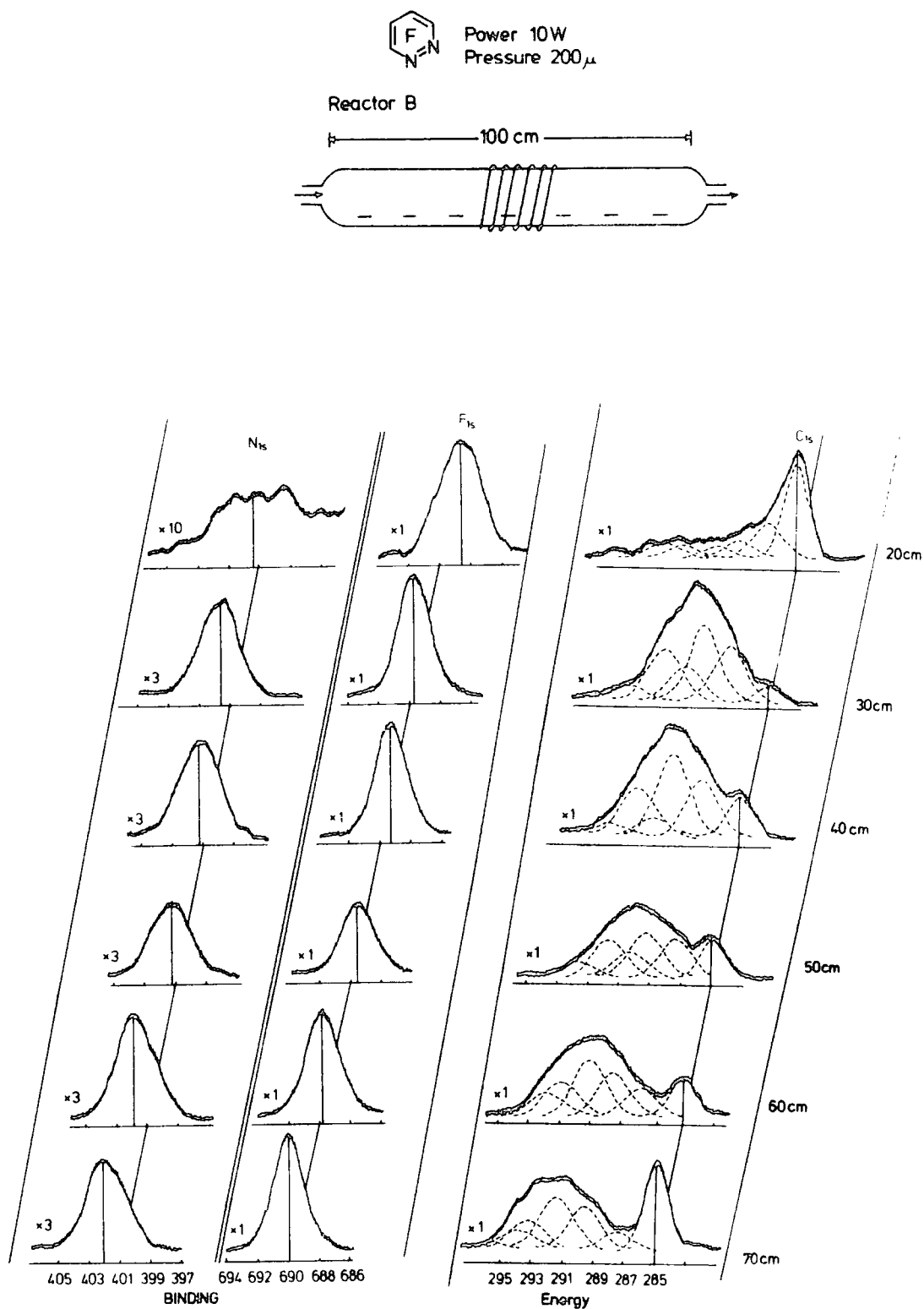


Figure 5.7.  $C_{1s}$ ,  $N_{1s}$  and  $F_{1s}$  spectra of plasma polymers deposited on gold substrate at different site of deposition in reactor B at power 10W and a pressure 200 $\mu$ . (The coil located in the centre of the reactor.)

coil region is moved upstream as is evident from the data acquired in configuration 2, with the coil located 25 cms. from the entrance to the reactor, which is presented in Table 5.8. The upstream and coil region materials are

Table 5.8. Stoichiometric ratios and percentage contribution to the  $C_{1s}$  envelopes in the plasma polymers prepared in reactor B on gold substrate at 10W and  $200\mu$  as a function of site of deposition. (The coil located 25 cms. from the entrance of the reactor.)

Position	C/F comp.	C/F ratio	C/N	C/O	C-CF	CF	CF <sub>2</sub>	CF <sub>3</sub>	$\pi \rightarrow \pi^*$
10 cm.	0.85	0.9	2.2	19.2	23	45	15	14	3
25 cm.	0.80	0.85	2.1	21.0	23	43	20	14	-
45 cm.	0.81	0.68	1.9	12.1	24	41	23	12	-
60 cm.	0.71	0.67	1.5	6.6	16	42	22	17	3
80 cm.	0.84	0.83	1.4	2.6	22	50	15	13	-

closely similar, with the material deposited downstream being higher in fluorine and nitrogen content. From the  $C_{1s}$  spectra displayed in Figure 5.8., it is again clearly revealed that plasma polymerisation is accompanied by extensive molecular rearrangement and the gross structural features are very dependent on the site of deposition.

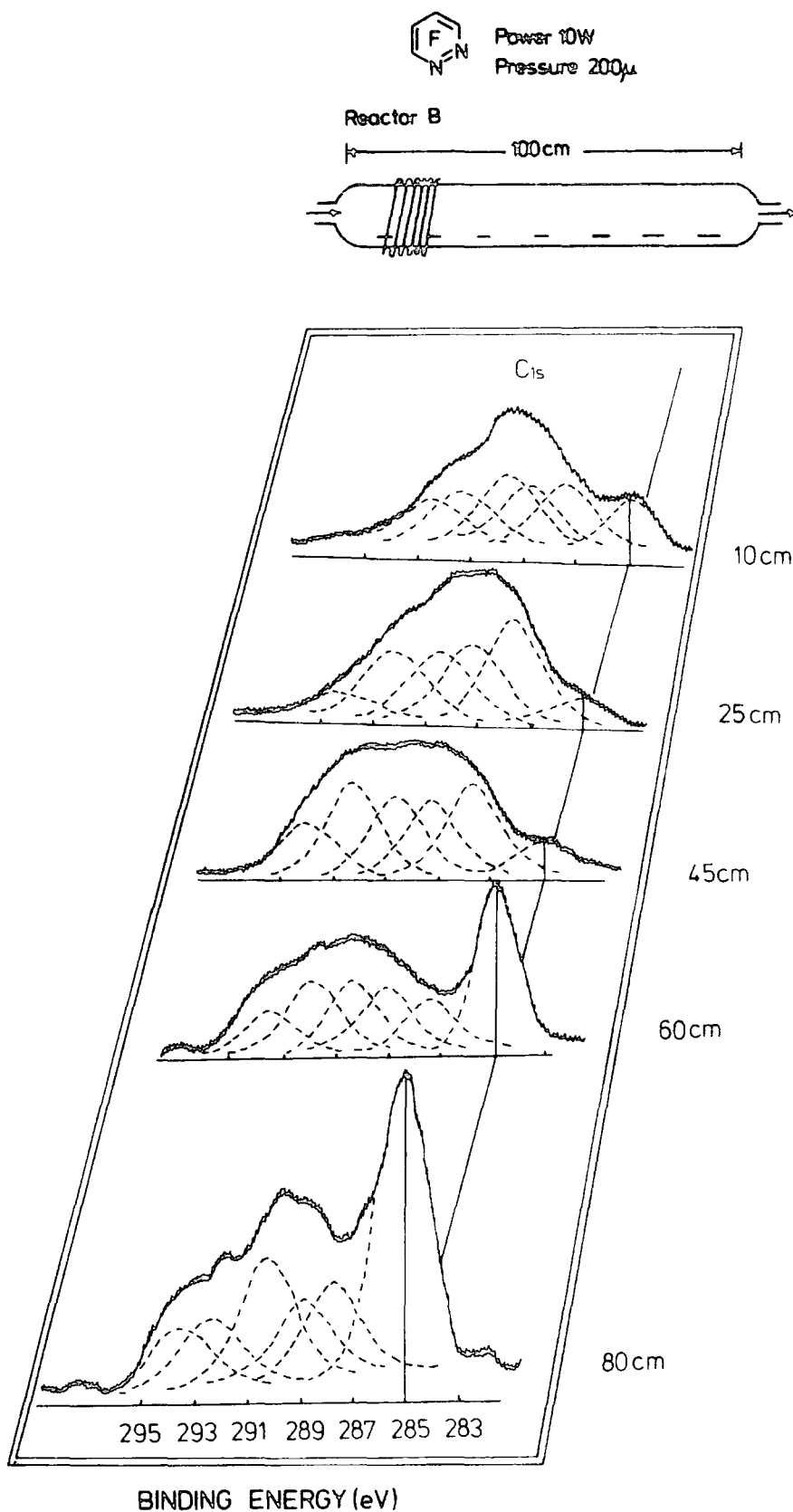


Figure 5.8. C<sub>1s</sub> spectra for various structural features in the plasma polymers prepared in reactor B on gold substrate at 10W and 200 $\mu$  as a function of site of deposition. (The coil located 25 cms. from the entrance of the reactor.)

A comparison has also been drawn with films deposited on aluminium foil substrates, the relevant data being displayed in Table 5.9. There is a close similarity in behaviour for depositions on the two substrates indicating that once the initial interface is formed the composition etc. is independent of the substrate.

Table 5.9. Stoichiometric ratios and percentages to the  $C_{1s}$  envelopes in the plasma polymers prepared in reactor B, on Al foil substrate at 10W and 200 $\mu$  as a function of site of deposition. (The coil located in the centre of the reactor.)

Position	C/F comp.	C/F ratio	C/N	C/O	C-CF	CF	CF <sub>2</sub>	CF <sub>3</sub>	$\pi \rightarrow \pi^*$
25 cm.	0.88	0.89	2.7	6.8	16	55	22	4	2
38 cm.	0.8	0.84	2.1	15.8	16	45	33	5	1
50 cm.	0.9	0.95	2.0	10.4	28	39	24	7	2
68 cm.	0.81	0.80	1.7	9.2	23	42	20	13	2
75 cm.	0.80	0.84	1.7	8.3	15	55	18	10	2
88 cm.	0.7	0.6	1.4	6.2	9	51	24	14	2

(iv) Other measurements

(a) Contact angles

For films deposited in the free-standing reactor it was soon noted that samples studied at varying periods after the end of the deposition apparently had differing contact angles with water.

Figure 5.9., shows data for a sample which has studied immediately after deposition. From an initial contact angle

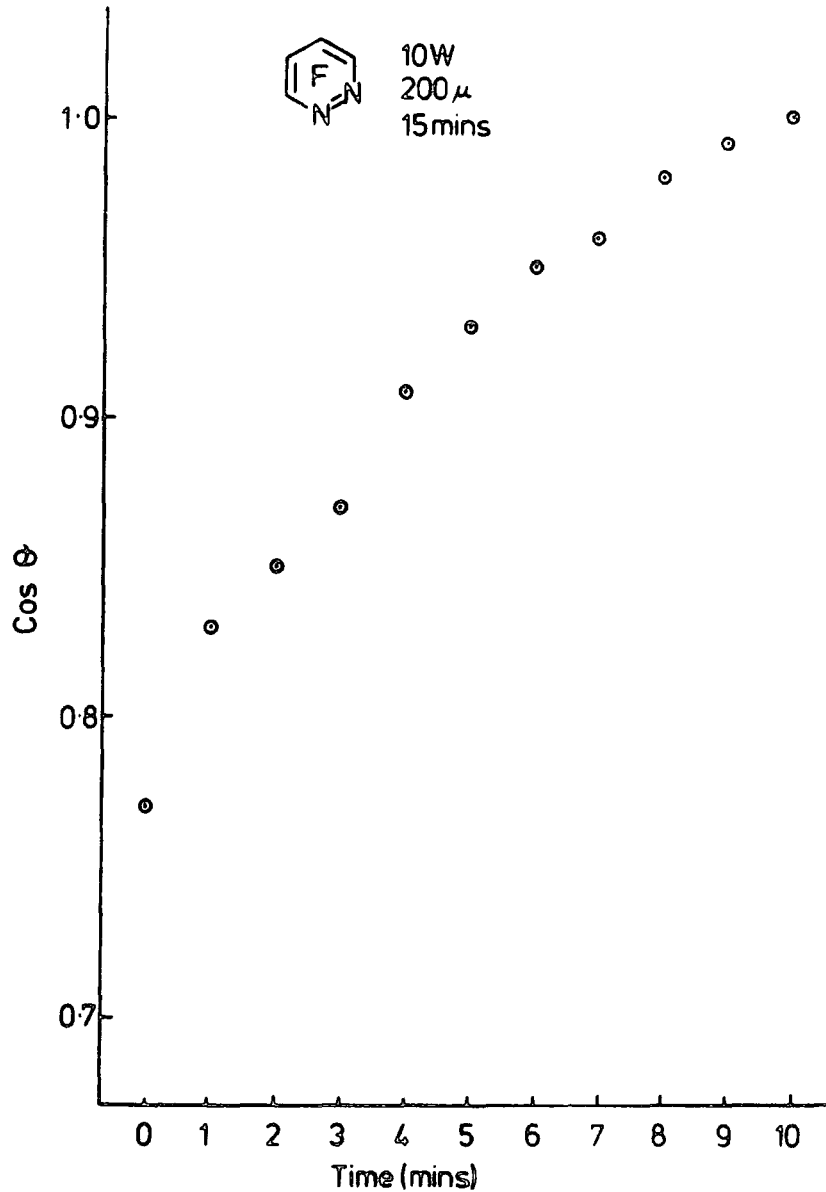


Figure 5.9. Contact angle with water (cos  $\theta$ ) vs. time (mins.).

of  $\sim 40^\circ$  there is a rapid decrease such that after a period of 10 minutes, the droplet had completely spread and started penetrating the sample. This indicates the hydrophilic nature



of the final surface. In an attempt to understand the changes in surface chemistry accompanying this process films deposited onto HDPE at 10W and 200 $\mu$  for 15 minutes have been studied by means of ESCA immediately after preparation and after treatment with water, allowing water droplets to spread on the films and subsequently pumping the water off. The measured  $C_{1s}$ ,  $N_{1s}$ ,  $F_{1s}$  and  $O_{1s}$  core levels are displayed in Figure 5.5. and indicate an extensive rearrangement before and after the treatment. The intensity ratios are displayed in Table 5.10. along with the component analysis of the  $C_{1s}$  spectrum at 30 $^{\circ}$  take-off angle, excluding the component at 285 eV arising from extraneous contamination and from the substrate itself (HDPE).

Table 5.10. Comparison of the area ratios and percentage contribution of the  $C_{1s}$  envelopes in plasma polymer films deposited onto HDPE at 10W and 200 $\mu$  before treatment and after treatment with water.

Polymer deposited onto HDPE, at (10W 200 $\mu$ , 15 mins.)	Angle	$F_{1s}/N_{1s}$	$F_{1s}/O_{1s}$	$N_{1s}/O_{1s}$	% $C_{1s}$ Contribution			
					C-CF	C-F	CF <sub>2</sub>	CF <sub>3</sub>
Before treatment	30 $^{\circ}$	3.8	11.2	3.0	36	42	16	6
After treatment with water	30 $^{\circ}$	4.9	9.9	2.0	22	63	11	4
	70 $^{\circ}$	5.3	9.0	1.7				

It is clear that, before treatment the level of oxygen is highest at the surface (lower  $F_{1s}/O_{1s}$ ,  $F_{1s}/N_{1s}$  and  $N_{1s}/O_{1s}$  ratio at 30 $^{\circ}$  take-off angle). After water treatment the level of oxygen relative to nitrogen is comparable for the surface and subsurface. The  $F_{1s}/N_{1s}$  ratios indicate that oxygen incorporation is accompanied by loss of nitrogen suggesting hydrolysis of imine functionalities.<sup>19</sup> Consistent with this

hypothesis is the apparent increase in contribution from  $\underline{\text{C}}\text{-F}$  structural features at the expense of carbons which do not have an  $\alpha$ -fluorine substituent. One interpretation of this is that  $\underline{\text{C}}\text{=N-}$  functionalities,<sup>65,70</sup> which overlap in binding energy with  $\underline{\text{C}}\text{-CF}_n$  structural types, have been converted to  $\underline{\text{C}}\text{=O}$  structural features with binding energy virtually coincident with that for  $\underline{\text{C}}\text{-F}$  structural features.

(b) Infra-red studies

Powdered samples of polymers from both the sleeve and the wall of the free-standing reactor A, have been studied in the form of KBr disks. The spectra in both cases are displayed in Figure 5.10. This shows broad intense absorptions centred at

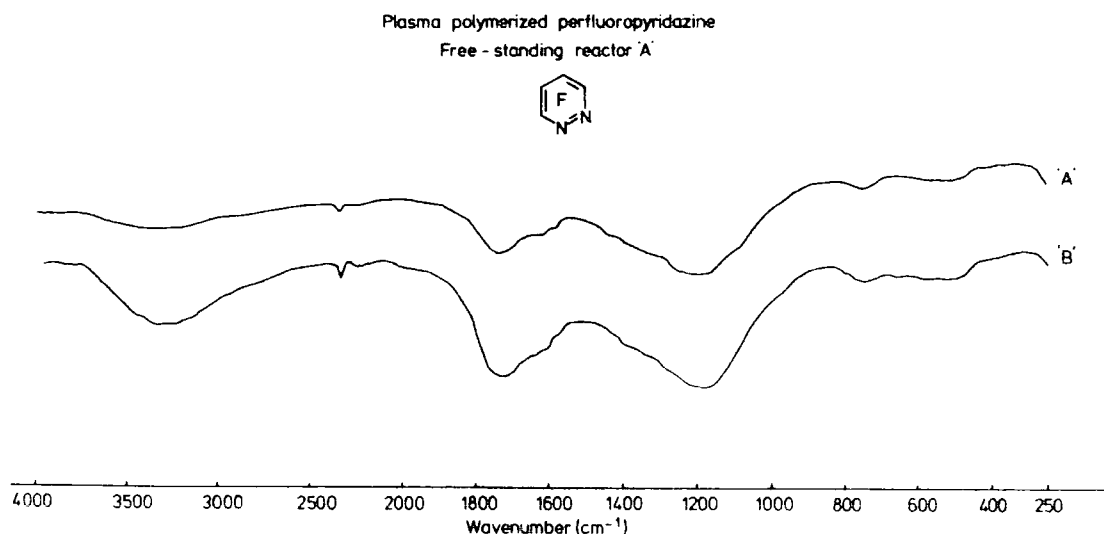


Figure 5.10. Infra-red spectra of plasma polymerised perfluoropyridazine prepared in free-standing reactor configuration A, (sample (a) from the reactor, sample (b) from the sleeve).

$\sim 1200 \text{ cm.}^{-1}$  and  $\sim 1730 \text{ cm.}^{-1}$ , regions associated with  $\underline{\text{C}}\text{-F}$  and  $\underline{\text{C}}=\text{CF}_2$  structural features respectively. Strong intensity, broad absorptions in the region  $\sim 3300 \text{ cm.}^{-1}$  associated with  $\text{-O-H}$  and  $\text{-N-H}$ , stretching modes are also observed, and these are attributed to surface hydrolysis of the plasma polymer films produced from tetrafluoropyridazine.

(c) Thermogravimetry (TG)

Samples of the power removed from both sleeve and from the wall of the free-standing reactor A have been investigated by TG, (Stanton Redcroft TG-750). These studies, presented in Figure 5.11., indicate no well-defined transitions. In contrast to the plasma polymerised films of tetrafluoropyridazine significant weight loss occurs even at relatively low temperatures ( $< 100^\circ\text{C}$ ).

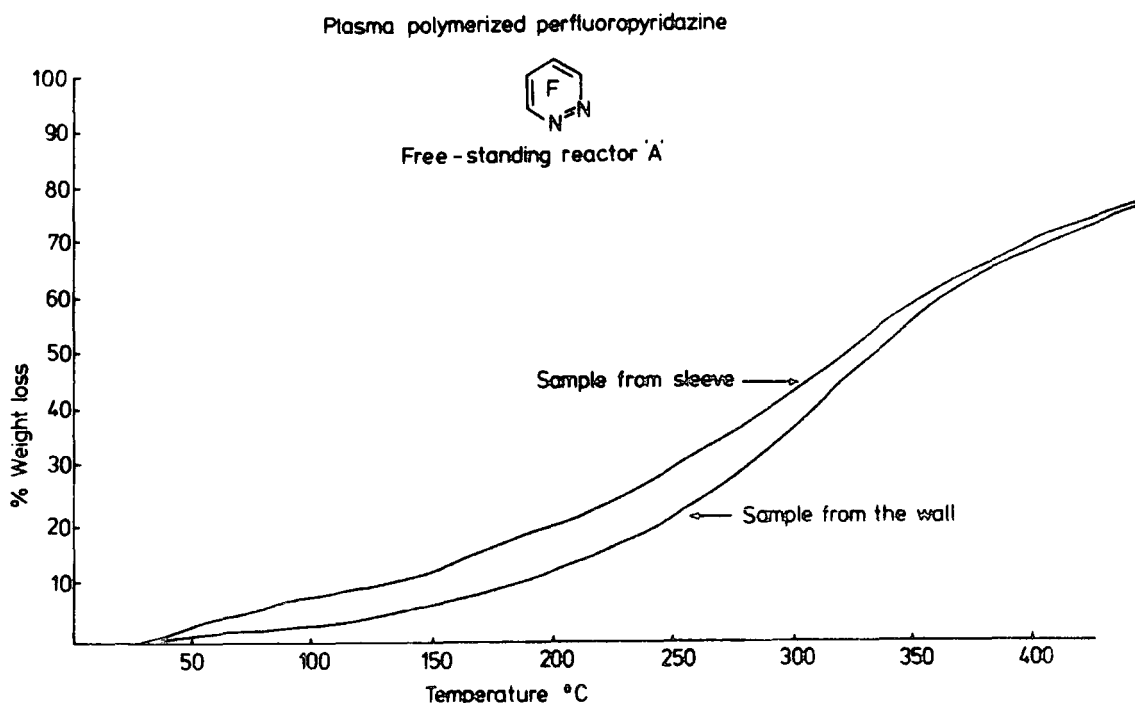


Figure 5.11. Thermogravimetry analysis of plasma polymerised tetrafluoropyridazine in the free-standing reactor, (operating conditions, nitrogen atmosphere, heating rate  $20^\circ\text{C}/\text{min.}$ ).

(d) Adhesion

Recent studies<sup>222-223</sup> of the adhesion aspects of plasma polymer deposition prompts a few generalizations from the studies presented in this chapter.

The extent of adhesion of thin plasma polymer films, prepared in the free-standing reactor A, depends on the substrate. Some observations already noted show that films of  $\sim 3000\text{\AA}$  deposited onto a glass surface exhibit relatively poor adhesion since it is possible to peel films intact directly from the wall in the glow region. Samples of  $\sim 300\text{\AA}$  deposited onto flamed gold substrates behaved similarly to those deposited on glass and could be readily peeled from the metal. Samples of the same thickness deposited onto aluminium foil adhered strongly and could not be removed other than by strong abrasion. Since the film thicknesses are the same for the three substrates and since the structure of the plasma polymer is also the same, the difference in behaviour must arise from the difference in interface chemistry<sup>222-223</sup> as opposed to internal stresses. This indicates how the adhesion of the polymer films is strongly influenced by the substrate.

The substrate dependence of the adhesion has not been so readily apparent in previous studies of plasma polymers based on fluoroaromatics,<sup>15-18</sup> and this again emphasises the difference in chemistry for the heterocyclic systems.

(v) Sleeve effects

The fact that in the coil region the deposition was uniform only on the inside of the sleeve prompted an

investigation of the mode of deposition on sleeves with differing diameters compared to that of the reactor. To this end sleeves were constructed from 85 mm. long pyrex tubing with four legs to enable the tube to be axially located in the reactor.

In addition to the sleeve of diameter 30 mm., tubes of diameter 45 mm. and 10 mm. have been investigated.

The region of greatest emission of light in the visible region was the inside of the tube in the coil region, except in the case of the smallest diameter tube, where the glow region was brightest in the annular space between the tube and the reactor walls.

For the intermediate size sleeve (diameter 30 mm.), deposition was clearly on the inside of the tube with little deposition on the walls of the reactor in the coil region. On removal of the sleeve, clearly defined boundaries for deposition in the region before and after the coil were evident in Figure 5.12. For the smallest tube the flow pattern was such that deposition was exclusively on the outside of the sleeve. This suggests that even with a relatively uncontrolled deposition (as opposed to, for example, a magnetically focussed audiofrequency plasma),<sup>224</sup> it should be relatively straightforward to arrange a configuration where deposition occurs on the desired surface.

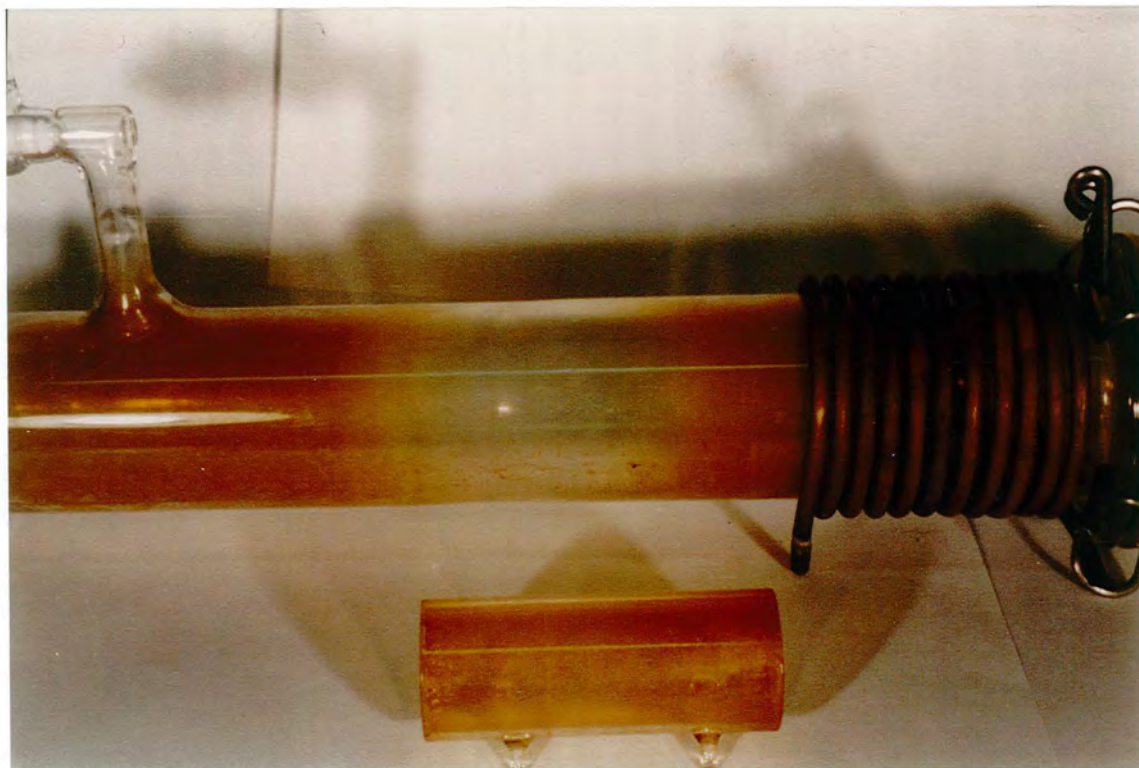


Figure 5.12. Configuration reactor A, shows the sleeve effects of plasma polymerised perfluoropyridazine.

CHAPTER SIX

CHAPTER SIXPLASMA POLYMERISATION: A COMPARISON OF THE PLASMA  
POLYMERISATION OF THE ISOMERIC PERFLUORINATED  
DIAZINESAbstract

Plasma polymers synthesised by inductively coupled RF techniques have been investigated as a function of operating parameters for the isomeric perfluorinated diazines (pyrazine, pyrimidine and pyridazine). A combination of ESCA and microanalytical studies show that the plasma polymers are produced via rearrangement mechanisms; the C:F and C:N stoichiometries being closely similar to that for the starting monomers over a range of operating parameters. Comparison of rates of formation of plasma polymer films reveals distinctive differences between the isomeric diazines, suggesting that equilibration of valence isomers occurs on a substantially slower time-scale than for isomeric fluorinated benzenes,<sup>213-216</sup> which in general polymerise at essentially the same rates. In contrast to the remarkably low critical surface tension for plasma polymers based on perfluorobenzenes ( $\sim 20$  dynes  $\text{cm}^{-2}$ ), the plasma polymer films from the perfluorinated diazines which are initially hydrophobic become hydrophilic in contact with water droplets. This is attributed to hydrolytic instability of the films associated with the labilising influence of nitrogen on nucleophilic displacement of fluoride which is a feature of the chemistry of the monomers themselves.



### 6.1. Introduction

It has been shown how the ESCA technique may be applied to a systematic investigation of how the gross structural features and rates of formation of ultra-films depend on the initial starting material and the operating parameters of the plasma instrumentation.<sup>219</sup> In the particular case of fluorinated<sup>213-216</sup> benzenes, such studies have shown that positional isomers produce essentially the same polymer at the same rate and this has been taken as evidence of a rearrangement mechanism for polymerisation in which ring scrambling plays an important part.

Semi-empirical SCF MO computations<sup>214,225</sup> have indicated that the relative energies of positional isomers of fluorine substituted benzenes are closely similar. As an important adjunct to these studies, Chapter five presented the results of an investigation of the plasma polymerisation of perfluoropyridazine where the replacement of ring carbons by nitrogen strongly influences the relative energetic of the various positional isomers.<sup>218</sup> The strong electronic perturbation consequent upon replacement of ring carbon by nitrogen on going from the homo to heteroaromatic system is manifest in the striking differences in reactivity towards nucleophiles for example.<sup>220,226</sup>

In the previous two chapters (4 and 5), it has been noted that the plasma polymers synthesised from perfluoropyridine and perfluoropyridazine although initially of low critical surface tension rapidly became wettable, (e.g. by water) on standing, and this has been taken as evidence of the

labilising influence of nitrogen towards hydrolysis in the surface regions.<sup>217-218</sup>

The distinctive difference in both the chemistry of the "monomers" and of the resultant polymers for the hetero and homoaromatic systems has prompted an extension of these studies to encompass all of the isomeric perfluorodiazines.

This chapter reviews the important features to emerge from a comparative study of the low power RF plasma polymerisation of the perfluorinated pyridine, pyridazine, pyrimidine and pyrazine heterocyclic systems.

## 6.2. Experimental

Two types of reactor configuration, A and C, as described in Chapter four, have been employed to synthesise plasma films from perfluoropyrimidine and pyrazine.

In reactor C for the in-situ polymerisation, the structures of the polymers have been studied as a function of power, pressure and time. The rates of deposition were measured by investigation of the signal attenuation of the gold substrate  $Au_{4f}$  levels as a function of power.

In reactor A the rates of deposition of the polymer films were determined by deposition onto aluminium foil as a function of power and pressure, by measuring the weight increase of the foil using a CAHN electromicrobalance. For a contact angle with water the polymer films were deposited onto High Density Polyethylene (HDPE). Sufficient quantities of the polymer for microanalysis were obtained by removing the polymer which was deposited on the walls of the pyrex reactor inside and outside the coil region.

ESCA spectra were recorded on an ES200A/B spectrometer using  $Mg_{k\alpha_{1,2}}$  radiation, and were analysed as described in previous chapters.

The starting monomers pyrimidine and pyrazine were prepared by fluorination of tetrachloropyrimidine and tetrachloropyrazine respectively, according to standard procedures.<sup>220</sup> The monomers were shown to be pure by G.L.C. and were degassed prior to use.

### 6.3. Results and Discussion

#### 6.3.1. Introduction

It is convenient to briefly describe the main features of the plasma polymerisation of each "monomer" of perfluoropyrimidine and perfluoropyrazine separately, and then to draw a comparison with data previously reported on perfluoropyridine and pyridazine in Chapters four and five respectively.

#### 6.3.2. Perfluoropyrimidine

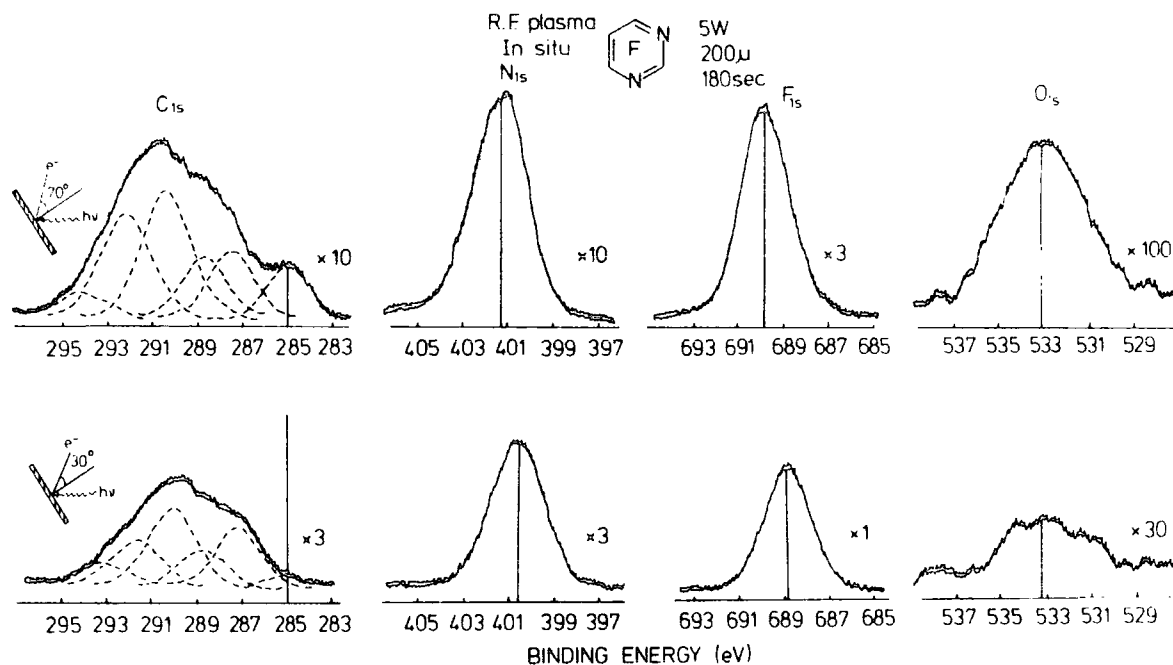
The following aspects have been studied:-

- (i) Gross structural features and composition as a function of the operating parameters;
- (ii) Angular dependence as a function of pressure;
- (iii) Rates of deposition as a function of operating parameters;
- (iv) Contact angles as a function of time.

#### (i) The gross structural features and composition

The core level spectra for plasma films of perfluoropyrimidine deposited on a gold substrate in-situ reactor at 5W and 200 $\mu$  for a period of 180 secs. at two take-off angles

$30^\circ$  and  $70^\circ$ , are shown in Figure 6.1. The spectra reveal that the  $C_{1s}$  levels show a broad structure extending from  $\sim 285$  eV



**Figure 6.1.**  $C_{1s}$ ,  $N_{1s}$ ,  $F_{1s}$  and  $O_{1s}$  spectra of the plasma polymerised tetrafluoropyrimidine prepared in-situ reactor at 5W discharge power and 200μ for 180 secs. at take-off angles  $30^\circ$  and  $70^\circ$ .

to  $\sim 294$  eV with a standard line shape analysis revealing components arising from  $\underline{CH}$ ,  $\underline{C-CF}$ ,  $\underline{CF-C}$ ,  $\underline{CF-CF}_n$ ,  $\underline{CF}_2$  and  $\underline{CF}_3$ . Whilst the spectra at  $70^\circ$  take-off angle indicate a large level of a low binding energy  $\underline{CH}$  hydrocarbon component, compared with spectra at  $30^\circ$  take-off angle, and this arises from extraneous hydrocarbon contamination. This, as previously noted, indicates that the plasma polymer of the 1,2-perfluorodiazine exhibits a relatively high level of surface contamination, compared with the plasma polymer film from perfluorobenzene for example,<sup>216</sup> and this is attributed to the

surface hydrolysis of these materials,<sup>217-218</sup> (see section iv).

The spectra in Figure 6.1. also reveal that the nitrogen peak centred at  $\sim 401$  eV is broadened indicative of a range of bonding environment,<sup>70</sup> and there is also a low level of oxygen apparent, slightly greater at the very surface.

The standard line shape analysis and the stoichiometric ratios as a function of power at constant pressure (200 $\mu$ ), are displayed in Table 6.1. It is clear from this, that at

Table 6.1. C/F, C/N and C/O stoichiometric ratios and percentage contribution of  $C_{1s}$  envelope of plasma polymerised tetrafluoropyrimidine prepared in-situ reactor at 200 $\mu$ , as a function of power, CF groups encompass ( $-\underline{CF}-C$  and  $\underline{CF}-CF_n$ ).

Power	Angle	Stoichiometry Ratios				% $C_{1s}$ Contribution			
		C/F comp.	C/F	C/N	C/O	C-CF	CF	CF <sub>2</sub>	CF <sub>3</sub>
0.1W	30°	1.09	1.0	1.95	9.2	25	59	15	1
	70°	-	-	-	-	-	-	-	-
0.5W	30°	1.0	1.02	1.90	16.8	24	56	16	4
	70°	1.05	1.05	1.90	19.6	26	56	15	3
3W	30°	0.92	1.0	1.8	28.8	23	51	20	6
	70°	-	-	-	-	-	-	-	-
5W	30°	0.90	0.95	1.6	25.5	24	47	22	7
	70°	0.86	0.93	1.5	20.0	20	49	25	6
10W	30°	0.88	0.95	1.5	23.5	24	45	24	7
	70°	0.90	1.08	1.5	15.1	25	46	22	7

low powers the C:F and C:N stoichiometric ratios are essentially the same as for the starting "monomer". However, at higher power the C:N and C:F stoichiometries indicate a slightly greater incorporation of both nitrogen and fluorine in the polymer films. In the case of fluorine the  $C_{1s}$  line shape analysis indicates that the slightly increased fluorine content arises from an increased contribution of  $CF_2$  and  $CF_3$  structural features as a function of power.

(ii) Angular dependent studies

The angular dependent data in Figure 6.1. reveals slight differences in the relative structural features as a function of depth into the sample. For this reason the angular dependent studies have been carried out by ESCA for plasma polymer films of polyfluoropyrimidine deposited on a gold substrate in-situ reactor at a power of 3W and pressure of  $100\mu$  and  $200\mu$ , at different take-off angles  $5^\circ$ ,  $15^\circ$ ,  $30^\circ$ ,  $45^\circ$  and  $70^\circ$ . The ESCA data are displayed in Table 6.2., and this indicates that at a pressure of  $200\mu$ , the surface is reasonably homogeneous on a vertical depth scale appropriate to the ESCA experiment. At a lower pressure ( $100\mu$ ), however, the ESCA gross structural features show a significantly larger depth dependence,<sup>227</sup> and this is apparent from the  $C_{1s}$  contribution profile which is shown in Figure 6.2. The  $CF_3$  structural features are higher at lower pressures ( $100\mu$ ), compared with the  $200\mu$ , but the  $CF_2$  structural features are lower at lower pressure. Also Table 6.2. shows the overall  $C_{1s}/F_{1s}$  intensity ratios, which indicate there is less fluorine at the very surface of the sample for both pressures

**Table 6.2.** Intensity ratios and percentage contribution of  $C_{1s}$  envelope of plasma polymerised tetrafluoropyrimidine prepared in-situ reactor at 3W power and 100 $\mu$  and 200 $\mu$  pressure, as a function of take-off angles.

Pressure $\mu$	Intensity Ratios				% $C_{1s}$ Contribution			
	C/F comp.	$C_{1s}/F_{1s}$	$C_{1s}/N_{1s}$	$C_{1s}/O_{1s}$	C-CF	CF	CF <sub>2</sub>	CF <sub>3</sub>
100 $\mu$	0.79	0.57	1.04	3.8	16	51	23	10
200 $\mu$ $\theta = 5^\circ$	0.85	0.42	1.2	-	20	49	24	7
100 $\mu$	0.81	0.60	1.3	4.6	17	52	21	10
200 $\mu$ $\theta = 15^\circ$	0.87	0.51	1.4	31.8	24	44	25	7
100 $\mu$	0.86	0.72	1.3	4.3	21	52	17	10
200 $\mu$ $\theta = 30^\circ$	0.89	0.51	1.4	35.7	26	43	24	7
100 $\mu$	0.91	0.69	1.3	3.9	21	56	15	8
200 $\mu$ $\theta = 45^\circ$	0.92	0.53	1.4	20.5	27	43	24	6
100 $\mu$	0.95	0.78	1.3	3.8	23	55	16	6
200 $\mu$ $\theta = 70^\circ$	0.97	0.63	1.5	14.5	30	42	23	5

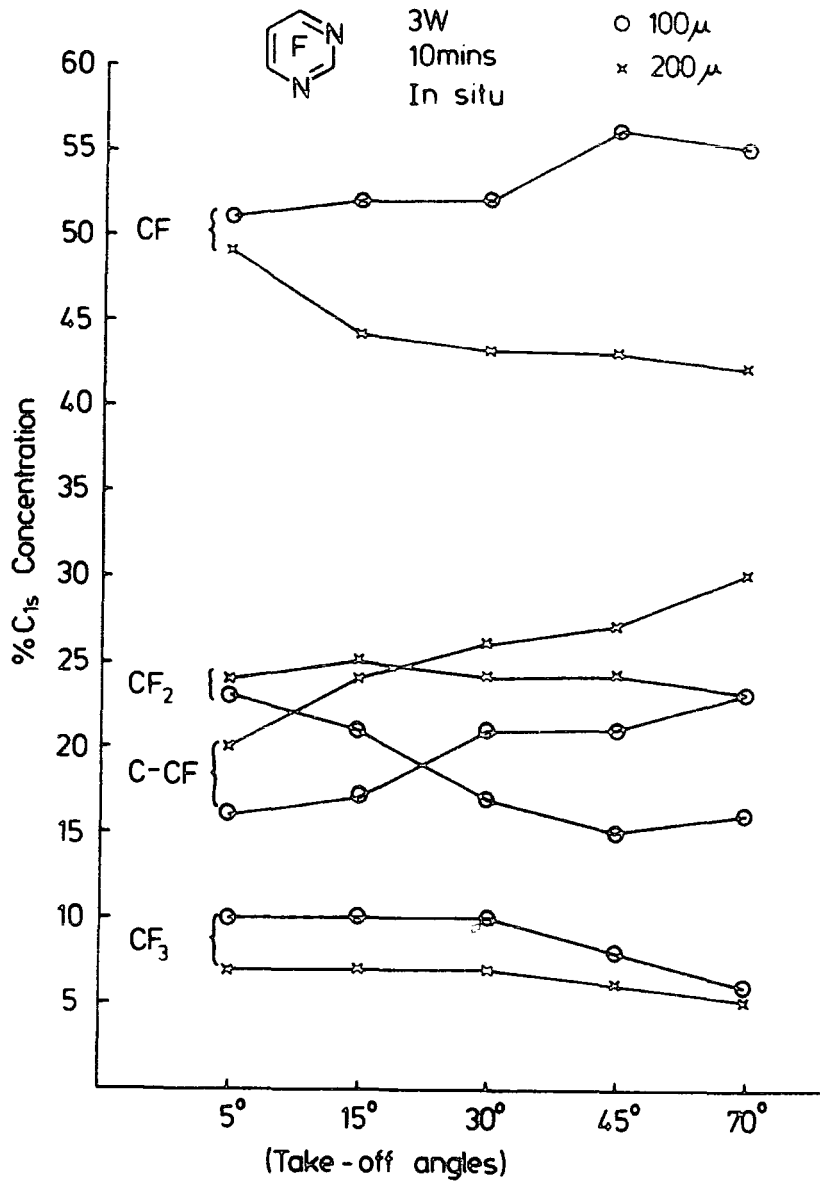


Figure 6.2. Percentage contribution of  $C_{1s}$  envelope of plasma polymerised tetrafluoropyrimidine prepared in-situ at 3W discharge power and pressure at  $100\mu$  and  $200\mu$ , as a function of take-off angles.

( $100\mu$  and  $200\mu$ ), but the  $C_{1s}/F_{1s}$  ratio is higher, (lower fluorine) at the lower pressure as a function of take-off angles. The lower level of fluorine at lower pressures may arise from the surface hydrocarbon contamination which will attenuate the signal from the  $F_{1s}$  level. The high level of



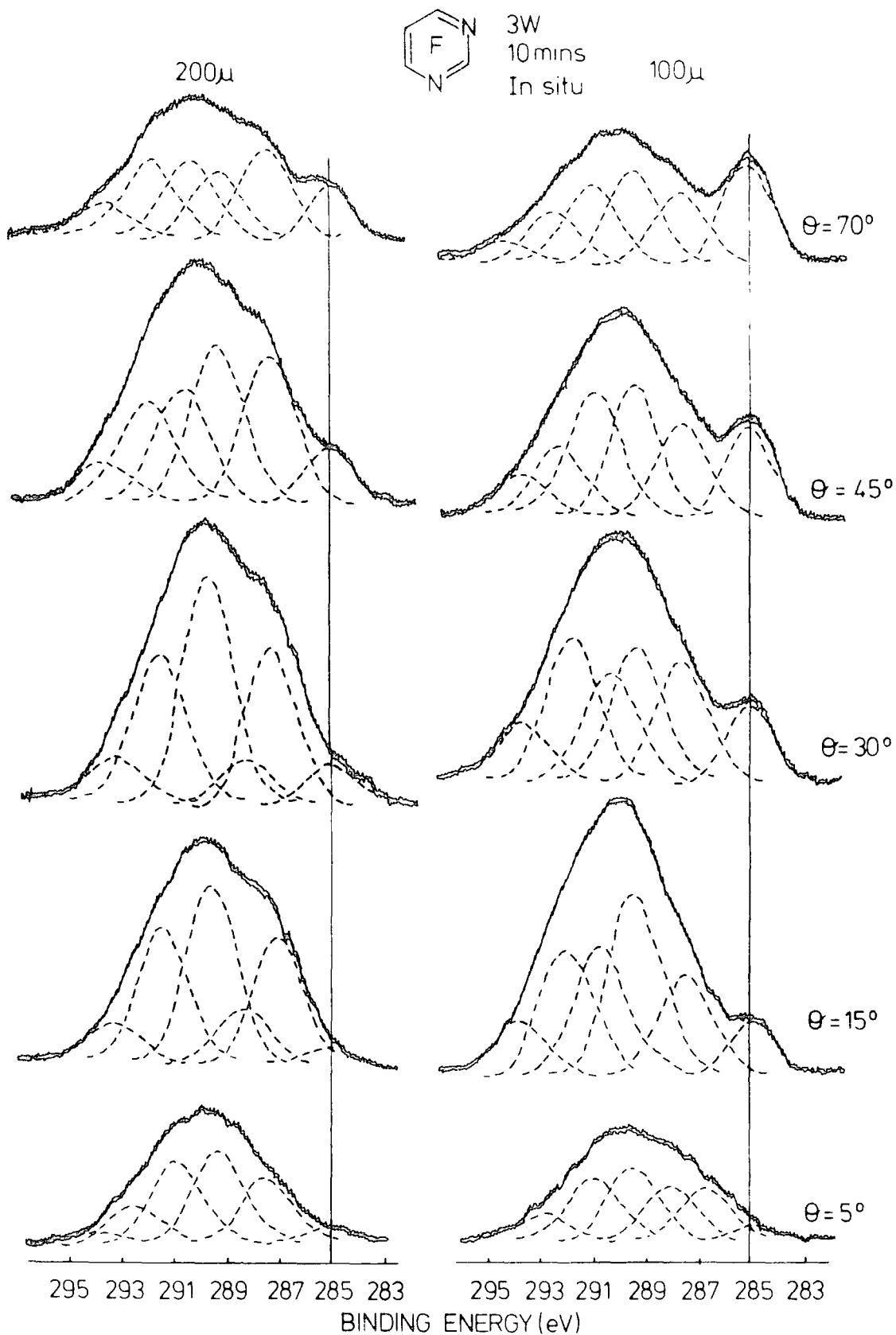
the hydrocarbon contamination at low pressure (100 $\mu$ ) is clearly shown in Figure 6.3.

The  $C_{1s}/N_{1s}$  intensity ratio also decreases (higher nitrogen content), for both pressures (100 $\mu$  and 200 $\mu$ ) at lower take-off angles. The level of extraneous oxygen as monitored by the  $C_{1s}/O_{1s}$  intensity ratios is significantly lower at higher pressures (viz. at 30 $^\circ$   $C_{1s}/O_{1s}$  ratios are 4 and 36 for 100 $\mu$  and 200 $\mu$  respectively). This suggests that ablation from the reactor walls of oxygen containing species is more of a problem at the lower pressures (higher W/FM).

Figure 6.3. shows the  $C_{1s}$  contribution to the overall line profile, and this also reveals that the gross chemical composition and structural features evident from ESCA studies are slightly influenced by the angular dependence. This again indicates that the plasma polymer films produced from fluoroheteroaromatic systems shows a more distinct dependence than the homoaromatic systems.

### (iii) Rates of deposition

The rates of deposition monitored by means of the attenuation of the  $Au_{4f}$  signal of gold substrates as a function of time are shown in Figure 6.4., for in-situ depositions in reactor configuration C. It is clear that the rate of deposition at 100 $\mu$  increases on going from a power input of 0.1 watt to 0.4 watt being 0.44 $\text{\AA} \text{ s}^{-1}$  to 0.86 $\text{\AA} \text{ sec.}^{-1}$  respectively. Also the rate of deposition increases rapidly at the higher pressures from 0.44 $\text{\AA} \text{ sec.}^{-1}$  at 100 $\mu$  to 2.5 $\text{\AA} \text{ sec.}^{-1}$  at 200 $\mu$  for a power input of 0.1 watt.



**Figure 6.3.**  $C_{1s}$  levels of plasma polymerised perfluoropyrimidine prepared in-situ reactor at 3W and pressures 100 $\mu$  and 200 $\mu$ , as a function of take-off angles.

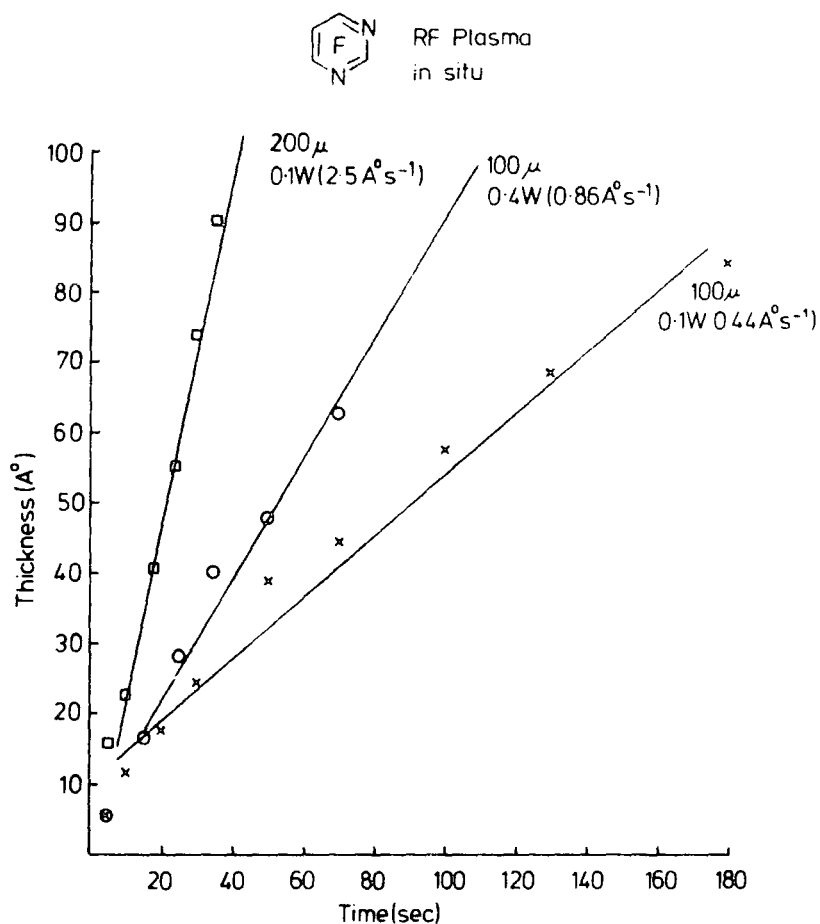


Figure 6.4. Thickness (Å) vs. time (secs.) for plasma polymerised tetrafluoropyrimidine.

It is clear from this that the rate of deposition is strongly dependent on  $W/FM$ .<sup>219,228</sup>

For deposition in the free-standing reactor the data of the rate of deposition are displayed in Table 6.3. The data indicate that at  $100\mu$  the rate of deposition at 10 watts input power is less than at 5 watts whereas at  $200\mu$  the rates increase slightly in going from 5 to 10 watts.

Table 6.3. Rate of depositions of plasma polymers prepared from tetrafluoropyrimidine and tetrafluoropyrazine in reactors A and C, as a function of power and pressure.

Power	Pressure	1,3-diazine	1,4-diazine	Reactor
0.1W	100 $\mu$	0.44 $\text{\AA s}^{-1}$	0.31 $\text{\AA s}^{-1}$	C
	200 $\mu$	2.5 $\text{\AA s}^{-1}$	-	C
0.4W	100 $\mu$	0.86 $\text{\AA s}^{-1}$	0.55 $\text{\AA s}^{-1}$	C
5W	100 $\mu$	3.2 $\text{\AA s}^{-1}$	0.30 $\text{\AA s}^{-1}$	A
	200 $\mu$	21.0 $\text{\AA s}^{-1}$	8.80 $\text{\AA s}^{-1}$	A
10W	100 $\mu$	1.8 $\text{\AA s}^{-1}$	0.44 $\text{\AA s}^{-1}$	A
	200 $\mu$	24.0 $\text{\AA s}^{-1}$	7.80 $\text{\AA s}^{-1}$	A

(iv) Contact angle with water as a function of time

In a previous chapter it has been noted that there are distinctive differences between the surface wettabilities of plasma polymer films prepared from fluorinated aromatic and heteroaromatic systems.<sup>217-218</sup> The contact angles with water for the fluorinated aromatic systems are higher, indicative of very low surface free energies than those for heteroaromatic systems. This is attributed to the presence of nitrogen<sup>220</sup> in the polymer of the heteroaromatic at about the same level as in the starting monomer. Since the polymers produced from perfluoropyrimidine also fall into this category, we might anticipate similar behaviour. This is indeed the case as is readily apparent from the data displayed in Figure 6.5.

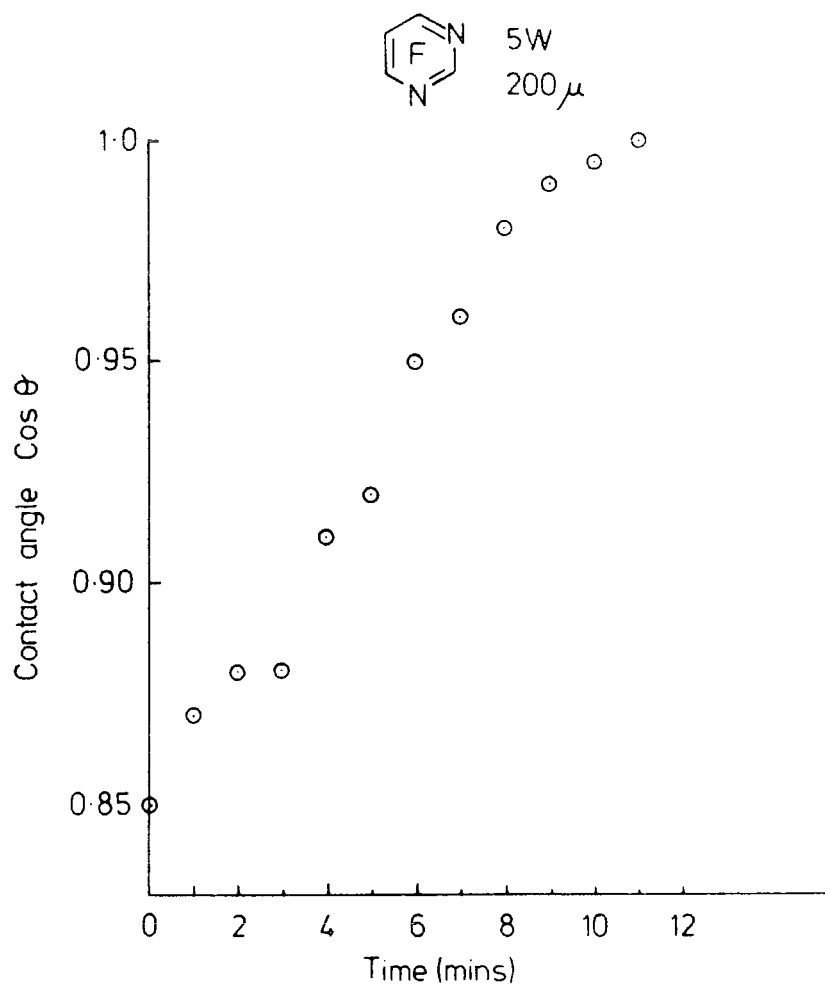


Figure 6.5. Contact angle with water vs. time (mins.), for plasma polymerised tetrafluoropyrimidine films deposited onto HDPE.

The microanalysis of polymer samples produced in the free-standing reactor configuration A, confirms that over extended periods of exposure to the atmosphere the C/N ratio remains essentially constant, whilst the C/F stoichiometric ratio increases by  $\sim 40\%$ , with a concomitant increase in oxygen. The data are displayed in Table 6.4., and this suggests that the dominant reaction is hydrolysis of the polymer.

Table 6.4. Stoichiometric ratios measured by microanalysis as a function of exposure time.

<u>Date</u>	<u>C/N</u>	<u>C/F</u>
1.10.82	1.82	1.25
2.3.83	1.77	1.51

### 6.3.3. Perfluoropyrazine

#### (i) Gross structural features and composition

A typical core level spectra for plasma polymer films of polyfluoropyrazine deposited on gold substrates in-situ reactor at a power input of 10 watts and pressure  $200\mu$  for 180 seconds, are shown in Figure 6.6. The ESCA spectra indicate that the  $C_{1s}$ ,  $N_{1s}$  and  $F_{1s}$  levels were similar to

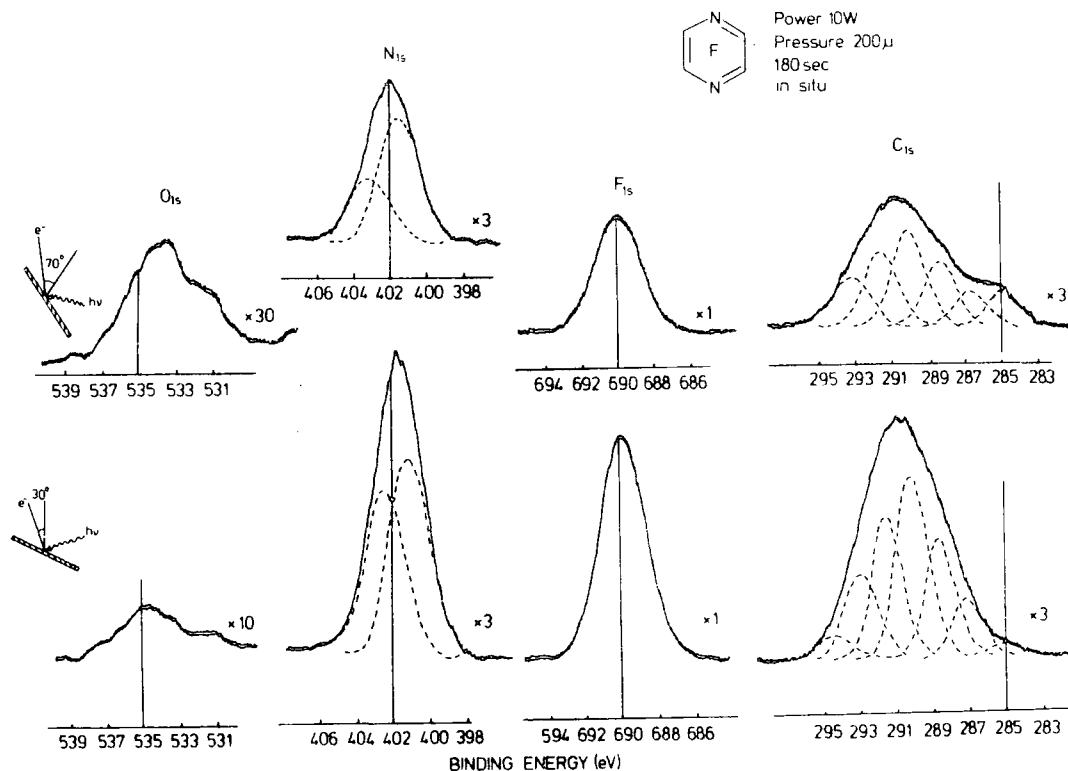


Figure 6.6.  $C_{1s}$ ,  $N_{1s}$ ,  $F_{1s}$  and  $O_{1s}$  spectra of the plasma polymerised tetrafluoropyrazine prepared in-situ reactor at 10W discharge power and  $200\mu$  for 180 secs. at take-off angles  $30^\circ$  and  $70^\circ$ .

those for the other isomeric diazines previously described. The  $C_{1s}$  component analysis and derived stoichiometric ratios as a function of power are shown in Table 6.5. A similar trend is apparent for the other isomer in that at a given

Table 6.5. C/F, C/N and C/O stoichiometric ratios and percentage contribution of the  $C_{1s}$  envelope of plasma polymerised tetrafluoropyrazine prepared in-situ reactor at  $200\mu$ , as a function of power, CF groups encompass ( $-\underline{C}F-C$  and  $\underline{C}F-CF_n$ ).

Power	Angles $\theta$	Stoichiometric Ratio				% $C_{1s}$ Contribution				
		C/F comp.	C/F	C/N	C/O	$\underline{C}-CF$	$\underline{C}F$	$\underline{C}F_2$	$\underline{C}F_3$	$\pi \rightarrow \pi^*$
0.5W	$30^\circ$	1.15	0.95	1.8	32.0	30	54	15	1	-
	$70^\circ$	1.25	1.02	1.9	25.0	33	54	13	-	-
1W	$30^\circ$	1.05	1.02	1.9	27.0	25	57	15	3	-
	$70^\circ$	1.05	1.03	1.9	18.0	23	59	16	2	-
5W	$30^\circ$	0.90	0.97	1.6	20.0	20	54	19	6	1
	$70^\circ$	0.89	0.98	1.7		21	52	20	7	-
10W	$30^\circ$	0.85	0.98	1.6	38.0	17	51	23	7	2
	$70^\circ$	0.81	0.97	1.6	24.5	18	50	23	9	-
20W	$30^\circ$	0.74	0.75	1.2	15.6	12	50	26	11	1
	$70^\circ$	-	-	-	-	-	-	-	-	-

pressure ( $200\mu$ ), the data also indicate that increasing the power leads to increased incorporation of both fluorine and nitrogen. At the lowest power loadings studied, the C/F and C/N stoichiometric ratios are closely similar to those for the starting monomer, (C/F and C/N ratios of 1.0 and 1.9 at 1 watt respectively). The C/O stoichiometry ratio suggests a very

low level of oxygen (cf. Figure 6.6.).

The increased fluorine content at higher powers derives largely from an increase in intensity of the components attributed to  $\text{CF}_3$  and  $\text{CF}_2$  groups, consistent with greater extent of rearrangement at higher average electron energy. Therefore, it is clear that the gross chemical composition and structural features evidenced by ESCA (data shown in Table 6.5.) reveals subtle changes for the plasma polymerised perfluoropyrazine over a range of power inputs.

(ii) Rates of deposition

The rates of deposition have been determined in both the free-standing reactor A, by weight increase of Al foils and in-situ reactor C, by deposition and monitoring of attenuation of  $\text{Au}_{4f}$  signals for gold substrates, as previously described. The data of rates of deposition for the in-situ reactor are shown in Figure 6.7., whilst that for the free-standing reactor are given in Table 6.2. It is clear from this data that the rates of deposition are lower for perfluoropyrazine compared with other isomeric diazines. A comparison of data for the isomeric diazine and perfluoropyridine will be given later in section 6.3.4

(iii) Time dependence

The previous chapters (4 and 5) have indicated that for the plasma polymerisation of fluoroheteroaromatic systems, the composition and the structural features are dependent on time of deposition.

Perfluoropyrazine shows similar behaviour, as is clearly evident from the components of the  $\text{C}_{1s}$  analysis in Figure 6.8.,



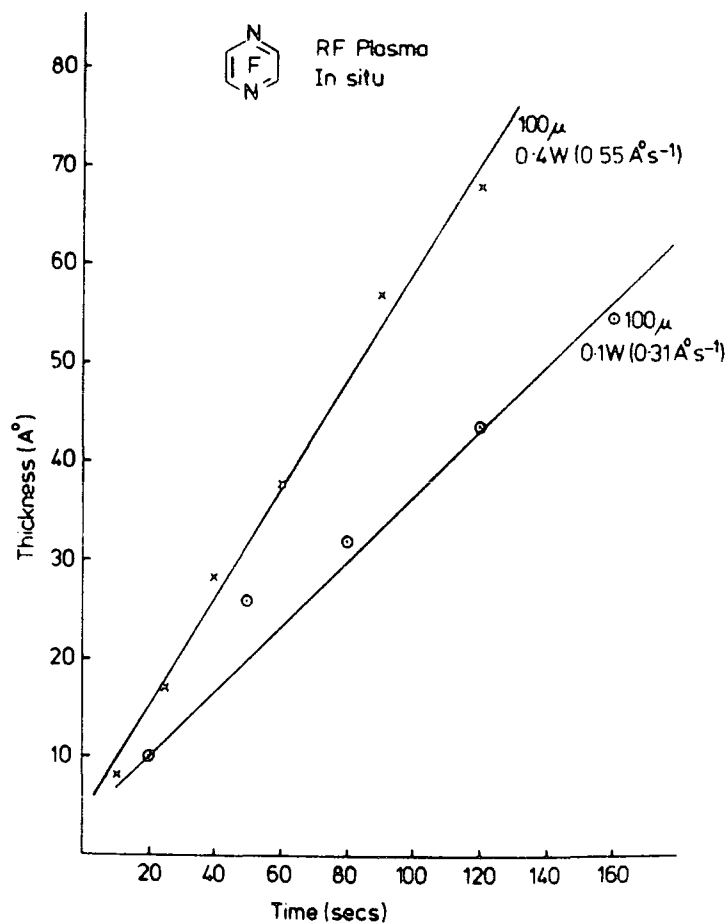


Figure 6.7. Thickness (Å) vs. time (secs.) for plasma polymerised tetrafluoropyrazine.

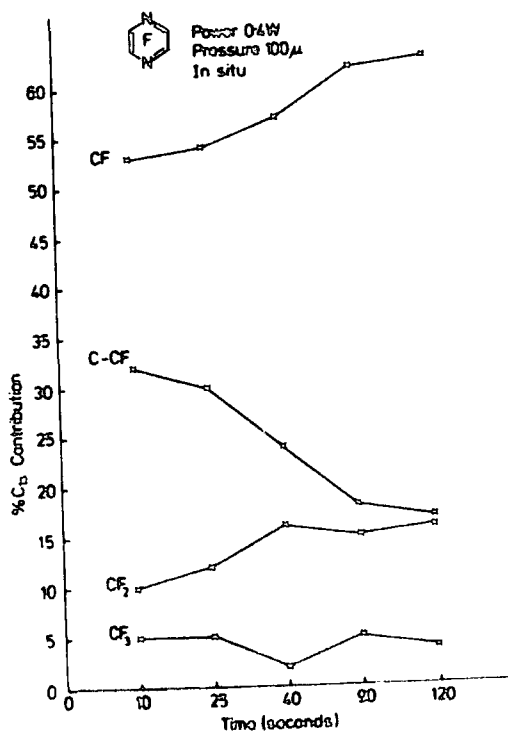


Figure 6.8. % contribution of the C<sub>1s</sub> envelope of plasma polymer films prepared in-situ at 0.4W and 100 μ, as a function of time, CF groups encompass (-CF-C and CF-CF<sub>n</sub>).

for films deposited at 0.4W and 100 $\mu$  in-situ reactor C, for varying periods of time. The data indicate that, as the film is deposited there is an increase of  $\text{CF}_2$  structural features. This may suggest that initially deposited films of this reactive monomer are much more dependent on the totality of operating parameters than for the corresponding fluorinated benzenes.

(iv) Contact angle with water as a function of time

The qualitative behaviour of polymer films produced from the 1,4-diazine towards water droplets placed on the surface is similar to that for the 1,3-diazine. Thus Figure 6.9. shows the variation of  $\cos \theta$  versus time with the

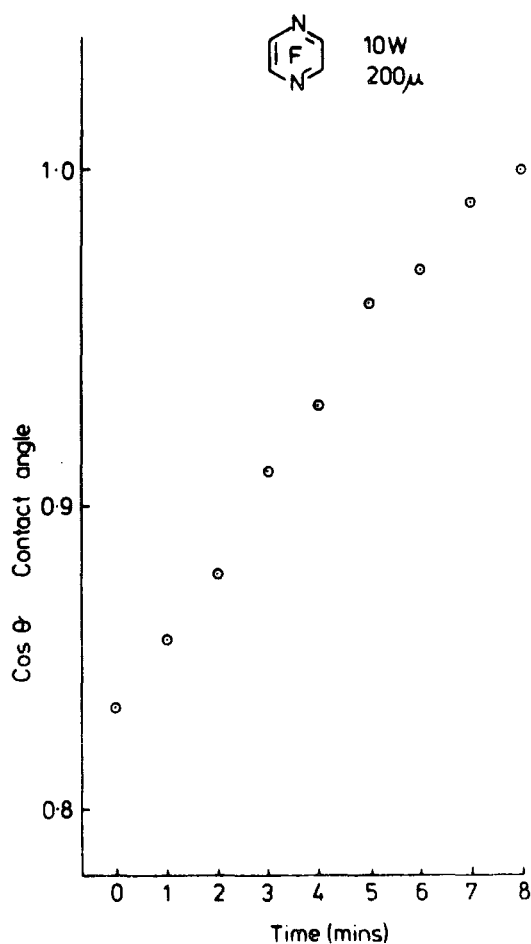


Figure 6.9. Contact angle with water vs. time (mins.), for plasma polymerised tetrafluoropyrazine films deposited onto HDPE.

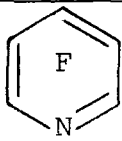
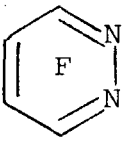

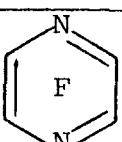
surface becoming completely wettable on a substantially shorter time-scale than for the 1,3-diazine.

#### 6.3.4. Comparison of plasma polymer films from perfluoropyridine and the Isomeric Diazines

The ESCA analysis of polymers prepared from perfluoropyridine and perfluoropyridazine have been previously described in Chapters four and five. This section draws a comparison of these data with data for perfluoropyrimidine and pyrazine.

Representative comparative data on the composition of polymers at 200 $\mu$  in the in-situ reactor as a function of power are shown in Table 6.6. The C/F stoichiometric ratios

Table 6.6. Comparison of stoichiometric ratios and percentage contribution of the C<sub>1s</sub> envelope of plasma polymerised of perfluoropyridine and the isomeric diazines, prepared in-situ reactor C, at 200 $\mu$ , as a function of power.

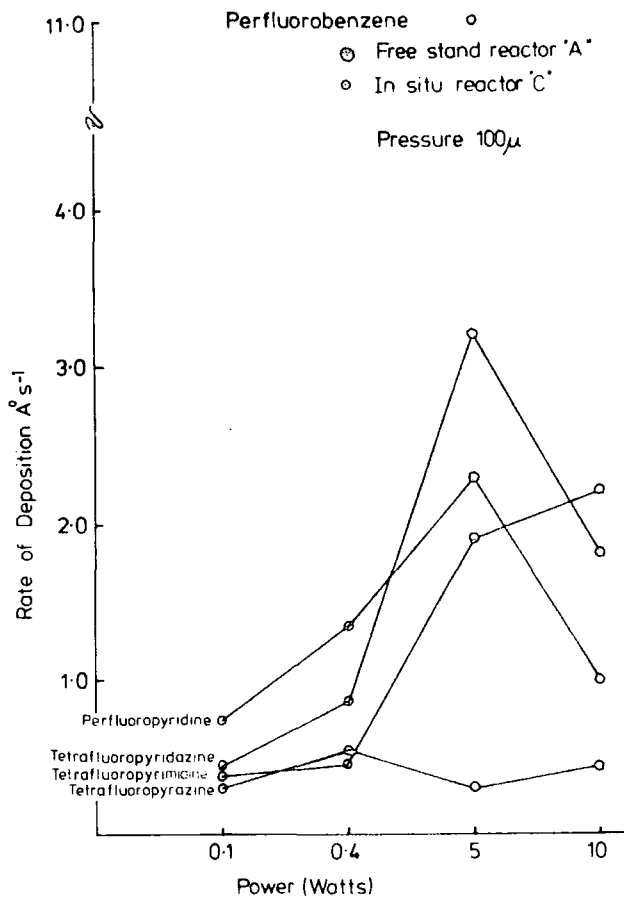
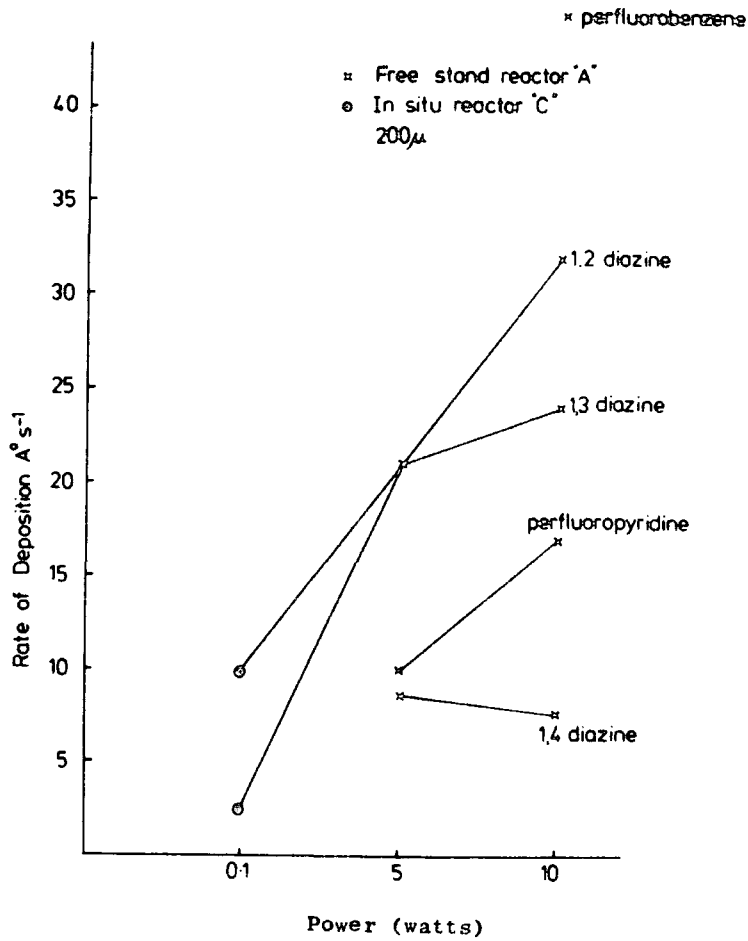
	Power (watts)	Stoichiometry Ratio (in situ reactor)				% C <sub>1s</sub> Contribution				
		C/F comp.	C/F	C/N	C/O	C-CF	CF	CF <sub>2</sub>	CF <sub>3</sub>	$\pi \rightarrow \pi^*$
	0.5W	-	-	-	-	-	-	-	-	-
	5W	0.92	0.97	3.0	8.0	22	54	20	5	-
	10W	0.82	0.96	2.6	7.0	21	43	29	7	-
	0.5W	0.93	1.04	2.3	-	19	60	15	6	1
	5W	0.86	1.0	2.0	21.0	17	56	17	8	2
	10W	1.0	1.0	1.9	48.0	29	46	19	6	-
	0.5W	1.0	1.02	1.9	17.0	24	56	16	4	-
	5W	0.90	0.95	1.6	26.0	24	47	22	7	-
	10W	0.88	0.95	1.5	23.0	24	45	24	7	-
	0.5W	1.15	0.95	1.8	30.0	30	54	15	1	-
	5W	0.90	0.97	1.6	20.0	20	54	19	6	1
	10W	0.80	0.98	1.6	28.0	17	51	23	7	2

are close to that for the starting monomers, however, the C/N stoichiometries show slightly increased levels of nitrogen in the polymers in each case. The component analyses reveal a remarkable similarity in component distribution for all four systems, although as will become apparent the rates of deposition are substantially different.

Increasing the power at a given pressure leads to an increased contribution arising from  $\text{CF}_2$  structural features. Comparison of the heterocyclic systems with perfluorobenzene,<sup>216</sup> reveal that the heterocyclic system produces polymers under the same conditions with substantially higher levels of  $\text{CF}_2$  groups. It has previously been noted that facile skeletal rearrangements occurring in the excited state manifold provides a ready route for interconversion of positional isomers in the fluorobenzene series.<sup>213-216</sup> The striking feature evident from the previous studies on the isomeric fluorobenzenes was the close similarity in structural features, compositions and rates of depositions for the various positional isomers, consistent with a rearrangement plasma polymerisation route which involved equilibration of isomeric structures.<sup>213-216</sup> The corresponding isomeric structures for perfluoropyridine,<sup>217</sup> and for the diazines differ substantially in relative energies, and recently<sup>225</sup> a detailed theoretical investigation of this point has been carried out. The fact that interconversion of isomeric structures involves substantially higher barriers than for the benzene series is manifest by the different rates of polymer formation exhibited by the

various heterocyclic monomers. Figures 6.10. and 6.11., for example, show the rates of deposition as a function of power and pressure. At 100 $\mu$  and 5 watts the rate of deposition of the 1,4-diazine is substantially lower than for the other isomers, and the rates of deposition increase in the order pyrimidine > pyridine > pyridazine and pyrazine. At lower powers at (0.1W, 200 $\mu$ ) the isomers show slightly different rates of deposition in the order pyridine > pyrimidine > pyridazine and pyrazine (0.73, 0.44, 0.39, 0.31 $\text{\AA}^0 \text{sec}^{-1}$  respectively). The power dependence at fixed pressure and pressure dependence at fixed power is substantially different for the isomeric diazines, and under all conditions the rates of deposition are lower for the fluoroheterocyclic systems compared with perfluorobenzene. <sup>216</sup>

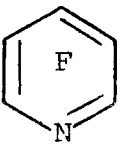
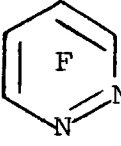
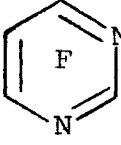
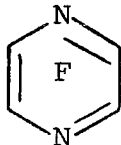
In all the isomeric diazines the polymers synthesised from the heterocyclic systems show time dependent phenomena of contact angles, which contrasts strongly with the time independent hydrophobic nature of the perfluorinated polymer produced from the corresponding benzene. This hydrolytic instability of the polymers is consistent with the striking difference in chemistry for the starting monomers; perfluorobenzene being inert to water whilst the isomeric diazines undergo very rapid hydrolysis. Indeed microanalysis of samples of the polymers prepared in the free-standing reactor reveals from the C/F and C/N stoichiometries and from the oxygen level (by difference), increasing hydrolytic instability in the order pyrazine > pyrimidine > pyridazine and pyridine (see Table 6.7.), similar to that found in nucleophilic substitution in the monomers. <sup>220</sup>



Figures 6.10. and 6.11.

Comparison of the rates of deposition of plasma polymers prepared from perfluorobenzene, perfluoropyridine and the isomeric diazines, as a function of power and pressure in reactors A and C.

Table 6.7. C/F and C/N stoichiometries and percentage of C, F, N and H of microanalysis of plasma polymerised perfluoropyridine and isomeric perfluorodiazine in the free-stand reactor.

Plasma polymerised powder	Stoichiometric ratios (Bulk analysis)		% of microanalyses in weight
	C/F	C/N	
	0.96	4.5	- - - -
	1.18	2.45	33 : 44 : 16 : -
	1.25	1.82	28 : 36 : 18 : 2
	2.03	1.67	28 : 22 : 20 : 2

As previously noted in chapters 4 and 5 the hydrolytic stability may have an important bearing on the observation that for the perfluoroheterocyclic systems there is an initial time dependence for the structures as a function of deposition.

#### 6.3.4. Conclusions

The data presented here indicates that the plasma polymer formation from perfluorinated nitrogen heterocyclic systems proceeds via a rearrangement mechanism. The relative energetics of the species involved means that the rate of deposition and structural features for positional isomers of

the diazines differ, which contrasts with the behaviour exhibited by the corresponding benzenes. The polymers produced all become wettable over a period of time when in contact with water and the retention of nitrogen in the polymer structure is directly responsible for the hydrolytic instability.



CHAPTER SEVEN

CHAPTER SEVENTHE ESCA INVESTIGATION OF THE SURFACE CHEMISTRY OF  
POLYETHYLENE AND POLYESTER LAMINATE FILMSAbstract

ESCA may now be regarded as a standard analytical tool, in which large sections of industry have invested. ESCA has been used to investigate laminate films based on low-density polyethylene and polyester (Melinex) adhesively bonded with polyurethane adhesives.

The consideration of the surface chemistry of these materials, especially their surface characterisations, is in order to understand the migration and segregation of the low molecular weight materials from the bulk to the surface. It has been found that the migration is strongly dependent on the nature of the slip agents in the laminate films of PE, and on the type of the adhesive.

The dynamic coefficient of friction (COF) has been measured for the base polymer (PE) and for the laminate films; the results indicate that the COF is also dependent on the slip agent.

### 7.1. Introduction

During the past thirty years or so, a vast technology has grown up that now produces materials which have a wide range of properties. These can be tailored to particular applications.<sup>229-235</sup>

The modern high polymer industry began with the discovery of techniques for the chemical modification of natural polymers. Examples of important modification processes include rubber vulcanization and cellulose acetylation etc. These processes opened many new fields of application. Within the past few decades, along with the development of synthetic and modified natural polymers, there has been, of necessity, a parallel development of techniques for the conversion of polymeric materials of all kinds into useful products, such as packaging films and surface coatings.<sup>236-237</sup> The term polymer processing is used to describe the conversion operations of the high polymer industry. A particularly important example is provided by the lamination process, which involves the bonding of two films together to produce a laminate film with better mechanical properties, better chemical resistance and better appearance. These have found a wide range of applications in various fields.<sup>238</sup>

There are over 300 different kinds of laminates. The principle advantages of laminated materials are, that the laminate may have certain properties that are not apparent in, or characteristic of the individual component films. The advantages of these laminated materials may be summarised as follows:-<sup>239</sup>

- (1) Mechanical and physical properties, such as strength, permeability etc.
- (2) Ease of fabrication and considerable design versatility, such as shape and size.
- (3) Resistance to a wide range of chemicals.
- (4) Resistance to weathering and UV exposure.
- (5) Thermal properties and fire resistance.
- (6) Electrical properties.

Another factor which is relevant to any materials selection process is that of the cost of these materials. In the case of laminated polymer films, which are derived from oil, cost is related to crude oil price.<sup>239</sup>

The laminate films which are the subject of study in this chapter, were produced by applying certain types of polyurethane adhesives with heat and pressure to polyethylene and polyester films, forming composite structures.

The principal advantage of adhesively combining in the lamination processes is, that the laminate films may have certain properties that were not characteristic of the individual substrates, as previously discussed. Also, the adhesive imparts to the laminate important properties, such as increased flexibility (or rigidity), improved barrier properties, puncture resistance and chemical resistance.<sup>240</sup>

There are two types of adhesive commonly used.<sup>241-242</sup> These are either water or organic solvent based. The latter are the most widely used adhesives today. The advantages of solvent based systems include the fact that most have dry film compositions suitable for use as food packaging adhesives

(e.g. polyurethane adhesive). Another advantage offered by these systems is that they have low surface tensions, providing easy wetting of a wide variety of substrates. The disadvantages arise from the migration of low molecular weight species from the adhesive to the laminate film surfaces. Also, solvents may be trapped in the laminate due to incomplete drying, and these may subsequently be a source of odour in food packaging applications. In addition to this, solvents will attack sensitive functional coatings and films.<sup>242</sup>

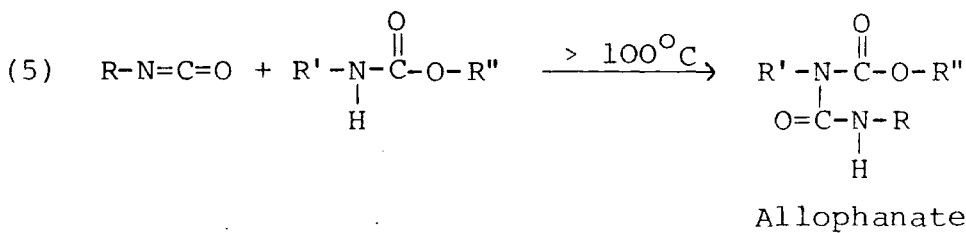
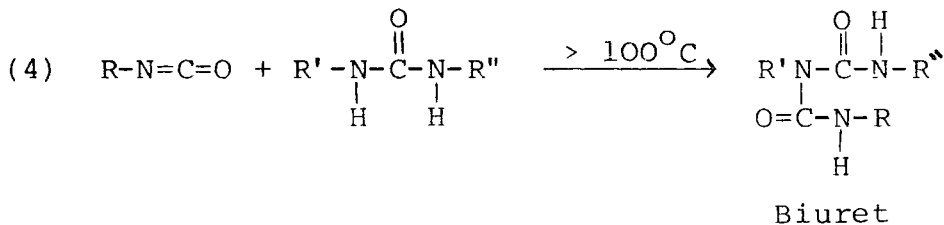
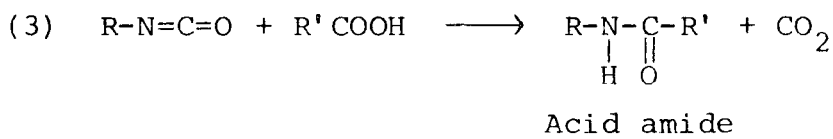
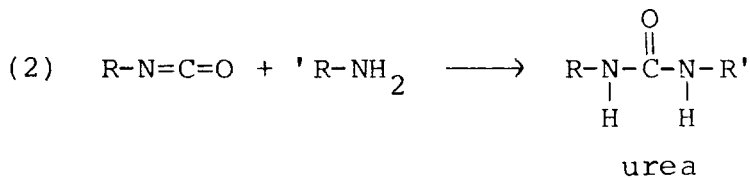
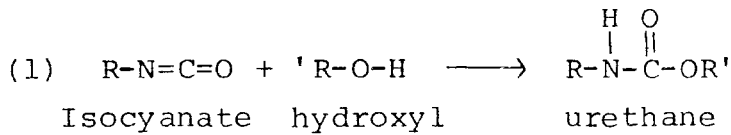
The polyurethane adhesives are of interest for the lamination processes because of their strong adhesion to many surfaces,<sup>242</sup> as shown in Table 7.1.

Table 7.1.

<u>Material bonded</u>	<u>Adhesive used</u>	<u>Average tensile strength of bond</u>
Steel to steel	TDI based	1600 psi
Aluminium to Aluminium	TDI based	>2000 psi
Aluminium to Cellulose	TDI based	450 psi
Aluminium to Acrylic	MDI based	350 psi
Aluminium foil to LDPE	MDI based	360 psi
Polyamide to LDPE	MDI based	960 psi
Polyester to LDPE	MDI based	350 psi

Generally an adhesive can be said to be a "polyurethane" if it contains, in the final adhesive, joint urethane groups. These are invariably formed by isocyanate groups with compounds containing active hydrogen atoms, either linear or

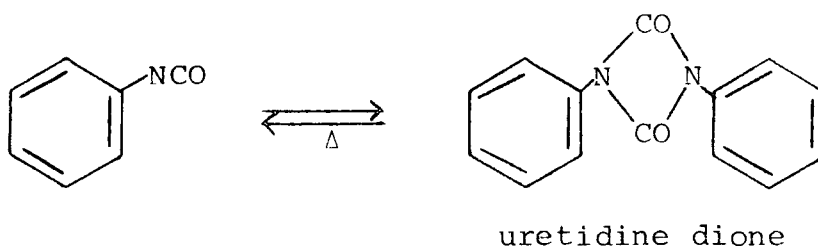
cross-linked polymers being formed.<sup>241-243</sup> As the isocyanate group is particularly reactive other potential reactions can take place through other reactive hydrogen groups, as follows:-<sup>243</sup>



Generally, the object of a urethane polymer chemist is to achieve a final adhesive with high strength and this usually means high linear molecular weight.

The effectiveness of isocyanate-based adhesives involves a combination of several features which are characteristic of the materials:-<sup>241</sup>

- (1) Isocyanates react with a variety of other functional groups containing active hydrogen atoms, as described before. There are three classes of compounds containing active hydrogen atoms, namely compounds containing hydroxyl groups, (such as polyester etc.), carboxylic acids and amines. In general the order of reactivity is: primary  $\text{NH}_2$  > aromatic  $\text{NH}_2$  > primary OH > water > secondary OH > tertiary OH > COOH and  $\text{RNHCOOR}'$ .
- (2) Di- and polyisocyanates can undergo self polymerisation, i.e. reaction with other isocyanate groups, "In-situ polymerisation".



- (3) Solubility characteristics, these promote adhesion by allowing the isocyanate to penetrate the adherend. Good strength and flexibility characteristics in the boundary film formed between the adhered members by the isocyanate-based adhesives.
- (4) The reaction of di- and polyisocyanates with hydroxyl-bearing polyesters and polyethers, produces the relatively polar, highly hydrogen bonded polyurethanes which wet and show strong attraction for a variety of surfaces.
- (5) Isocyanates react even with hydrated oxide layers on metal surfaces, thus producing a clean surface.

These factors may be responsible for the ability of the

polyurethane to adhere strongly to many substances, including: resin rubber shoe soling, nylon and polyester fabrics, a wide variety of flexible packaging films, metals and polypropylene and polyethylene, surface treated to form some surface hydroxyl groups, as presented in this chapter. For example,<sup>242</sup> strong bonds may be obtained with leather by reaction of the amino groups in the leather with isocyanate groups in the adhesive. It has been suggested that the strong bonds produced between metals such as aluminium foil and rubbers may be due to reaction of the isocyanate groups with the hydrated oxide layer on the metal surface, as described before.

Commonly used isocyanates are, toluene diisocyanate (TDI), and 4,4'-diphenyl methane diisocyanate (MDI). The isocyanate is usually added in the form of a prepolymer so as to decrease the actual free pure isocyanate content, especially if TDI has been used; and also to ensure that the mixed polyurethane solution does not set or cure in an unacceptably fast time. Several adhesive manufacturers now have adhesives that contain "excess isocyanate" that have a "pot life" extended to several months, but in which further reaction occurs rapidly when the solvent is evaporated.<sup>243</sup> The free isocyanate monomer is present in very small quantities in all isocyanate based laminating adhesives. This chapter will consider the surface chemistry of the laminate films in order to understand the migration of the isocyanate groups from the adhesive into the laminate surfaces.



Polyurethane adhesives have been found suitable for laminating a wide range of flexible packaging films including polyester, nylon, coated cellulose films, olefins and aluminium foil for general purpose and some biological applications. Most of the applications have good thermal insulation properties, structural strength, buoyancy characteristics and shock resistance combined with light weight.

In the particular case of laminate films of polyethylene and polyester with polyurethane adhesives for packaging, it has been found that the isocyanate groups in the polyurethane adhesive react very strongly with the polyester to produce strong bonds. Polyethylene is one of the cheapest thermoplastics, and as well as possessing excellent impact properties, it is very flexible. These properties and those outlined previously provide advantages for laminate films of polyethylene and polyester, also there are other advantages which have been described before.

One important influence in the formation of a good adhesive bond between two substances is the surface or interfacial chemistry.<sup>244</sup>

The question is often asked, "which is the best surface chemistry tool for research on adhesive bonding"? This question is difficult to answer because it depends on the aspect of adhesion which is being studied. Often a combination of instruments must be used to take advantage of the strong points of each.<sup>245-247</sup>

Spectrochemical techniques such as ISS, SIMS, AES and

ESCA combined with microscopy, can be usually used to gain a clear picture of where an adhesive joint has failed. The failure surfaces obtained by these techniques have been compared with lap shear and peel test.<sup>245-247</sup> Figure 7.1. shows the surface science of the adhesion.

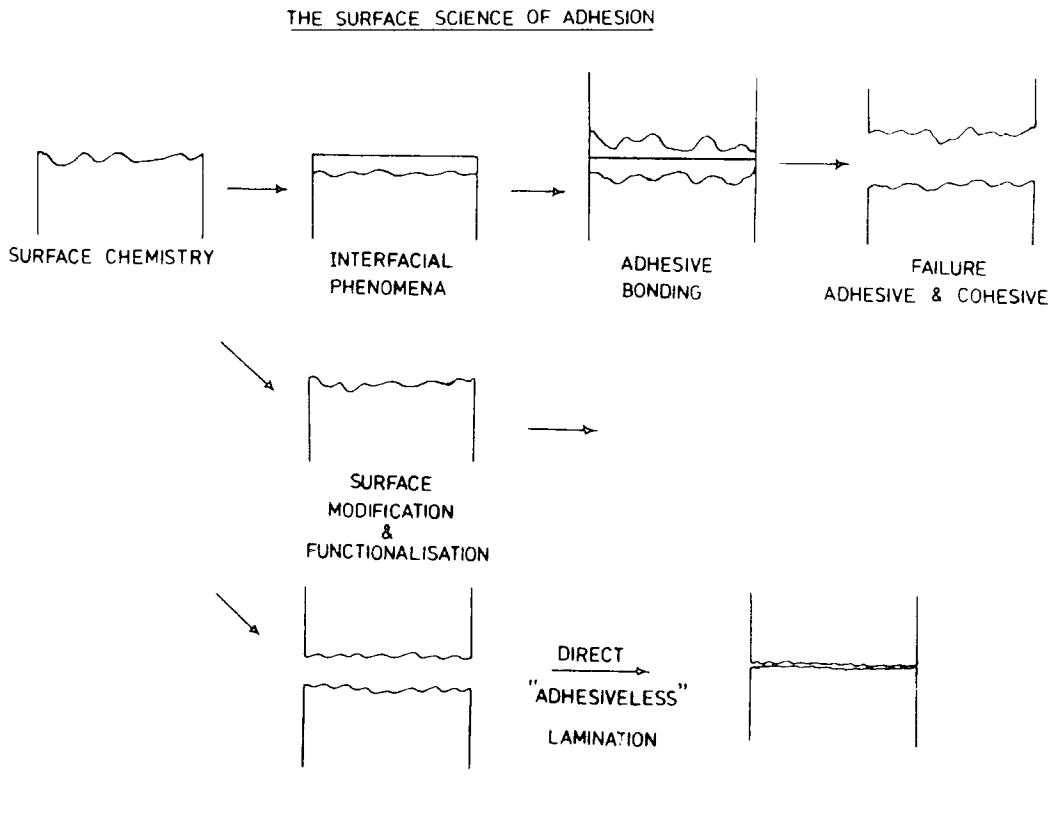


Figure 7.1. The surface science of adhesion, showing the lamination process.

ESCA is now the most widely used non-destructive technique for characterisation of the adhesive and for surface analysis because of the large amount of data which it provides, (see Chapter one).

The presence of unwanted chemical species, "contamination" within the interphase region of an adhesive bond becomes an extremely important consideration in the overall

performance of bonded materials.<sup>248</sup> This region includes all the material from some point in the bulk adhesive toward and through the boundary between adhesive and adherend to a point in the adherend where the local properties are the same as the bulk properties. Contaminants within this region, originating from the original adherend surfaces, adherend bulk and bulk adhesive, can adversely affect bonding mechanisms (i.e. wetting and adhesion), as well as bond performance (i.e. strength and durability). However, combinations of spectrochemical techniques such as ISS, SIMS, AES and ESCA were used to chemically characterise the surface of materials which make up adhesively bonded structures.<sup>249</sup>

In this chapter examples of surface characterisation data from ESCA are presented which provides a means of studying the chemical species and the migration products from the bulk to the surface for laminated films of low-density polyethylene (low and high-slip agent) and polyester film with polyurethane adhesives.

The data will be considered as follows:-

- (1) Base polymer films
  - (a) Low-density polyethylene
  - (b) Polyester
- (2) Polyurethane adhesives
- (3) Laminate films.

## 7.2. Experimental

Samples of polyurethane adhesives A - G were supplied independently, each manufacture providing details about the

commercial formulation. The general procedure in each case involved making adhesive samples according to the details given by the suppliers. In all cases, Analar grade ethylacetate was used as the dilution solvent. The adhesive samples were mixed with the solvent, and homogenized with a high speed mixer prior to use. The mixing ratio of each adhesive with the solvent, and the details of the suppliers formulation are presented in Table 7.2.

A specially fabricated handle was used to dip the degreased aluminium foil into the diluted adhesive, giving a film of each adhesive for ESCA analysis. All handling of adhesives was carried out in a clean well ventilated fume hood.

Two samples of each adhesive were analysed. The first sample was cured for one minute at 70°C, (in a lab. oven), and then stored for a period of about two weeks before ESCA examination; the second sample, uncured, was left for one hour in a fume hood before inserting into the ESCA spectrometer.

Polymer films of low and high-slip polyethylene and polyethyleneterephthalate (Melinex), provided by I.C.I. were received as a rolled sheet. The polymer films for all cases have been examined by ESCA on both sides, (inside and outside).

Laminate films in the form of a rolled sheet were made by Metal Box Ltd., from either high or low-slip polyethylene films with the appropriate polyurethane adhesive A - G, and Melinex films. Polyethylene low and high-slip surfaces were examined by means of ESCA, and in appropriate cases studies were also made of the surface chemistry of the Melinex

Table 7.2. The commercial formulation of the polyurethane adhesives A - G from the suppliers, and the components based on each system, and the mixing ratios of the Analar grade ethylacetate solvent with each adhesive.

Polyurethane adhesives	Suppliers	Components	Mixing ratios with solvent (gms.)
Adhesive A	Bondmaster Ltd.	Single component MDI based	100 gms. adhesive: 35 gms. solvent
Adhesive B	Holden Surface Coatings Ltd.	Single component MDI based	100 gms. adhesive: 35 gms. solvent
Adhesive C	Wikolin Polymer Chemie	Two component MDI based	100 gms. component A: 45 gms. solvent: 50 gms. component C
Adhesive D	Berger Adhesives	Two component MDI based	100 gms. EPS 72: 40 gms. component 403: 57 gms. solvent
Adhesive E	Wikolin Polymer Chemie	Single component TDI based	100 gms. adhesive: 35 gms. solvent
Adhesive F	Morton Williams	Single component MDI based	100 gms. component G <sub>1</sub> : 2.8 gms. of catalyst F <sub>1</sub> : 30 gms. solvent
Adhesive G	Morton Williams	Two component TDI based	100 gms. component G <sub>1</sub> : 4 gms. component G <sub>2</sub> : 25 gms. solvent

surface of the low and high-slip PE laminates. In certain cases laminate samples of low and high-slip were studied after a further period of storage to investigate the time dependence of the surface chemistry.

In all cases, samples were cut from the centre of each film to a convenient size for direct mounting on the tip of the ESCA probe, by means of double-sided "Scotch" insulating tape.

ESCA analysis was performed using either an AEI ES200A/B or Kratos ES300 electron spectrometer, at two different take-off angles,  $30^\circ$  and  $70^\circ$  or  $(50^\circ)$ . In all cases  $Mg_{k\alpha_{1,2}}$  radiation was used as the exciting source, and spectra were recorded in the fixed retardation ratio scanning mode (FRR). Under the conditions of these experiments the  $Au_{4f_{7/2}}$  level at 84 eV, used for calibration, had a full width at half maximum (FWHM) of 1.15 eV. Analysis of unresolved line shapes was carried out by standard line shape techniques using a Dupont 310 Analogue Computer.

### 7.3. Results and Discussion

#### 7.3.1. Base Polymer Films

Before considering the ESCA results obtained for the laminates, it is convenient to consider the relevant data for the base polymer films of low and high-slip polyethylene and polyester, and the adhesive samples.

##### (i) Low-Density Polyethylene (LDPE)

###### (a) Low-slip agent

A film of low-slip PE was examined by ESCA at two

different take-off angles  $30^\circ$  and  $70^\circ$  for both sides (inside and outside). The ESCA spectra displayed in Figure 7.2. show that the inside surface was corona treated (cf. chapter

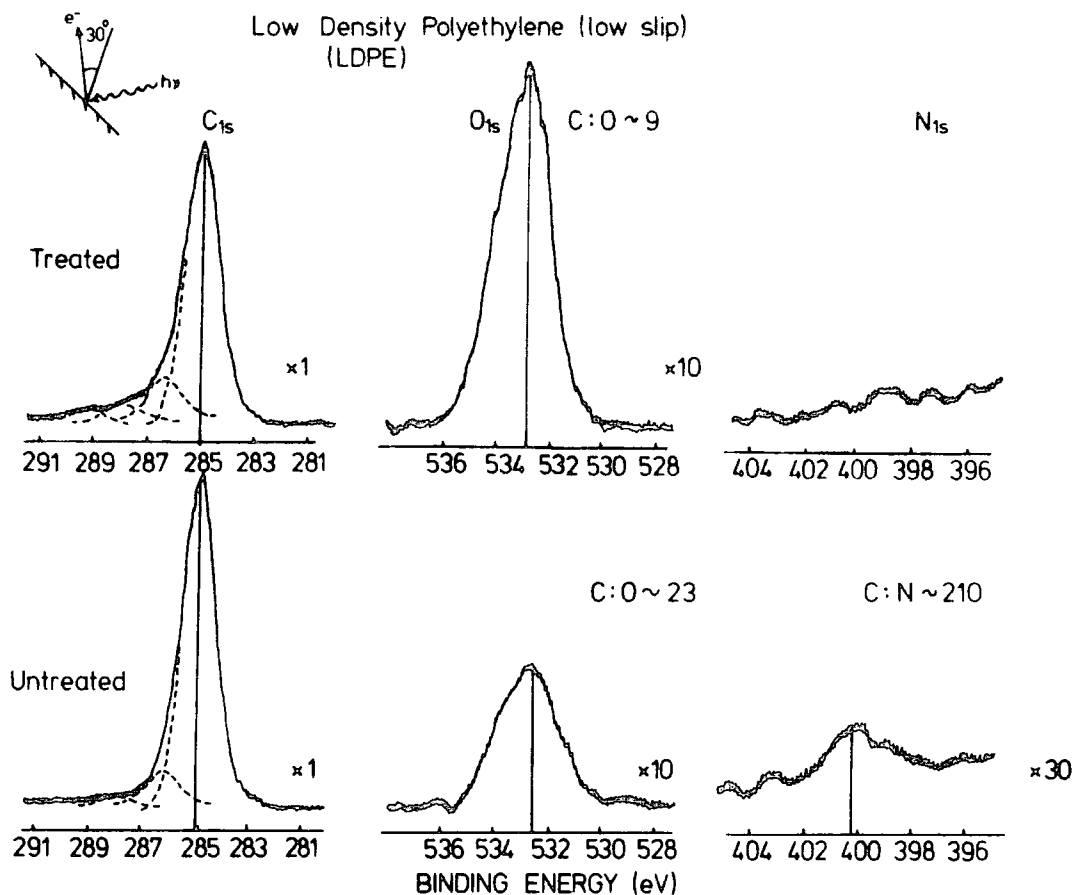


Figure 7.2.  $C_{1s}$ ,  $O_{1s}$  and  $N_{1s}$  spectra for the base polymer low-density polyethylene (low-slip), of the inside surface (corona treated) and outside surface (untreated) at a  $30^\circ$  take-off angle.

two), ( $C_{1s}/O_{1s}$  much lower than the outside).

The spectra for the corona treated side shows a relatively intense  $O_{1s}$  peak, which exhibits considerable asymmetry. This is indicative of a variety of functionalities which are also evident in the high binding energy tail of the  $C_{1s}$  peak.

The line shape analysis of the  $C_{1s}$  levels at take-off angle  $30^\circ$  shows evidence for components of  $\underline{C}H$  (285.0 eV),  $\underline{C}-O$  (286.6 eV),  $\begin{array}{c} \diagup \\ C=O \\ \diagdown \end{array}$  (287.9 eV) and  $O-\underline{C}=O$  (289.2 eV), with relative intensities of 100:15:4:1 respectively. The ESCA data displayed in Table 7.3. show that the  $C_{1s}/O_{1s}$  area ratios are 5.2 and 6.6 at  $30^\circ$  and  $70^\circ$  take-off angles respectively, indicating a small degree of vertical inhomogeneity in stoichiometry on the ESCA depth sampling scale ( $\sim 50\text{\AA}$ ). The area ratio of 5.2 gives a C:O stoichiometry of  $\sim 8:1$ , and this indicates a reasonable degree of oxygen functionalities on the surface which react with the polyurethane adhesives at the lamination interface. This will be discussed in a later section.

The reverse side of the LDPE is of interest because, it is the surface involved in heat sealing in the lamination processes. The ESCA spectra in Figure 7.2. show that the  $O_{1s}$  levels are much lower than for the corona treated side, indicating that this side was untreated. The ESCA data in Table 7.3. show the  $C_{1s}/O_{1s}$  ratios of 13.5 and 13.2 at  $30^\circ$  and  $70^\circ$  take-off angles, indicating a C:O stoichiometry of  $\sim 23:1$ , and a vertically homogeneous sample on the ESCA depth sampling scale. The  $C_{1s}$  line profile reflects this low level of oxygen functionality. The high binding energy component with a very low intensity of  $\sim 2\%$  of the main peak corresponds in binding energy to  $-N-\overset{|}{\underline{C}}=O$  at 288.0 eV, and although not specified as an additive, this suggests a very low level of amide is present at the surface.

The  $N_{1s}$  levels are weak but nonetheless statistically



Table 7.3. The relevant area ratios, binding energies, percentage of  $C_{1s}$  contribution, and the coefficient of friction (COF) for the base polymer low-slip polyethylene for outside and inside surfaces at  $30^\circ$  and  $70^\circ$  take-off angles.

LDPE Low slip	Angle	Area Ratios		Binding Energies		% of $C_{1s}$ Contribution				Coefficient of Friction		
		$C_{1s}/O_{1s}$	$C_{1s}/N_{1s}$	$C_{1s}$	$O_{1s}$	$\underline{C-H}$	$\underline{C-O}$	$\diagup C=O$	$\begin{array}{c} \diagup C=O \\ \diagdown OH \end{array}$	Time sec.	Peak value	Average
Outside surface	$30^\circ$	13.5	176.8	286.4, 288.1	532.5, 534.0	89	9	2	-	10	0.17	0.18
	$70^\circ$	13.2	94.7	286.3, 287.9 289.0	532.6, 534.0	90	8	1.5	0.5	50	0.20	0.19
Inside surface	$30^\circ$	5.2	-	286.4, 287.9 289.2	532.3, 534.8	83	13	3	1	10	0.28	0.25
	$70^\circ$	6.6	-	286.3, 287.9 289.2	532.2, 534.6	79	14	5	2	50	0.27	0.25

significant, and the  $C_{1s}/N_{1s}$  area ratios of 177 and 95, at  $30^\circ$  and  $70^\circ$  take-off angles respectively, indicate a high degree of vertical inhomogeneity. This also shows that the nitrogen functionality is located at the surface. The  $C_{1s}/N_{1s}$  area ratio of 177 would correspond to  $\sim 1$  nitrogen per  $\sim 211$  carbons, i.e. a very low level indeed. It is interesting to note that, the level of nitrogen functionality in the surface regions of the corona treated side is substantially smaller (i.e. undetected), suggesting that the corona treatment lowers the level of nitrogen functionality; this will be discussed in the next section on high-slip PE.

(b) High-slip agent

The films of high-slip LDPE were examined by ESCA on both sides, and it became evident that the outside surface was corona treated ( $C_{1s}/O_{1s}$  ratio much lower; indicative of oxidative functionalisation).

The representative spectra for both sides are displayed in Figure 7.3. The spectra for the corona treated surface indicate that the nitrogen functionality is present, (BE  $399.8 \text{ eV} - \text{C} \begin{array}{l} \text{O} \\ // \\ \text{N} \end{array}$ ) at substantially higher levels than for the low slip films. The  $O_{1s}$  levels show extensive fine structure to high binding energy, consistent with oxidative functionalisation, ( $\text{C}-\text{O}$ ,  $\text{C}=\text{O}$  and  $\text{C}-\text{OH}$ ). The ESCA data displayed in Table 7.4., indicate that the  $C_{1s}/N_{1s}$  area ratios are 39 and 32 at  $30^\circ$  and  $70^\circ$  take-off angles respectively; this is a distinctive difference from the low-slip and consistent with the known additives. A  $C_{1s}/N_{1s}$  area ratio of  $\sim 39$  gives C:N stoichiometry in the subsurface of  $\sim 46$ .

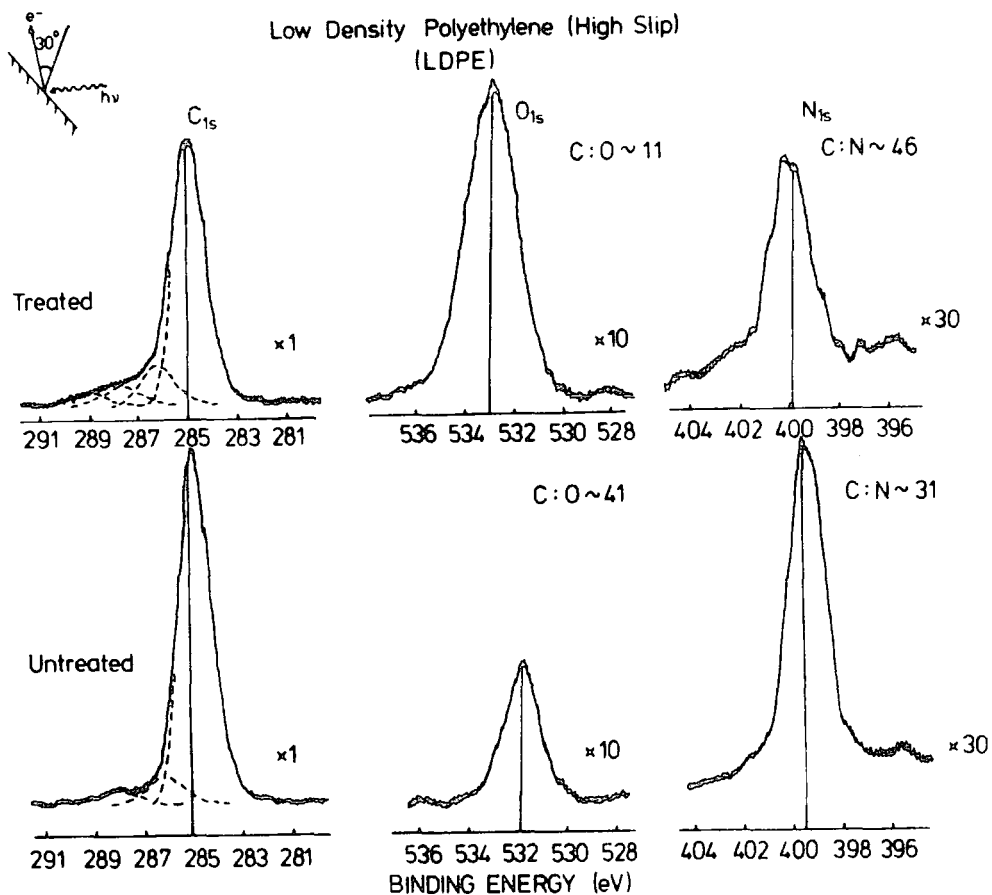


Figure 7.3.  $C_{1s}$ ,  $O_{1s}$  and  $N_{1s}$  spectra for the base polymer low-density polyethylene (high-slip), of the outside surface (corona treated) and inside surface (untreated) at a  $30^\circ$  take-off angle.

The  $C_{1s}/O_{1s}$  area ratios of 6.5 and 6.7 at take-off angles  $30^\circ$  and  $70^\circ$  respectively, indicate vertical homogeneity comparable with the low-slip sample.

The spectra for the inside, (untreated side) are also shown in Figure 7.3. The  $C_{1s}$  levels show the distinctive level associated with a straight chain amide on the PE surface, ( $-\overset{\text{O}}{\parallel}{\text{C}}-\text{NH} \sim 288.1 \text{ eV}$ ). The  $C_{1s}/N_{1s}$  intensity ratios in Table 7.4. of 26 and 26 at take-off angle  $30^\circ$  and  $70^\circ$  respectively, indicate a degree of vertical homogeneity.

Table 7.4. The relevant area ratios, binding energies, percentage  $C_{1s}$  contributions, and the COF for the base polymer high-slip polyethylene for the outside and inside surfaces at  $30^\circ$  and  $70^\circ$  take-off angles.

LDPE High-slip	Angle	Area Ratios		Binding Energies			% of $C_{1s}$ Contribution				Coefficient of Friction		
		$C_{1s}/O_{1s}$	$C_{1s}/N_{1s}$	$C_{1s}$	$O_{1s}$	$N_{1s}$	$\underline{C-H}$	$\underline{C-O}$	$\begin{array}{c} \diagup \\ C=O \\ \diagdown \end{array}$	$\begin{array}{c} O \\ // \\ C \\ \backslash \\ OH \end{array}$	Time sec.	Peak value	Average
Outside surface	$30^\circ$	6.5	38.9	286.4, 287.7 288.6	532.8, 534.0	399.8	80	10	5	5	10	0.29	0.26
	$70^\circ$	6.7	31.5	286.3, 287.8 288.7	532.6, 534.1	399.9	78	16	3	3	50	0.24	0.22
Inside surface	$30^\circ$	24.4	26.2	286.3, 288.1	531.8, 533.3	399.6	91	6	3	-	10	0.24	0.23
	$70^\circ$	18.2	26.3	286.2, 288.1	532.0, 533.4	399.7	88	8	4	-	50	0.24	0.22

A  $C_{1s}/N_{1s}$  area ratio of  $\sim 26$  would give a stoichiometry of  $\sim 30$ , which is consistent with a high level of nitrogen functionality in the surface regions. The additive in the high-slip LDPE is oleamide, which has a stoichiometry  $\sim 18$ . This demonstrates the substantial segregation of the slip agent to the surface. However, it is clear that the corona treatment lowers the level of nitrogen functionalities in the surface, (the change in  $C_{1s}/N_{1s}$  area ratios from  $\sim 39$  to  $\sim 26$  in going from the corona treated surface to the untreated surface).

(ii) Polyester

The polyethyleneterephthalate (PET) films were studied by ESCA at different take-off angles  $30^\circ$  and  $70^\circ$ , for both sides (outside and inside).

The representative spectra for both sides are displayed in Figure 7.4. The line profile of the  $C_{1s}$  peak of the inside surface, at take-off angle  $30^\circ$  suggests components of  $\underline{C-H}$  at 285.0 eV,  $\underline{C-O}$  at 286.6 eV and  $O-\underline{C=O}$  at 289.0 eV, with relative intensities of 100:33:25 respectively. The component at  $\sim 291.2$  eV is a broad peak consistent with  $\pi \rightarrow \pi^*$  shake-up<sup>58</sup> satellites, with intensity  $\sim 4\%$  of that of the main peak. The  $O_{1s}$  levels show the characteristic double structure  $C-\underline{O}$  and  $C=\underline{O}$ .

The ESCA data are displayed in Table 7.5., indicating that the  $C_{1s}/O_{1s}$  area ratio of 2.1 and 2.5 at  $30^\circ$  and  $70^\circ$  take-off angles respectively are evidence for some surface contamination, and there is no evidence for any nitrogen functionality. The data for the outside surface show that

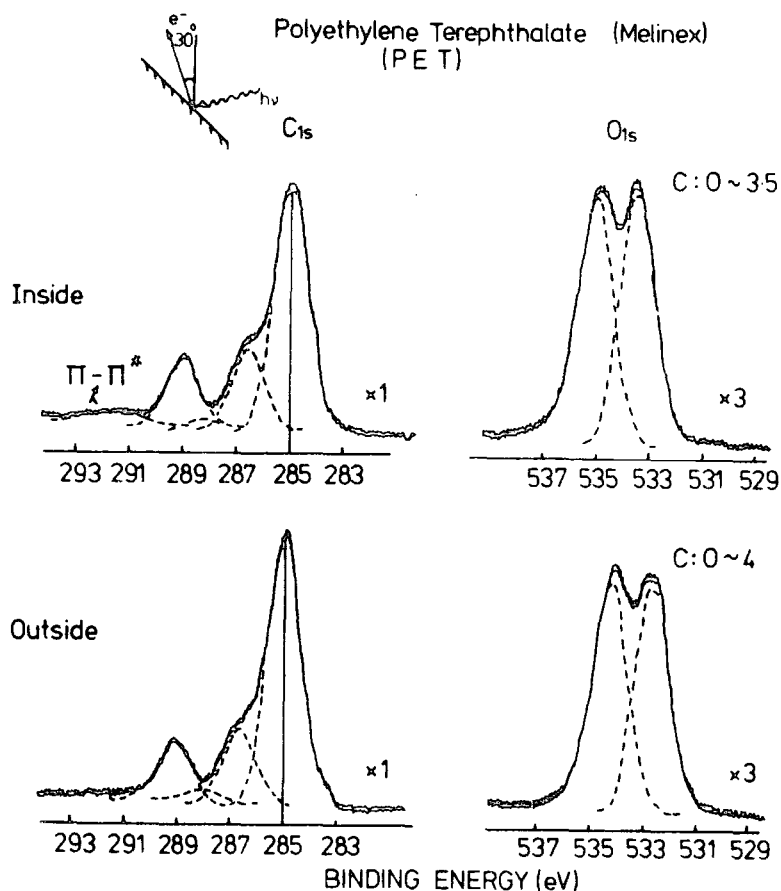


Figure 7.4.  $C_{1s}$  and  $O_{1s}$  spectra of base polymer polyester, polyethyleneterephthalate (Melinex) of the inside and outside surfaces at a  $30^\circ$  take-off angle.

the  $C_{1s}/O_{1s}$  intensity ratios are 2.4 and 2.7 at  $30^\circ$  and  $70^\circ$  respectively, indicating a slightly higher level of surface contamination than for the inside surface. This could be due to an additive.

To summarise, the main points are:-

- (1) The high-slip PE film shows extensive surface coverage by the slip agent.
- (2) The PE films had been corona treated by the corona discharge method, (the outside of the high-slip

Table 7.5. The area ratios and the binding energies of  $C_{1s}$  and  $O_{1s}$  levels, and the percentage of  $C_{1s}$  contributions of the base polymer polyester (PET) film, for the outside and the inside surfaces at  $30^\circ$  and  $70^\circ$  take-off angles.

Polyester (PET)	Angle	Area Ratio		Binding Energy		% of $C_{1s}$ Contribution			
		$C_{1s}/O_{1s}$	$C_{1s}/N_{1s}$	$C_{1s}$	$O_{1s}$	$\underline{C-H}$	$\underline{-C-O}$	$\underline{-C=O}$	$\pi \rightarrow \pi^*$
Outside surface	$30^\circ$	2.4	-	286.7, 288.3 289.3	532.9, 534.4	68	18	14	-
	$70^\circ$	2.7	-	286.6, 289.1	532.6, 534.2	70	17	13	-
Inside surface	$30^\circ$	2.1	-	286.6, 288.1 289.1, 291.7	533.6, 535.2	62	20	16	2
	$70^\circ$	2.5	-	286.5, 288.0 289.1, 291.5	532.7, 534.2	65	19	14	2

and the inside of the low-slip PE).

- (3) The corona treated surfaces of PE are of interest because of their involvement in the laminate films.
- (4) There is little or no nitrogen functionality on either the low-slip PE or the polyester surfaces.
- (5) The corona treatment lowers the level of nitrogen functionality in the surface.
- (6) The dynamic coefficient of friction (COF) is dependent on the slip agent on the PE surfaces.

### 7.3.2. Polyurethane Adhesives

This section will describe the surface chemistry of the adhesive samples A - G, individually for both uncured and cured states.

#### (i) Adhesive A

ESCA examinations for adhesive A were made for films of the cured and uncured adhesives on the aluminium foil substrate. The wide scan spectrum reveals the presence of  $C_{1s}$ ,  $N_{1s}$  and  $O_{1s}$  levels as expected. The high resolution spectra of  $C_{1s}$ ,  $N_{1s}$  and  $O_{1s}$  levels are shown in Figure 7.5. For both uncured and cured samples the  $C_{1s}$  spectrum shows that the polyurethane adhesive is polyether based, (see Tables 7.6. and 7.8.).

The line profile of the  $C_{1s}$  levels of the uncured sample, at take-off angle  $30^\circ$  suggests components of  $\underline{C}$ -H at  $\sim 285$  eV,  $\underline{C}$ -O at 286.6 eV,  $-\underline{C}=\overset{N}{O}$  at 288.0 eV and  $X-\overset{N}{C}=\overset{N}{O}$  at 289.5 eV with relative intensities of 91:100:5:6 respectively, (see Table 7.6.). The component at  $\sim 292.0$  eV is a broad peak consistent with  $\pi \rightarrow \pi^*$  shake-up satellites.<sup>58</sup> The intensity of



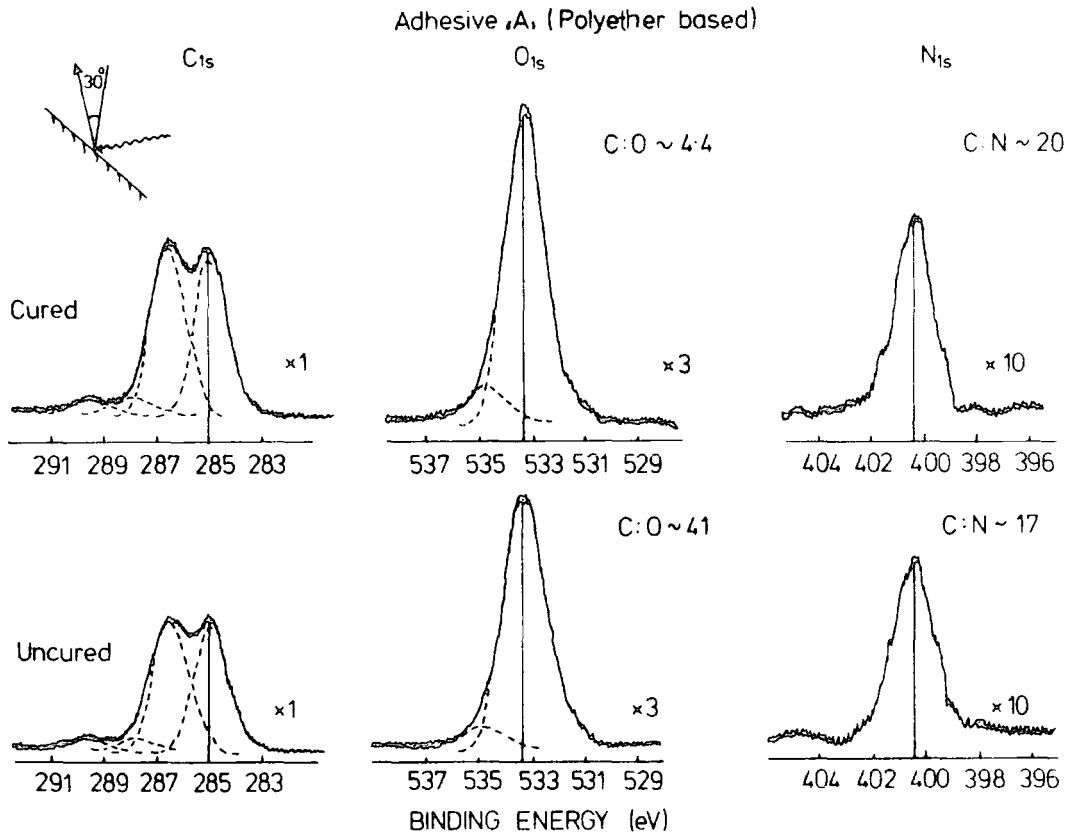


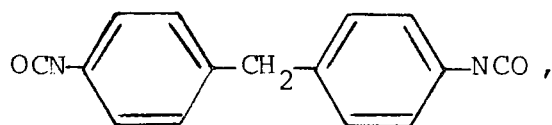
Figure 7.5. C<sub>1s</sub>, O<sub>1s</sub> and N<sub>1s</sub> of polyurethane adhesive A, "polyether based", for cured and uncured samples at 30° take-off angle.

this, ~ 2% of the intensity of the main peak, is of relevance to the assessment of the overall level of MDI containing material.

The ESCA data for the uncured sample displayed in Table 7.7., shows the C<sub>1s</sub>/O<sub>1s</sub> intensity ratios of 2.4 and 3.1 at take-off angles 30° and 70° respectively. This indicates a degree of vertical inhomogeneity. The C<sub>1s</sub>/N<sub>1s</sub> area ratios of 15 (30°) and 23 (70°) are also indicative of vertical inhomogeneity, but taking the former as a starting point the surface stoichiometry is in the region of C:N of 18.

For MDI the stoichiometry is 6.5, therefore the ESCA indicates a fairly high proportion of MDI based functionalities in the surface regions.

The component at 289.5 eV in the  $C_{1s}$  spectrum almost certainly corresponds to urethane linkages  $-NH-\overset{O}{\parallel}C-O-$  shifted to higher binding energy than  $-\overset{O}{\parallel}C-O-$ .<sup>65,70</sup> However, the polyether based the adhesive is almost certainly based on propylene glycol ( $O-\overset{CH_3}{\underset{|}{CH}}-CH_2-O$ ), in which case the contribution to the  $\underline{C}H$  component would be  $\frac{100}{2} \times 1 = 50$ , (derived from the  $\underline{C}-O$  component at 286.6 eV with relative intensity of 100, see Table 7.6.). The remaining  $\underline{C}-H$  intensity i.e.  $91 - 50 = 41$ , could be the intensity of  $\underline{C}H$  component from MDI based. The relative intensity of  $\sim 5$  of the higher binding energy component  $-NH-\overset{O}{\parallel}C-O-$  at 289.5 eV suggest a contribution of 32.5 from MDI to the  $\underline{C}-H$  intensity, (the ratio of the carbon in the isocyanate group  $-O-\overset{O}{\parallel}C-N$  to that in the rest of the MDI



is  $2:13 = 6.5$ , and the carbon attached to nitrogen will contribute slightly to the components assigned to  $\underline{C}-H$  and  $\underline{C}-O$ , however the contribution to the  $\underline{C}H$  from the component  $-N-\overset{O}{\parallel}C-O-$  is approximately  $5 \times 6.5 = 32.5$ ). The remaining intensity of  $(41 - 32.5)$  could be assigned to the intermediate binding energy component at  $\sim 287.8$  eV possibly due to  $-\overset{O}{\parallel}C-N-\overset{O}{\parallel}C-$  functionalities.<sup>65,70</sup>

The  $N_{1s}$  peak in Figure 7.5. is somewhat broadened, but

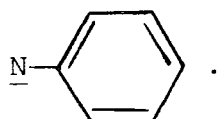
Table 7.6. The relative intensities of  $C_{1s}$  contribution of the uncured adhesives A - G at  $30^\circ$  and  $70^\circ$  take-off angles.

Samples	Angles	$C_{1s}$ Contribution				Shake-up
		H-C	O-C	O=C-	X-C=O	
Adhesive "A" uncured	70	96	100	7	10	2.9
	30	91	100	5	6	2.4
Adhesive "B" uncured	70	77	100	6	6	-
	30	72	100	7	5	-
Adhesive "C" uncured	70	59	100	6	4	-
	30	66	100	8	4	-
Adhesive "D" uncured	70	100	40	11	21	-
	30	100	43	10	25	-
Adhesive "E" uncured	70	70	100	7	7	1.1
	30	70	100	9	8	1.8
Adhesive "F" uncured	70	100	34	-	28	2.8
	30	100	34	-	26	2.7
Adhesive "G" uncured	70	100	35	-	30	2.9
	30	100	35	-	27	2.9

Table 7.7. The  $C_{1s}/O_{1s}$  and  $C_{1s}/N_{1s}$  area ratios and the binding energies of the  $C_{1s}$ ,  $O_{1s}$  and  $N_{1s}$  levels of the uncured adhesives A - G at  $30^\circ$  and  $70^\circ$  take-off angles.

Name	Angle	Area Ratio		Binding Energy		
		$C_{1s}/O_{1s}$	$C_{1s}/N_{1s}$	$C_{1s}$	$O_{1s}$	$N_{1s}$
Adhesive "A"	70	3.1	22.9	286.6, 287.8 289.6	533.1, 534.6	400.4
	30	2.4	14.6	286.6, 287.8 289.5	533.4, 534.9	400.4
Adhesive "B"	70	2.4	22.5	286.7, 287.8 289.7	533.3, 535.0	400.5
	30	2.6	20.9	286.7, 287.9 290.0	533.4, 534.9	400.6
Adhesive "C"	70	2.5	30.5	286.6, 287.8 289.4	533.3, 534.8	400.3
	30	2.5	22.3	286.5, 287.7 289.5	533.1, 534.4	400.4
Adhesive "D"	70	3.0	13.2	286.6, 287.4 289.5	532.8, 534.4	400.5
	30	2.5	11.0	286.3, 287.3 289.5	532.8, 534.4	400.5
Adhesive "E"	70	2.3	16.1	286.6, 287.5 289.2	533.1, 534.7	400.2
	30	2.7	16.7	286.7, 287.9 289.7	533.0, 534.7	400.2
Adhesive "F"	70	2.1	135	286.5, 288.9	532.7, 534.2 534.6	399.6
	30	1.7	120	286.5, 288.9	532.6, 534.0 535.3	399.9
Adhesive "G"	70	2.1	43.9	286.6, 289.0	532.6, 534.2 535.1	399.8
	30	1.9	41.2	286.6, 289.0	532.6, 534.2 535.1	400.1

the main peak is at  $\sim 400.5$  eV, significantly higher in binding energy than for the amide functionalities.<sup>70</sup> The nitrogen peak also shows evidence of shake-up structure, suggesting the group:



The spectra for the cured sample are also shown in Figure 7.5. The ESCA data are displayed in Table 7.8. and Table 7.9. They are remarkably similar to those for the uncured sample, the main change being a fairly uniform  $C_{1s}/O_{1s}$  ratio as a function of take-off angles  $2.6$  ( $30^\circ$ ) and  $2.7$  ( $70^\circ$ ). The  $N_{1s}$  levels still show a small vertical inhomogeneity from  $C_{1s}/N_{1s}$  ratios of 17 and 21 at take-off angles  $30^\circ$  and  $70^\circ$  respectively. It seems likely from this, that the outermost few tens of Angstroms of the "uncured" sample have already undergone reaction during the time scale between preparation and analysis.

(ii) Adhesive B

The films of the cured and uncured of adhesive B on aluminium foil substrate were analysed by ESCA. The spectra indicated a close correspondence between the two samples, and also show that the polyurethane adhesive B is polyether based, like adhesive A, (see Figure 7.5.). The overall intensities of the components of the  $C_{1s}$  levels suggests that the polyether is based on a propylene glycol system  $-O-\underset{\text{CH}_3}{\text{CH}}-\text{CH}_2-\text{O}-$ , as previously described, (see Tables 7.6. and 7.8.).

Table 7.8. The relative intensities of the  $C_{1s}$  contribution of the cured adhesives A - G at  $30^\circ$  and  $70^\circ$  take-off angles.

Samples	Angles	$C_{1s}$ Contribution				Shake-up
		H-C	O-C	O=C-	X-C=O	
Adhesive "A" cured	70	93	100	10	8	2.6
	30	92	100	7	8	2.3
Adhesive "B" cured	70	76	100	6	6	1.3
	30	82	100	7	6	1.9
Adhesive "C" cured	70	63	100	8	4	low
	30	84	100	14	6	low
Adhesive "D" cured	70	100	24	-	16	-
	30	100	28	3	17	-
Adhesive "E" cured	70	64	100	8	9	3.2
	30	60	100	9	6	3.1
Adhesive "F" cured	70	100	35	3	25	1.1
	30	100	36	2	26	1.7
Adhesive "G" cured	70	100	34	4	27	3.0
	30	100	37	3	31	1.9

Table 7.9. The  $C_{1s}/O_{1s}$  and  $C_{1s}/N_{1s}$  area ratios and the binding energies of the  $C_{1s}$ ,  $O_{1s}$  and  $N_{1s}$  levels of the cured adhesives A - G at  $30^\circ$  and  $70^\circ$  take-off angles.

Name	Angle	$C_{1s}/O_{1s}$	$C_{1s}/N_{1s}$	$C_{1s}$	$O_{1s}$	$N_{1s}$
Adhesive "A" cured at $70^\circ\text{C}$	70	2.6	21.1	286.6, 287.8 289.5	533.3, 534.9	400.4
	30	2.7	17.2	286.6, 287.6 289.3	533.4, 534.8	400.4
Adhesive "B" cured at $70^\circ\text{C}$	70	2.5	24.7	286.7, 287.9 289.5	533.5, 534.8	400.4
	30	2.6	20.4	286.7, 287.8 289.7	533.2, 534.5	400.4
Adhesive "C" cured at $70^\circ\text{C}$	50	1.9	16.2	286.7, 288.0 289.8	532.5, 534.1	400.4, 402.3
	30	2.0	15.1	286.6, 287.8 289.5	532.5, 534.0	399.8, 401.7
Adhesive "D" cured at $70^\circ\text{C}$	70	4.0	21.9	286.4, 289.1	532.2, 533.7 535.0	399.9
	30	3.4	17.2	286.6, 287.8 289.3	533.0, 534.7 536.0	400.7
Adhesive "E" cured at $70^\circ\text{C}$	70	2.3	15.0	286.6, 287.4 289.5	533.2, 534.7	400.3
	30	2.4	14.6	286.7, 287.9 289.7	533.1, 534.5	400.7
Adhesive "F" cured at $70^\circ\text{C}$	70	2.3	143.8	286.5, 287.7 289.0	532.5, 533.9 534.9	399.8
	30	1.9	111.8	286.4, 287.8 288.8	532.4, 533.8 534.8	399.6
Adhesive "G" cured at $70^\circ\text{C}$	70	2.0	82.5	286.8, 288.0 289.1	532.6, 534.0 535.2	400.1
	30	1.8	76.6	286.8, 288.1 289.3	532.8, 534.3 535.5	400.1

The ESCA data, displayed in Tables 7.7. and 7.9., provide direct indication that the cured samples are remarkably similar to those for the uncured samples. The  $C_{1s}/O_{1s}$  ratios of 2.6 and 2.4 at take-off angles  $30^\circ$  and  $70^\circ$  respectively, indicate that the uncured sample has a reasonable degree of homogeneity, as do the  $C_{1s}/N_{1s}$  ratios of 21 ( $30^\circ$ ) and 23 ( $70^\circ$ ). The overall  $C_{1s}$  line profile shows:  $\underline{C}$ -H at 285.0 eV,  $\underline{C}$ -O at 286.6 eV and  $X-\overset{O}{\parallel}{C}-N$  at ( $\sim 287.8$  eV and  $\sim 289.7$  eV), with relative intensities of 72, 100 and 12 respectively (see Table 7.6.). The  $N_{1s}$  peak is at  $\sim 400.5$  eV significantly higher than for amide.

The ESCA data for the cured sample in Table 7.9. indicates that it exhibits a reasonable degree of homogeneity; the  $C_{1s}/O_{1s}$  ratios are 2.6 and 2.5 at  $30^\circ$  and  $70^\circ$  take-off angles, giving stoichiometries of 4.2 and 4.0 respectively. The  $C_{1s}/N_{1s}$  ratios of 20.4 ( $30^\circ$ ) and 24.7 ( $70^\circ$ ) corresponding to stoichiometries of  $\sim 24$  and  $\sim 30$  respectively are indicative of considerable vertical inhomogeneity and also suggest a considerable segregation of MDI based functionalities in the surface region, (compare MDI stoichiometry of 6.5). It is interesting to note that the MDI based material is slightly more concentrated at the surface compared with the subsurface.

From the  $\underline{C}$ -O intensity of 100 for the cured sample, (see Table 7.8.), it is deduced that, if the system is based on propylene then, the contribution to the  $\underline{C}$ -H intensity would be 50, (see adhesive A). This leaves an intensity of  $82 - 50 = 32$  for the  $\underline{C}$ -H component derived from MDI, and this gives a surface loading of  $\sim (-O-\overset{\text{CH}_3}{\underset{|}{\text{CH}}}-\text{CH}_2-\text{O}-)$ : MDI of 20:1.



(iii) Adhesive C

ESCA examinations were made of the films of cured and uncured adhesives on aluminium foil substrate. The  $C_{1s}$  and  $O_{1s}$  spectra show that, like adhesive A the polyurethane is polyether based, (see Figure 7.5., Tables 7.6. and 7.8.).

The dominant feature in the case of the cured and uncured adhesives is a component at 286.6 eV corresponding to  $\underline{C}$ -O structural features. The low binding energy component at 285.0 eV is attributable to the  $C_{1s}$  levels of the MDI and those carbons of the polyether attached only to carbon or hydrogen. The component at 287.8 eV arises from  $-C(=O)N$  components, whilst that at 289.4 eV is attributable to  $-O-C(=O)N$  functionalities.<sup>65,70</sup>

The ESCA data for uncured samples are displayed in Table 7.7. The  $C_{1s}/O_{1s}$  area ratios at  $30^\circ$  and  $70^\circ$  take-off angles of 2.5., indicate that the sample exhibits vertical homogeneity with respect to oxygen stoichiometry. By contrast the  $C_{1s}/N_{1s}$  intensity ratio varies from 22 to 31 as a function of take-off angles  $30^\circ$  and  $70^\circ$ ; indicative of considerable vertical inhomogeneity.

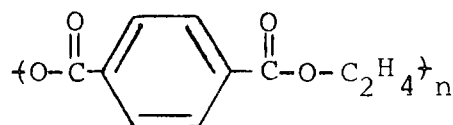
On curing samples, the area ratios in Table 7.9., show that there are very significant changes in surface chemistry compared with uncured samples. The oxygen content increases on curing ( $C_{1s}/O_{1s} \sim 2$ ), and the nitrogen functionality also increases ( $C_{1s}/N_{1s} \sim 16$ ). In addition the  $N_{1s}$  levels for the cured sample show an extra high binding energy component at  $\sim 402.0$  eV corresponding, in binding energy, to an amine functionality,<sup>70</sup> and this is  $\sim 30\%$  of the total signal

intensity. The change in  $C_{1s}/N_{1s}$  area ratios from  $\sim 22$  to  $\sim 16$  in going from the uncured to the cured samples thus stems largely from the appearance of this extra component in the  $N_{1s}$  level of the cured samples.

Considering the cured sample the C:N and C:O stoichiometries are  $\sim 19$  and  $\sim 3$  respectively, compared with the MDI stoichiometry of 6.5 for both nitrogen and oxygen. This suggests a considerable segregation of MDI based functionalities into the surface regions. It is interesting to note that the shake-up intensity is lower than might be anticipated if the aromatic system of MDI remained unmodified during the curing process.

(iv) Adhesive D

ESCA examinations were made of films of the cured and uncured adhesive samples on the Al foil substrate. The ESCA spectra reveal the  $O_{1s}$  levels characteristic of two components,  $C-O$  and  $C=O$  separated by their natural line width, whilst the  $C_{1s}$  levels are basically of three distinctive components,  $\overset{O}{\parallel}C-O$ ,  $\overset{O}{\parallel}C-O$  and  $\underline{C}-H$  environments (see Tables 7.6. and 7.8.). Thus the  $C_{1s}$  and  $O_{1s}$  levels are all characteristic of a polyester based system



(cf. Figure 7.6.).

The ESCA data for the uncured sample are displayed in Table 7.7., and this indicates that the  $C_{1s}/O_{1s}$  and  $C_{1s}/N_{1s}$  area ratios have some dependence on take-off angles, and this

is indicative of some small vertical inhomogeneity. The  $C_{1s}$  levels show evidence of shake-up structure consistent with the presence of phthalate residues.<sup>58</sup> The high binding energy component at  $\sim 289.5$  eV is due to ester groups,<sup>65,70</sup> and the intensity ratio of the  $\text{-}\overset{\text{O}}{\parallel}\text{C}\text{-O}$  and  $\text{CH}$  components (25:100) suggests a functionality ratio of 4, (see Table 7.6.). For a phthalate based system the ratio should be 1:3, whilst for adipate the ratio should be 1:2; this indicates that there are other contributions to the low binding energy  $\text{C-H}$  component at 285.0 eV from the MDI.

The  $N_{1s}$  levels are a single component consistent in BE with it being the  $\text{-O-}\overset{\text{O}}{\parallel}\text{C-N-}$  functionality. The  $C_{1s}/N_{1s}$  area ratio, at  $30^\circ$  take-off angle, of 11 gives a stoichiometry of  $\sim 13$ , and since the stoichiometry from MDI based on 6.5 this indicates a very high loading of MDI based residues in the surface region.

The ESCA data for the cured sample are displayed in Table 7.9. This indicates that the  $C_{1s}/O_{1s}$  and  $C_{1s}/N_{1s}$  area ratios vary with angular dependence, showing degree of vertical inhomogeneity. The decrease in  $O_{1s}$  and  $N_{1s}$  levels is associated with an increase in the low binding energy component at 285.0 eV of the  $C_{1s}$  levels. The  $C_{1s}/O_{1s}$  and  $C_{1s}/N_{1s}$  area ratios of 3.4 and 17.2 at  $30^\circ$  take-off angle, correspond to stoichiometries  $\sim 5$  and  $\sim 20$  respectively. This again indicates a very high loading of MDI in the surface region, and the angular data at  $30^\circ$  and  $70^\circ$  show that the MDI is more concentrated at the surface than the subsurface.

(v) Adhesive E

The ESCA spectra for both uncured and cured samples show that the  $C_{1s}$  levels are characteristic of a polyether based system, as previously described, (see Figure 7.5.). The single component  $N_{1s}$  levels are consistent with urethane functionalities as is the binding energy of the component  $C_{1s}$  level at  $\sim 289.4$  eV.<sup>70</sup> The ESCA data are displayed in Tables 7.7. for uncured sample and 7.9. for cured sample. These indicate that the  $C_{1s}/O_{1s}$  and  $C_{1s}/N_{1s}$  area ratios of 2.7 and 16.7 (at a  $30^\circ$  take-off angle) for the uncured sample change very little on curing, (2.4 and 14.6 respectively). The corresponding stoichiometries for the cured sample are  $\sim 4$  (C:O) and 17 (C:N).

The high binding energy component of the  $C_{1s}$  levels attributable to  $-N-\overset{\text{O}}{\parallel}{C}-O$  functionalities, and the observation of  $\pi \rightarrow \pi^*$  shake-up satellites, show the high degree of functionalisation in the surface regions arising from the TDI.

(vi) Adhesive F

The ESCA measurements were carried out for both uncured and cured samples. The spectra show that the two equal intensity components of the  $O_{1s}$  levels are distinctive of ester functionalities, whilst the  $C_{1s}$  levels show three components from  $\underline{C}-H$ ,  $\underline{C}-O$  and  $-\overset{\text{O}}{\parallel}{C}-O$ , with an additional high binding energy component arising from the  $\pi \rightarrow \pi^*$  shake-up satellites, (see Tables 7.6. and 7.8.). This indicates that adhesive F is based on an aromatic polyester system (cf. Figure 7.6.). The  $N_{1s}$  signal is detected at very low intensity for both cured and uncured samples.

The ESCA data, displayed in Tables 7.7. for the uncured and 7.9. for the cured sample, indicate that the  $C_{1s}/O_{1s}$  and  $C_{1s}/N_{1s}$  area ratios, at a  $30^\circ$  take-off angle, are  $\sim 1.8$  and  $\sim 120$  respectively for both the cured and uncured samples; these correspond to stoichiometries of  $\sim 2.7$  and  $\sim 130$  respectively. Thus, this system exhibits very low loading of MDI based functionalities at the surface region. The angular data also show that the samples are reasonably homogeneous on the ESCA depth sampling scale.

(vii) Adhesive G

ESCA was used to study the films of the cured and uncured samples on the aluminium foil substrate. The ESCA spectra of the two samples are displayed in Figure 7.6. The  $C_{1s}$  levels

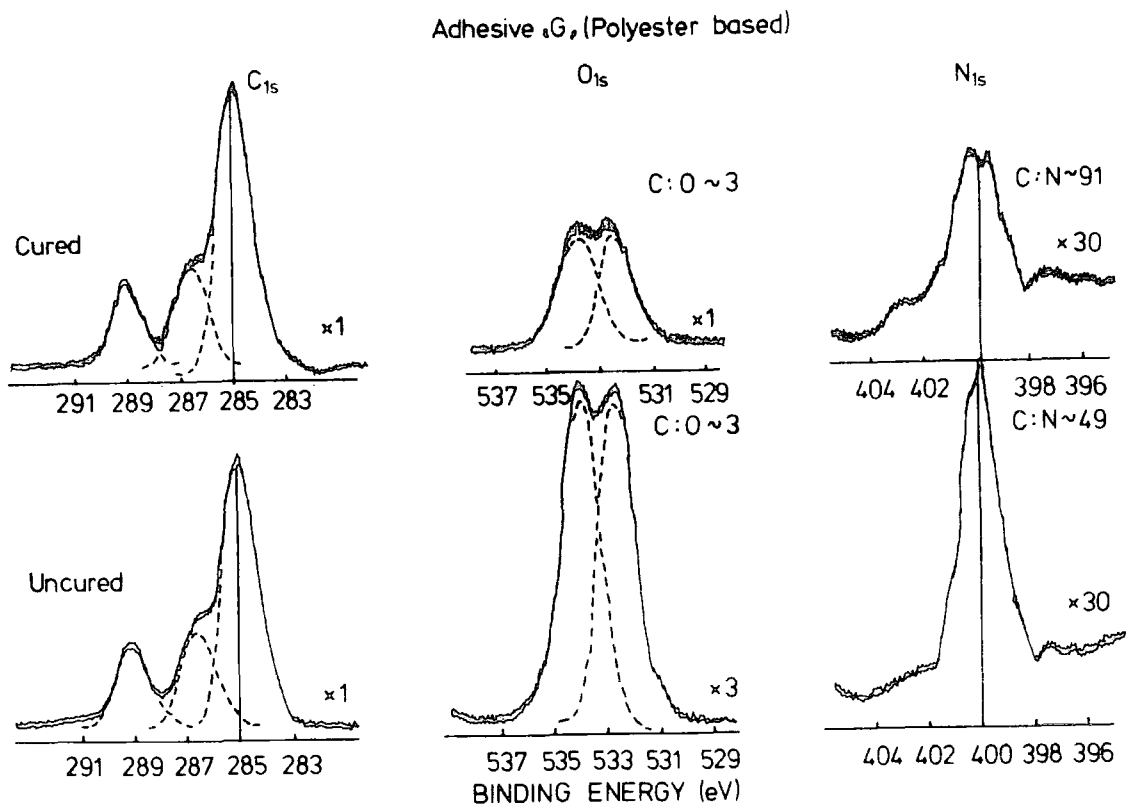


Figure 7.6.  $C_{1s}$ ,  $O_{1s}$  and  $N_{1s}$  of polyurethane adhesive G, "polyester based", for cured and uncured samples at a  $30^\circ$  take-off angle.

are basically four components viz.  $\underline{\text{C}}\text{-H}$ ,  $\underline{\text{C}}\text{-O}$ ,  $\text{-}\overset{\text{O}}{\parallel}\text{C}\text{-O}$  and  $\pi\rightarrow\pi^*$  shake-up satellites (see Tables 7.6. and 7.8.), and the  $\text{O}_{1s}$  spectra is characteristic of two components separated by their natural line width,  $\underline{\text{O}}\text{-C}$  and  $\underline{\text{O}}\text{=C}$  in this case. Thus the  $\text{C}_{1s}$  and  $\text{O}_{1s}$  levels are distinctive of an aromatic based polyester system, (PET).

The ESCA data displayed in Table 7.7. for the uncured sample and 7.9. for the cured sample shows that the  $\text{C}_{1s}/\text{O}_{1s}$  area ratios are comparable with those for adhesive F, for which both the cured and uncured samples have been previously described. The  $\text{C}_{1s}/\text{O}_{1s}$  ratios of 1.8 and 2.0 at take-off angles  $30^\circ$  and  $70^\circ$  respectively, indicate a degree of vertical homogeneity for both samples cured and uncured. The  $\text{C}_{1s}/\text{N}_{1s}$  area ratios of  $\sim 41$  and  $\sim 77$  at  $30^\circ$  take-off angle for uncured and cured samples respectively show that the nitrogen functionalities on the surface are at low level. This indicates that the loading from the TDI based adhesive G is significantly low. It is also seen that the effect of curing is a reduction in nitrogen functionality by a factor of  $\sim 2$ , (see Figure 7.6.). The  $\text{C}_{1s}/\text{N}_{1s}$  area ratios show that there is a change in stoichiometry from  $\sim 50$  to  $\sim 100$  in going from the uncured to cured samples. The angular dependent data show a high degree of vertical homogeneity in the sample.

### 7.3.3. Laminate Films

This section considers the surface chemistry of the laminated samples of PE and PET. It is convenient to discuss the low and high-slip PE laminates of each adhesive separately. In appropriate cases the surface chemistry of the PET is also

Table 7.10. The  $C_{1s}/O_{1s}$  and  $C_{1s}/N_{1s}$  area ratios, the binding energies of the  $C_{1s}$ ,  $O_{1s}$  and  $N_{1s}$  levels and the coefficient of friction (COF), of the low-slip polyethylene laminate films with polyurethane adhesives A - G, at  $30^\circ$  and  $70^\circ$  take-off angles.

Name	Angle	Area Ratio		Coefficient of Friction			Binding Energy		
		$C_{1s}/O_{1s}$	$C_{1s}/N_{1s}$	Time sec.	Peak value	Average	$C_{1s}$	$O_{1s}$	$N_{1s}$
LDPE low slip "A"	70	138.8	277.5	10	0.29	0.27	286.3, 287.9	532.4	-
	30	235.7	-	50	0.24	0.25	286.4, 287.9	533.0	-
LDPE low slip "B"	70	60.5	-	10	0.27	0.22	286.0, 287.8	532.3, 533.7	-
	30	75.0	-	50	0.24	0.23	286.1, 287.7	532.3, 533.8	-
LDPE low slip "C"	50	140.2	-	10	0.23	0.22	286.2	531.2, 532.8	-
	30	193.8	238.5	50	0.24	0.23	286.1, 287.4	532.0, 532.9	399.9
LDPE low slip "D"	50	45.4	-	10	0.30	0.24	286.1, 287.6	531.3, 532.4	-
	30	91.2	-	50	0.29	0.24	286.1, 287.5	530.7, 532.4	-
LDPE low slip "E"	50	72	-	10	0.26	0.20	286.1 -	very low	-
	30	146	-	50	0.21	0.23	286.2 -	532.0	-
LDPE low slip "F"	50	59.1	-	10	0.25	0.20	286.0, 287.7	531.1, 532.1	-
	30	93.3	-	50	0.23	0.20	286.1, 287.5	530.6, 532.3	-
LDPE low slip "G"	50	48.6	-	10	0.25	0.20	286.2	532.2	-
	30	105.7	-	50	0.23	0.21	286.2, 287.7	531.2, 532.4	-

Table 7.11. The  $C_{1s}/O_{1s}$  and  $C_{1s}/N_{1s}$  area ratios, the binding energies of  $C_{1s}$ ,  $O_{1s}$  and  $N_{1s}$  levels and the coefficient of friction (COF), of the high-slip polyethylene laminate films with polyurethane adhesives A - G, at  $30^\circ$  and  $70^\circ$  take-off angles.

Name	Angle	Area Ratio		Coefficient of Friction			Binding Energy		
		$C_{1s}/O_{1s}$	$C_{1s}/N_{1s}$	Time sec.	Peak value	Average	$C_{1s}$	$O_{1s}$	$N_{1s}$
LDPE high slip "A"	50	70.2	-	10	0.30	0.21	286.3	530.8, 532.3	-
	30	136.0	-	50	0.32	0.22	286.2, 287.5	532.1	-
LDPE high slip "B"	50	171.2	-	10	0.31	0.245	286.3	531.7	-
	30	123.0	-	50	0.31	0.23	286.3	530.4, 531.7	-
LDPE high slip "C"	50	87.0	very low	10	0.25	0.20	286.9	532.5	very low
	30	537.5	488.6	50	0.23	0.20	286.4, 287.5	532.5	400.6
LDPE high slip "D"	50	15.7	17.7	10	0.24	0.16	286.1, 288.7	531.3	399.3
	30	15.9	21.1	50	0.20	0.18	286.6, 288.5	530.6, 531.8	398.8
LDPE high slip "E"	50	31.8	-	10	0.32	0.18	286.2	531.3	-
	30	103.8	-	50	0.33	0.18	286.1, 288.2	532.1	-
LDPE high slip "F"	50	11.9	22.2	10	0.22	0.16	286.2, 287.8	531.2, 532.4	398.9
	30	17.4	22.5	50	0.21	0.16	286.4, 288.3	531.4, 533.0	399.3
LDPE high slip "G"	50	16.2	18.7	10	0.296	0.18	286.2, 288.1	531.6, 532.6	398.6
	30	20.5	28.5	50	0.19	0.17	286.2, 288.3	531.4, 532.8	399.6



discussed. The ESCA data are displayed in Tables 7.10. and 7.11.

(i) Adhesive A

ESCA measurements were carried out for both low and high-slip PE laminates of adhesive A. The ESCA data, displayed in Tables 7.10. and 7.11., indicate that the  $C_{1s}$  line profile shows a very intense component due to  $\underline{CH}$ , and a small intensity component due to  $\underline{C-O}$  structural features.

The dominant feature in each case is an essentially single component  $C_{1s}$  spectrum with very low intensity signals from  $O_{1s}$  and  $N_{1s}$  levels. It is instructive to compare the relevant area ratios, and these are set out in Table 7.12.

Table 7.12.

	$\frac{C_{1s}/O_{1s}}$		$\frac{C_{1s}/N_{1s}}$	
	$30^\circ$	$70^\circ$	$30^\circ$	$70^\circ$
Low-slip PE "base polymer"	14	13	95	177
Low-slip laminate of adhesive A	236	139	-	278
High-slip PE "base polymer"	24	18	39	32
High-slip laminate of adhesive A	136	70	-	-
Cured adhesive A	2.7	2.6	17	21
Uncured adhesive A	2.4	3.1	15	23

This indicates that the nitrogen functionality is barely detectable for the laminates, and the oxygen functionality is also of low intensity for both the high and low-slip laminate samples. Therefore, the laminate surfaces indicate a clean polyethylene surface with no evidence of migration products originating from the adhesive.

The reverse side (PET surfaces) of the high and low-slip

Table 7.13. The  $C_{1s}/O_{1s}$  and  $C_{1s}/N_{1s}$  area ratios and the binding energies of  $C_{1s}$ ,  $O_{1s}$  and  $N_{1s}$  levels of polyester (PET) laminated films with low and high-slip polyethylene laminates at  $30^\circ$  and  $70^\circ$  take-off angles.

Polyester (PET) film	Angle	Area Ratios		Binding Energies		
		$C_{1s}/O_{1s}$	$C_{1s}/N_{1s}$	$C_{1s}$	$O_{1s}$	$N_{1s}$
with low-slip "A"	70	4.2	59.1	286.6, 287.9 293.3	532.8, 534.3	399.3
	30	2.9	78.7	286.5, 287.8 289.1, 291.5	532.5, 534.1	400.1
with low-slip "B"	70	3.7	78.4	286.6, 289.3	532.8, 534.3 535.5	400.3
	30	2.6	96.6	286.6, 287.2 289.2, 291.6	532.4, 534.0 535.5	400.2
with low-slip "E"	70	2.5	-	286.7, 289.1	532.7, 534.2	-
	30	2.2	-	286.6, 289.3	532.8, 534.5	-
with low-slip "F"	70	5.3	305.5	287.0, 288.4 289.4	532.7, 534.4	400.1
	30	5.3	189.4	286.4, 287.7 288.8	532.8, 534.5	400.2
with low-slip "G"	70	3.6	-	286.7, 289.3	532.8, 534.3 535.1	-
	30	2.4	-	286.7, 289.0 291.8	532.6, 534.2 535.5	-
with high-slip "A"	50	4.1	104.6	286.3, 287.7 289.3	532.3, 533.7	400.0
	30	2.7	64.8	286.3, 287.6 284.2	532.0, 533.7	399.7
with high slip "F"	50	2.9	40.2	286.4, 287.9 290.0	532.1, 533.6 534.8	399.7
	30	2.4	61.9	286.5, 287.9 289.1, 291.2	531.8, 533.5 534.4	399.7

lamine samples have been studied by ESCA. The  $C_{1s}$  and  $O_{1s}$  levels are characteristic of polyethyleneterephthalate (see section 7.3.1.); thus the  $O_{1s}$  levels show the distinctive 1:1 doublet structure, (corresponding to  $\underline{O}-C$  and  $C=\underline{O}$ ), whilst the  $C_{1s}$  levels show four components corresponding to  $\underline{C}-H$ ,  $\underline{C}-O$ ,  $\begin{array}{c} \underline{C} \\ \diagup \quad \diagdown \\ O \quad O \end{array}$  and  $\pi \rightarrow \pi^*$  shake-up satellites.

The ESCA data of PET in the laminates are displayed in Table 7.13., indicating that the  $C_{1s}/O_{1s}$  area ratios are somewhat similar to the base polymer (PET) (see Table 7.5.), whereas the angular dependence indicates a degree of vertical inhomogeneity. The  $C_{1s}/N_{1s}$  area ratios of  $\sim 79$  and  $\sim 65$ , at  $30^\circ$  take-off angle, give stoichiometries of  $\sim 94$  and  $\sim 77$  for low and high-slip PE respectively. This indicates increased nitrogen functionality in the surface regions of PET compared with the clean surface of the original sample. Therefore, the data suggest selective diffusion of nitrogen functionalised material, originating from the adhesive, into the PET phase.

(ii) Adhesive B

The ESCA analysis for low and high-slip PE laminated with adhesive B, is displayed in Table 7.10. for low-slip, and Table 7.11. for high-slip.

The dominant feature in both cases is an essentially single component  $C_{1s}$ , with very low levels of oxygen and nitrogen functionalities, indicative of surfaces which are cleaner than the initially studied base polymer films of PE. Table 7.14. sets out a comparison of the relevant area ratios.

Table 7.14.

	$\frac{C_{1s}}{O_{1s}}$		$\frac{C_{1s}}{N_{1s}}$	
	$30^\circ$	$70^\circ$	$30^\circ$	$70^\circ$
Low-slip PE "base polymer"	14	13	95	177
Low-slip PE laminate of adhesive B	75	61	-	-
High-slip PE "base polymer"	24	18	39	32
High-slip PE laminate of adhesive B	123	171	-	-
Cured adhesive B	2.6	2.5	20	25
Uncured adhesive B	2.6	2.4	21	23

The data show no evidence for migration of nitrogen functionalities from the adhesive; indeed the surfaces of the laminate samples for both low and high-slip PE are cleaner than those for the base polymer.

The low-slip PE laminate was re-examined after a further period of storage of about 7 months. The ESCA data are compared with the sample which has been discussed before, (Table 7.15.).

Table 7.15.

<u>Date studied</u>	$\frac{C_{1s}}{O_{1s}}$		$\frac{C_{1s}}{N_{1s}}$	
	$30^\circ$	$70^\circ$	$30^\circ$	$70^\circ$
29.6.80	75	61	-	-
4.2.81	101	74	-	-

The  $\frac{C_{1s}}{O_{1s}}$  area ratio indicates a small decrease, since the sample was originally studied, which shows that after a period of storage the low degree of oxygen functionality has generally decreased even further, and there is no evidence for

any nitrogen functionality at the surface.

Adhesive B was selected for study of the PET surface, which was laminated with low-slip PE. The ESCA data are displayed in Table 7.13. The  $C_{1s}/O_{1s}$  area ratios of 2.6 and 3.7 at  $30^\circ$  and  $70^\circ$  take-off angles respectively, indicate a degree of vertical inhomogeneity. The  $C_{1s}/N_{1s}$  area ratio of 97 at  $30^\circ$  take-off angle, gives a stoichiometry of  $\sim 115$ . This shows that low level of nitrogen functionalisation, which are comparable in fact to that for the corresponding low-slip PE base polymer, (see Table 7.3.). This suggests selective diffusion of nitrogen functionalised material into the PET phase.

(iii) Adhesive C

ESCA examinations were made for both low and high-slip laminate with adhesive C. The ESCA analysis is shown in Table 7.10. for low-slip and Table 7.12. for high-slip. The data indicate that the laminate PE has a clean, uncontaminated surface, with very low levels of oxygen and nitrogen functionalities. This is best appreciated by comparison of relevant area ratios, which are shown in Table 7.16.

Table 7.16.

	$C_{1s}/O_{1s}$		$C_{1s}/N_{1s}$	
	$30^\circ$	$70^\circ$	$30^\circ$	$70^\circ$
Low-slip PE "base polymer"	14	13	95	177
Low-slip laminate of adhesive C	194	140	239	-
High-slip PE "base polymer"	24	18	39	32
High-slip PE laminate of adhesive C	540	87	490	-
Cured adhesive C	2.0	1.9	15	16
Uncured adhesive C	2.5	2.5	22	31

The data for the  $C_{1s}/O_{1s}$  and  $C_{1s}/N_{1s}$  area ratios of both low and high-slip PE laminate with adhesive C show very low levels of oxygen and nitrogen functionalities, indicative of clean PE surfaces with no evidence for migration of products originating from the adhesive.

(iv) Adhesive D

ESCA analysis for low-slip PE laminate surface, displayed in Table 7.10., shows the  $C_{1s}/O_{1s}$  area ratios of 45 and 91 at  $30^\circ$  and  $70^\circ$  take-off angles, indicating high degree of vertical inhomogeneity, and that the stoichiometry changes from  $\sim 147$  to  $\sim 73$  on going from the surface to the subsurface. This suggested that the oxygen functionalities are mainly on the surface. The  $N_{1s}$  levels are of very low level, but the  $C_{1s}$  levels show high binding energy components at  $\sim 287.6$  eV originating from  $-\overset{\text{O}}{\underset{\text{X}}{\text{C}}}$  functionalities.<sup>65,70</sup>

The corresponding data for the high-slip sample displayed in Table 7.11., indicate that the concentration of oxygen and nitrogen functionalities is much higher than in the low-slip sample, and is comparable with that for the original base polymer of high-slip PE, (see Table 7.4.). The  $N_{1s}$  level at binding energy at  $\sim 399.5$  eV suggests the presence of an amide group<sup>70</sup> and this corresponds to the high binding energy component of the  $C_{1s}$  levels at  $\sim 288.0$  eV, originating from the  $-\overset{\text{O}}{\underset{\text{X}}{\text{C}}}$  functionality.<sup>65,70</sup>

The area ratios of  $C_{1s}/O_{1s}$  and  $C_{1s}/N_{1s}$  for the base polymer PE, for the laminate samples and for the adhesive itself are shown in Table 7.17.

Table 7.17.

	$\frac{C_{1s}/O_{1s}}{}$		$\frac{C_{1s}/N_{1s}}{}$	
	$30^\circ$	$70^\circ$	$30^\circ$	$70^\circ$
Low-slip PE "base polymer"	14	13	95	177
Low-slip PE laminate of adhesive D	91	45	-	-
High-slip PE "base polymer"	24	18	39	32
High-slip PE laminate of adhesive D	16	16	21	18
Cured adhesive D	3.4	4.0	17	22
Uncured adhesive D	2.5	3.0	11	13

The  $C_{1s}/O_{1s}$  and  $C_{1s}/N_{1s}$  area ratios of the low-slip laminate, indicate a degree of vertical inhomogeneity. For the high-slip laminate the data shows clear evidence for migration from the adhesive to the surface region. For this reason the high-slip was re-examined after a further period of storage. The data are shown in Table 7.18. as a function of examined time.

Table 7.18.

<u>Date of study</u>	$\frac{C_{1s}/O_{1s}}{}$		$\frac{C_{1s}/N_{1s}}{}$	
	$30^\circ$	$70^\circ$	$30^\circ$	$70^\circ$
30.6.80	16	16	21	18
21.7.80	16	17	21	22

The data shows very small changes after the longer period of storage, and that from the different angles indicates uniform functionalisation at the surface.

(v) Adhesive E

The ESCA analysis for both the low and high-slip laminated

with adhesive E, are displayed in Tables 7.10. and 7.11. The dominant feature in each case is an essentially single component  $C_{1s}$ , with very low intensity signals in the  $O_{1s}$  and  $N_{1s}$  spectra.

Table 7.19. shows a comparison, between the PE, base polymer of PE and the adhesive of cured and uncured, of the important  $C_{1s}/O_{1s}$  and  $C_{1s}/N_{1s}$  area ratios.

Table 7.19.

	$\frac{C_{1s}}{O_{1s}}$		$\frac{C_{1s}}{N_{1s}}$	
	$30^\circ$	$70^\circ$	$30^\circ$	$70^\circ$
Low-slip PE "base polymer"	14	13	95	177
Low-slip laminate of adhesive E	146	72	-	-
High-slip PE "base polymer"	24	18	39	32
High slip PE laminate of adhesive E	104	32	-	-
Cured adhesive E	2.4	2.3	15	15
Uncured adhesive E	2.7	2.3	17	16

For both low and high-slip laminate samples, the nitrogen and oxygen functionalities are barely detectable. The  $C_{1s}/O_{1s}$  area ratios at different take-off angles indicate a degree of vertical inhomogeneity. The data also show that the laminate samples have a clean PE surfaces, with no evidence of migration from the adhesive.

The low-slip PE laminate was studied after a further period of storage. ESCA analysis is shown in Table 7.20.

The  $O_{1s}$  levels reveal a very low level of oxygen functionalisation, which generally decreased even further after a period of storage. The  $C_{1s}/O_{1s}$  area ratios of 175



Table 7.20.

<u>Date Studied</u>	$\frac{C_{1s}}{O_{1s}}$		$\frac{C_{1s}}{N_{1s}}$	
	$30^\circ$	$70^\circ$	$30^\circ$	$70^\circ$
2.7.80	146	72	-	-
5.2.81	175	178	-	-

and 178 at  $30^\circ$  and  $70^\circ$  take-off angles give surface stoichiometries which are uniform than for this sample when studied previously, ( $C_{1s}/O_{1s}$  of 146 and 72 at  $30^\circ$  and  $70^\circ$  respectively). The  $N_{1s}$  levels are undetectable; therefore, there is no evidence for any nitrogen functionality at the surface.

Additional studies have been made of the polyester surfaces (PET), of the low-slip laminate with adhesive E. The ESCA data are displayed in Table 7.13. The  $C_{1s}$  and  $O_{1s}$  core levels are distinctive and characteristic of polyethylene-terephthalate, (see section 7.3.1.). The  $C_{1s}/O_{1s}$  area ratios of 2.2 and 2.5 at  $30^\circ$  and  $70^\circ$  take-off angle respectively indicate a degree of vertical homogeneity. No evidence for nitrogen functionality apparent in the surface region indicating a clean PET surface.

(vi) Adhesive F

The low and high-slip PE laminates of adhesive F, have been examined by ESCA at two take-off angles,  $30^\circ$  and  $50^\circ$ , and the analysis data is displayed in Tables 7.10. and 7.11.

The data of low-slip laminate shows a very low level of oxygen on the surface, and the nitrogen functionality is barely detectable. The high-slip laminate, however, is

strikingly different; the amount of nitrogen and oxygen functionality at the surface is comparable to that for the high-slip PE, base polymer film. Table 7.21. shows a comparison of  $C_{1s}/O_{1s}$  and  $C_{1s}/N_{1s}$ .

Table 7.21.

	$\frac{C_{1s}}{O_{1s}}$		$\frac{C_{1s}}{N_{1s}}$	
	$30^\circ$	$70^\circ$	$30^\circ$	$70^\circ$
Low-slip PE "base polymer"	14	13	95	177
Low-slip PE laminate of adhesive F	93	54	-	-
High-slip PE "base polymer"	24	18	39	32
High-slip PE laminate of adhesive F	17	12	23	22
Cured adhesive F	1.9	2.3	112	144
Uncured adhesive F	1.7	2.1	120	135

The data indicate that, whilst the low-slip sample has a clean surface, the surface region of the high-slip sample contains nitrogen functionality, which has migrated from the adhesive.

The low-slip laminate was examined again after a further period of time. The ESCA analysis is shown in Table 7.22.

Table 7.22.

<u>Date studied</u>	$\frac{C_{1s}}{O_{1s}}$		$\frac{C_{1s}}{N_{1s}}$	
	$30^\circ$	$50^\circ$	$30^\circ$	$50^\circ$
2.7.80	93	54	-	-
5.2.81	110	91	-	-

The  $C_{1s}$  and  $O_{1s}$  levels reveal a clean PE surface, with low oxidative functionalisation, lower than the same sample

previously studied. The  $N_{1s}$  level is undetectable, so there is no evidence for nitrogen functionalities. The angularly dependent area ratios of  $C_{1s}/O_{1s}$  110 ( $30^\circ$ ) and 91 ( $70^\circ$ ) reveal that the stoichiometry is relatively uniform over the ESCA depth sampling scale ( $\sim 50\text{\AA}$ ).

ESCA was also used to examine the polyester surface of both the low and high-slip laminates. The data are displayed in Table 7.13. The  $C_{1s}$  and  $O_{1s}$  levels are distinctive and characteristic of a polyester, as previously described in section 7.3.1.

The data show evidence of migration to the surface, of oxygen and nitrogen functionalities for the polyester laminated to both low and high-slip PE, but this is greater for the high-slip than for the low-slip. The  $C_{1s}/N_{1s}$  area ratios are  $\sim 189$  and  $\sim 62$ , (at  $30^\circ$  take-off angle) for low-slip and high-slip respectively, corresponding to stoichiometries of  $\sim 225$  and  $75$ . This indicates migration, from the adhesive to the surface region, which is higher in the high-slip than the low-slip.

The  $C_{1s}/O_{1s}$  area ratios for the different take-off angles also indicate a high degree of vertical homogeneity.

(vii) Adhesive G

The low and high-slip PE laminated with adhesive G have been investigated by ESCA. The analysis data are displayed in Table 7.10. for low-slip and Table 7.11. for high-slip. The  $C_{1s}$ ,  $N_{1s}$  and  $O_{1s}$  levels for the low-slip laminate are strikingly different from those of the high-slip. A comparison of  $C_{1s}/O_{1s}$  and  $C_{1s}/N_{1s}$  area ratios for the low and

high-slip laminate and base polymer PE samples are displayed in Table 7.23.

Table 7.23.

	$\frac{C_{1s}/O_{1s}}$		$\frac{C_{1s}/N_{1s}}$	
	$30^\circ$	$70^\circ$	$30^\circ$	$70^\circ$
Low-slip PE "base polymer"	14	13	95	177
Low-slip PE laminate of adhesive G	106	49	-	-
High-slip PE "base polymer"	24	18	39	32
High-slip PE laminate of adhesive G	21	16	29	19
Cured adhesive G	1.8	2.0	77	83
Uncured adhesive G	1.9	2.1	41	44

The data indicate that, the low-slip laminate surface shows no evidence of nitrogen functionality, and it has a low degree of oxygen functionality. The angular dependence of  $C_{1s}/O_{1s}$  area ratios show considerable vertical inhomogeneity, nonetheless the surface is cleaner than for the low-slip PE base polymer.

The high-slip laminate shows  $C_{1s}/O_{1s}$  and  $C_{1s}/N_{1s}$  area ratios comparable with those for the high-slip PE base polymer. For this reason the high-slip laminate was re-investigated after a further period of storage; the ESCA data are shown in Table 7.24., as a function of time.

Table 7.24.

<u>Date studied</u>	$\frac{C_{1s}/O_{1s}}$		$\frac{C_{1s}/N_{1s}}$	
	$30^\circ$	$50^\circ$	$30^\circ$	$50^\circ$
1.7.80	21	16	29	19
21.7.80	33	22	52	64

On storage, there is clearly a substantial change, with a significant reduction in both the oxygen and nitrogen functionalities.

The low-slip laminate PE was also examined after a further period of storage. The ESCA analysis is shown in Table 7.25.

Table 7.25.

<u>Date studied</u>	<u>C<sub>1s</sub>/O<sub>1s</sub></u>		<u>C<sub>1s</sub>/N<sub>1s</sub></u>	
	<u>30°</u>	<u>50°</u>	<u>30°</u>	<u>50°</u>
2.7.80	93	54	-	-
5.2.81	110	91	-	-

This indicates that low-slip PE surface is "clean" with only a low level of surface functionalisation. Also the angular dependent data reveal that the stoichiometry is relatively uniform over the ESCA depth sampling scale.

The polyester surface of low-slip PE has also been examined by ESCA, and the data are displayed in Table 7.13. The C<sub>1s</sub> and O<sub>1s</sub> levels are characteristic of PET, (see section 7.3.1.). The C<sub>1s</sub>/O<sub>1s</sub> area ratios of 2.9 and 3.6 at 30° and 70° take-off angles respectively, are similar to those of the original PET base polymer. The ESCA data also show a clean surface with no evidence of nitrogen functionality.

#### 7.4. Conclusion

The ESCA analysis of base polymer films reveals that the high and low-slip PE films have been corona treated,

(the outside of high-slip and the inside of low-slip were treated), and that this treatment lowers the level of nitrogen functionality in PE surface. The corona surface which comes in contact with the adhesive appears to have comparable oxidative functionalisation for both the low and high-slip samples. The high-slip PE shows a high level of nitrogen functionality, indicating that there is extensive surface coverage by the slip agent, but there is little or no nitrogen functionality on either the low-slip PE or PET surface.

ESCA data for the freshly coated "uncured" and cured adhesives indicate that adhesives A - E show comparable levels of nitrogen functionality, whilst adhesives F and G show significantly lower levels. In general adhesive samples show small changes in surface chemistry on curing, however, adhesive G does show considerable change. The main indication of the changes in the surface chemistry of the adhesive samples is derived from the overall relative intensity of the  $C_{1s}/O_{1s}$  and  $C_{1s}/N_{1s}$ . The  $C_{1s}/N_{1s}$  area ratios for all the uncured adhesive samples are shown in Figure 7.7., and for the cured in Figure 7.8. These indicate, from the different take-off angles used, vertical inhomogeneity. The  $C_{1s}/O_{1s}$  area ratios for uncured and cured adhesive samples are shown in Figures 7.9. and 7.10. These indicate that whilst some adhesives are inhomogeneous, for the cured system there is a general trend towards homogeneity. Whilst the  $C_{1s}$  and  $O_{1s}$  levels of adhesives A, B, C and E are characteristic of polyurethane

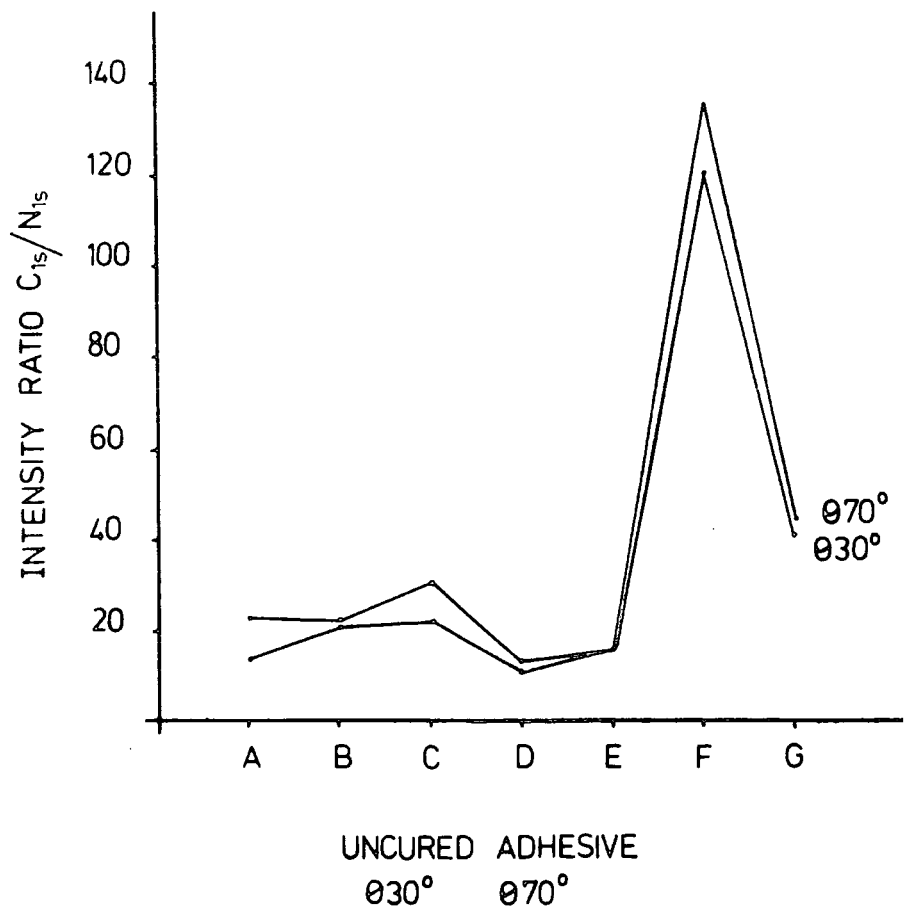


Figure 7.7. Comparison of  $C_{1s}/N_{1s}$  area ratios for the uncured polyurethane adhesives A - G at two different take-off angles ( $30^\circ$  and  $70^\circ$ ).

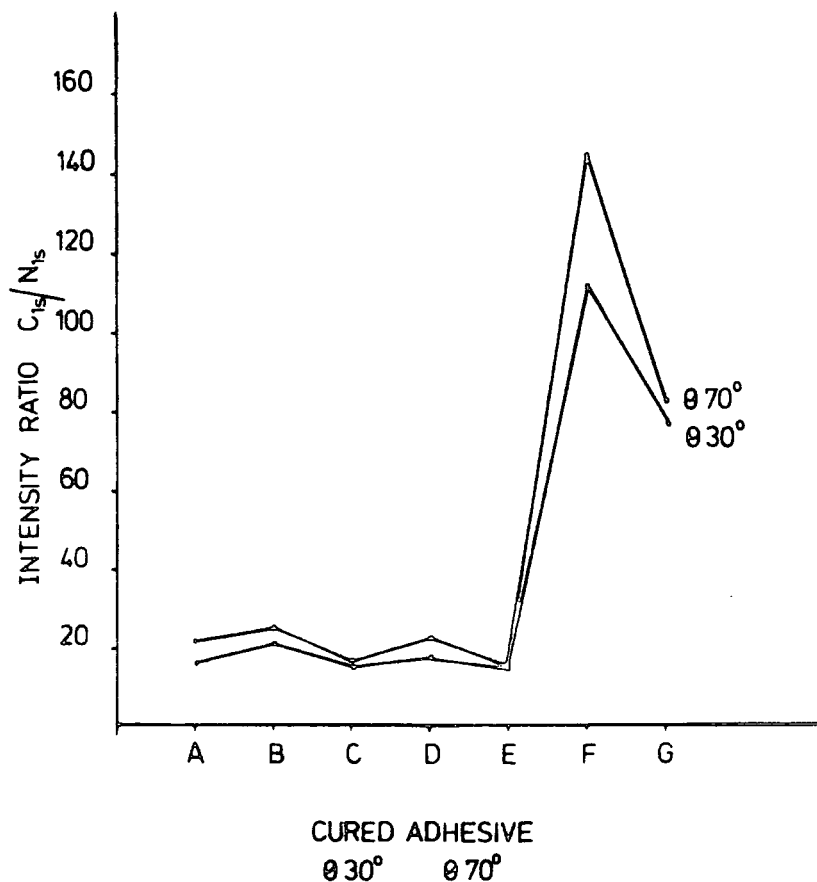


Figure 7.8. Comparison of  $C_{1s}/N_{1s}$  area ratios for the cured polyurethane adhesives A - G at  $30^\circ$  and  $70^\circ$  take-off angles.

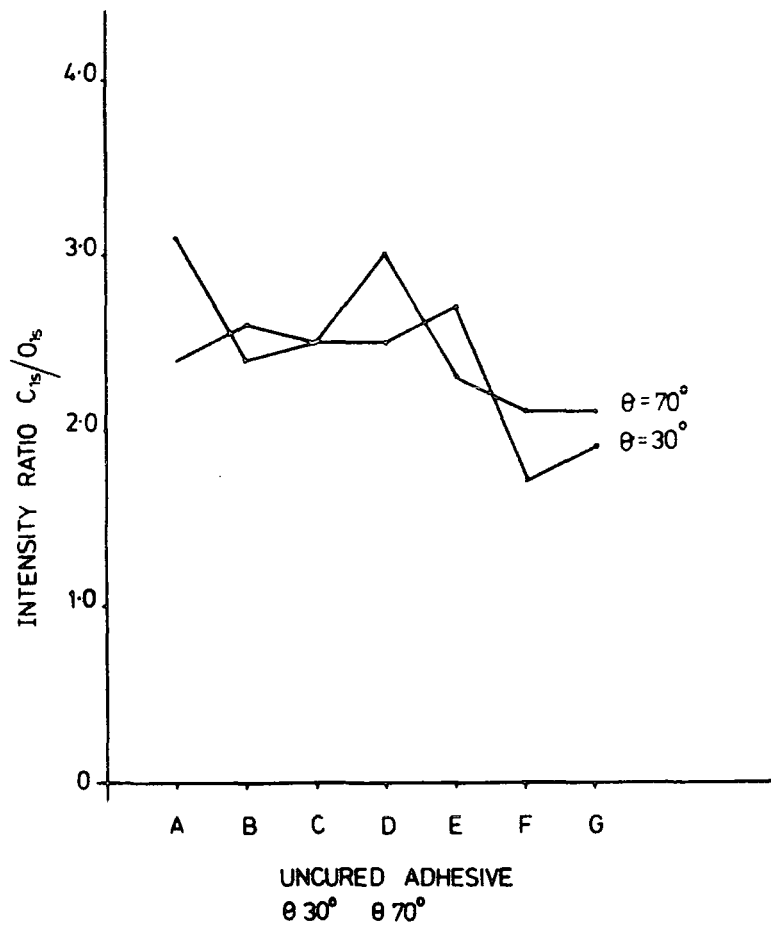


Figure 7.9. Comparison of  $C_{1s}/O_{1s}$  area ratios for the uncured polyurethane adhesives A - G at  $30^\circ$  and  $70^\circ$  take-off angles.

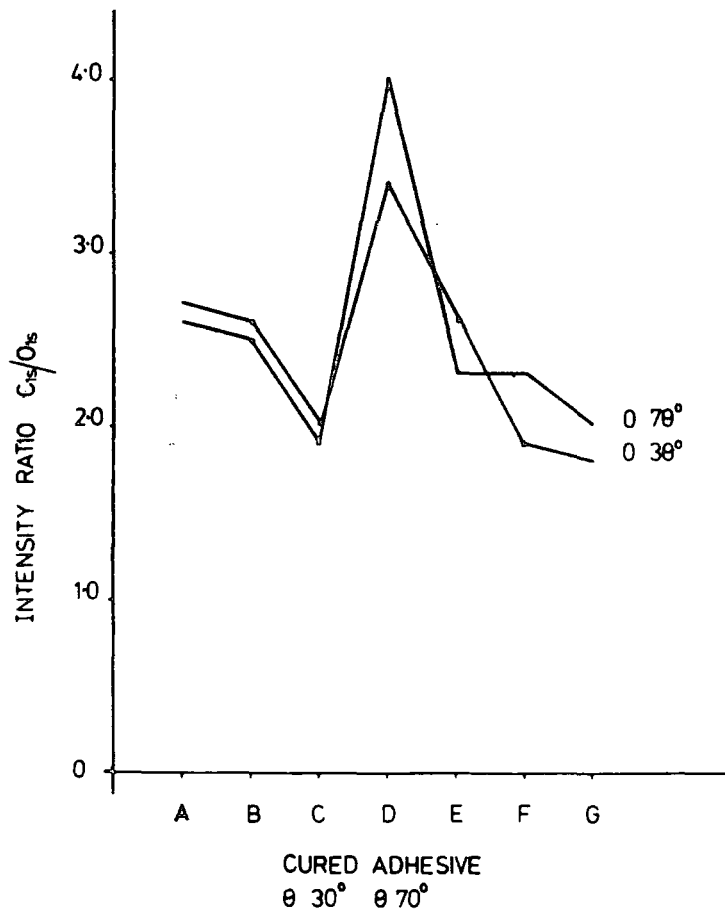


Figure 7.10. Comparison of  $C_{1s}/O_{1s}$  area ratios of the cured polyurethane adhesives A - G at  $30^\circ$  and  $70^\circ$  take-off angles.



adhesives based on a polyether, those of adhesive D, F and G are characteristic of a polyester, (e.g. Figures 7.5. and 7.6.).

The laminated samples have been examined by ESCA for low and high-slip PE and PET surfaces. The low-slip laminate surface shows no evidence for nitrogen functionality, and only low levels of oxygen functionality. This indicates "clean" PE surfaces, much cleaner in fact than the base polymer PE; therefore there is no evidence for migration of species originating from the adhesives. This is evident from the  $C_{1s}/O_{1s}$  area ratios, at two take-off angles,  $30^\circ$  and  $70^\circ$ , for all the low-slip laminate samples, which are displayed in Figure 7.11. The high-slip laminate surfaces also show

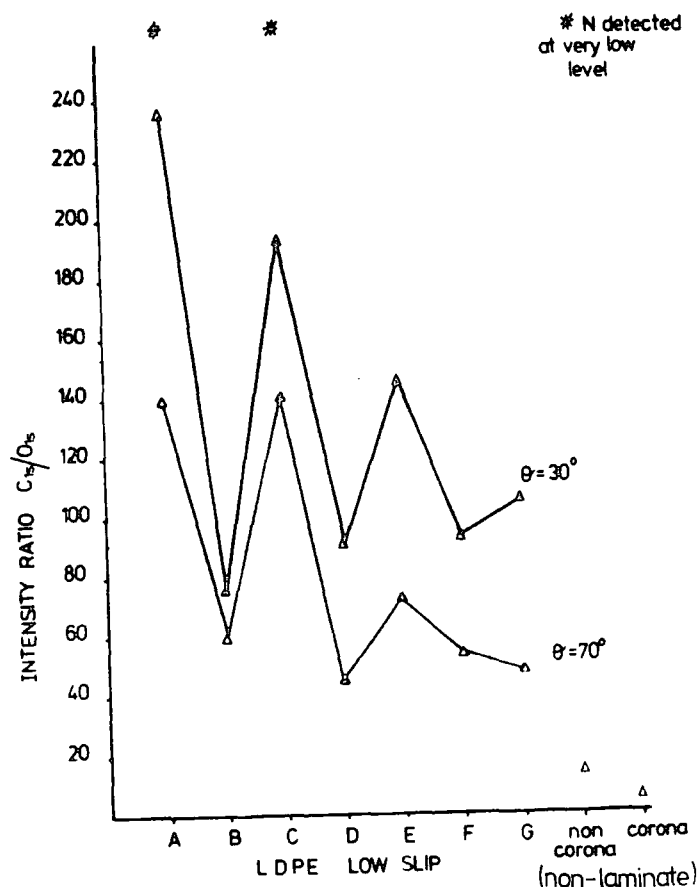


Figure 7.11. Comparison of  $C_{1s}/O_{1s}$  area ratios of the low-slip polyethylene laminate films with polyurethane adhesives A - G and the base-polymer polyethylene at  $30^\circ$  and  $70^\circ$  take-off angles.

very clean surfaces with a low degree of oxygen and nitrogen functionalities for samples A, B, C and E, whereas, samples D, F and G show levels of nitrogen and oxygen functionalities comparable to the high-slip base polymer. Figure 7.12.

presents the  $C_{1s}/O_{1s}$  area ratios of the high-slip laminate samples and the base polymer PE.

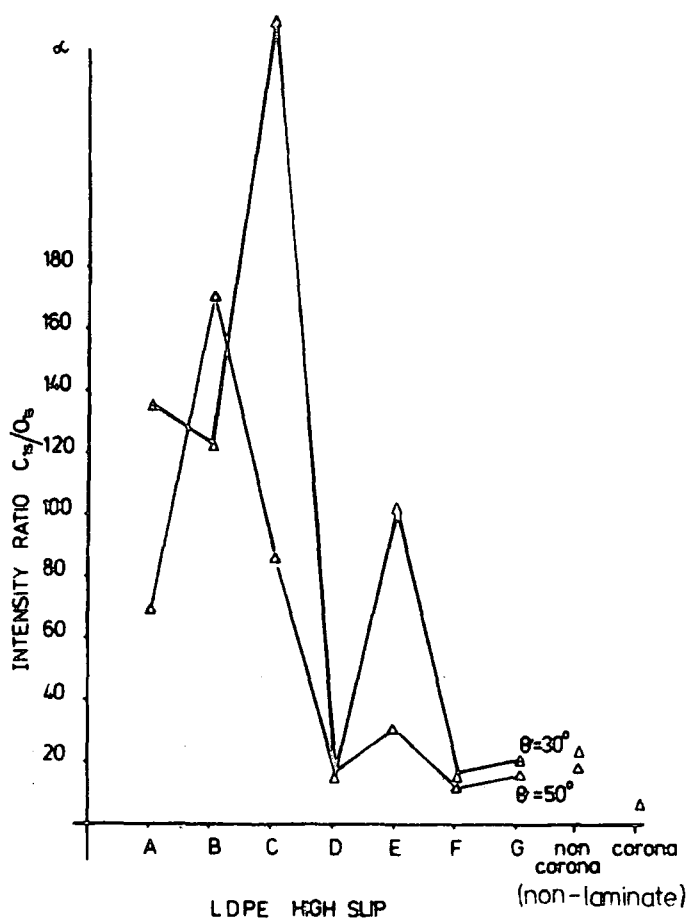


Figure 7.12. Comparison of  $C_{1s}/O_{1s}$  area ratios for the high-slip polyethylene laminate films with polyurethane adhesives A - G and the base-polymer polyethylene at 30° and 50° take-off angles.

The PET surfaces have been studied for low-slip PE laminates with samples A, B, E, F and G.

The PET surface of samples A and B show increased nitrogen

functionalities, compared with the clean surface of the original film, samples E and G showed no sign of the nitrogen functionalities, which indicate a very clean PET surface. Sample F is substantially different, exhibiting a very low level of nitrogen functionality, and as the  $C_{1s}$  and  $O_{1s}$  levels show, a surface which is extensively contaminated compared with the other samples. These changes of PET surfaces are evident in Figure 7.13., which presents the  $C_{1s}/O_{1s}$  and  $C_{1s}/N_{1s}$  and

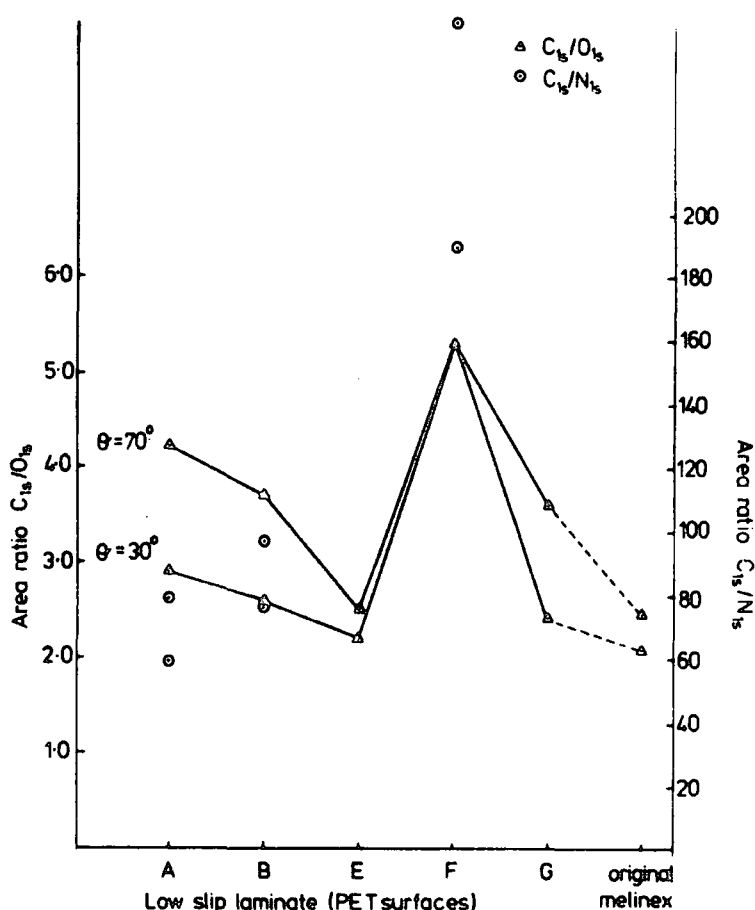


Figure 7.13. Comparison of  $C_{1s}/O_{1s}$  and  $C_{1s}/N_{1s}$  area ratios of the polyester (PET) laminate surfaces for the low-slip polyethylene laminate with adhesives A, B, E, F and G, at  $30^\circ$  and  $70^\circ$  take-off angles.

$C_{1s}/N_{1s}$  area ratios. The PET surface was also studied for the high-slip laminates with samples A and F. The PET surfaces also show significant nitrogen functionality, compared with the original film. This could be due to the migration of products originating from the adhesive.

Time dependent studies on the low-slip laminates B, E, F and G show that after a storage interval of about seven months, the low degree of oxygen functionality has generally decreased even further, and there is no evidence of any nitrogen functionality at the surface (e.g. see Figure 7.14.). Similar

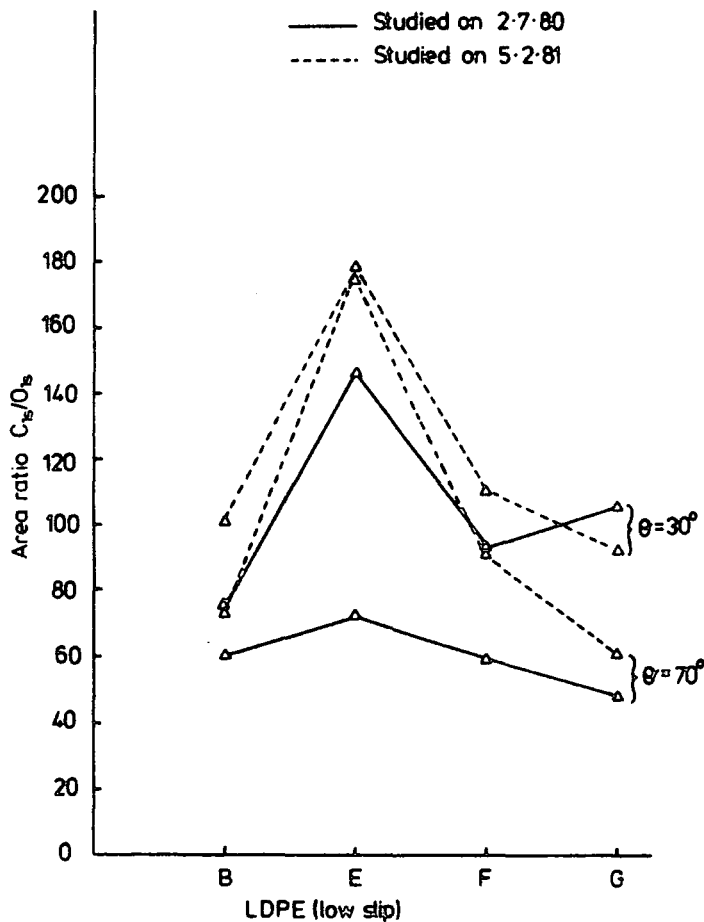


Figure 7.14. Comparison of  $C_{1s}/O_{1s}$  area ratios of the low-slip polyethylene laminate films with adhesives B, E, F and G, as a function of storage time, at  $30^\circ$  and  $70^\circ$  take-off angles.

studies for the high-slip laminates reveal that, whereas sample D shows very little change after an additional three weeks storage, sample G shows substantial differences (see Figure 7.15.).

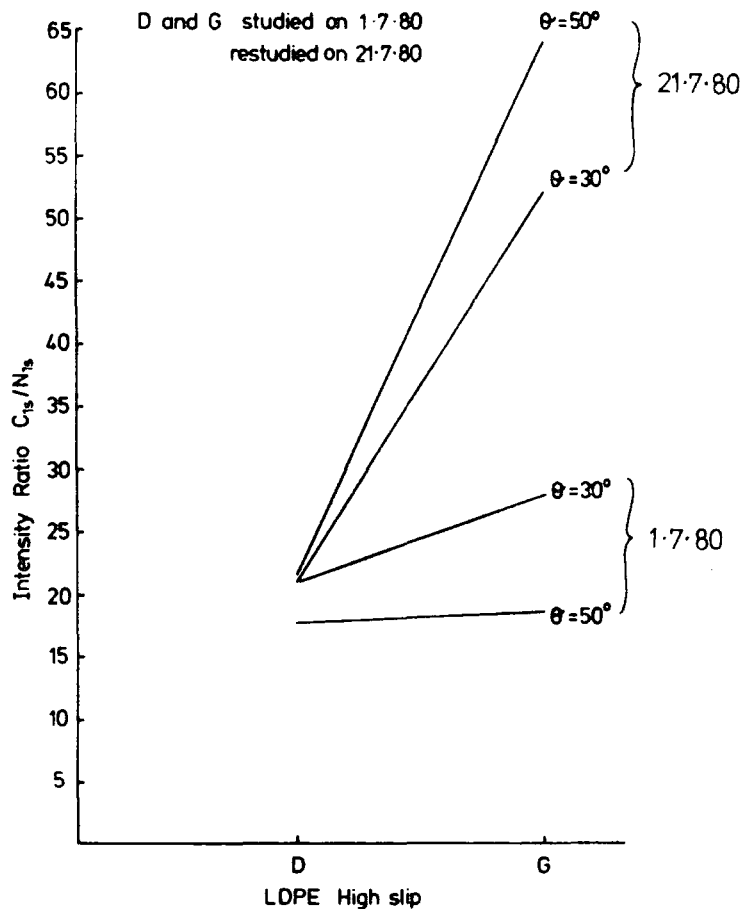


Figure 7.15. Comparison of  $C_{1s}/N_{1s}$  area ratios of the high-slip polyethylene laminate films with adhesives D and G, as a function of storage time, at  $30^\circ$  and  $50^\circ$  take-off angles.

The dynamic coefficient of friction (COF) has been measured for the base polymer PE low and high-slip; the data are displayed in Table 7.3. for low-slip; and in Table 7.4. for high-slip. The data indicate that the COF is similar for both sides, the untreated and treated side, of the high-slip,

and for the treated side of the low-slip PE; whereas the untreated side of the low-slip exhibits significantly smaller coefficient.

From the data collected in Tables 7.10. and 7.11., it is evident that the average value of the COF is somewhat similar for the low and high-slip laminates but the peak value of COF is slightly lower for the samples which exhibit significant nitrogen functionalities, (i.e. high-slip laminates).

CHAPTER EIGHT

CHAPTER EIGHTAN ESCA INVESTIGATION OF THE SURFACE CHEMISTRY OF HEAT  
TREATED POLYETHYLENE TEREPHTHALATE AND POLYETHYLENEAbstract

ESCA has been used to study the effect of heat treatment for a range of temperatures from room temperature - 120°C for LDPE, and from room temperature - 210°C for PET in the absence of oxygen inside the source chamber of the spectrometer, at a base pressure of  $\sim 10^{-8}$  torr. The ESCA data indicates a great loss of oxygen functionality, which reveals that in the outermost few tens of Angstroms, where chain mobility, (particularly in its influence on molecular rearrangements are concerned) and crystallinity will be different than in the bulk. Also ESCA data at room temperature of PET suggests a patched overlayer coverage which arises from extraneous hydrocarbon contamination, which is analysed in terms of a substrate-overlayer model.



### 8.1. Introduction

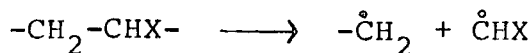
The fabrication and indeed the end use of polymers often involves temperatures well above ambient and as such, thermally induced processes are of considerable importance.<sup>237,239</sup> Many studies on the polymer reactions involved have been carried out in order to improve the nature of polymeric materials. Polymer degradation is one of the most fundamental reactions as is grafting and crosslinking. The motivation for studying these reactions is to understand the elementary reactions in thermal, photo and radiation degradation of polymers with reference to their chemical structures.<sup>250</sup>

When polymers are heated or irradiated by UV or ionising radiation under vacuum, several phenomena may occur. Examples being:-<sup>250</sup>

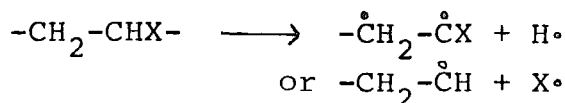
- (i) a decrease of molecular weight;
- (ii) the production of low-molecular weight compounds;
- (iii) crosslinking.

These changes are dependent mainly on the nature of the chemical structure of the polymers and reaction conditions. The elementary initiation reactions involving the pure polymer  $\{CH_2-CHX\}_n$  are main-chain, and side-chain scission.<sup>250</sup>

main-chain scission



side-chain scission



A vast literature exists on the thermal degradation of polymers in general, and in particular polyethylene terephthalate<sup>251-252</sup> (PET) and polyethylene (PE);<sup>253</sup> the emphasis being almost exclusively on thermally induced processes occurring in the bulk. There has been little attempt to monitor the changes in structure and bonding in the interface with the outside world namely the surface despite the obvious importance of surface phenomena to a wide range of properties such as adhesion, printability, dyeability etc. Clark and co-workers<sup>254-255</sup> have suggested that thermally promoted reactions at a surface might well be different than those occurring in the bulk. For processing at elevated temperatures, in air for example, the partial pressure of oxygen is orders of magnitude higher at the surface compared with the bulk. Recent studies<sup>179,256-257</sup> have emphasized the distinctive difference arising from this cause in photodegradation. The questions of thermal gradients, of differences, in chain mobilities, in surface vs. bulk crystallinities, and in orientation effects, all suggest that the surface might well behave differently than the bulk in thermal processing. The variety of techniques which have been employed in the surface characterisation of PET have been reviewed recently by Gillberg and Kemb,<sup>258</sup> whilst attempts have been made at defining differences in bulk and surface, (viewed on a macroscopic scale). Crystallinity in PET has been described by Sung et al<sup>259</sup> using FTAR-IR spectroscopy.

The diffusion of low molecular weight moieties during the thermal treatment could also lead to distinctive differences.

The thermal degradation of both polyethylene terephthalate and polyethylene has been extensively studied from the bulk point of view and the studies may be put into four distinct categories:

- (i) Monitoring changes in properties of the bulk;
- (ii) Examination of volatiles arising during heat treatment;
- (iii) Structural studies of the residue after heat treatment;
- (iv) Examination of model systems.

The general scheme in Figure 8.1., gives the conditions under which polymer decomposition can be studied and the possible analytical methods by which the degradation products can be identified.<sup>260</sup>

Valuable reviews on polymer degradation in general have been provided by Conley,<sup>261</sup> Hemminger<sup>262</sup> and Grassie.<sup>263</sup>

For PET, approach (i) is exemplified by the studies of Marshall and Todd<sup>264</sup> of the changes in melt viscosity for samples heated in an oxygen free atmosphere, and by Gupta and Kumar,<sup>265</sup> who investigated the effect of heat setting on the structure and mechanical properties of samples in fibre form; the samples being heat treated in silicon oil in the temperature range 100 - 220°C with treatment times ranging from 1 minute to 1 hour. They found that the changes were related to structure and morphology. These changes influence the dynamic mechanical properties without any detailed discussion of changes in structure and bonding at the molecular level. A similar situation is obtained for PE where

## GENERAL ANALYTICAL SCHEME

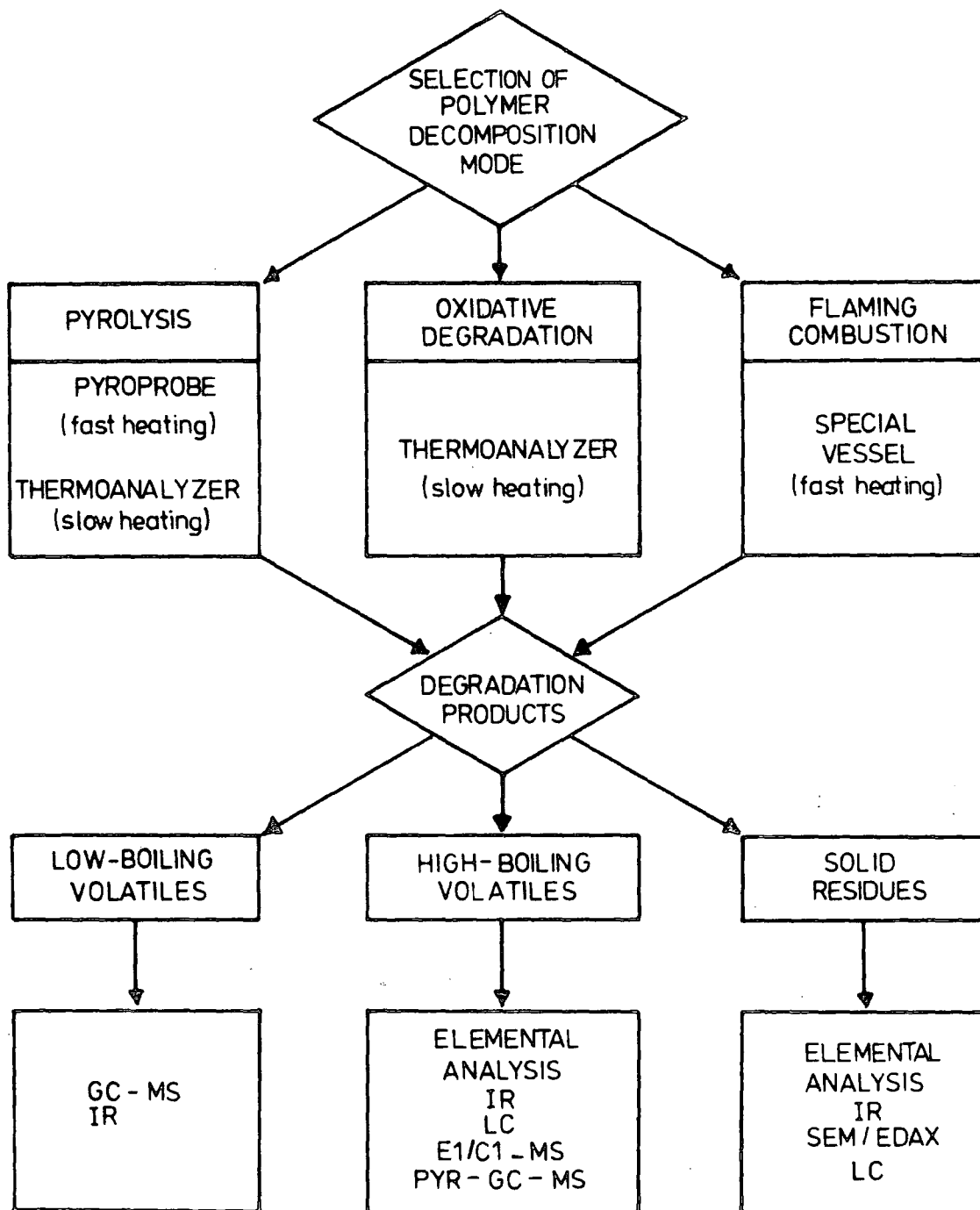


Figure 8.1. General analytical scheme of polymer degradation.

the influence of thermal history on chain conformation and morphology has been extensively studied. Viscosity measurements have been used to monitor the rapid decrease in molecular weight for PE heat treated in inert atmospheres, and the results have been interpreted in terms of random chain scission.<sup>266-267</sup>

In approach (ii), considerable insights into the mechanism of thermal degradation of PET and PE has come from studies of volatiles. Gooding<sup>252</sup> studied the pyrolysis of PET in nitrogen atmospheres and noted the formation of gaseous products, (acetaldehyde is the major product) and low molecular weight compounds such as terephthalic acid. Direct detection of volatiles arising during the thermal degradation of PET has been made under high vacuum conditions in a mass spectrometer source,<sup>268</sup> and from the data a random chain scission leading to low molecular weight oligomers was inferred. The combustion and pyrolysis of PET has been studied by Wiles et al,<sup>269</sup> with particular emphasis on the flash pyrolysis gas chromatographic mass spectrometry, (GC/MS) for the identification of low M.Wt. material, and the role of flame retardants in inhibiting the reactions involved.

The thermal degradation of polyethylene in a nitrogen atmosphere of low oxygen content has been studied by Holmstrom and Sörvik,<sup>266-267</sup> at temperatures between 284 and 355°C. Changes in molecular weight distribution (MWD), molecular weight averages and degree of long-chain branching (LCB) were followed by gel permeation chromatography (GPC)

and viscosity measurements. Other structural changes were investigated by infrared spectroscopy and differential scanning calorimetry (DSC). It was found that increasing the heating time and the temperature gave an increase in the formation of low molecular weight material, LCB and volatile products.

The organic volatile products formed during the thermo-oxidation of PE at 150°C and 160°C, at 760 torr oxygen pressure were investigated by gas chromatographic analysis.<sup>270</sup> Aldehydes and ketones are the major components. Similar products were also obtained by Hoff and Jacobsson,<sup>271</sup> who investigated the thermo-oxidative degradation of low-density PE, at 264 - 289°C using the GC/MS.

In approach (iii), the structure of the residues after heat treatment of PET and PE is studied. Complications result from the crosslinked, black residue formed from solid PET, which severely limits analytical techniques. IR analysis by the KBr disc method has been used.<sup>252,260,272</sup> IR investigations have led to identification of various products including aromatic anhydrides, (both linear and cyclic),<sup>260</sup> carboxylic acids,<sup>272</sup> vinyl benzoate and polyenes.<sup>260</sup> Recent studies by Wiles and co-workers<sup>273</sup> of the pyrolysis of PET fibres using the DRIFT technique, have shown that for PET, the partial pressure of oxygen in which the sample is heated is relatively unimportant. Similar results being obtained for samples heated in air and in nitrogen. They found that carboxylic acid end groups and linear anhydrides are the major involatile residues based on infrared absorbances.

By contrast the partial pressure of oxygen strongly influences the products formed from PE.

In approach IV, Ritchie<sup>251</sup> studied the mechanism of thermal degradation of PET, using a related number of esters as model compounds, at 340<sup>o</sup> - 375<sup>o</sup>C. It was found that the vinyl ester and carboxylic acid, which then further reacted to give acetaldehyde, acid anhydrides and methyl ketones, are the main products of the degradation. Gooding<sup>252</sup> has chosen glycol dibenzoate as a model for PET in order to study the rate of thermal decomposition. It has also been found that PET on pyrolysis gives similar products as the glycol dibenzoate, (carbon monoxide, acetaldehyde and carboxyl groups).

The thermo-oxidative degradation of PET was investigated by heating at 263 - 300<sup>o</sup>C under nitrogen flow.<sup>274</sup> A relation was found between the crosslinking and the formation of vinyl ester groups, by heating the vinyl methyl terephthalate as a model compound at 300<sup>o</sup>C for 2 hrs., and the PET decomposition.

From the previous investigations, it is clear that the thermal degradation of PET, even in the presence of oxygen, is viewed as a series of rearrangements and eliminations. The thermal degradation of PE involves a well known sequence of radical reactions leading to low molecular weight oxidatively functionalised species (e.g. HCOOH, CH<sub>3</sub>-COOH etc.).

In summary, the main reactions in the thermal degradation of PET and PE are shown in Figure 8.2. and 8.3.

It is clear that in the decomposition of PET in the absence of oxygen (pyrolysis), carboxyl and vinyl ester end-

THE THERMODEGRADATION OF PET IN THE ABSENCE OF OXYGEN

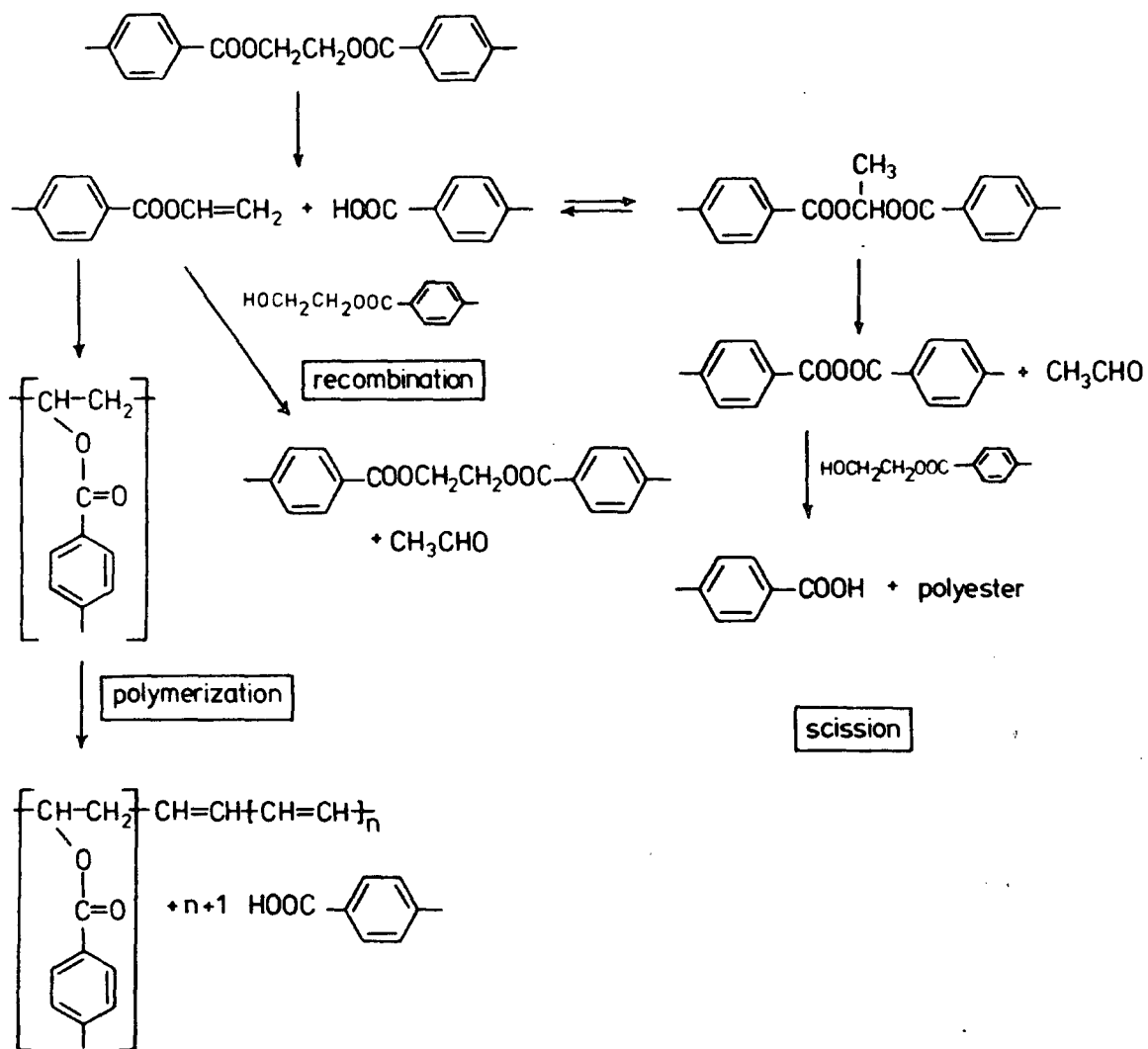


Figure 8.2. The general mechanism of the thermodegradation of PET in the absence of oxygen.



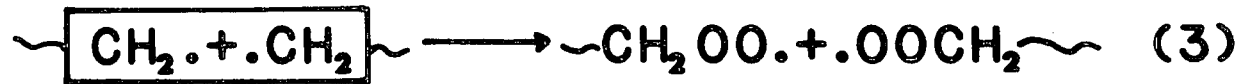
## Thermal degradation of PE



recombination



disproportionation



oxidation

Figure 8.3. General scheme of thermal degradation of PE.

groups are formed in the first step. Three different consecutive reactions occur: polymerisation of vinyl ester to form polyene, transesterification of vinyl ester with original glycol ester end-groups, resulting in recombination, and chain scission accompanied by liberation of free formaldehyde.<sup>260</sup> The primary decomposition of PE acts as an initiation reaction producing a primary free radical, which can undergo either of the following reactions:- (a) recombination, (b) disproportionation, (c) oxidation by reactions involving oxygen and stabilizer.<sup>275</sup>

In this chapter we consider the surface aspects of the heat treatment of PET and PE (low-density) in the absence of oxygen. Such studies form a useful complement to those in the literature on bulk aspects of thermal degradation.

## 8.2. Experimental

Polyethylene terephthalate (PET), and high- and low-slip low-density polyethylene (LDPE) were received as films in 1 metre roll form. The physical properties were typical of those for commercially produced films by I.C.I.

The polymer films were studied by ESCA on both sides, (inside and outside). The ESCA analysis of LDPE indicate that the inside surface of low-slip and the outside of the high-slip were corona treated.

The PET, the corona surface of low-slip PE and the untreated surface of high-slip PE films, were chosen for the heat treatment studies.

Samples were cut from the centre of each film to a convenient size for direct mounting on the tip of the ESCA

probe. The spectra were recorded at two different take-off angles,  $30^\circ$  and  $70^\circ$ . Each sample was heated inside the source chamber of the spectrometer under UHV conditions, (the base pressure being  $\sim 10^{-8}$  torr), using the heating facilities of the spectrometer probe. After holding the sample at a fixed temperature for a constant time  $\sim 15$  mins., the spectra were re-recorded. The heat treatment was investigated for a range of temperature from  $30 - 120^\circ\text{C}$  for LDPE, and from  $45 - 210^\circ\text{C}$  for PET. The temperatures were monitored using a thermocouple gauge, ( $-150 - 500^\circ\text{C}$ ). The spectra were recorded at each temperature setting.

Another set of samples were heated at  $210^\circ\text{C}$  (PET), and  $120^\circ\text{C}$  (LDPE), and then cooled to ambient temperature using the liquid nitrogen cooling facilities of the spectrometer probe. The spectra were then re-recorded.

Core level spectra were recorded on an AEI ES200A/B spectrometer using  $\text{Mg}_{k\alpha_{1,2}}$  x-ray radiation. The  $\text{C}_{1s}$  CH level at 285.0 eV binding energy was used for energy calibration. Integration of spectra was accomplished on a Dupont 310 curve resolver.

Two samples of PET film were heated inside the pyrolysis tube of a "Lindberg", (type 55035A, Lindberg, Watertown, Wisconsin, U.S.A.) pyrolysis furnace, under a vacuum of  $\sim 4 \times 10^{-2}$  torr. One sample was heated at  $150^\circ\text{C}$  for 24 hr. and the other was heated at  $240^\circ\text{C}$  for 36 hr. IR spectra were then measured for these samples.

### 8.3. Results and Discussion

#### 8.3.1. High-slip polyethylene (HSPE)

The HSPE formulation was known to be based on LDPE together with 0.18% micronised silica, 0.05% Butylated hydroxy toluene (BHT) and 0.11% of oleamide slip agent.

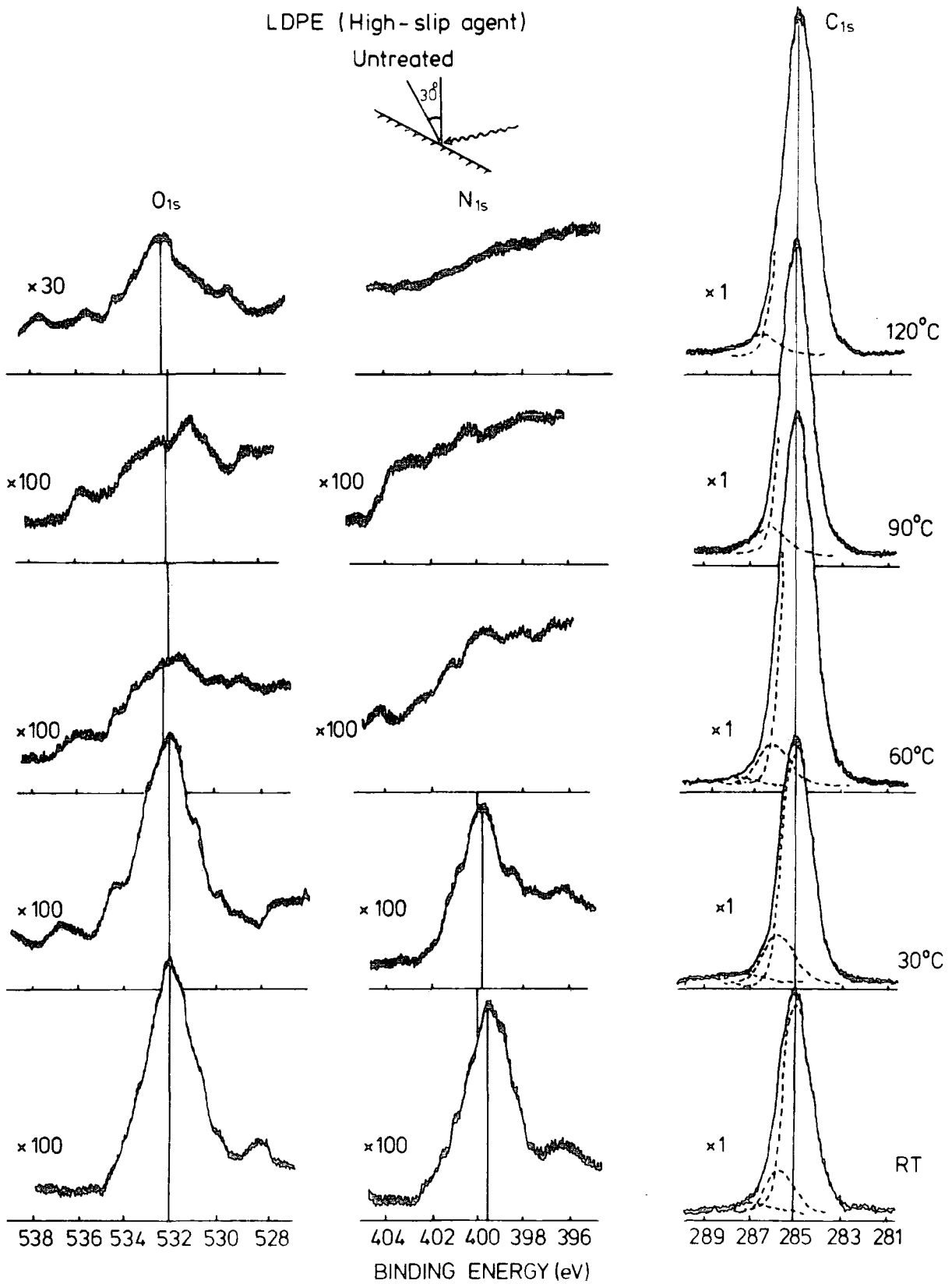
The film sample received in roll form was examined by ESCA on both sides, (the inside and outside surfaces), and the level of oxidative functionalisation immediately revealed that the outside surface had been corona treated, (see section 7.3.1.(i)).

Chapter seven commented on the fact that oxidatively functionalised surfaces of PE which are of high surface energy undergo reorientation at the surface to produce lower surface free energy surfaces by migration of e.g. carboxyl groups into the subsurface. The focus of attention in this chapter has therefore been on the untreated, (non-oxidatively functionalised) inside surface of the films. The ESCA data displayed in Table 8.1., and the spectra shown in Figure 8.4., reveal the presence of both oxygen and nitrogen containing functionalities.

At room temperature and 30° take-off angle, the spectra

Table 8.1.  $C_{1s}/O_{1s}$  and  $C_{1s}/N_{1s}$  area ratios of high-slip polyethylene at two take-off angles, 30° and 70°, as a function of heat treatments.

Area ratio	Angle	R. T.	30°C	60°C	90°C	120°C
$C_{1s}/O_{1s}$	30°	65	85	230	220	65
	70°	27	51	195	80	42
$C_{1s}/N_{1s}$	30°	68	155	-	-	-
	70°	49	132	-	-	-



**Figure 8.4.** The  $C_{1s}$ ,  $N_{1s}$  and  $O_{1s}$  levels of high-slip LDPE, (the inside surface) at  $30^\circ$  take-off angle, as a function of heat treatments.

show the nitrogen functionality is present, (at BE 399.8 eV) at substantially high level, and this associated with the high binding energies of the  $C_{1s}$  levels at 288.1 eV ( $-\overset{\text{O}}{\parallel}{\text{C}}-\text{NH}$ ). This corresponds to amide functional groups. Also the  $C_{1s}/N_{1s}$  and  $C_{1s}/O_{1s}$  area ratios of 68 and 65 at  $30^\circ$  take-off angles indicating stoichiometries of  $\sim 81$  and  $\sim 100$  respectively. As a crude first estimate, one may use bulk derived sensitivity factors to provide an estimated C:N:O stoichiometry of  $\sim 80:1:0.8$ , compared with a statistical ratio of 18:1:1 for the oleamide slip agent. This demonstrates the substantial segregation of the slip agent to the surface. The angular dependent data of  $C_{1s}/O_{1s}$  and  $C_{1s}/N_{1s}$  area ratios show an increase in relative concentrations of both oxygen and to a lesser extent nitrogen functionalities at the surface. The area ratios strongly suggest a patched overlayer of slip agent at the surface together with BHT, however, there is no evidence for silica in the surface regions. The  $C_{1s}/N_{1s}$  intensity ratios suggest that the oleamide slip agent is oriented at the surface with the hydrophobic hydrocarbon chain directed outwards.

It is of interest before considering the effect of heat treatment to briefly consider the time dependence of the data for a given film. Although repeat measurements on separate samples taken from the same batch of film at a given time were reproducible, samples of film studied after an interval of 9 months did show distinctive differences. This is readily apparent from the data shown in Table 8.2. The sample received shortly after manufacture reveals a higher

Table 8.2.  $C_{1s}/O_{1s}$  and  $C_{1s}/N_{1s}$  area ratios of high-slip PE at  $30^\circ$  and  $70^\circ$  take-off angles as a function of period of storage.

Date	Angle	$C_{1s}/O_{1s}$	$C_{1s}/N_{1s}$
11.6.80	$30^\circ$	24	26
	$70^\circ$	18	26
25.3.81	$30^\circ$	65	68
	$70^\circ$	27	49

level of both nitrogen and oxygen functionality. The  $C_{1s}/O_{1s}$  and  $C_{1s}/N_{1s}$  area ratios of 24 and 26 at  $30^\circ$  take-off angle respectively, indicating a surface dominated by oleamide slip agent; the angular dependence indicating a level of an additional oxygen containing species (BHT) at the surface. A storage period, (in air, in the dark) of  $\sim 9$  months leads to a substantial loss of slip agent as is readily apparent from the intensity ratios in Table 8.2., (the  $C_{1s}/N_{1s}$  area ratio changes from  $\sim 26$  to  $\sim 68$  at  $30^\circ$  take-off angle, as a function of period of storage).

The rate processes responsible for loss of oleamide from the surface over a long period of time are clearly accelerated at elevated temperatures. Thus at  $30^\circ\text{C}$ , there is a very great reduction in intensity of the  $O_{1s}$  and  $N_{1s}$  levels consistent with loss of slip agent to the vacuum system. The  $C_{1s}/O_{1s}$  and  $C_{1s}/N_{1s}$  area ratios of 85 and 155 at  $30^\circ$  take-off angle, give stoichiometries of  $\sim 135$  and  $\sim 185$  respectively, indicating that the oxygen and nitrogen functionalities decreased at the surface region. This is

very clear when the sample had been heated at temperature  $60^{\circ}\text{C}$ . The nitrogen functionality has disappeared, and the  $\text{C}_{1\text{s}}/\text{O}_{1\text{s}}$  of  $\sim 200$  indicates a very low level of surface contamination of the sample. Therefore at this range of temperature the sample is indicative of clean PE surfaces, with no evidence of slip agent at the surface.

At  $90^{\circ}\text{C}$  there is a slight increase in oxidative functionality at the surface. The  $\text{C}_{1\text{s}}/\text{O}_{1\text{s}}$  area ratios of 220 and 80 at  $30^{\circ}$  and  $70^{\circ}$  respectively indicate that the oxygen functionalities are more concentrated at the surface than the subsurface, and this could correspond to an increased rate of diffusion of anti-oxidant to the surface, a less likely alternative being that the oxidative functionalisation arises from thermal oxidation involving reaction with dissolved oxygen from the bulk. In this connection it is interesting to note that the level of oxidative functionalisation in the surface region increases at the higher temperature ( $120^{\circ}\text{C}$ ), at which temperature the film has softened. Diffusion of both oxygen and low molecular weight species such as BHT would be enhanced under these conditions.

Independent evidence for the importance of diffusion from the bulk in determining the surface chemistry is provided by ESCA analysis of samples taken through a heating/cooling cycle. The relevant data are displayed in Table 8.3. A sample heated from room temperature to  $30^{\circ}\text{C}$  shows  $\text{C}_{1\text{s}}/\text{O}_{1\text{s}}$  area ratios, indicative of vertical inhomogeneity with there being more oxygen actually at the



Table 8.3.  $C_{1s}/O_{1s}$  and  $C_{1s}/N_{1s}$  area ratios of high-slip PE at  $30^\circ$  and  $70^\circ$  take-off angles as a function of heating/cooling cycle.

Area ratio	Angle	$120^\circ\text{C}$	Cooled to $90^\circ\text{C}$	$90^\circ\text{C}$	Cooled to $30^\circ\text{C}$
$C_{1s}/O_{1s}$	$30^\circ$	65	128	220	135
	$70^\circ$	42	111	80	60
$C_{1s}/N_{1s}$	$30^\circ$	-	-	-	-
	$70^\circ$	-	-	-	-

very surface (see Table 8.1.). A sample heated to  $90^\circ\text{C}$  and then cooled to  $30^\circ\text{C}$  shows an inhomogeneity which is the exact reverse with oxygen being less at the very surface. The sample which has been taken to higher temperature also reveals no evidence for nitrogen functionality. Viz. the slip agent in the surface is largely at the very surface and rapidly desorbs. The surface chemistry for the sample heated to  $120^\circ\text{C}$  and then cooled to  $90^\circ\text{C}$  is remarkably similar to that from room temperature up to  $90^\circ\text{C}$ , perhaps providing evidence for increased mobility of the oxygen containing species at the elevated temperature. Viz. above  $90^\circ\text{C}$  the mobility is such that the surface is enriched in the oxygen containing species rather than the subsurface.

### 8.3.2. Low-slip polyethylene (LSPE)

The low-slip PE film was studied on both sides. The ESCA data displayed in Table 8.4. show distinctive differences between the inside and the outside surfaces in terms of the oxidative functionalisation.

Table 8.4.  $C_{1s}/O_{1s}$  and  $C_{1s}/N_{1s}$  area ratios of the low-slip PE for the outside and inside surfaces at  $30^\circ$  and  $70^\circ$  take-off angles.

low-slip PE	Angle	$C_{1s}/O_{1s}$	$C_{1s}/N_{1s}$
outside	$30^\circ$	13.5	177
	$70^\circ$	13.2	95
inside	$30^\circ$	6.3	-
	$70^\circ$	5.3	-

The outside surface of the wound reel of film shows evidence for very low levels of nitrogen with binding energy appropriate to an amide. It appears that from the commercial formulation of LDPE, 0.19% micronised silica, 0.02% ethylene oxide condensate and 0.05% BHT are present. Although the commercial formulation does not claim to have a slip agent added this is nonetheless present at low levels in the surface regions. The angular dependent data confirms the surface nature of the nitrogen containing functionality. The  $C_{1s}$  and  $O_{1s}$  spectra reveal a relatively high level of oxygen functionality which the angular dependent data suggests is vertically homogeneous, (the  $C_{1s}/O_{1s}$  of 13.5 and 13.2 at  $30^\circ$  and  $70^\circ$  take-off angles). The  $C_{1s}$  spectra show evidence for  $\underline{C}-O$  as the major structural feature, (see Figure 7.2.) and the data overall suggests that the untreated surface has a significant level of BHT present.

The prime focus of interest for the LSPE has, however, been the heat treatment of the inside surface which ESCA reveals to have been corona treated. This is most clearly

evident from the  $C_{1s}/O_{1s}$  intensity ratios in Table 8.4. However, corona treatment clearly removes low levels of slip agent since nitrogen is not detected for this surface, (see section 7.3.1.(i)).

The core level spectra as a function of temperature are shown in Figure 8.5. The most evident feature is the considerable reduction in intensity of the  $O_{1s}$  peak even at  $30^\circ$  take-off angle. The  $C_{1s}$  spectra shows the gradual decrease in the high binding energy tail which changes most abruptly between  $90^\circ\text{C}$  and  $120^\circ\text{C}$ . This is also true of the  $O_{1s}$  spectra, and the data overall reveal that in vacuo, migration or "turning in" of high surface energy oxygen containing functionalities occurs, and that the rate is considerably enhanced above the softening point for PE.

Whilst at room temperature, the corona surface in Table 8.5.

Table 8.5.  $C_{1s}/O_{1s}$  area ratios of low-slip PE at  $30^\circ$  and  $70^\circ$  take-off angles, as a function of heat treatments.

Area ratio	Angle	R.T.	$30^\circ\text{C}$	$60^\circ\text{C}$	$90^\circ\text{C}$	$120^\circ\text{C}$
$C_{1s}/O_{1s}$	$30^\circ$	6.3	6.9	7.9	8.4	18.8
	$70^\circ$	5.3	6.6	6.7	8.1	20.7

of the  $C_{1s}/O_{1s}$  area ratios are 6.3 and 5.3 at  $30^\circ$  and  $70^\circ$  take-off angles respectively. This gives C:O stoichiometries of  $\sim 10:1$  ( $30^\circ$ ) and  $\sim 8:1$  ( $70^\circ$ ), indicating a relatively small degree of vertical inhomogeneity, with the tendency for more oxygen functionalities to be at the very surface. The reverse is true above the melting point. Thus at  $120^\circ\text{C}$  the level of oxygen functionalities has drastically been

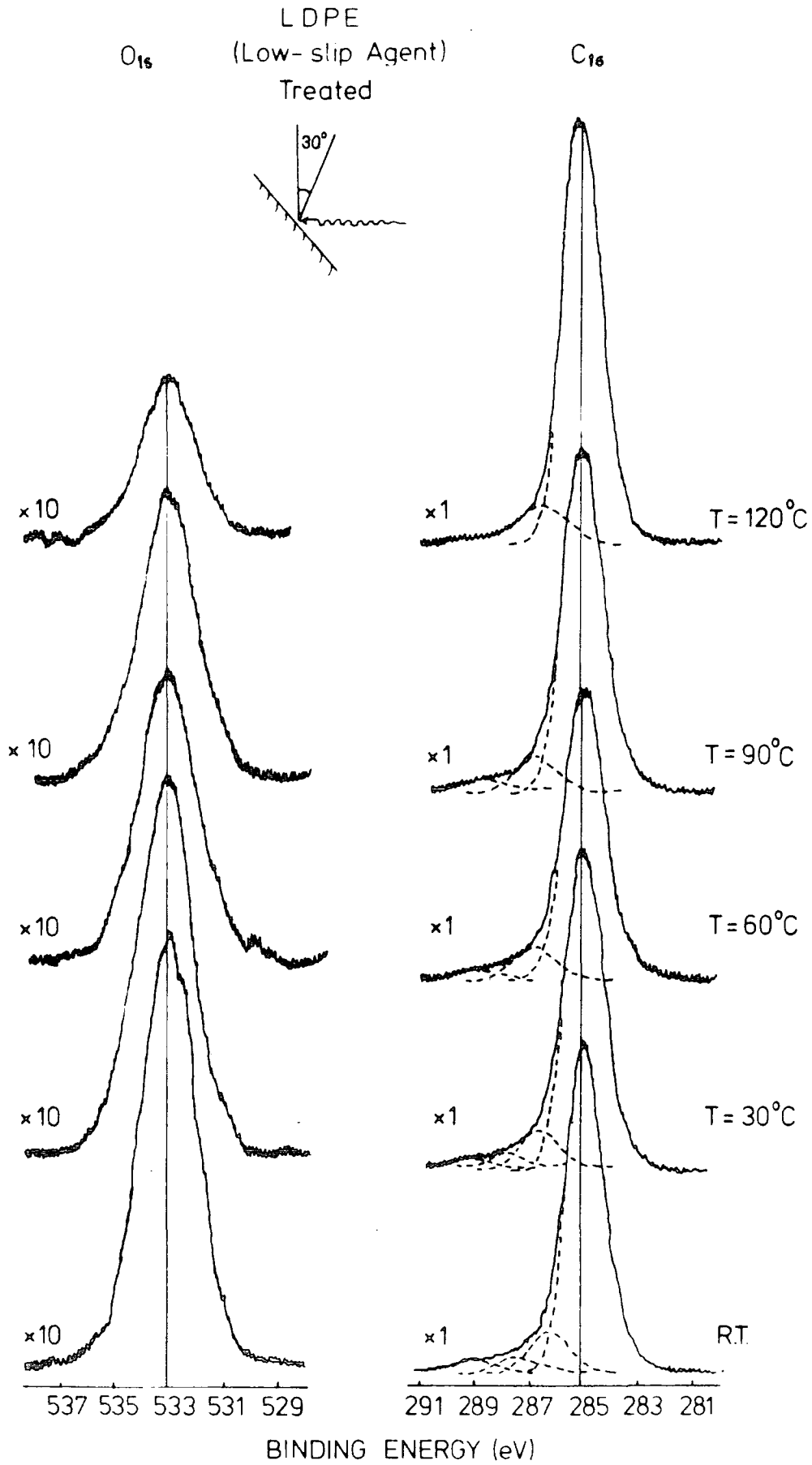


Figure 8.5. The  $C_{1s}$  and  $O_{1s}$  levels of low-slip LDPE, (the inside surface) at  $30^\circ$  take-off angle as a function of heat treatment.

reduced. The  $C_{1s}/O_{1s}$  area ratios of 18.8 and 20.7, give stoichiometries of  $\sim 30$  and  $\sim 33$  at  $30^\circ$  and  $70^\circ$  respectively. This reveals that the vertical inhomogeneity is now such as to suggest less oxygen functionalities at the very surface as required by a kinetic process in which e.g.  $-\overset{\text{O}}{\underset{\text{OH}}{\text{C}}}$  groups migrate into the subsurface.

On taking the sample heated to  $120^\circ\text{C}$  through a progressive cooling cycle to  $90^\circ\text{C}$  and thence  $60^\circ\text{C}$ , the  $C_{1s}/O_{1s}$  area ratios in Table 8.6. show that the oxygen functionalities

Table 8.6.  $C_{1s}/O_{1s}$  area ratio of low-slip PE at  $30^\circ$  and  $70^\circ$  take-off angles as a function of heating/cooling cycle.

Area ratio	Angle	$120^\circ\text{C}$	Cooled to $90^\circ\text{C}$	Cooled to $60^\circ\text{C}$	$90^\circ\text{C}$	Cooled to $60^\circ\text{C}$	Cooled to $30^\circ$
$C_{1s}/O_{1s}$	$30^\circ$	18.8	25.1	24.7	8.4	10.6	11.2
	$70^\circ$	20.7	22.8	23.5	8.1	9.9	9.7

increase slightly, and a similar effect is seen in cooling the sample from  $90^\circ\text{C}$  to  $60^\circ\text{C}$  to  $30^\circ\text{C}$ . Therefore the surface chemistry is largely dominated, as might have been anticipated, by the more rapid rate processes at elevated temperatures.

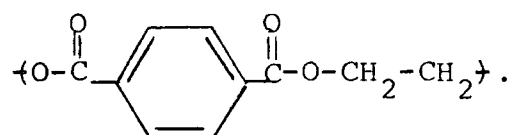
### 8.3.3. Polyethylene terephthalate (PET)

The PET, (Melinex type) is a commercially produced film by I.C.I. The film was examined by ESCA at two different take-off angles,  $30^\circ$  and  $70^\circ$ . It is of interest to study the surface chemistry of PET at room temperature (R.T.) before considering the effect of heat treatment. The relevant ESCA data are displayed in Table 8.7. The  $C_{1s}/O_{1s}$  area ratios of 1.85 and 2.44 at  $30^\circ$  and  $70^\circ$  take-off angles respectively,

Table 8.7.  $C_{1s}/O_{1s}$  area ratio and the  $C_{1s}$  envelope contribution of PET at  $30^\circ$  and  $70^\circ$  take-off angles, as a function of heat treatments.

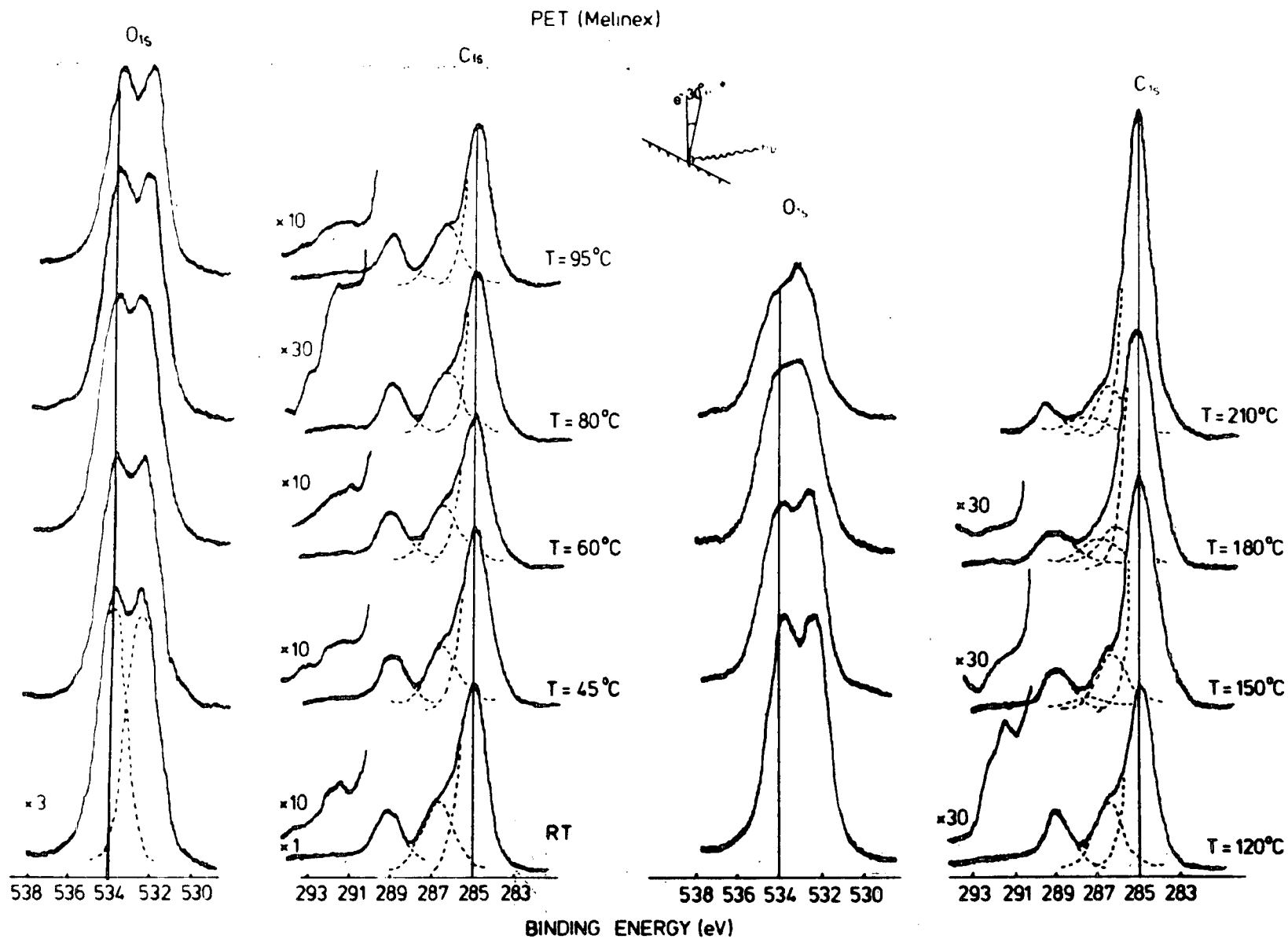
Temperature	Angle	$C_{1s}$ envelope contribution					
		$C_{1s}/O_{1s}$	$\underline{C-H}$	$\underline{C-O}$	$O-\underline{C=O}$	$\underline{C=O}$	$\pi \rightarrow \pi^*$
R.T.	$30^\circ$	1.85	60	21	16	-	3
	$70^\circ$	2.44	67	18	13	-	2
$45^\circ\text{C}$	$30^\circ$	1.85	63	21	15	-	3
	$70^\circ$	2.22	66	18	14	-	2
$60^\circ\text{C}$	$30^\circ$	1.61	57	23	19	-	2
	$70^\circ$	1.78 <sub>1</sub>	60	22	16	-	2
$80^\circ\text{C}$	$30^\circ$	1.72	59	23	17	-	1
	$70^\circ$	2.04	64	21	14	-	1
$95^\circ\text{C}$	$30^\circ$	2.04	63	20	15	1	1
	$70^\circ$	1.96	65	20	14	-	1
$120^\circ\text{C}$	$30^\circ$	2.00	63	20	15	1	1
	$70^\circ$	2.38	67	19	13	-	1
$150^\circ\text{C}$	$30^\circ$	3.13	72	16	10	2	-
	$70^\circ$	3.03	74	15	9	2	-
$180^\circ\text{C}$	$30^\circ$	3.33	74	12	8	6	-
	$70^\circ$	3.33	75	13	6	6	-
$210^\circ\text{C}$	$30^\circ$	4.32	78	10	6	5	-
	$70^\circ$	5.88	82	8	4	6	-

reveal a considerable degree of vertical inhomogeneity on the ESCA depth scale  $\sim 50\text{\AA}$ . The  $C_{1s}/O_{1s}$  area ratios give apparent stoichiometries, (using bulk derived sensitivity factors) of  $\sim 2.9$  ( $30^\circ$ ) and  $\sim 3.9$  ( $70^\circ$ ), indicating that the oxygen functionalities are less at the surface than at the subsurface. The repeat structural unit for PET is:-



This gives C:O stoichiometry of 2.5:1, therefore the ESCA data suggests a fairly high proportion of contamination in the surface regions. Also there is no evidence of any nitrogen functionalities, indicating no slip agent in the surface.

Representative spectra of PET are displayed in Figure 8.6. Analysis of the line profile of the  $C_{1s}$  region at a take-off angle of  $30^\circ$ , at R.T. suggests components of C-H (285.0 eV),  $\underline{\text{C}}-\text{O}$  (286.6 eV) and  $\text{O}-\underline{\text{C}}=\text{O}$  (289.0 eV), with relative intensities of 100:35:26. The component at  $\sim 291.2$  eV is a broad peak consistent with  $\pi \rightarrow \pi^*$  shake-up satellites, with intensity  $\sim 5\%$  of that of the main peak. The  $O_{1s}$  levels show the characteristic doublet structure attributed to  $\text{C}-\underline{\text{O}}$  and  $-\overset{\text{O}}{\parallel}{\text{C}}-\underline{\text{O}}$  structural features. The repeat structural unit of PET gives theoretical relative ratios of the  $C_{1s}$  levels of CH:C-O:O-C=O of 3:1:1. Thus, the higher  $C_{1s}/O_{1s}$  area ratio at higher take-off angle coupled with the lower ratio of high ( $\underline{\text{C}}=\text{O}$  and  $\underline{\text{C}}-\text{O}$ ) to low (CH) binding energy carbon suggests that, as a starting point the data at lower



**Figure 8.6.** The  $C_{1s}$  and  $O_{1s}$  levels of PET, (Melinex) at  $30^\circ$  take-off angle, as a function of heat treatments.



temperatures may be analysed in terms of a substrate-overlayer model where the overlayer arises from extraneous hydrocarbon. This will be described as model I, in terms of standard equations.

Methods of calculation of substrate-overlayer intensity attenuation

Model (I)

Figure 8.7., indicates the overlayer contaminant which arises from extraneous hydrocarbon.

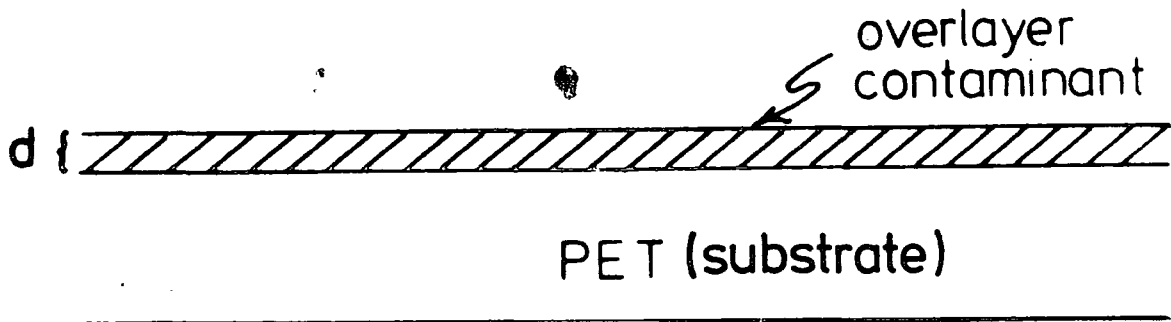


Figure 8.7. Substrate/overlayer model I.

The expressions which describe model (I) in terms of standard equations based on substrate-overlayer intensity ratios, (see section 1.5.2.) are shown below. The overlayer arising from hydrocarbon contaminants gives:-

$$I_{\text{overlayer}} = k_1(1 - e^{-d/\lambda_1 \cos \theta}) \quad 8.1$$

The substrate based on PET gives:-

$$I_{\text{PET}} = k_1(e^{-d/\lambda_1 \cos \theta}) \quad 8.2$$

Therefore:-

$$\frac{I_{\text{over}}}{I_{\text{PET}}} = \frac{1 - e^{-d/\lambda_1 \cos \theta}}{e^{-d/\lambda_1 \cos \theta}} \quad 8.3$$

When the substrate is based on the  $O_{1s}$  intensity ratio:-

$$I_{O_{1s}} = k_2 (e^{-d/\lambda_2 \cos \theta}) \quad 8.4$$

Therefore, by combining eq. 8.1 and 8.2, (which represents the total  $C_{1s}$  intensity ratios), and dividing by eq. 8.4 gives:-

$$\frac{I_{C_{1s}}}{I_{O_{1s}}} = \frac{(1 - e^{-d/\lambda_1 \cos \theta}) + (e^{-d/\lambda_1 \cos \theta}) \cdot \frac{k_1}{k_2}}{(e^{-d/\lambda_2 \cos \theta})} \quad 8.5$$

Therefore:-

$$\frac{I_{C_{1s}}}{I_{O_{1s}}} = \frac{1}{e^{-d/\lambda_2 \cos \theta}} \cdot \frac{k_1}{k_2} \quad 8.6$$

The assumed  $\lambda_1$  and  $\lambda_2$  mean free paths for photoemitted electrons of kinetic energy  $\sim 968$  eV ( $C_{1s}$ ) and  $\sim 720$  eV ( $O_{1s}$ ) of  $15\text{\AA}$  and  $10\text{\AA}$  respectively derive from previous studies in Durham laboratories.<sup>93</sup>

If we consider firstly the ratio of extraneous hydrocarbon signal to PET signal for the  $C_{1s}$  levels, the experimental data in Table 8.7., indicates values of 0.25 ( $30^\circ$ ) and 0.54 ( $70^\circ$ ) for the original sample studied at room temperature.

Comparison with the appropriate computations as a function of overlayer thickness indicates tolerable agreement for a value of thickness (d) of  $\sim 3\text{\AA}$  considerably less than a typical monolayer ( $\sim 5\text{\AA}$ ). The corresponding analysis of the  $C_{1s}/O_{1s}$  intensity ratios also indicates rough correspondence of theory and experiment for an overlayer thickness d of  $\sim 2\text{\AA}$ .

Since a typical monolayer thickness is  $\sim 5\text{\AA}$  the preliminary

analysis suggests only partial monolayer coverage. As will become apparent the totality of core level data only becomes understandable in terms of an initial patched overlayer structure as indicated in Figure 8.8. The patched overlayer

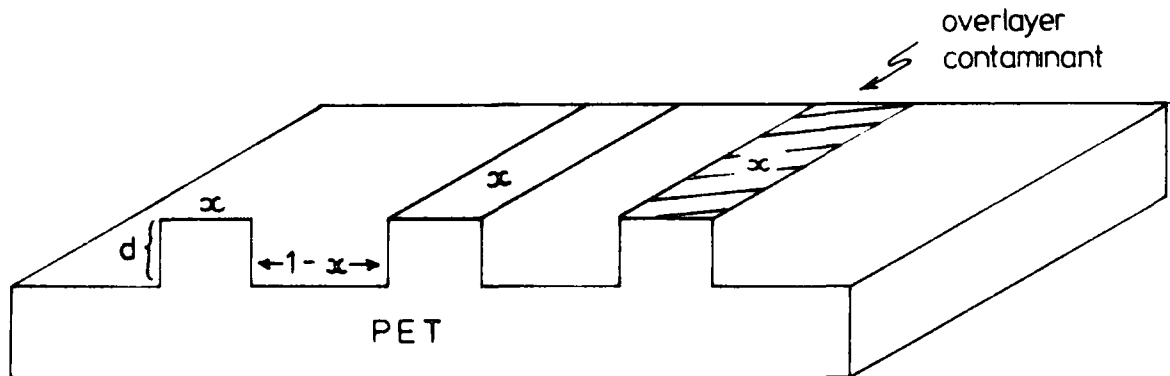


Figure 8.8. Substrate/overlayer model II, shows the patched overlayer coverage ( $x$ ) at the surface of PET film.

coverage will be described as model (II) in terms of standard equations based on the expressions of model (I).

Model (II)

From eq. 8.3, therefore

$$\frac{I_{\text{over}}}{I_{\text{PET}}} = \frac{x(1 - e^{-d/\lambda_1 \cos \theta})}{(1-x) + x(e^{-d/\lambda_1 \cos \theta})} \quad 8.7$$

and, eq. 8.6 gives:-

$$\frac{I_{C_{1s}}}{I_{O_{1s}}} = \frac{1}{(1-x) + x(e^{-d/\lambda_2 \cos \theta})} \cdot \frac{k_1}{k_2} \quad 8.8$$

whereas,  $x$  is the patched overlayer percentage coverage, and  $d$  is the thickness of monolayer coverage. The values of

relevant intensity ratios which have been computed for a matrix, values of  $d$  and  $x$ , the fractional overlayer coverage based in eq. 8.7 and 8.8, are displayed in Tables 8.8. and 8.9. A close examination of the data indicates good agreement for the angular dependence at room temperature data with  $\sim 55\%$  monolayer ( $5\text{\AA}$ ) coverage with extraneous hydrocarbon.

On raising the temperature to  $45^{\circ}\text{C}$  the experimental data of the ratio of extraneous hydrocarbon signal to PET signal for the  $\text{C}_{1s}$  levels, indicates values of 0.33 and 0.43 at  $30^{\circ}$  and  $70^{\circ}$  take-off angles respectively. The corresponding analysis of the  $\text{C}_{1s}/\text{O}_{1s}$  intensity ratios of 1.85 ( $30^{\circ}$ ) and 2.22 ( $70^{\circ}$ ). These experimental data seems well described by  $\sim 30\%$  coverage by an overlayer  $\sim 10\text{\AA}$  thick; the implication being that surface migration leads to an initial agglomeration of the hydrocarbon contamination as the temperature is initially raised.

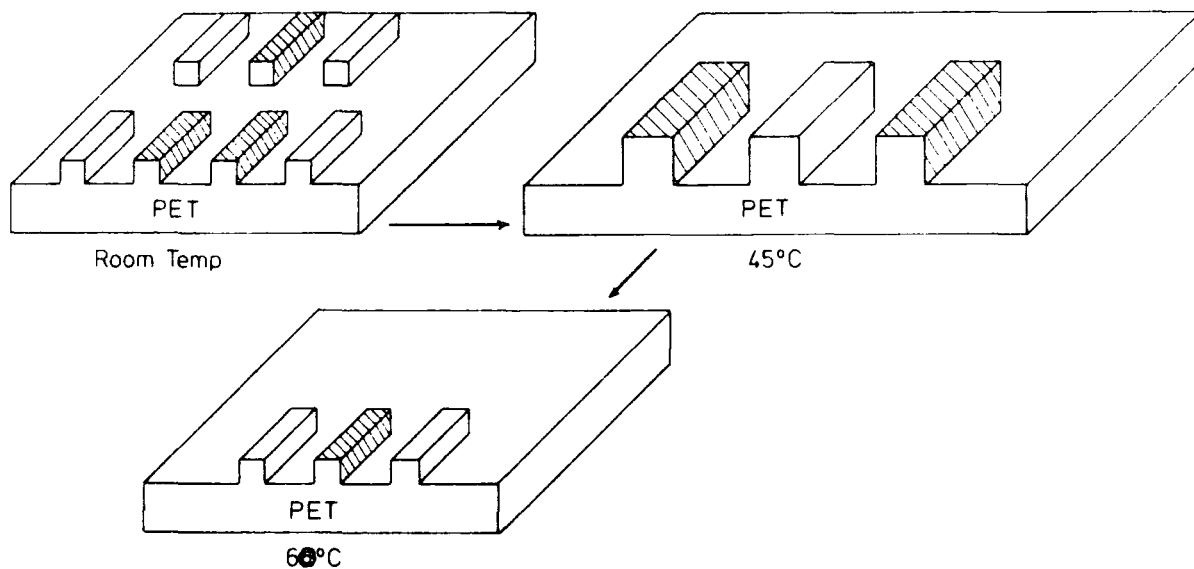
As the temperature is raised to  $60^{\circ}\text{C}$ , the relevant intensity ratios in Table 8.7., indicate a relatively clean surface with  $\sim 15\%$  of a  $5\text{\AA}$  monolayer of hydrocarbon contamination. The general scheme of the patched overlayer coverage for samples heated from room temperature to  $45^{\circ}\text{C}$  and  $60^{\circ}\text{C}$ , are shown in Figure 8.9. The temperature from  $60^{\circ}\text{C}$  to  $80^{\circ}\text{C}$ , shows a small increase in the relative intensity of the low binding energy component of the  $\text{C}_{1s}$  spectrum, and this is accompanied by a corresponding small increase in the  $\text{C}_{1s}/\text{O}_{1s}$  intensity ratios, (the  $\text{C}_{1s}/\text{O}_{1s}$  area ratio of 1.61 and 1.78 at  $30^{\circ}$  and  $70^{\circ}$  take-off angles respectively change to 1.72 ( $30^{\circ}$ ) and 2.04 ( $70^{\circ}$ ) from  $60^{\circ}$  to  $80^{\circ}\text{C}$

Table 8.8. The calculated  $\frac{I_{\text{over}}}{I_{\text{PET}}}$  intensity ratios for model II at  $30^\circ$  and  $70^\circ$  take-off angles, as a function of overlayer coverage ( $x$ ) and thicknesses ( $d$ ).

$x \%$	Angle	$d = 1\text{\AA}$	$d = 2\text{\AA}$	$d = 3\text{\AA}$	$d = 4\text{\AA}$	$d = 5\text{\AA}$	$d = 6\text{\AA}$	$d = 7\text{\AA}$	$d = 8\text{\AA}$	$d = 9\text{\AA}$	$d = 10\text{\AA}$
10	$30^\circ$	0.007	0.014	0.021	0.027	0.033	0.038	0.044	0.048	0.053	0.057
	$70^\circ$	0.02	0.03	0.05	0.057	0.066	0.074	0.080	0.086	0.090	0.094
20	$30^\circ$	0.015	0.03	0.04	0.06	0.07	0.08	0.09	0.10	0.11	0.12
	$70^\circ$	0.04	0.07	0.10	0.12	0.14	0.16	0.19	0.19	0.20	0.21
30	$30^\circ$	0.02	0.04	0.06	0.09	0.11	0.12	0.15	0.16	0.18	0.19
	$70^\circ$	0.05	0.11	0.15	0.19	0.23	0.27	0.28	0.32	0.33	0.35
40	$30^\circ$	0.03	0.06	0.09	0.12	0.15	0.17	0.20	0.23	0.25	0.27
	$70^\circ$	0.08	0.15	0.22	0.28	0.33	0.38	0.42	0.46	0.49	0.52
50	$30^\circ$	0.04	0.08	0.12	0.16	0.19	0.23	0.27	0.30	0.33	0.37
	$70^\circ$	0.10	0.19	0.28	0.37	0.45	0.53	0.59	0.66	0.71	0.75
60	$30^\circ$	0.05	0.09	0.14	0.19	0.24	0.29	0.33	0.38	0.43	0.48
	$70^\circ$	0.12	0.24	0.36	0.48	0.60	0.71	0.81	0.85	0.90	1.10
70	$30^\circ$	0.06	0.11	0.18	0.23	0.28	0.35	0.41	0.47	0.54	0.61
	$70^\circ$	0.14	0.28	0.45	0.61	0.75	0.92	1.10	1.22	1.38	1.50
80	$30^\circ$	0.06	0.13	0.20	0.27	0.34	0.42	0.50	0.58	0.67	0.75
	$70^\circ$	1.16	0.35	0.55	0.76	0.99	1.23	1.47	1.72	1.92	2.19
90	$30^\circ$	0.08	0.15	0.23	0.32	0.41	0.49	0.61	0.69	0.82	0.96
	$70^\circ$	0.18	0.41	0.67	0.96	1.27	1.63	2.03	2.45	3.00	3.35
100	$30^\circ$	0.08	0.16	0.26	0.36	0.46	0.58	0.72	0.86	0.99	1.10
	$70^\circ$	0.21	0.48	0.79	1.18	1.64	2.22	2.90	3.76	4.75	6.03

Table 8.9. The calculated  $\frac{I_{C_{1s}}}{I_{O_{1s}}}$  intensity ratios for model II at  $30^\circ$  and  $70^\circ$  take-off angles, as a function of  $x$  and  $d$ .

X %	Angle	$d = 1\text{\AA}$	$d = 2\text{\AA}$	$d = 3\text{\AA}$	$d = 4\text{\AA}$	$d = 5\text{\AA}$	$d = 6\text{\AA}$	$d = 7\text{\AA}$	$d = 8\text{\AA}$	$d = 9\text{\AA}$	$d = 10\text{\AA}$
10	$30^\circ$	1.58	1.60	1.61	1.62	1.64	1.64	1.65	1.66	1.67	1.68
	$70^\circ$	1.59	1.64	1.67	1.67	1.69	1.69	1.72	1.72	1.72	1.73
20	$30^\circ$	1.60	1.63	1.66	1.69	1.71	1.74	1.77	1.78	1.79	1.81
	$70^\circ$	1.65	1.71	1.77	1.81	1.85	1.87	1.89	1.91	1.92	1.93
30	$30^\circ$	1.62	1.67	1.71	1.76	1.80	1.84	1.87	1.91	1.94	1.97
	$70^\circ$	1.69	1.80	1.89	1.97	2.03	2.08	2.12	2.14	2.17	2.18
40	$30^\circ$	1.63	1.70	1.77	1.83	1.89	1.95	2.01	2.06	2.11	2.15
	$70^\circ$	1.74	1.90	2.04	2.16	2.26	2.33	2.40	2.45	2.49	2.51
50	$30^\circ$	1.65	1.74	1.83	1.92	2.00	2.08	2.16	2.24	2.31	2.38
	$70^\circ$	1.79	2.01	2.21	2.38	2.54	2.66	2.77	2.85	2.92	2.97
60	$30^\circ$	1.67	1.78	1.90	2.01	2.12	2.23	2.34	2.45	2.55	2.65
	$70^\circ$	1.86	2.13	2.41	2.67	2.90	3.10	3.27	3.41	3.53	3.62
70	$30^\circ$	1.69	1.83	1.97	2.11	2.25	2.40	2.55	2.70	2.85	3.00
	$70^\circ$	1.90	2.26	2.64	3.02	3.38	3.71	4.00	4.25	4.46	4.63
80	$30^\circ$	1.71	1.87	2.04	2.22	2.41	2.60	2.81	3.02	3.24	3.46
	$70^\circ$	1.96	2.42	2.93	3.49	4.05	4.62	5.15	5.64	6.07	6.43
90	$30^\circ$	1.73	1.92	2.12	2.34	2.58	2.84	3.12	3.42	3.73	4.07
	$70^\circ$	2.02	2.60	3.29	4.12	5.06	6.11	7.23	8.37	9.48	10.5
100	$30^\circ$	1.75	1.97	2.21	2.48	2.78	3.12	3.51	3.94	4.42	4.96
	$70^\circ$	2.09	2.80	3.76	5.03	6.74	9.03	12.10	16.21	21.71	29.09



**Figure 8.9.** The patched overlayer coverage ( $x$ ) at the surface of PET film as a function of temperature, (R.T.,  $45^{\circ}\text{C}$  and  $60^{\circ}\text{C}$ ).

respectively). This change corresponds to a decrease in oxygen functionality. This trend continues up to  $150^{\circ}\text{C}$  by which temperature the films are vertically homogeneous, but with a greatly decreased level of oxygen. The  $C_{1s}/O_{1s}$  area ratio at  $150^{\circ}\text{C}$  are 3.13 and 3.03 at  $30^{\circ}$  and  $70^{\circ}$  take-off angles respectively, indicating a C:O stoichiometry of  $\sim 5$  ( $30^{\circ}$ ) and  $\sim 4.8$  ( $70^{\circ}$ ). This reveals that the oxygen functionalities are rapidly decreased compared with the relatively clean surface at  $60^{\circ}\text{C}$ . At temperatures approaching the melting point  $210^{\circ}\text{C}$  (cf.  $\sim 265^{\circ}\text{C}$ )<sup>276</sup>, there is a further decrease in oxygen functionality such that the low binding energy  $C_{1s}$  component of  $\text{O}-\underline{\text{C}}$  and  $\text{O}-\underline{\text{C}}=\text{O}$  in Figure 8.6., completely dominates the spectrum with the  $C_{1s}/O_{1s}$  ratios being 2 - 3 times larger than for the initial sample, (the  $C_{1s}/O_{1s}$  area

ratio at 210°C are 4.35 and 5.88 at 30° and 70° take-off angles respectively).

In section 8.1. a brief summary was provided of work described in the literature pertaining to the bulk thermal degradation of PET. In almost all cases the temperature range encompassed by these studies was substantially larger than that employed in this work. Nonetheless the dramatic changes in surface chemistry, (irrespective of those initially occurring from desorption of low molecular weight hydrocarbon based contamination) imply very substantial changes in molecular structure in the surface regions which are clearly not necessarily reflected throughout the bulk.

Recent IR studies have identified loss of  $\text{CH}_3\text{CHO}$  as a major route in the thermal degradation of PET. However, even if the loss occurs uniformly throughout the ESCA depth sampling scale, from each diad unit of PET; the C:O stoichiometry would only change from 2.5 to 2.6. The ~ 100% change in  $\text{C}_{1s}/\text{O}_{1s}$  intensity ratio in going from 60°C to samples heated at 180°C, (the area ratios of 1.61 (60°C) change to 3.13 (180°C) at 30° take-off angle). This indicates a much greater loss of oxygen functionality which can only be reasonably accommodated by extensive decarboxylation in the surface regions. Figure 8.10. for example illustrates decarboxylation occurring for a given diad sequence which leads to a C:O stoichiometry of 3.2:1. This corresponds in stoichiometry to the sample heated to 95°C or so emphasising the fact that in the surface region the decarboxylation is very substantial even at relatively modest temperatures.



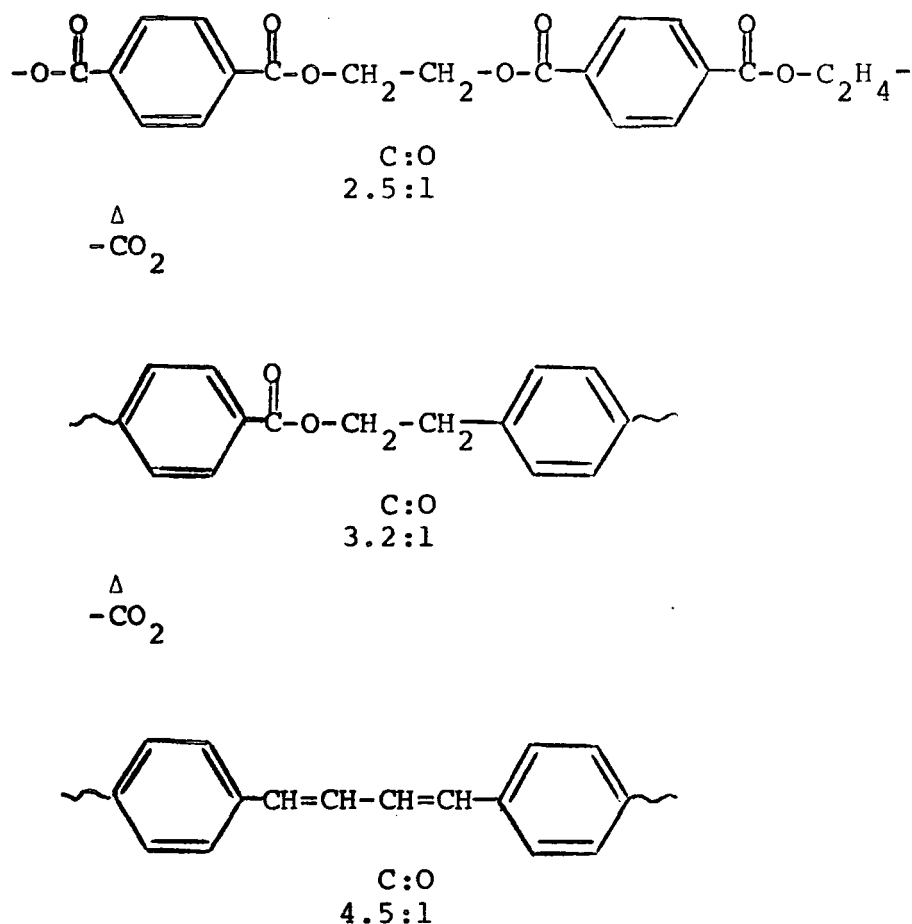


Figure 8.10. (Reaction scheme of decarboxylation)

Further decarboxylation to produce an extended conjugated system as in Figure 8.10. provides a C:O stoichiometry of 4.5:1 which is in tolerable agreement with the stoichiometry derived from the ESCA data in Table 8.7. for the sample heated to 150°C. The transmission IR spectra generally are frequently poorer in quality and poorly resolved bands than DRIFT spectra for example. The IR spectra for PET film heated at 240°C show a very low intensity band at 1608 cm<sup>-1</sup> which has been attributed to a conjugated hydrocarbon system, (polyenes -CH=CH-CH=CH-) suggesting that this is confined to the surface regions. Rohringer et al have detected bands at 1608, 1795

and  $1852\text{ cm}^{-1}$  from the low temperature pyrolysis of PET, they attributed these bands to polyenes at  $1608\text{ cm}^{-1}$ , linear anhydride at  $1795\text{ cm}^{-1}$  and cyclic anhydride at  $1786$  and  $1852\text{ cm}^{-1}$ .

At even higher temperatures further loss of oxygen functionalities must lead to extended linear conjugated systems which further heat treatment could conceivably convert into graphitic material.

PET samples heated to  $210^{\circ}\text{C}$  have also been studied after cooling to  $180^{\circ}\text{C}$  and the relevant data are included in Table 8.10. The cooled sample is much closer in C:O stoichiometry to its higher temperature precursor than the sample heated directly to  $180^{\circ}\text{C}$ , (see Table 8.7.). Studies have also been made of samples taken from  $180^{\circ}\text{C}$  to progressively lower temperature. The data in Table 8.10., again reveals that the surface structure developed at higher temperatures remains essentially intact on cooling.

Table 8.10. The  $C_{1s}/O_{1s}$  area ratios of PET at  $30^{\circ}$  and  $70^{\circ}$  take-off angles as a function of heating/cooling cycle.

Area ratio	Angle	$210^{\circ}\text{C}$	Cooled to $180^{\circ}\text{C}$	$180^{\circ}\text{C}$	Cooled to $150^{\circ}\text{C}$	Cooled to $120^{\circ}\text{C}$	Cooled to $90^{\circ}\text{C}$
$C_{1s}/O_{1s}$	$30^{\circ}$	4.4	4.0	3.3	3.2	3.1	3.0
	$70^{\circ}$	5.9	7.5	3.3	3.6	3.0	3.5

It is interesting to note that any dissolved oxygen in the film samples which would in any case be expected to be at a very low level do not give rise to thermal oxidation

artefacts in the surface regions; the clear trend being that as the temperature is increased oxidative functionalisation decreases. The fundamentally significant result deriving from the ESCA studies is that in the outermost few tens of Angstroms, where chain mobility, (particularly in its influence on molecular rearrangements are concerned), and crystallinity may well be different than in the bulk, there is a substantial change in surface chemistry at relatively modest temperatures. Under conditions where techniques for monitoring bulk chemistry reveal little change, that occurring in the surface regions may be well advanced towards graphitization.

The essential disappearance of the discrete shake-up component associated with  $\pi \rightarrow \pi^*$  transition in the benzenoid rings which is clearly evident in Figure 8.6., e.g. at R.T. is then explicable in terms of a broad diffuse shake-up arising from the multiplicity of transitions that are possible for an extended conjugated chain system.

Since it is the external surface of a material which communicates with the rest of the world such profound changes have considerable importance and relevance to a number of fields. The most likely route for understanding the drastic changes in surface chemistry which are observed involve a series of decarboxylations, as described before (see Figure 8.10.).

REFERENCES

1. D.T. Clark, "Chemical Aspects of ESCA", in "Electron Emission Spectroscopy", Eds., W. Dekeyser and D. Reidel, D. Reidel Publishing Co., Dordrecht, Holland, 373 (1973).
2. H. Robinson and W.F. Rawlinson, *Phil. Mag.*, 28, 277 (1914).
3. H. Robinson, *Proc. Roy. Soc.*, A104, 455 (1923).
4. H. Robinson, *Phil. Mag.*, 50, 241 (1925).
5. M. de Broglie, *Compt. Rend.*, 172, 274 (1921).
6. J.A. Van Akker and E.C. Watson, *Phys. Rev.*, 37, 1631 (1931).
7. M. Farence, Jr., *Phys. Rev.*, 51, 720 (1937).
8. A. Bazin, *Zhurnal Eksperimental noi Theoreticheskoi Fiziki*, 14, 23 (1944).
9. R.G. Steinhardt, Jr., F.A.D. Granados and G.I. Post, *Anal. Chem.*, 27, 1046 (1955).
10. B.L. Henke, Tech. Report No. 6, Contract No. AF 49 (638), Air Force Office of Scientific Research (1962).
11. K. Siegbahn and K. Eduarson, *Nucl. Phys.*, 1, 137 (1956).
12. C. Nordling, E. Sokolowski and K. Siegbahn, *Phys. Rev.*, 105, 1676 (1957); E. Sokolowski, C. Nordling and K. Siegbahn, *Ark. Fys.*, 12, 301 (1957); C. Nordling, E. Sokolowski and K. Siegbahn, *Ark. Fys.*, 13, 282, 288 (1958).

13. K. Siegbahn, C. Nordling, A. Fahlman, R. Nordberg, K. Hamrin, J. Hedman, G. Johansson, T. Berkmark, S.E. Karlsson, I. Lidgren and B. Lindberg, "ESCA, Atomic, Molecular and Solid State Structure Studied by Means of Electron Spectroscopy", Almqvist and Wiksells, Uppsala (1967).
14. A.E. Lindh, in "Handbuch der Experimental-Physik", 24 2, Eds., W. Wien and F. Haines, Leipzig (1930).
15. H.W.B. Skinner and J.E. Johnston, Proc. Roy. Soc., A161, 420 (1937).
16. C. Nordling, E. Sokolowski and K. Siegbahn, Ark. Fys., 13, 483 (1958).
17. S. Hagstrom, C. Nordling and K. Siegbahn, Phys. Letts., 9, 235 (1964).
18. C. Nordling, S. Hagstrom and K. Siegbahn, Z. Physik, 178, 433 (1964).
19. J.G. Jenkin, R.C.G. Leckey and J. Liesegang, J. Photoelect. Spec. and Rel. Phen., 12 (1), 1 (1977).
20. K. Siegbahn, C. Nordling, G. Johansson, J. Hedman, P.F. Heden, K. Hamrin, U. Gelius, T. Berkmark, L.D. Werme, R. Manne and Y. Baer, "ESCA Applied to Free Molecules", North-Holland Publishing Co., Amsterdam (1969).
21. K. Siegbahn, "Electron Spectroscopy - An Outlook", J. Elect. Spec. and Rel. Phen., 5, 3 (1974).
22. K. Siegbahn, "Electron Spectroscopy for Chemical Analysis". A survey presented at the Third International Conference on Atomic Physics at the University of Colorado, Boulder, Colorado (1972).

23. K. Siegbahn, "Electron Spectroscopy and Molecular Structure". A survey presented at XVIIIth Colloquium Spectroscopium International at Grenoble, Fr., (Sept. 1975).
24. K. Siegbahn, "Electron Spectroscopy for Solids, Surfaces, Liquids and Free Molecules, Uppsala University, Sweden (1976).
25. D.W. Turner, C. Baker, A.D. Baker and C.R. Brundle, Eds., "Molecular Photoelectron Spectroscopy", Wiley, N.Y. (1970).
26. D.T. Clark, "Structure and Bonding in Polymers as Revealed by ESCA", in "Electronic Structure of Polymers and Molecular Crystals", J. Ladik and J.M. Andre, Eds., Plenum Press, N.Y. (1975).
27. L.S. Cederbaum and W. Domcke, J. Elect. Spect. and Rel. Phen., 13, 161 (1978).
28. P. Auger, Compt. Rend., 65, 180 (1925).
29. J.J. Lander, Phys. Rev., 91, 1382 (1953).
30. D. Coster and R. de L. Kronig, Physica, 2, 13 (1935).
31. E.H.S. Burhop, Ed., "The Auger Effect and Other Radiationless Transitions", Cambridge Univ. Press, (1952).
32. C.F. Carlsson, Ed., "Photoelectron and Auger Spectroscopy", Plenum Press, N.Y. (1975).
33. C.C. Chang, Surface Sci., 25, 53 (1971).
34. J.P. Coad, M. Getting and J.G. Riviere, Farad. Disc. Chem. Soc., 60, 269 (1975).

35. A.E. Sandstrom, in "Handbook of Physics XXX. X-rays",  
Ed., S.F. Flugge, Springer Verlag, Berlin (1975), p.164.
36. A. Rosen and I. Lindgren, Phys. Rev., 176, 114 (1968).
37. P.S. Bagus, Phys. Rev., 139A, 619 (1965).
38. D.A. Shirley, in "Advances in Chemical Physics", 23,  
85 Eds., I. Prigogine and S.A. Rice, Wiley, N.Y.  
(1973).
39. U. Gelius and K. Siegbahn, Farad. Disc. Chem. Soc.,  
54, 257 (1972).
40. L.C. Synder, J. Chem. Phys., 55, 95 (1971).
41. D.B. Adams and D.T. Clark, Theoret. Chim. Acta, 31,  
171 (1973).
42. M.F. Guest, I.H. Hillier, V.R. Saunders and  
M.H. Wood, Proc. Roy. Soc., A333, 201 (1973).
43. D.T. Clark, I. Scanlan and J. Muller, Theoret. Chim.  
Acta, (Berl.) 35, 341 (1974).
44. T.A. Koopmans, Physika, 1, 104 (1933).
45. J.S. Levinger, Phys. Rev., 90, 11 (1953).
46. M.O. Krause, T.A. Carlson and R.D. Dismukes, Phys. Rev.,  
37, 170 (1968).
47. R. Manne and T. Aberg, Chem. Phys. Letts., 7, 282  
(1970).
48. J.W. Gadzuk, in "Electronic Structure and Reactivity  
of Metal Surfaces", Eds., E.G. Doroudne and  
A.A. Lucas, Plenum Press, N.Y. (1976).
49. I.H. Hillier and J. Kendrick, J. Elect. Spec.  
and Rel. Phen., 6, 325 (1975).
50. I.H. Hillier and J. Kendrick, Faraday Trans., 11, 71,  
1369 (1975).

51. S. Pignataro and G. Distofano, *Z. Naturforsch* A309, 815 (1975).
52. Ohta, Toshiaki, Fukitawa, Takashi, Furoda, Haruo, *Chem. Phys. Letts.*, 32, 369 (1975).
53. L. Yin, I. Adler, T. Tsang, L.J. Matienzo and S.O. Grim, *Chem. Phys. Letts.*, 24, 81 (1974).
54. T. Robert and G. Offergeld, *Chem. Phys. Letts.*, 29 606 (1974).
55. D.T. Clark, A. Dilks, J. Peeling and H.R. Thomas, *Faraday Disc.*, 60, 183 (1975).
56. (a) D.T. Clark and D.B. Adams, *J. Elect. Spec. and Rel. Phen.*, 7, 401 (1975).  
(b) D.T. Clark, D.B. Adams, A. Dilks, J. Peeling and H.R. Thomas, *J. Elect. Spec. and Rel. Phen.*, 8, 51 (1976).
57. D.T. Clark and A. Dilks, *J. Polym. Sci., Polym. Chem. Ed.*, 14, 533 (1976).
58. D.T. Clark and A. Dilks, *J. Polym. Sci., Polym. Chem. Ed.*, 15, 5 (1977).
59. R.D. Chambers, D.T. Clark, D. Kilcast and S. Partington, *J. Polym. Sci., Polym. Chem. Ed.*, 12, 1647 (1974).
60. M.A. Brisk and A.D. Baker, *J. Elect. Spec. and Rel. Phen.*, 7, 197 (1977).
61. L. Hedin and S. Lundqvist, in "Solid State Physics", 23 1, Eds., H. Ehrenreich, F. Seitz and H. Turnbull, Academic Press, N.Y. (1969).
62. M. Sunjic, D. Sokcevic and C. Lucas, *J. Elect. Spec. and Rel. Phen.*, 5, 963 (1974).



63. M.P. Hooker, J.T. Grant and T.W. Haas, *J. Vac. Sci. Technol.*, 13, 296 (1976).
64. S. Hagstrom, C. Nordling and K. Siegbahn, *Z. Physik*, 178, 439 (1964).
65. D.T. Clark, B.J. Cromarty and A. Dilks, *J. Polym. Sci., Polym. Chem. Ed.*, 16, 3173 (1978).
66. D.T. Clark and H.R. Thomas, *J. Polym. Sci., Polym. Chem. Ed.*, 14, 1671 (1976).
67. B.E. Mills, R.L. Martin and D.A. Shirley, *J. Am. Chem. Soc.*, 98 (9), 2380 (1976).
68. W.L. Jolly and T.F. Schaaf, *J. Am. Chem. Soc.*, 98 (11), 3178 (1976).
69. C.D. Wagner, W.M. Riggs, L.E. Davis, J.F. Moulder and G.E. Muilenberg, "Handbook of X-ray Photoelectron Spectroscopy", Perkin Elmer Corporation, Physical Electron Division (1979).
70. D.T. Clark and A. Harrison, *J. Polym. Sci., Polym. Chem. Ed.*, 19, 1945 (1981).
71. W.L. Jolly and D.N. Henrickson, *J. Am. Chem. Soc.*, 92, 1863 (1970).
72. J.N. Murrell and B.J. Ralston, *J. Chem. Soc., Faraday Trans.*, 11, 68, 1393 (1972).
73. M.E. Schwartz, *Chem. Phys. Letts.*, 6, 631 (1970).
74. D.A. Shirley, *Chem. Phys. Letts.*, 15, 325 (1972).
75. C.S. Fadley, "Basic Concepts of X-ray Photoelectron Spectroscopy", in "Electron Spectroscopy Theory Techniques and Applications", Vol. 2, 1, Eds., C.R. Brundle and A.D. Baker, Academic Press (1978).

76. C.F.H. Fellner-Feldagg, U. Gelius, B. Wannberg, A.G. Nilsson, E. Basilier and K. Siegbahn, *J. Elect. Spec. and Rel. Phen.*, 5, 643 (1974).
77. C.F.N. Beatham and A.F. Orchard, *J. Elect. Spec. and Rel. Phen.*, 9, 129 (1976).
78. A.F. Carley and R.M. Joyner, *J. Elect. Spec. and Rel. Phen.*, 16, 1 (1979).
79. T. Novakov and J.M. Hollander, *Phys. Rev. Lett.*, 21, 1113 (1968).
80. L.G. Parrat, *Rev. Mod. Phys.*, 31, 616 (1959).
81. R.E. Watson and A.J. Freeman, in "Hyperfine Interactions", Eds. A.J. Freeman and R.B. Frankel, Academic Press, N.Y. (1967).
82. C.S. Fadley, D.A. Shirley, A.J. Freeman, P.S. Bagus and J.V. Mallow, *Phys. Rev. Lett.*, 23, 1397 (1969).
83. J.V. Van Vleck, *Phys. Rev. Lett.*, 45, 405 (1934).
84. C.S. Fadley, in "Electron Spectroscopy", Ed., D.A. Shirley, North Holland, Pg. 781 (1972).
85. D.A. Shirley and D.W. Davis, *J. Chem. Phys.*, 56, 669 (1972).
86. G.K. Wertheim, "Mössbauer Effect: Principles and Applications", Academic Press, N.Y. (1964).
87. G.M. Bancroft, I. Adams, H. Lampe and T.K. Sham, *Chem. Phys. Letts.*, 32, 173 (1975).
88. R.D. Gupta and S.K. Shen, *Phys. Rev. Lett.*, 28, 1311 (1972).
89. D.T. Clark and A. Dilks, *J. Polym. Sci., Polym. Chem. Ed.*, 15, 2321 (1977).

90. B.L. Henke and R.L. Elgim, *Advan. X-ray Anal.*, 13, 639 (1970).
91. C.J. Powell, *Surface Sci.*, 44, 29 (1974).
92. D.R. Penn, *J. Elect. Spec. and Rel. Phen.*, 9, 29 (1976).
93. D.T. Clark and H.R. Thomas, *J. Polym. Sci., Polym. Chem. Ed.*, 15, 2843 (1977).
94. (a) R.J. Baird and C.S. Fadley, *J. Elect. Spec. and Rel. Phen.*, 11 (1), 39 (1977).  
(b) B.L. Henke, *J. Phys. (Paris)*, C4, 115 (1971).
95. J.H. Schofield, Lawrence Livermore Laboratory Report, U.G.R.L., 51326, Jan. (1973).
96. J.H. Schofield, *J. Elect. Spec. and Rel. Phen.*, 8, 129 (1976).
97. D.T. Clark and D. Shuttleworth, *J. Polym. Sci., Polym. Chem. Ed.*, 15, 2843 (1977).
98. D.T. Clark, "ESCA Applied to Polymers", in "Advance in Polymer Science", Springer-Verlag, Berlin (1977).
99. D.T. Clark and D. Shuttleworth, *J. Polym. Sci., Polym. Chem. Ed.*, 16, 1093 (1978).
100. D.T. Clark, Y.C.T. Fok and G.G. Roberts, *J. Elect. Spec. and Rel. Phen.*, 22, 173 (1981).
101. D.T. Clark, M.M. Abu-Shbak and W.J. Brennan, *J. Elect. Spec. and Rel. Phen.*, 28, 11 (1982).
102. E. Sokolowski, *Ark. Fys.*, 15, 1 (1959).
103. C. Nordling, *Ark. Fys.*, 15, 397 (1959).
104. G. Johansson, J. Hedman, A. Berndtsson, M. Klasson and R. Nilsson, *J. Elect. Spec. and Rel. Phen.*, 2, 295 (1973).

105. P. Ascarelli and G. Missoni, *J. Elect. Spec. and Rel. Phen.*, 5, 417 (1974).
106. D.T. Clark, H.R. Thomas, A. Dilks and D. Shuttleworth, *J. Elect. Spec. and Rel. Phen.*, 10 (4), 455 (1977).
107. K. Siegbahn, *J. Elect. Spec. and Rel. Phen.*, 5, 3 (1974).
108. R.M. Eisenberg, in "Fundamentals of Modern Physics", Chapter 14, J. Wiley and Sons, N.Y. (1981).
109. B.L. Henke, *Advan. X-ray Anal.*, 13, 1 (1969).
110. K. Yates, A. Barrie and F.J. Street, *J. Phys.*, E6, 130 (1973).
111. E.M. Purcell, *Phys. Rev.*, 54, 818 (1938).
112. J.C. Helmer and N.H. Weichert, *Appl. Phys. Lett.*, 13, 268 (1968).
113. C.D. Wagner, *Faraday Disc. Chem. Soc.*, 60, 306 (1975).
114. D.T. Clark and W.J. Feast, *J. Macromol. Sci.*, *Reviews in Macromol. Chem.*, C12, 191 (1975).
115. D.T. Clark, in "Structural Studies of Macromolecules by Spectroscopic Methods", Chapter 9, Eds. K. Ivin, J. Wiley and Sons, London (1976).
116. D.T. Clark, in "Advances in Polymer Friction and Wear", Vol. 5A, Ed., L.H. Lee, Plenum Press, N.Y. (1975).
117. D.T. Clark, in "Advances in Characterization of Polymer and Metal Surfaces", Ed. L.H. Lee, Academic Press, N.Y. (1976).
118. D.T. Clark, in "Chemistry and Physics of Solid Surfaces", Vol. 11, Ed., R. Vanselow, CRC Press, Boca Raton, Florida (1977).
119. D.T. Clark in "Polymer Surfaces", Eds., D.T. Clark and W.J. Feast, Wiley, London, Chapter 9 and 16 (1978).

120. D.T. Clark, in "Handbook of X-ray and Ultraviolet Photoelectron Spectroscopy", Ed., D. Briggs, Heyden, London, Chapter 6 (1977).
121. D.T. Clark, in "Photon, Electron and Ion Probes of Polymer Structure and Properties", Eds., D.W. Dwight, T.J. Fabish and H.R. Thomas, A.C.S. Symposium Series, 162, Washington, D.C., Chapter 17 (1981).
122. D.T. Clark, in "Advances in ESCA Applied to Polymer Characterization", Pure and Appl. Chem., Vol. 54, No. 2, 415 (1982).
123. A. Dilks, in "Electron Spectroscopy", Eds., C.R. Brundle and A.D. Baker, Academic Press (1981).
124. D.T. Clark and H.R. Thomas, J. Polym. Sci., Polym. Chem. Ed., 14, 1701 (1976).
125. R. Holm and S. Storp, Surf. and Interf., Vol. 2, No. 3, 961 (1980).
126. T.L. Barr, "Applications of ESCA in Industrial Research", Part II, Am. Lab., Vol. 10, 40 (1978).
127. T.L. Barr, "Applications of ESCA in Industrial Research", Part I, Am. Lab., p.65 (1978).
128. R. Holm and S. Storp, Surface Interf. Anal., 2 (1980).
129. R.J. Baird and C.S. Fadley, J. Elect. Spec. and Rel. Phen., 11 (1), 3 (1977) and references therein.
130. D.T. Clark, D. Kilcast, W.J. Feast and W.K.R. Musgrave, J. Polym. Sci., Polym. Chem. Ed., 11, 389 (1973).
131. D.T. Clark and H.R. Thomas, J. Polym. Sci., Polym. Chem., 14, 1701 (1976).

132. D.T. Clark and H.R. Thomas, *J. Polym. Sci., Polym. Chem.*, 16, 791 (1978).
133. D.T. Clark and A. Dilks, *J. Polym. Sci., Polym. Chem.*, 17, 957 (1979).
134. D.T. Clark, W.J. Feast, I. Ritchie, W.K.R. Musgrave, M. Modena and M. Ragazzini, *J. Polym. Sci., Polym. Chem. Ed.*, 12, 1049 (1974).
135. (a) D.T. Clark, J. Peeling and J.M. O'Malley, *J. Polym. Sci., Polym. Chem. Ed.*, 14, 543 (1976).  
(b) J. Peeling, D.T. Clark, I.M. Evans and D. Boulter, *J. Sci. Fd. Agric.*, 27, 331 (1976).  
(c) D.T. Clark, H.R. Thomas, W.J. Feast and P.J. Tweedale, *J. Polym. Sci.* (1979).
136. (a) C.S. Paik Sung and C.B. Hu, in "Multiphase Polymers", Eds., S.L. Cooper and G.M. Estes, *Advances in Chemistry, Ser. No.*, 176 (1979).  
(b) C.S. Paik Sung and C.B. Hu, *J. Biomed. Mater. Res.*, 13, 161 (1979).  
(c) B.D. Ratner, in "Photon, Electron and Ion Probes of Polymer Structure and Properties", Eds., D.W. Dwight, T.J. Fabish and H.R. Thomas, *A.C.S. Symposium Series, No.*, 162, Washington, D.C., (1981).  
(d) C.B. Hu and C.S. Paik Sung, *A.C.S. Polymer Preprints*, 21 (1), 156 (1980).  
(e) B.D. Ratner, in "Physicochemical Aspects of Polymer Surfaces", Ed., K.L. Mittal, Vol. 2, Plenum Publishing Corporation (1983).  
(f) R.W. Paynter, B.D. Ratner and H.R. Thomas, *A.C.S. Polymer Preprints*, 24 (1), 13 (1983).

137. J.J. Pireaux, J. Riga, R. Caudane and J. Verbist, in "Photon, Electron and Ion Probes of Polymer Structure and Properties", Eds., D.W. Dwight, T.J. Fabish and H.R. Thomas, A.C.S. Symposium Series, 162, Washington, D.C., Chapter 13 (1981).
138. J.J. Pireaux, Polymer Preprints, 21, 123 (1980).
139. J.J. Pireaux, J. Riga, R. Caudane and Y. Gobillon, Phys. Scripta, 16, 329 (1977).
140. J.J. Pireaux, J. Riga, R. Caudane, J. Verbist, Y. Gobillon and S. Delhalle, J. Polym. Sci., Polym. Chem. Ed., 17, 1175 (1979).
141. L.B. Duke, A. Paton, W.R. Salaneck, H.R. Thomas, E.W. Plummer, A.J. Heeger and A.G. MacDiarmid, Chem. Phys. Letts., 59, 146 (1978); W.R. Salaneck, H.R. Thomas, C.B. Duke, A. Paton, E.W. Plummer and A.G. MacDiarmid, J. Chem. Phys., 71, 2044 (1979).
142. C.D. Wagner, in "Photon, Electron and Ion Probes of Polymer Structure and Properties", Eds., D.W. Dwight, T.J. Fabish and H.R. Thomas, A.C.S. Symposium Series, 162, Washington, D.C., Chapter 14 (1981).
143. C.D. Wagner and P. Bilven, Surf. Sci., 35, 82 (1973).
144. C.D. Wagner, L.H. Gale and R.H. Raymond, Anal. Chem., 51, 466 (1979).
145. C.D. Wagner, Chem. Soc., Far. Disc., 60, 291 (1975).
146. J.E. Castle, L.B. Hazell and R.H. West, J. Elect. Spec. and Rel. Phen., 16, 97 (1979).
147. J.E. Castle and R.H. West, J. Elect. Spec. and Rel. Phen., 16, 195 (1979) and 18, 355 (1980).

148. C.D. Wagner and J.A. Taylor, *J. Elect. Spec. and Rel. Phen.*, 20, 83 (1980).
149. D.T. Clark, A. Dilks and H.R. Thomas, *J. Polym. Sci, Polym. Chem. Ed.*, 16, 1461 (1978).
150. D.T. Clark, A. Dilks, H.R. Thomas and D. Shuttleworth, *J. Polym. Sci., Polym. Chem. Ed.*, 17, 627 (1979).
151. M. Hudis, in "Techniques and Applications of Plasma Chemistry", Eds., J.R. Hollahan and A.T. Bell, Chapter 3, Wiley, N.Y. (1974).
152. J. Gray, "Surface Treatments for Plastics Films" and "Containers in Plastics: Surface and Finish", Eds., S.H. Pinner and W.G. Simpson, Butterworths, London (1971).
153. C.B. Jones, *Soc. Plast. Eng. Tech. Pap.*, 25, 724 (1979).
154. M.M. Millard, *Anal. Chem.*, 44, 828 (1972).
155. M.M. Millard, K.S. Lee and A.E. Pavlath, *Text. Res. J.*, 42, 307 (1972).
156. D.T. Clark, W.J. Feast, W.K.R. Musgrave and I. Ritchie, in "Advances in Polymer Friction and Wear", Los Angeles, March 1974, Ed., L.H. Lee, Vol. 5A, N.Y. (1975).
157. D.T. Clark, A. Dilks and D. Shuttleworth, *J. Mat. Sci.*, 12, 2547 (1977).
158. D.T. Clark and A. Dilks, *J. Polym. Sci., Polym. Chem. Ed.*, 16, 911 (1978).
159. D. Briggs, D.M. Brewis and M.B. Konieczko, *J. Mat. Sci.*, 12, 429 (1977).
160. D. Briggs, D.M. Brewis and M. Konieczko, *J. Mat. Sci.*, 11, 1270 (1976).



161. D. Briggs, D.G. Rance, C.R. Kendall and A.R. Blythe, *Polymer*, 21, 895 (1980).
162. D.M. Brewis and D. Briggs, *Polymer*, 22, 7 (1981).
163. H.F. Beer, Ph. D. Thesis, University of Durham (1980).
164. D.T. Clark and A. Dilks, in "Characterization of Metal and Polymer Surfaces", Vol. 2, Ed., L.H. Lee, Academic Press, N.Y. (1977).
165. D.T. Clark and A. Dilks, *J. Elect. Spec. and Rel. Phen.*, 11, 225 (1977).
166. D.T. Clark and Y.C.T. Fok, *Thin Solid Films*, 78, 271 (1981).
167. D.T. Clark and R. Wilson, *J. Polym. Sci., Polym. Chem.*, 21, 837 (1983).
168. D. Briggs, D.M. Brewis, J. Comyn, R.H. Dahm, M.A. Green and M.B. Konieczko, *Surf. Interf. Anal.*, 2 (3), 107 (1980).
169. D.T. Clark and P.J. Stephenson, *Proceedings of Conference on Nitrocelluloses*, Waltham Abbey, Ed., T.J. Lewis, Plenum Press (1980).
170. D.T. Clark, P.J. Stephenson and F. Heatley, *Polymer*, 22, 1110 (1981).
171. D.T. Clark and P.J. Stephenson, *Polymer*, 22, 1303 (1981).
172. D.T. Clark and P.J. Stephenson, *Polymer*, 23, 1034 (1982).
173. D.T. Clark and A.H.K. Fowler, in press (1983).
174. R.B. Ranby and J.F. Rabek, *Photodegradation, Photo-oxidation and Photostabilization of Polymers*, Wiley, London (1975).
175. J.F. McKellar and N.S. Allen, *Photochemistry of Man-made Polymers*, Applied Science Publishers Ltd., London (1979).

176. A. Dilks and D.T. Clark, *J. Polym. Sci., Polym. Chem. Ed.*, 19, 2847 (1981).
177. A. Dilks, in "Dev. Polym. Charact.", 2, 145 (1980).
178. D.T. Clark and H.S. Munro, *Polym. Degrad. and Stab.*, 4, 83 (1982).
179. D.T. Clark and H.S. Munro, *Polym. Degrad. and Stab.*, 4, 441 (1982).
180. D.T. Clark and H.S. Munro, *Polym. Degrad. and Stab.*, in press (1983).
181. M.P. Seah and W.A. Dench, *Surf. Interf. Anal.*, 1, 2 (1979).
182. R.F. Roberts, D.L. Allara, C.A. Pryde, D.N.E. Buchanan and N.D. Hobbins, *Surf. Interf. Anal.*, 2, 5 (1980).
183. D.T. Clark, Y.C.T. Fok and G.G. Roberts, *J. Elect. Spec. and Rel. Phen.*, 22, 173 (1980).
184. D.T. Clark, in "Physico-Chemical Aspects of Polymer Surfaces", Ed., K.L. Mittal, A.C.S. Symposium Series (1981).
185. C.J. Powell, *Surface Sci.*, 44, 29 (1974).
186. W.F. Gorham, *J. Polym. Sci.*, A-1, 4000 (1966).
187. W.G. Gorham, in "Encyclopaedia of Polymer Science and Technology", Eds., H.F. Mark, N.G. Gaylord and N. Bikales, Interscience, N.Y. (1971), Vol. 15.
188. W.F. Gorham, U.S. Pat. 3, 342, 754 (Sept. 1976).
189. W.D. Niegisch, *J. Polym. Sci., B*, 4, 531 (1966); *J. Appl. Phys.*, 37, 4041 (1966); *J. Appl. Phys.*, 38, 4110 (1967).
190. S. Kubo and B. Wunderlich, *J. Appl. Phys.*, 42, 4558 (1971); *J. Appl. Phys.*, 42, 4565 (1971).

191. R.G. Steinhardt, J. Hudis and M.L. Perlman, Phys. Rev., B5, 1016 (1972).
192. M. Klasson, J. Hedman, A. Benndsson, R. Nilsson, C. Nordling and P. Melnik, Phys. Ser., 5, 93 (1972).
193. A.T. Bell, in "Techniques and Applications of Chemistry", Eds., J.R. Hollahan and A.T. Bell, Wiley, N.Y., Chapter 1, (1974).
194. E.O. Johnson and L. Matter, Phys. Rev., 80, 58 (1950).
195. J.D. Swift and M.J.R. Schwar, "Electrical Probes for Plasma Diagnostics", Liffé Books Ltd., London (1970) and references therein.
196. D.T. Clark and A. Dilks, A.C.S. Centennial Meeting, New York, April 1976, "International Symposium on Advances in Characterisation of Polymer Surfaces", 101, Ed., L.H. Lee, Academic Press, N.Y. (1976).
197. A.N. Mearns, Thin Solid Films, 3, 201 (1969).
198. V.M. Kolotyrkin, A.B. Gilliman and A.K. Tsapuk, Russ. Chem. Phys., 36, 579 (1967).
199. N. Morosoff and H. Yasuda, in "Plasma Polymerisation", Eds., M. Shen and A.T. Bell, A.C.S. Symposium Series, 108, Washington, D.C., Chapter 10, Chapter 17 (1979).
200. C.F. Panel, Discussion, "Symposium on Plasma Chemistry of Polymers", J. Macromol. Chem., A(10), 3 (1976).
201. F.K. McTaggart, in "Plasma Chemistry in Electrical Discharges", Elsevier Publishing Co., Amsterdam (1967).
202. M. Shen, in "Plasma Chemistry of Polymers", Marcel Dekker Inc., N.Y. (1976).

203. N. Morosoff, B. Crist, T. Hsu Bumgarner and H. Yasuda, *J. Macromol. Sci.-Chem.*, 10, 451 (1976).
204. H. Kobayashi, M. Shen and A.T. Bell, *J. Macromol. Sci.-Chem.*, 8, 373 (1974).
205. A. Dilks, S. Kaplan and A. van Laeken, *J. Polym. Sci., Polym. Chem. Ed.*, (1981).
206. S. Kaplan and A. Dilks, *Thin Solid Films*, (1981).
207. L.F. Thomson and K.J. Maghan, *J. Appl. Polym. Sci.*, 16, 2291 (1972).
208. P.J. Dynes and D.H. Kaelble, in "Plasma Chemistry of Polymers", Ed., M. Shen, Marcel Dekker, Inc., N.Y. (1976).
209. H. Schonhorn, in "Polymer Science", Eds., D.T. Clark and W.J. Feast, Wiley, N.Y., Chapter 10 (1978).
210. D.T. Clark and D. Shuttleworth, *J. Polym. Sci., Polym. Chem. Ed.*, 17, 1317 (1978).
211. D.T. Clark and D. Shuttleworth, *J. Polym. Sci., Polym. Chem. Ed.*, 18, 27 (1980).
212. D.T. Clark and D. Shuttleworth, *J. Polym. Sci., Polym. Chem. Ed.*, 18, 407 (1980).
213. D.T. Clark and M.Z. AbRahman, *J. Polym. Sci., Polym. Chem. Ed.*, 20, 691 (1982).
214. D.T. Clark and M.Z. AbRahman, *J. Polym. Sci., Polym. Chem. Ed.*, 20, 2689 (1981).
215. D.T. Clark and M.Z. AbRahman, *J. Polym. Sci., Polym. Chem. Ed.*, 19, 2129 (1981).
216. D.T. Clark and M.Z. AbRahman, *J. Polym. Sci., Polym. Chem. Ed.*, 20, 1717 (1982).

217. D.T. Clark and M.M. Abu-Shbak, *J. Polym. Sci. Polym. Letts.*, A-1 (1983).
218. D.T. Clark and M.M. Abu-Shbak, *J. Polym. Sci., Polym. Chem.*, in press (1983).
219. H. Yasuda and T. Hirotsu, *J. Polym. Sci., Polym. Chem. Ed.*, 16, 743 (1978).
220. R.D. Chambers, in "Fluorine in Organic Chemistry", Wiley, London (1973).
221. D.T. Clark, R.D. Chambers, D. Kilcast and W.K.R. Musgrave, *J. Chem. Soc., Faraday Trans.*, 2 (1972).
222. L.W. Crane and C.L. Hamermesh, in "Adhesion of Thin Plasma Polymer Films to Plastics", Ed., K.L. Mittal, American Society for Testing and Materials, p.101 (1978).
223. T. Smith, D.H. Kaelble and C.L. Hamermesh, *Surface Science*, 76, 203 (1978).
224. H. Suhr, in "Techniques and Applications of Plasma Chemistry", Eds., J.R. Hollahan and A.T. Bell, Wiley and Son, Chapter 2 (1974).
225. D.T. Clark, M.M. Abu-Shbak, W.J. Brennan and S.A. Johnson, unpublished (1983).
226. H.F. Beer and D.T. Clark, *J. Fluorine Chem.*, 4, 181 (1974).
227. D.T. Clark and D. Shuttleworth, *J. Elect. Spec. and Rel. Phen.*, 15, 17 (1979).
228. H. Yasuda, in "Plasma Polymerization", Eds., M. Shen and A.T. Bell, A.C.S. Symposium Series, 108, Washington, D.C. (1979).

229. G. Lubin, in "Handbook of Fibreglass and Advanced Plastics Composites", R.K. Krieger, Huntington, N.Y. (1975).
230. J.A. Brydson, in "Plastics Materials", Newnes and Butterworths, London (1975).
231. W. Brenner, D. Lum and M.W. Riley, in "High-Temperature Plastics", Chapman and Hall Ltd., London (1962).
232. R.M. Ogorkiewicz, in "Engineering Properties of Thermoplastics", Wiley and Sons Ltd., London (1970).
233. A.W. Birley and M.J. Scott, in "Plastics Materials Properties and Applications", Leonard Hill, London (1982).
234. L.K. Arnold, in "Introduction to Plastics", G. Allen and Unwin Ltd., London (1969).
235. F. Bueche, in "Physical Properties of Polymers", Wiley and Sons Ltd., London (1962).
236. D.C. Miles and J.H. Briston, in "Polymer Technology", Temple Press Books, London (1965).
237. J.M. McKelvey, in "Polymer Processing", Wiley and Sons Ltd., London (1962).
238. Y.B. Vasudeo and S.P. Potnis, J. Colour Soc., p.19, (1977).
239. R.G. Weatherhead, in "FRP Technology Fibre Reinforced Resin System", Applied Science Publishers Ltd., London (1980).
240. J.R. Caimi, Packing Technol., 4 (11), 11 (1981).
241. I. Skeist, in "Handbook of Adhesives", 2nd Edn., Van Nostrand Reinhold Co., N.Y. (1978).

242. W.J. Powers, in "Polymer Processes", Ed.  
C.E. Schildknecht, Wiley and Sons Ltd., London  
(1963).
243. A. Hardy and R.T. Agger, British Poly. J., 11 (2),  
(1979).
244. W.L. Baun, Applications of Surf. Sci., 4, 291 (1980).
245. W.L. Baum, in "Adhesion Measurement of Thin Films,  
Thick Films and Bulk Coating", ASTM STP, Ed.,  
K.L. Mittal, American Society for Testing and  
Materials, (1978), pp. 41-53.
246. H. Schonhorn, in "Polymer Surfaces", Eds., D.T. Clark  
and W.J. Feast, Wiley and Sons Ltd., London (1978).
247. E.H. Andrews and N.E. King, in "Polymer Surfaces,  
Eds., D.T. Clark and W.J. Feast, Wiley and Sons  
Ltd., London (1978).
248. L.T. Drzal, "Summary of the Workshop held on the  
Role of the Polymer Substrate Interphase in  
Structural Adhesion", Air Force Materials Laboratory,  
Technical Report, AFML-TR-77-129, July (1979).
249. W.L. Baun and J.S. Soloman, "Surface Contamination  
of Adhesive Bonding Materials", Air Force  
Materials Laboratory, Technical Report, AFML-TR-79-  
4165, December (1979).
250. V.T. Kagiga, K. Takemoto and M. Hagiwara, J. Appl.  
Polym. Sci., Appl. Polym. Sym., 35, 95 (1979).
251. P.D. Ritchie, in Soc. Chem. Ind. Monograph, No. 13,  
London, (1961), pp. 107-131.
252. E.P. Goodings, in Soc. Chem. Ind. Monograph, No. 13,  
London, (1961), pp. 211-228.

253. J. Polym. Sci., Sym. No. 57, 65 (1976).
254. U. Hayat, Ph.D. Thesis, Durham, unpublished.
255. H.S. Munro, unpublished data.
256. J. Peeling and D.T. Clark, Polym. Degrad., 3, 97 (1981) and 3, 177 (1981).
257. D.T. Clark and H.S. Munro, Polym. Degrad., 5, 237 (1983).
258. G. Gillberg and D. Kemp, J. Appl. Polym. Sci., 26, 2023 (1981).
259. J.P. Hobbs, C.S.P. Sung, K. Krishnan and S. Hill, Macromolecules, 16, 193 (1983).
260. R. Rohringer, E. Marti and S. Moss, in "Thermal Analysis", Ed. W. Hemminger, Vol. 2, Birkhäuser Verlage, England (1980).
261. "Thermal Stability of Polymers", Ed. R.T. Conley, Vol. 1, Marcel Dekker, Inc., New York (1970).
262. "Thermal Analysis", Ed. W. Hemminger, Vol. 2, Birkhäuser Verlage, England (1980).
263. "Developments in Polymer Degradation", Ed. N. Grassie, Vol. 1 - 4, Applied Science Publishers Ltd., Essex (1982).
264. I. Marshall and A. Todd, Trans. Faraday Soc., 49, 67 (1963).
265. V.B. Gupta and S. Kumar, J. Appl. Polym. Sci., 26, 1865-1905 (1981).
266. A. Holmström and E.M. Sörvik, J. Appl. Polym. Sci., 18, 761 (1974).
267. A. Holmström and E.M. Sörvik, J. Polym. Sci., Sym. No. 57, 33 (1976).



268. I. Lüderwald, in "Developments in polymer Degradation",  
Ed. N. Grassie, Vol. 2, Applied Science Publishers  
Ltd., England (1982).
269. M.E. Bednas, M. Day, K. Ho, R. Sander and D.M. Wiles,  
J. Appl. Polym. Sci., 26, 277 (1981).
270. K. Barabás, M. Iring, T. Kelen and F. Tüdös, J. Polym.  
Sci., Sym. No. 57, 65 (1976).
271. H. Hoff and S. Jacobsson, J. Appl. Polym. Sci.,  
26, 3409 (1981).
272. N. Inagaki, H. Onishi, H. Kunisada and K. Katsuura,  
J. Appl. Polym. Sci., 21, 217 (1977).
273. D.J. Carlsson, M. Day, T. Suprunhuk and D.M. Wiles,  
J. Appl. Polym. Sci., 28, 715 (1983).
274. K. Yoda, A. Tsuboi, M. Wada and R. Yamadera,  
J. Appl. Polym. Sci., 14, 2357 (1970).
275. G.R. Rideal and J.C. Padget, J. Polym. Sci., Sym.  
No. 57, 1 (1976).
276. "Polymer Handbook", Eds. J. Brandrup and E.H. Immergut,  
2nd Edn., Wiley (1975).
277. N. Inagaki, H. Onishi, H. Kunisada and K. Katsuura,  
J. Appl. Polym. Sci., 21, 217 (1977).

APPENDIX I

Lectures and Seminars attended during the period 1980-1983

21 May 1980

Dr. T.W. Bentley (University of Swansea),  
"Medium and Structural Effects in Solvolytic Reactions".

7 October 1980

Professor T. Fehlner (Notre-Dame University, U.S.A.),  
"Metalloboranes Cages or Coordination Compounds?".

16 October 1980

Dr. D. Maas (Salford University),  
"Reactions a Go-Go".

30 October 1980

Professor N. Grassie (Glasgow University),  
"Inflammability Hazards in Commercial Polymers".

6 November 1980

Professor A.G. Sykes (Newcastle upon Tyne University),  
"Metallo-Proteins: An Inorganic Chemists' Approach".

12 November 1980

Dr. M. Gerloch (University of Cambridge),  
"Magnetochemistry is about Chemistry".

13 November 1980

Professor N.N. Greenwood (Leeds University),  
"Metalloborane Chemistry".

19 November 1980

Dr. T. Gilchrist (University of Liverpool),  
"Nitroso-olefins as Synthetic Intermediates".

4 December 1980

Reverend R. Lancaster,  
"Fireworks".

18 December 1980

Dr. R. Evens (University of Brisbane, Australia),  
"Some Recent Communications to the Editor of the  
Australian Journal of Failed Chemistry".

29 January 1981

Mr. H. Maclean (I.C.I. Ltd.),  
"Managing in the Chemical Industry in the 1980s".

18 February 1981

Professor S. Kettle (University of East Anglia),  
"Variations in the Molecular Dance at the Crystal Ball".

25 February 1981

Dr. K. Bowden (University of Essex),  
"The Transmission of Polar Effects of Substituents".

17 March 1981

Professor W. Jencks (Brandeis University, Massachusetts),  
"When is an Intermediate not an Intermediate?".

7 May 1981

Professor M. Gordon (Essex University),  
"Do Scientists have to Count?".

10 June 1981

Dr. J. Rose (I.C.I. Plastics),  
"New Engineering Plastics".

21 September 1981

Dr. P. Plimmer (Dupont),  
"From Conception to Commercialisation of a Polymer".

14 October 1981

Professor E. Kluk (University of Katowice),  
"Some Aspects of the Study of Molecular Dynamics -  
Simple Molecular Liquids".

22 October 1981

Dr. P.J. Corrish (Dunlop Ltd.),  
"What would life be like without Rubber".

6 November 1981

Dr. W. Moddeman (Monsanto Ltd., U.S.A.),  
"High Energy Materials".

12 November 1981

Professor A.I. Scott (University of Edinburgh),  
"An Organic Chemist's View of Life in the N.M.R. Tube".

26 November 1981

Dr. W.O. Ord (Northumbrian Water Authority),  
"The Role of the Scientist in a Regional Water Authority".

2 December 1981

Dr. G. Beamson (University of Durham),  
"Photoelectron Spectroscopy in a Strong Magnetic Field".

20 January 1982

Dr. M.R. Bryce (University of Durham),  
"Organic Metals".

28 January 1982

Professor I. Fells (University of Newcastle upon Tyne),  
"Balancing the Energy Equations".

3 February 1982

Dr. D. Parker (University of Durham),  
"Modern Methods for the Determination of Enantiomeric  
Purity".

10 February 1982

Dr. D. Pethrick (University of Strathclyde),  
"Conformational Dynamics of Small and Large Molecules".

17 February 1982

Professor D.T. Clark (University of Durham),  
"Structure, Bonding, Reactivity and Synthesis of  
Surfaces as revealed by ESCA".

3 March 1982

Dr. P. Bamfield (I.C.I. Organics Division),  
"Computer Aided Synthesis Design: A view from Industry".

19 May 1982

Professor R.D. Chambers (University of Durham),  
"Fluorocarbanions - some 'Alice in the Looking Glass'  
Chemistry".

28 June 1982

Professor D.J. Burton (University of Iowa),  
"Some Aspects of the Chemistry of Fluorinated Phosphonium  
Salts and Phosphonates".

13 September 1982

Professor R. Neidlein (University of Heidelberg),  
"New Aspects and Results of Bridged Annulene Chemistry".

27 September 1982

Dr. W.K. Ford (Xerox Research Centre, Webster, New York),  
"The Dependence of the Electronic Structures of Polymers  
on their Molecular Architecture".

13 October 1982

Dr. W.J. Feast (University of Durham),  
"Approaches to the Synthesis of Conjugated Polymers".

28 October 1982

Professor M.F. Lappert, F.R.S. (University of Sussex),  
"Approaches to Asymmetric Synthesis and Catalysis Using  
Electron-Rich Olefins and Some of Their Metal Complexes".

15 November 1982

Dr. G. Bertrand (University of Toulouse),  
"Curtius Rearrangement in Organometallic Series: A Route  
for New Hybridised Species".

24 November 1982

Professor G.G. Roberts (University of Durham),  
"Langmuir-Blodgett Films".

24 November 1982

Professor F.R. Hartley (R.M.C.S. Shrivenham),  
"Supported Metal Complex Hydroformylation Catalysts:  
A Novel Approach Using  $\gamma$ -radiation".

2 December 1982

Dr. G.M. Brooke (University of Durham),  
"The Fate of the Ortho-Fluorine in 3,3-Sigmatropic  
Reactions Involving Polyfluoro-aryl and -heteroaryl  
Systems".

9 February 1983

Dr. P. Moore (University of Warwick),  
"Mechanistic Studies in Solution by Stopped Flow  
F.T. NMR and High Pressure NMR Line Broadening".

2 March 1983

Dr. D. Bloor (Queen Mary College, University of London),  
"The Solid-State Chemistry of Diacetylene monomers and  
Polymers".

11 March 1983

Professor H.G. Viehe (University of Louvain),  
"Oxidations on Sulphur".

16 March 1983

Dr. I. Gosney (University of Edinburgh),  
"New Extrusion Reactions: Organic Synthesis in a  
Hot Tube".

25 March 1983

Professor F.G. Baglin (University of Newark),  
"Interaction Induced Raman Spectroscopy in Supracritical  
Ethane".

21 April 1983

Professor J. Passmore (University of New Brunswick),  
"Novel Selenium-Iodine Cations".

4 May 1983

Professor P.H. Plesch (University of Keele),  
"Binary Ionisation Equilibria Between Two Ions and Two  
Molecules. What Ostwald Never Thought Of".

10 May 1983

Professor K. Berger (University of Munich),  
"New Reaction Pathways from Trifluoromethyl-Substituted  
Heterodienes to Partially Fluorinated Heterocyclic  
Compounds".

11 May 1983

Dr. N. Isaacs (University of Reading),  
"The Application of High Pressures to the Theory and  
Practice of Organic Chemistry".

13 May 1983

Dr. R. de Kock (Calvin College, Grand Rapids, Michigan),  
"Electronic Structural Calculations on Organometallic  
Cobalt Cluster Molecules: Implications for Metal  
Surfaces".



APPENDIX II

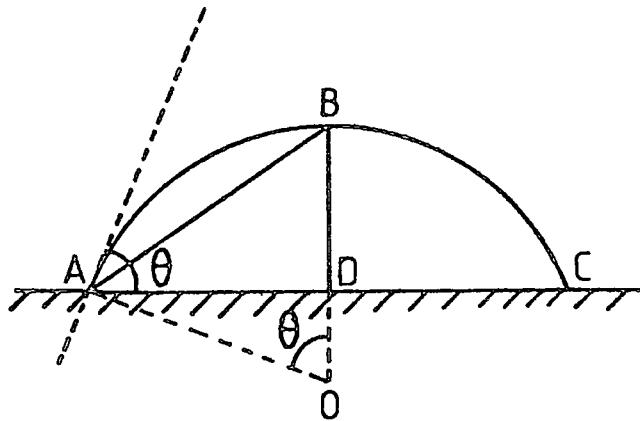
Conferences Attended During the Period 1980-1983

- (1) Polymer Characterisation Symposium, July 1981, Durham.
- (2) Graduate Symposium, Durham 1982.
- (3) Graduate Symposium, April 1983, Durham.

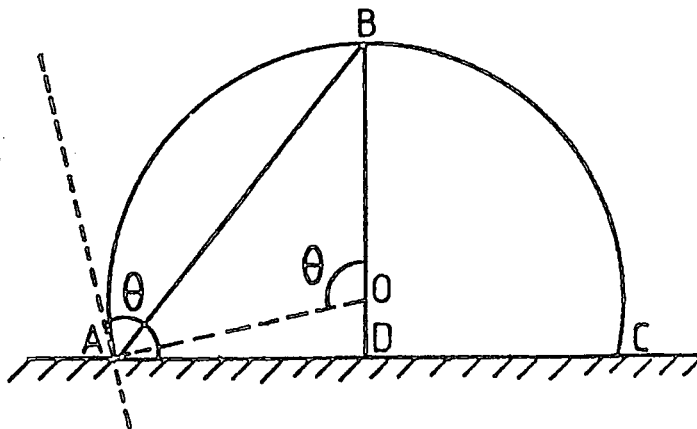
APPENDIX III

Determination of Contact Angles from Dimensions  
of Liquid Drops

a)  $\theta \leq 90^\circ$



b)  $\theta \geq 90^\circ$



$$\theta = 2 \tan^{-1} \frac{BD}{AD}$$

